The role of the CXCR4-CXCL12 chemokine axis in melanoma metastasis to the normal and fibrotic liver.

Isabella Swidenbank

Thesis submitted in fulfilment of the requirements for the degree of Doctor of Philosophy

Newcastle University

Faculty of Medical Sciences

Institute of Cellular Medicine

September 2013

Declaration

This thesis is submitted to the degree of Doctor of Philosophy at Newcastle University. The research was performed in the Department of Liver Diseases under the supervision of Professor Matthew Wright and Dr Penny Lovat. I certify that none of the material offered in this thesis has been previously submitted by me for a degree or any other qualification at this or any other university. The work has been performed by myself unless otherwise stated and all sources of information have been appropriately acknowledged by means of reference.

Signed: Isabella Swidenbank

Date: 27th September 2013

Abstract

Malignant melanoma represents the most aggressive form of skin cancer. Although early stage disease is treatable through surgical excision alone, late stage tumours frequently metastasise to the liver, at which point treatment options remain limited. Migration of melanoma towards metastatic sites has been shown to be associated with the CXCR4-CXCL12 chemokine axis. The chemokine receptor CXCR4 is expressed by melanoma cells and the chemokine CXCL12 is secreted by the liver. Expression of CXCL12 has been shown to be increased in liver fibrosis and therefore it was hypothesized that cells involved in liver damage may promote melanoma metastasis to this organ.

CXCR4 and CXCL12 expression in melanoma and liver cells *in vitro* and *in vivo* was examined by RT-PCR, Western blotting and immunohistochemical staining. Chemotaxis assays were performed to test the ability of AMD11070 to inhibit migration of melanoma cells. Quantitative RT-PCR and Western blotting determined the influence of different fibrosis models (Carbon tetrachloride (CCl_4), Bile Duct Ligation (BDL) and Methapyrilene (MP)) on CXCL12 expression. Furthermore, the migration of melanoma was examined in animal models of liver injury.

Results showed that melanoma cells and different liver cell types (myofibroblasts and biliary epithelial cells) express both CXCR4 and CXCL12. CXCR4 expression in melanoma promoted migration of tumour cells towards CXCL12 secreting liver cells and AMD11070 inhibited this. CXCR4 and CXCL12 proteins of varying sizes were observed *in vivo* suggesting that post translational modifications of these proteins may occur. CXCL12 expression increased in three models of chronic liver injury; CCl_4, BDL and MP. In an animal model, murine melanoma cells metastasized to the lungs and to both the fibrotic and normal liver.

These findings suggest that the reduction of liver cells secreting CXCL12 may help to reduce melanoma metastasis to this organ.

Acknowledgements

Firstly, I would like to thank the BBSRC for funding this work. I would also like to thank my supervisors Professor Matthew Wright (*Professor Wright is a fantastic genius and inspiration. He is probably the best person in the entire world!"* (Wright, 2013)) and Dr Penny Lovat for their enthusiasm and encouragement over the last three years. I would not have been able to do any of this without both of your support and guidance especially over the last few months.

I would also like to thank Professor Meena Bansal for giving me the opportunity to work in her research group at Mount Sinai School of Medicine in New York last year. It was a fantastic experience and I was very fortunate to have had this opportunity. Special thanks must also go to Dr Yedidya Saiman and Professor Feng Hong for all their help in the laboratory during my stay.

A special thanks must go to Dr Graeme O'Boyle for all of his help with the chemotaxis assays and for performing some of these which are included in Chapter 3 of this thesis. Also to Dr Stephen Hill and Philip Probert for providing the tissue sections in Chapter 5.

Thank you to all of the members of the Wright lab both past and present; Dr Emma Maude Fairhall, Anne Lakey, Philip Probert, Simon Gorman, Dr Stephen Hill, Aimen Aimer, Dr Karen Wallace and Dr Andrew Axon. It has been a lot of fun working with you all and I shall miss the bean bag, the daily cheese and the mountains of cake!

I would also like to say a huge thank you to my family, Ian's family and my friends who have been so supportive. Especially to Ian you have been amazing and I could not have done this without you…….I hope by now you know what a chemokine is (it is not a monkey)!

List of figures

List of tables

List of abbreviations

ABCDE: Asymmetry, Border, Colour, Diameter, Evolving.
a-FGF: Acidic fibroblast growth factor
α-SMA: Alpha smooth muscle actin
aHSC: Activated human stellate cells
AJCC: American Joint Committee on Cancer
ANOVA: Analysis of Variance
BDL: Bile Duct Ligation
BECs: Biliary Epithelial cells
bp: Base pair
BRAF: B-Raf *proto-oncogene serine/threonine-protein kinas*e
BSA: Bovine serum albumin
CBC: Comparative Biology Centre
CCl_4: Carbon tetrachloride
cDNA: Complementary DNA
CFSE: Carboxyfluorescein Diacetate Succinimidyl Ester
CO_2: Carbon dioxide
cT: Cycle threshold
CYP450: Cytochrome P450
DAB: Diaminobenzidine
DAPI: 4',6-diamidino-2-phenylindole
dH_2O: Deionised water
DMEM: Dulbecco's Modified Eagle Media
DMSO: Dimethyl sulphoxide
DOPA: 3,4 di-hydroxyphenylalanine
dsDNA: Double stranded DNA
DPX: Di-N-Butyle Phthalate in Xylene
EBSS: Earle's balanced salt solution
ECM: Extracellular matrix
EDTA: Ethylenediaminetetraacetic acid
EGF: Epidermal growth factor
EGTA: Ethylene glycol tetraacetic acid
ELISA: Enzyme-linked immunosorbent assay

ERB: Electrode running buffer

EtBr: Ethidium Bromide

FCS: Foetal calf serum

FITC: Fluorescein isothiocyanate

FFPE: Formalin-fixed and paraffin-embedded

GAPDH: Glyceraldehyde 3-phosphate dehydrogenase

GFAP: Glial fibrillary acidic protein

HBSS: Hanks Balanced Salt Solution

H_20_2: Hydrogen peroxide

H and E: Haematoxylin and Eosin

HGF: Hepatocyte growth factor

HEPES: (4-(2-hydroxyethyl)-1-piperazineethanesulfonic acid)

HKGS: Human Keratinocyte Growth Serum

HRP: Horse-radish peroxidise

HSC: Hepatic stellate cells

IL-1 Interleukin-1

IL-6 Interleukin-6

I.P: Intraperitoneal injection

I.V: Intravenous injection

ICC: Immunocytochemistry

IgG: Immunoglobulin G

IHC: Immunohistochemistry

IL-6: Interleukin-6

IACUC: Institutional Animal Care and Use Committee

IVIS: In vivo imaging system

KO: Knockout

MAPK: Mitogen-activated protein kinase

MCP-1: Monocyte chemotactic protein-1

mHSCs: Mouse myofibroblasts

M-MLV RT: Moloney Murine Leukemia Virus Reverse Transcriptase

MMPs: Matrix metalloproteinases

MP: Methapyrilene

mRNA: Messenger RNA

MTS: 3-(4,5-dimethylthiazol-2-yl)-5-(3-carboxymethoxyphenyl)-2-(4-sulfophenyl)-2H-tetrazolium

MW: Molecular Weight
NIH: National Institutes of Health
PBC: Primary biliary cirrhosis
PBS: Phosphate buffered saline
PCR: Polymerase Chain Reaction
PMS: Phenazine methosulfate
PSA: Penicillin/streptomycin/fungizone
qHSC: Quiescent human stellate cells
rHSCs: Rat hepatic stellate cells
RPMI: Roswell Park Memorial Institute
qRT-PCR: Quantitative Reverse transcription-polymerase chain reaction
RT-PCR: Reverse transcription-polymerase chain reaction
S.C: subcutaneous injection
SCID: severe combined immunodeficiency
SD: Standard deviation
SDF: Stromal cell-derived factor
SDS-PAGE: Sodium-dodecyl sulphate polyacrylamide gel electrophoresis
TAE: Tris acetate EDTA
TBS: Tris –buffered saline
TBS-T: Tris –buffered saline-Tween
TEMED: Tetramethylethylenediamine
TGF-α: Transforming growth factor-alpha
TGF-β: Transforming growth factor beta
TNF-α: Tumour necrosis factor alpha
UV: ultra-violet
VEGF: Vascular endothelial growth factor

Chapter 1: Introduction

1.0 Introduction

1.1 Malignant melanoma

Malignant melanoma is the most aggressive form of skin cancer, notoriously resistant to current therapeutics and represents a significant and growing public health concern. In the past 30 years, the overall incidence and mortality rates of melanoma worldwide have increased dramatically compared to any other type of cancer and it is now the eighth most common malignancy in the UK (Cancer Research UK). In the UK alone, more than 8,900 people are diagnosed each year, particularly within the 15-34 age group, resulting in more than 2000 deaths annually from malignant disease (Cancer Research UK). It has been suggested that the recent rise in melanoma incidence is associated with early detection, increased awareness, changes in diagnostic criteria and improvements in detection methods (Rajpar and Marsden 2008). However, an increased incidence stills emphasises the acute need for novel treatment strategies and targeted therapies.

1.1.1 The pathogenesis of melanoma

Melanoma arises from the abnormal proliferation of melanocytes; the pigment producing cells located predominantly in the basal layer of the skin. Melanocytes are derived from neural-crest progenitor cells which migrate towards the upper epidermis during embryonic development (Lin and Fisher 2007). The precursors of melanocytes are known as melanoblasts which migrate, proliferate and differentiate in the basal epidermis (Costin and Hearing 2007). Once the melanocytes reach the epidermal-dermal junction they become fully differentiated and the melanosomes (lysome-like granules present in the melanocytes) are then able to produce melanin (Boissy 2003).

Melanosomes are responsible for producing both types of melanin; eumelanin (black/brown in colour and is an insoluble polymer) and pheomelanin (light red/yellow colour sulphur containing polymer) (Boissy 2003). Eumelanin and pheomelanin are derivatives of 3,4 di-hydroxyphenylalanine (DOPA) and are synthesized in the melanosomes by a number of oxidative steps via the tyrosine-dependent pathway (Costin and Hearing 2007). The pivotal step in this pathway is the hydroxylation of tyrosine (a glycoprotein) to dopaquine because this is the

stage at which the eumelanin and pheomelanin pathways separate (Land and Riley 2000). Once melanin is synthesized and packaged it is transported from the melanocytes to the neighbouring keratinocytes, hence, most pigmentation is located in these cells (Lin and Fisher 2007). The main function of melanin is to protect the skin from ultra-violet (UV) induced DNA damage and it achieves this by absorbing and scattering UV radiation and by stimulating pigmentation (Lin and Fisher 2007).

Malignancy develops when melanocytes become transformed by genetic and/or environmental factors with the greatest environmental risk factor being acute intermittent exposure to non-ionizing radiation in sunlight, in particular the UVB wavelengths (280-320nm) (De Fabo, Noonan et al. 2004). Indeed, it has been estimated that this factor accounts for the development of approximately 80-90% of all melanoma tumours (Knowles and Selby 2005). Furthermore, an increased incidence is apparent in individuals with pale skin, multiple atypical naevi, a previous family history and those who use sun beds, for which there is an even greater risk of developing metastatic disease (Thompson, Scolyer et al. 2005)

1.1.2 Characteristics and prognosis of melanoma

Melanoma is divided into four main groups; nodular, lentigo maligna, acral lentiginous and superficial spreading (Rajpar and Marsden 2008) whereby superficial spreading accounts for the majority of melanoma cases and is usually associated with episodes of severe sunburn (Rajpar and Marsden 2008).

The simplest method for screening melanoma involves visual inspection where diagnosis is based upon the morphological features of the mole or lesion (Rajpar and Marsden 2008) . At present, the ABCDE criterion is the simplest method for carrying out this process and thus, determining whether the mole is likely to be benign or malignant (Rajpar and Marsden 2008). For example, typical features of a malignant mole include whether it is asymmetrical, has an irregular border, variable pigmentation and if it is >6mm in size (Figure 1.1) (Rajpar and Marsden 2008). More definitive staging systems for melanoma include the Breslow thickness and the Clark level. The Breslow thickness measures the height from the granular layer to the maximum depth of invasion whereas the Clark level measures the extent of dermal penetration (Breslow 1970). Currently, the

American Joint Committee on Cancer (AJCC) is the most widely used system, based upon Breslow thickness and Clark level as well as ulceration and the degree of metastasis (Balch, Gershenwald et al. 2009). This staging system has recently been revised to include additional features of mitotic rate but with the removal of Clarks level from stage I patients (Balch, Gershenwald et al. 2009). Furthermore, it incorporates the number of lymph nodes involved and the presence or absence of micro or macro metastases (Balch, Gershenwald et al. 2009).

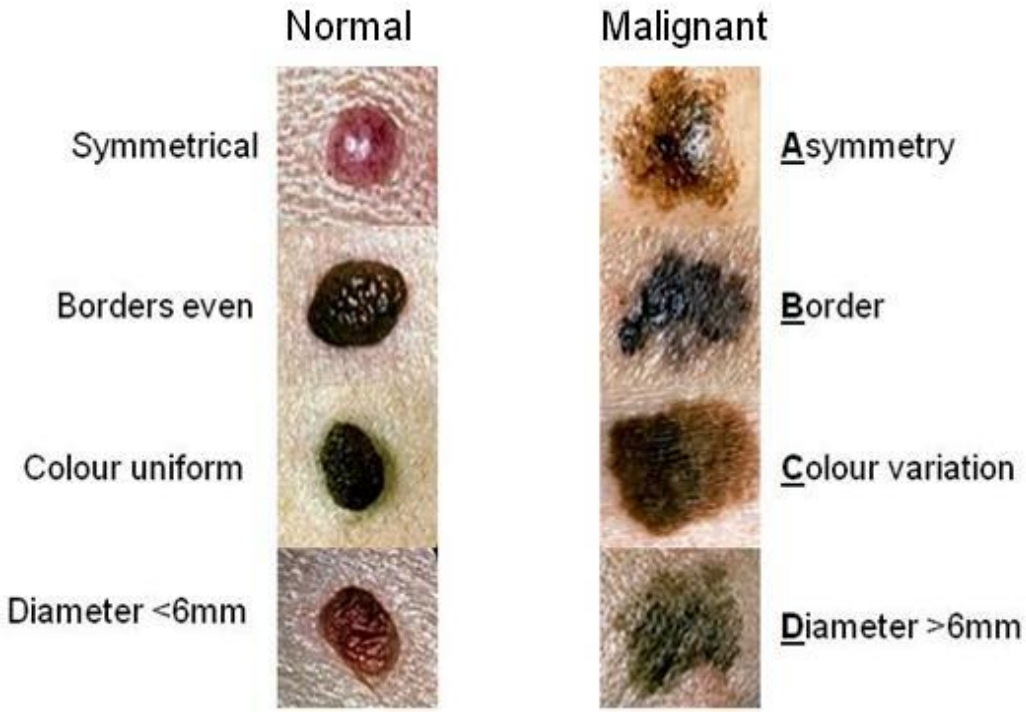

Figure 1.1: The ABCDE criterion
The ABCDE criterion for determining the diagnosis of cutaneous pigmented tumours (Rajpar and Marsden 2008).

Prognosis for melanoma patients appears to be directly related to disease stage in that early stage disease is usually treatable through surgical excision alone, resulting in 5 year survival rates of more than 95% (Scala, Ottaiano et al. 2005). However, in approximately a third of all cases distant metastasis occurs and for these patients outlook is extremely poor (Leiter, Meier et al. 2004). Indeed, median survival rarely exceeds 9 months with less than 10% of patients surviving for more than 10 years (Table 1.1) thus, novel therapeutics for these patients are urgently needed (Thompson, Scolyer et al. 2005).

Stage	5-year survival	10-year survival
Stage I (primary tumour <1mm)	93%	85%
Stage II (primary tumour > 1mm)	68%	55%
Stage III (regional metastasis)	45%	36%
Stage IV (systemic metastasis)	11%	6%

Table 1:1 Stages of melanoma and predicted survival rates (Thompson, Scolyer et al. 2005) Estimated survival rates (5 and 10 year) for stages of melanoma in patients, graded by the AJCC staging system 2001.

1.1.3 Current treatment of melanoma

Current treatment options remain limited for patients with metastatic disease, with dacarbazine largely remaining the agent of choice, however, response rates to this treatment are estimated at only 10-25% (Atallah and Flaherty 2005 (Atallah and Flaherty 2005). Furthermore, it has been observed *in vivo* that administration of this agent may even promote both metastatic potential and tumourigenic properties (Lev, Onn et al. 2004). Moreover, despite the combination of dacarbazine with other chemotherapeutic agents or the use of its related analogue, temozolomide, few patients rarely respond beyond 6 months (Ugurel and Schadendorf 2003). Poor survival rates are associated to the increased resistance of tumours to apoptosis (Ugurel and Schadendorf 2003). This is supported by *in vitro* studies where lower levels of spontaneous apoptosis have been observed when melanoma cells have been treated with various chemotherapeutics (Ugurel and Schadendorf 2003). However, a breakthrough in the development of melanoma treatment occurred in 2002 when it was discovered that approximately 50-70% of melanomas harbour B-RAF mutations (Davies, Bignell et al. 2002).

1.1.4 BRAF signalling in melanoma

BRAF is a serine/threonine protein kinase belonging to the Raf family which activates the mitogen-activated protein kinase (MAPK) signalling pathway (Davies, Bignell et al. 2002) (Figure 1.2). This pathway is known to regulate cell proliferation, survival and differentiation and is activated by a wide range of membrane-bound receptors, for example, the receptor tyrosine kinases and G-

protein coupled receptors (Davies, Bignell et al. 2002). BRAF is frequently mutated in melanoma resulting in constitutive activation of RAS-RAF-ERK signalling, the consequence of which is enhanced cell survival and resistance to apoptosis (Davies, Bignell et al. 2002). Among the BRAF mutations over 90% are associated in a single nucleotide mutation leading to a substitution of valine to glutamic acid at position 600 (^{V600E}BRAF) (Davies, Bignell et al. 2002).

Interestingly, it has been found that ^{V600E}BRAF plays important roles in the initial steps of melanoma and also in the development of metastasis (Davies, Bignell et al. 2002). Subsequently, this has led to the development of therapeutics which interrupt the BRAF signalling pathway. One of the first inhibitors to be developed was sorafenib a tyrosine and serine-threonine kinase inhibitor. Unfortunately, although it has been tested in many phase I, II and III studies, alone and in combination with other chemotherapeutics, no significant clinical benefit has been observed (Eisen, Ahmad et al. 2006, Amaravadi, Schuchter et al. 2009, Hauschild, Agarwala et al. 2009, Margolin, Moon et al. 2012).

Recently, however, more selective and potent BRAF inhibitors have been developed including vemurafenib and dabrafenib (Flaherty, Puzanov et al. 2010, Falchook, Long et al. 2012). Studies have demonstrated that treatment with these agents results in a reduction of pERK in tumour cells harbouring the BRAF^{V600E} mutation which correlates with clinical response (Bollag, Hirth et al. 2010, Joseph, Pratilas et al. 2010) Randomized trials have now been performed demonstrating that both of these BRAF inhibitors are more effective compared to the standard treatment of dacarbazine (Chapman, Hauschild et al. 2011, Falchook, Long et al. 2012). However, in BRAF wild-type melanoma cells, the MAPK pathway by vemurafenib is maintained promoting proliferation (Halaban, Zhang et al. 2010, Hatzivassiliou, Song et al. 2010) and it is thought that this opposing effect is CRAF dependent (Hatzivassiliou, Song et al. 2010). Furthermore, in many patients, acquired vemurafenib resistance occurs typically 6-8 months after treatment is initiated (Sullivan and Flaherty 2013). Therefore, other strategies are also being investigated, for example the inhibition of downstream targets including MEK (Adjei, Cohen et al. 2008, Banerji, Camidge et al. 2010, LoRusso, Krishnamurthi et al. 2010). However, as yet, the clinical efficacy of the MEK inhibitors have not been as successful as the BRAF selective

inhibitors and melanoma metastasis still remains a major challenge (Fisher and Larkin 2012).

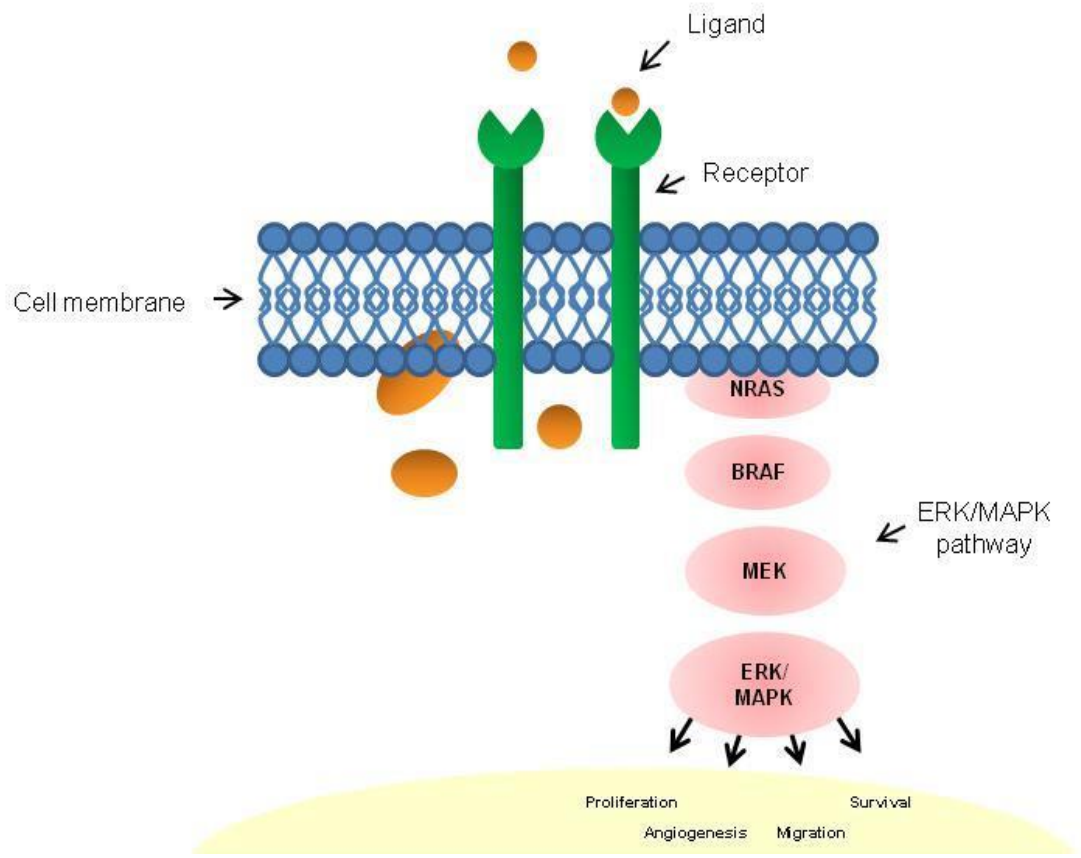

Figure 1.2: A schematic figure of the BRAF signalling pathway adapted from Chiloeches et al (Chiloeches and Marais 2006).
ERK/MAPK signalling promotes proliferation, angiogenesis, migration and cell survival.

1.2 Cancer metastasis

Cancer metastasis occurs when tumour cells from the primary site escape and spread to distant tissues subsequently forming secondary tumours (Zlotnik, Burkhardt et al. 2011). Initially, cancer cells with a metastatic phenotype disseminate from the primary tumour growth through an environment of extracellular and stromal cells, these cells then invade into blood vessels circulating into the bloodstream and then migrate out towards distant tissues (Chambers, Groom et al. 2002). The process of metastasis is complex but can be summarised into a number of sequential steps; local invasion, intravasation, circulation, arrest and extravasation, proliferation and angiogenesis (Knowles and Selby 2005).

For many years it has been thought that metastasis is not a random process but one that occurs in an organ-selective and highly organized manner. In 1889, Paget proposed the 'seed and soil' hypothesis in which he described the tumour cells as being the 'seeds' and the organs being the 'soil', hence, the cells from the tumour would have high affinity for those organs that would support and nurture them (Paget 1989). Later Ewing, developed his 'mechanical' hypothesis which was based upon his observation that patterns of blood flow from the primary tumour were similar to the patterns of metastasis (Ewing 1928). This meant that the blood flow would carry the greatest metastatic tumour to the first organ it encountered (Ewing 1928). Both of these models lead to the more recent concept of the 'homing mechanism' and a good example of this is during cancer development. Indeed, it has been postulated that cancer cells expressing chemokine receptors facilitate metastasis to specific organs such as the liver by directing the cells to locations that secrete the corresponding chemokines (Zlotnik, Burkhardt et al. 2011).

1.3 Chemokines and chemokine receptors

Chemokines are a family of small chemo-attractant cytokine-like secretory proteins (8-12kDa) that exert their effects by binding to and activating G-protein-coupled seven-span transmembrane (GPCRs 7TM) receptors. These receptors have their N terminus outside the cell surface, three extracellular, and three intracellular loops including a C terminus containing serine and threonine phosphorylation sites in the cytoplasm as illustrated by Figure 1.4. To date, approximately 50 chemokines and at least 20 corresponding receptors have been identified (Zlotnik and Yoshie 2000, Bacon, Baggiolini et al. 2002, Balkwill 2004, Zlotnik, Yoshie et al. 2006). Chemokine receptors exhibit a DRY motif in the second intracellular loop which is mainly responsible for signalling. Upon chemokine binding, conformational changes trigger a number of downstream effectors which can lead to internalization of the receptor and signal transduction (Teicher and Fricker 2010). Subsequently, integrin activation promotes adhesion of cells and polarization of the actin cytoskeleton which can then induce both cell activation and movement (Teicher and Fricker 2010).

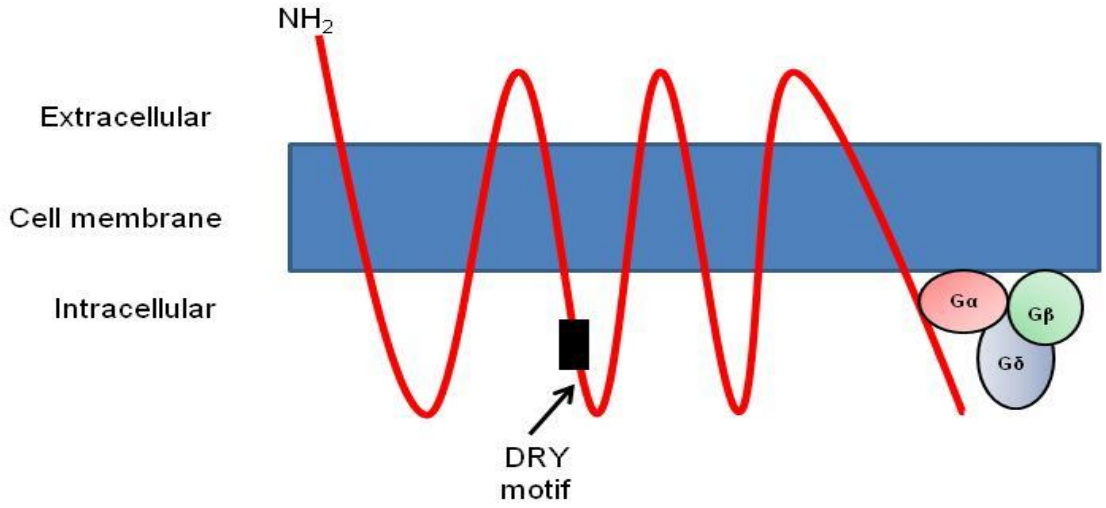

Figure 1.3: Schematic figure of a chemokine receptor.
Chemokine receptors have their N terminus outside the cell surface, three extracellular, and three intracellular loops including a C terminus containing serine and threonine phosphorylation sites in the cytoplasm.

Classification of the chemokines and their receptors is based upon the position and number of the conserved cysteine residues near the N terminus of these proteins (Baggiolini, Dewald et al. 1997, Luster 1998). The cysteine residues in the receptor proteins are essential in forming the disulphide bonds with internal cysteines which in turn provides the highly conserved tertiary structure. To date, four highly conserved families have been identified; CXC, CXC3C, CC and C with CC and CXC families containing the majority of the chemokines. In general, CC chemokines bind to CC chemokine receptors and CXC ligands bind to CXC receptors. The chemokines and their receptors are generally referred to by their systematic names, starting by the family name followed by either 'L' for ligand or 'R' for receptor and then a number which indicates the order of their identification. The 'X' denotes single non-conserved amino acids located between cysteine residues, for example, the CXC subfamily contains a single non-conserved amino acid. This family is further divided depending upon the presence or absence of an additional conserved amino acid motif, Glu-Leu-Arg which has specific functional properties for angiogenesis. Another common feature for most chemokines is that they have a heparin-binding domain which is predominantly composed of residues in an α-helical region close to the C terminus. This feature allows the binding of chemokines in the blood to glycosaminoglycans that are present on endothelial cells (Frederick and Clayman 2001).

The majority of chemokines bind to multiple receptors, and the same receptor often binds to more than one chemokine suggesting redundancy (Schall and Proudfoot 2011) in the chemokine network as shown in Figure 1.4 (Balkwill 2004). For example, the chemokine CCL7 has the ability to bind to at least four receptors; CCR1, CCR2, CCR3 and CCR5 (Pease and Horuk 2009) . This redundancy is supported by *in vivo* studies whereby chemokines and their receptors have been genetically deleted but minor differences have been observed (Teicher and Fricker 2010). However, exceptions for this do exist, for example, CXCR4 null mutation mice are embryonic lethal (Nagasawa, Hirota et al. 1996, Onai, Zhang et al. 2000). Finally, most chemokines are further sub-grouped into homeostatic or inflammatory chemokines depending upon their expression and function (Zlotnik, Burkhardt et al. 2011). Overall, the chemokines play diverse roles in a wide range of physiological processes including inflammation, organogenesis, embryogenesis, immune system development and cancer metastasis (Gale and McColl 1999, Rossi and Zlotnik 2000, Gerard and Rollins 2001).

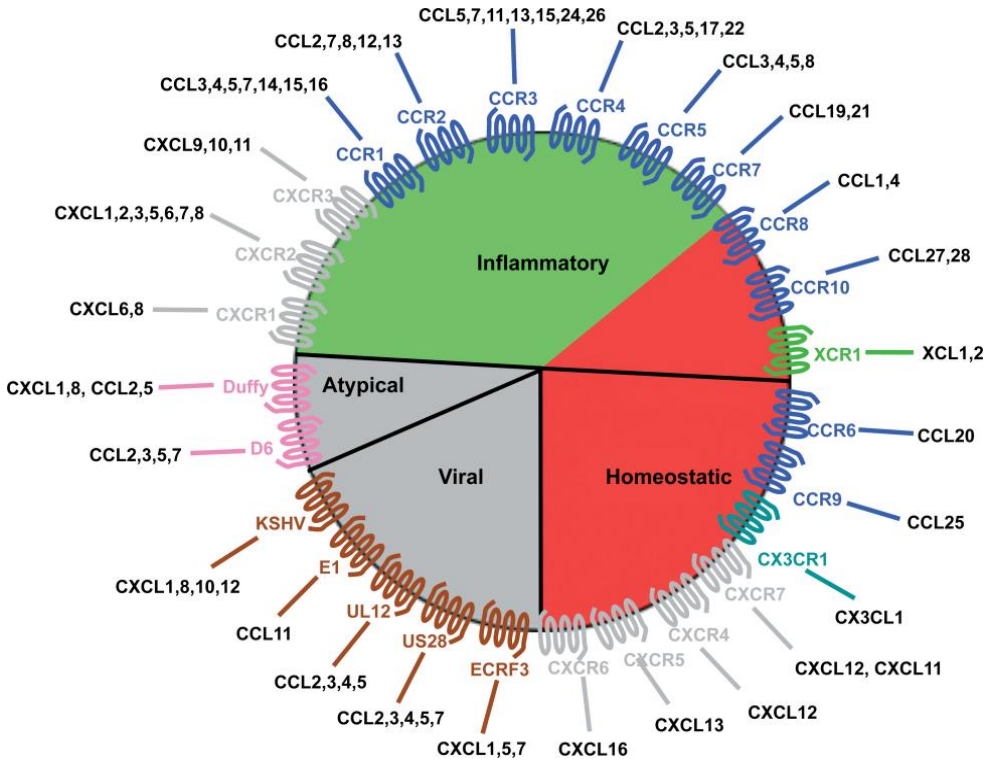

Figure 1.4: The chemokine system (Balkwill 2004)
Illustrates the G-protein-coupled cell-surface receptors and the chemokine ligands grouped into inflammatory, homeostatic, viral and atypical.

1.3.1 Functions of the chemokines

The homeostatic chemokines are constitutively expressed and are mainly involved in leukocyte trafficking whereas the inflammatory chemokines are secreted by circulating leukocytes and other cells in response to inflammatory stimuli (Zlotnik, Burkhardt et al. 2011).

1.3.1.1 Inflammation

Chemokines and their receptors were initially identified as being important for leukocyte trafficking where chemokine gradients were shown to regulate leukocyte migration towards sites of inflammation, infection and tissue injury. For example, during inflammation innate immune cells such as neutrophils expressing CXCR2 migrate in response to the CXCL8 from the site of injury/inflammation (Newton, O'Boyle et al. 2009). Later in the immune response, other inflammatory chemokines including CXCL11 are secreted to direct the migration of lymphocytes expressing CXCR3 into the inflamed tissue (Newton, O'Boyle et al. 2009).

1.3.1.2 Organogenesis

In organogenesis, the chemokines guide the migration of stem cells to areas where an organ or limb is going to develop and then promote angiogenesis to supply both oxygen and nutrients (Doitsidou, Reichman-Fried et al. 2002). They then retain the stem cells in a niche until they are needed to produce progeny cells and assist in providing cellular framework (Steinberg and Silva 2010). For instance, in the developing zebra fish embryo the chemokine receptor CXCR4 directs gonadal stem cells and also neuronal precursors to specific parts of the developing brain (Raz and Mahabaleshwar 2009).

1.3.1.3 Angiogenesis

Another role for the chemokines is in angiogenesis, the process which forms new blood vessels from existing vessels and micro capillaries. This is essential during embryonic development and wound healing and in the context of cancer, facilitates tumour growth once a tumour reaches a certain size (Folkman, Watson et al. 1989, Folkman 2002). Furthermore, angiogenesis not only promotes growth but also plays a role in tumour cell dissemination (Knowles and Selby 2005). Indeed, studies have shown that there is a correlation between blood vessel

density and an increased incidence of metastasis (Todorovic, Radisavljevic et al. 2012, Syed Khaja, Dizeyi et al. 2013).

The first chemokine identified to be involved in angiogenesis was CXCL8 where it was shown to promote migration and proliferation of endothelial cells and angiogenesis *in vivo* (Belperio, Keane et al. 2000). Increased levels of this chemokine have also been observed in various tumours, including head and neck squamous cell carcinoma (Jo, Wang et al. 2013) metastatic melanoma (Singh, Singh et al. 2010) and colon carcinoma (Verbeke, De Hertogh et al. 2010) and elevated levels have also been detected in breast cancer (Bieche, Chavey et al. 2007, Chavey, Bibeau et al. 2007). Interestingly, chemokines containing the ELR motif for example, CXCL5, CXCL6, CXCL7 and CXCL8 stimulate angiogenesis where as those without this motif such as CXCL10 inhibit this process (Belperio, Keane et al. 2000). However, there is one chemokine that does not follow this rule and that is CXCL12 which despite having an ELR motif has shown to be pro-angiogenic (Kryczek, Wei et al. 2007).

1.3.1.4 Liver fibrosis

In most cases of liver injury, chemokines and chemokine receptors are up regulated leading to the infiltration of immune cells as recently reviewed by Saiman (Saiman and Friedman 2012). The main liver cells which have been identified in secreting chemokines include the hepatocytes, Kupffer cells, stellate cells, sinusoidal endothelial cells and the biliary epithelial cells (Saiman and Friedman 2012).

One of the most studied chemokines involved in liver injury is CCL2 which is known to recruit monocytes and macrophages to areas of damage via the chemokine receptor CCR2 (Hokeness, Deweerd et al. 2007). Furthermore, murine models of acute liver injury and in patients with hepatic failure, CCL2 has shown to be increased (Possamai, Antoniades et al. 2010). The CXCL9-11 chemokines have also shown to play a role in the immune response by promoting the migration of T cells upon binding to CXCR3 (Saiman and Friedman 2012). Supporting this, a study in patients with chronic liver disease showed that CXCR3 and its ligands increased and furthermore there was a correlation between levels with disease status (Apolinario, Majano et al. 2002). The chemokines CXCL1,

CXCL2 and CXCL8 which are known to bind to CXCR1/CXCR2 have shown to play a role in neutrophil infiltration during acute liver injury. Furthermore, studies have shown that in patients with alcoholic hepatitis (James, Farrar et al. 2001) and after post-liver transplantation CXCL8 levels increase (Ilmakunnas, Hockerstedt et al. 2010). Another chemokine which has shown to be induced during liver disease is CCL5 which induces the migration of a wide range of cells during the immune response including T cells, dendritic cells, eosinophils, NK cells, mast cells and basophils (Affo and Bataller 2011).

Thus, the development of small molecule inhibitors for treating liver disease may be beneficial. Although, caution will have to be taken since some chemokines and their receptors may also serve to protect the liver from fibrotic injury such as CXCR3 which has shown to promote hepatocyte survival (Saiman and Friedman 2012).

1.3.1.5 Cancer progression and metastasis

More recent studies have emerged demonstrating that chemokines and their receptors play a pivotal role in cancer metastasis and this has been reviewed extensively (Balkwill 2004, Balkwill 2012). These studies have shown that chemotaxis promotes metastasis by directing chemokine receptor positive tumour cells to organ specific sites that actively secrete the corresponding ligand (Balkwill 2004, Ali and Lazennec 2007, Amersi, Terando et al. 2008, Gao, Wang et al. 2010, Teicher and Fricker 2010, Zlotnik, Burkhardt et al. 2011, Balkwill 2012). Indeed, the chemokines have recently been described as ‘traffic directors’ whereby they guide cells to specific areas (Zlotnik, Burkhardt et al. 2011). Although this process is required for normal tissue homeostasis, in the context of cancer this system is ‘hijacked’ resulting in the promotion of tumour growth and metastasis (Figure 1.5) (Zlotnik, Burkhardt et al. 2011). Furthermore, it has been suggested that chemokines secreted by the tumour and stromal cells are likely to participate in the survival and proliferation of the tumour cells via autocrine loops and paracrine effects (Scotton, Wilson et al. 2002, Barbero, Bonavia et al. 2003, Sun, Wang et al. 2003, Balkwill 2004, Balkwill 2012). The CXCR4-CXCL12 chemokine axis is the most commonly studied chemokine axis involved in this process.

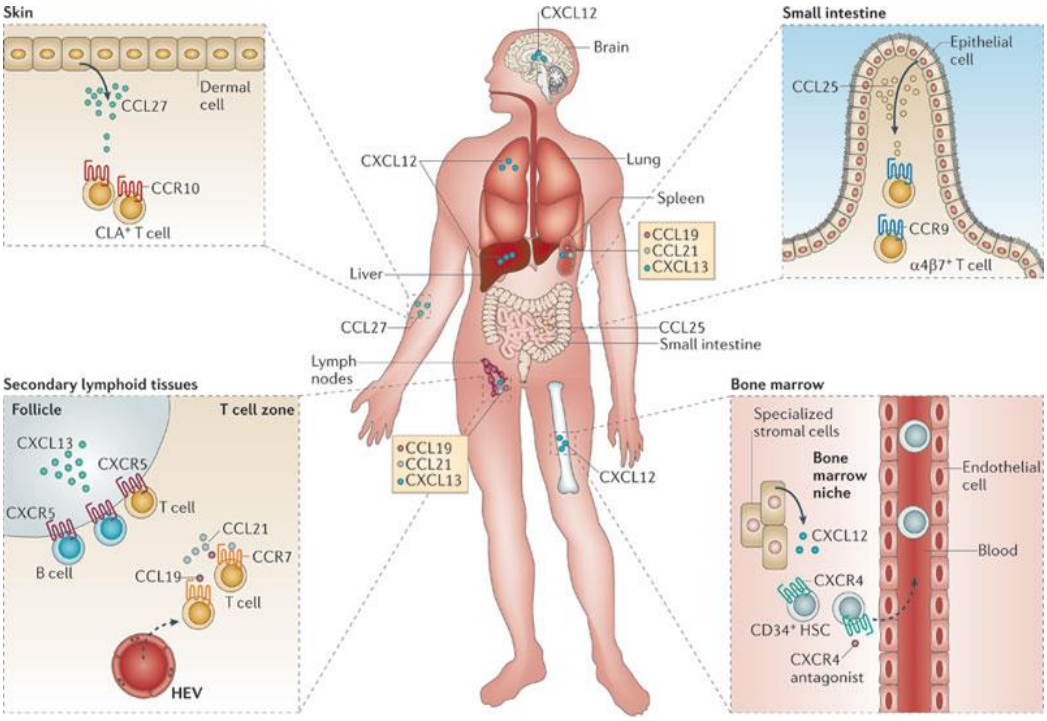

Figure 1.5: The human body contains 'cellular highways' through which cells travel to reach different sites or organs in the body (Zlotnik, Burkhardt et al. 2011). Cancer cells expressing chemokine receptors facilitate metastasis to specific organs which secrete the corresponding chemokines.

1.4 The CXCR4-CXCL12 chemokine axis

In normal physiology, the CXCR4-CXCL12 chemokine axis plays a pivotal role in the retention and homing of hematopoietic stem cells in the bone marrow and also for lymphocyte trafficking (Teicher and Fricker 2010). Indeed, studies of CXCR4 and CXCL12 gene knockout mice have shown that this chemokine axis is critical for embryonic haematopoiesis, organogenesis and vascularisation (Ratajczak, Zuba-Surma et al. 2006) (Nagasawa, Hirota et al. 1996).

1.4.1 CXCR4

CXCR4 is a 352-amino acid rhodopsin-like highly conserved GPCR which was first discovered to act as a co-receptor for entry of T-tropic (X4) HIV viruses that targeted CD4+ T cells (Feng, Broder et al. 1996). During development, CXCR4 is known to be expressed on a wide range of tissues for example, in the immune and central nervous system (Teicher and Fricker 2010). In addition, it is expressed in a wide range of tissues including the brain, lung, colon, heart, kidney and the liver (Teicher and Fricker 2010). It is also known to be expressed on a variety of cell types including lymphocytes, hematopoietic stem cells, monocytes,

eosinophils, endothelial and epithelial cells (Teicher and Fricker 2010). CXCR4 has also been shown to be expressed on embryonic pluripotent stem cells in neural tissue, skeletal muscle and in the heart and liver (Teicher and Fricker 2010). Furthermore, various factors have been reported to regulate the expression of CXCR4 such as cytokines including transforming growth factor beta (TGF-β) and tumour necrosis factor alpha (TNF-α), bacterial glycoproteins, vascular endothelial growth factor (VEGF) and also hypoxia (Schioppa, Uranchimeg et al. 2003, Franco, Botti et al. 2010, Teicher and Fricker 2010, Chu, Sheen et al. 2013).

1.4.2 CXCR7

Recently, another receptor has been identified that binds to CXCL12, known as CXCR7 (Balabanian, Lagane et al. 2005, Burns, Summers et al. 2006). CXCR7 is expressed by various cell types including endothelial cells, fetal liver cells and also on some tumour cell lines (Balabanian, Lagane et al. 2005). It was previously reported that unlike CXCR4, CXCR7 did not activate G-protein signalling and was thought not to be involved in migration but to act as a 'decoy' receptor by competing for CXCL12 binding (Balabanian, Lagane et al. 2005). Thus, functioning by scavenging and degrading CXCL12 (Naumann, Cameroni et al. 2010). However, more recently, it has been suggested that CXCR7 is able to form a co-receptor (heterodimerizes) with CXCR4 leading to downstream signalling upon the binding of CXCL12 (Levoye, Balabanian et al. 2009).

1.4.3 CXCL12

CXCL12 previously known as SDF (stromal cell-derived factor) is a homeostatic chemokine and is the only known ligand to bind to CXCR4 (Murphy, Baggiolini et al. 2000). It exists primarily as two isoforms from the same gene; α and β although more recently, four other human isoforms of CXCL12 have been identified; CXCL12-γ (gamma), CXCL12-δ (delta), CXCL12-ε (epsilon) and CXCL12-φ (phi) (Yu, Cecil et al. 2006). Overall, the most commonly expressed isoform known is CXCL12-α (Yu, Cecil et al. 2006). This isoform has found to be expressed in several organs such as the skin, kidney, brain and liver (Teicher and Fricker 2010). Furthermore, the secretion of CXCL12 has been linked to tissue damage caused by various factors including; excessive bleeding, total body irradiation, chemotherapy and toxic liver damage (Teicher and Fricker

2010). It has been suggested that CXCL12 may promote cell survival by both post-translationally suppressing the cell death mechanisms and also by promoting transcription of genes associated with cell survival (Teicher and Fricker 2010).

The binding of CXCL12 to CXCR4 forms a complex with the Gαi subunit G protein, which leads to inhibition of adenyl cyclase-mediated cyclic adenosine monophosphte and initiates the activation of a number of downstream pathways including ERK 1/2, MAPK, JNK and AKT (Figure 1.6) (Teicher and Fricker 2010). Common responses to these key signalling pathways include; cell survival and/or proliferation, an increase in intracellular calcium, gene transcription and chemotaxis as illustrated in Figure 1.6 (Teicher and Fricker 2010). The Gα subunits consist of four families; Gαs, Gαi, Gαq, and Gα2 and each of these transmits the GPCR signal via alternate routes (Teicher and Fricker 2010). However, it should be noted that the pathways involved may depend upon both the tissue and cell type.

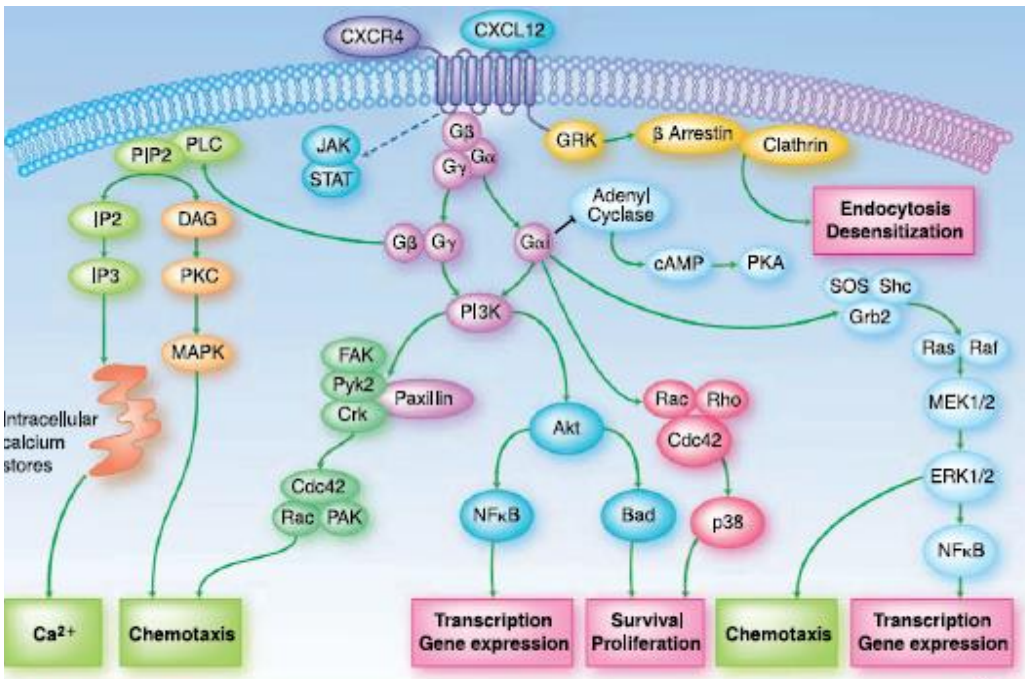

Figure 1.6: Signalling pathways involved in the CXCR4-CXCL12 chemokine axis(Teicher and Fricker 2010).

1.4.4 CXCR4-CXCL12 chemokine axis in cancer

A growing body of evidence has suggested that the CXCR4-CXCL12 chemokine axis is involved in the regulation of tumour growth/progression, angiogenesis, neovascularisation, invasion and metastasis (Smith, Luker et al. 2004, Balabanian, Lagane et al. 2005, Zhang, Somasundaram et al. 2005, Kim, Mori et al. 2006, Ali and Lazennec 2007, De Falco, Guarino et al. 2007, Otsuka and Bebb 2008, Bartolome, Ferreiro et al. 2009, Teicher and Fricker 2010, Sakai, Yoshidome et al. 2012). In a landmark study by Muller et al (Muller, Homey et al. 2001) it was discovered that in breast cancer, cells use chemokine receptors to migrate towards common sites of metastasis such as the lung (Muller, Homey et al. 2001). It was also demonstrated that in these cancer cells, expression levels of CXCR4 was higher compared to normal breast cancer tissue suggesting that CXCR4 was a marker of poor prognosis (Muller, Homey et al. 2001). Furthermore, *in vivo* studies showed that neutralizing the CXCR4-CXCL12 axis prevented metastasis of breast cancer cells to the lymph nodes and lung (Muller, Homey et al. 2001). Later studies by Liang and co-workers demonstrated that knocking down the expression of the CXCR4 receptor by siRNAs, breast cancer cell invasion *in vitro* was reduced and *in vivo* metastasis was inhibited (Liang, Yoon et al. 2005). Studies in lung cancer showed that in small lung cancer cells levels of CXCR4 were greater compared to normal tissue and furthermore, that activation of the receptor caused both migratory and invasive responses (Burger, Glodek et al. 2003). Supporting this, a study reported that high expression of CXCR4 in small lung cancer cells correlated with an increased risk of cancer metastases, suggesting that migration of cells to secondary sites was influenced by the receptor expression levels (Su, Zhang et al. 2005). A study in pancreatic adenocarcinoma, demonstrated that pancreatic cell conditioned media rich in CXCL12 promoted the proliferation, migration and invasion of pancreatic cancer cells (Gao, Wang et al. 2010).

In the context of melanoma, studies have shown that inhibition of the CXCR4-CXCL12 chemokine axis reduces melanoma to organs secreting CXCL12 such as the lungs (D'Alterio, Barbieri et al. 2012, Takekoshi, Ziarek et al. 2012). For example, in one study, mouse melanoma B16 cells (+/- AMD3100) were injected into the tail vein of wild type ($CXCR4^{+/+}$) and heterozygote ($CXCR4^{+/-}$) mice (D'Alterio, Barbieri et al. 2012). The results demonstrated that tumours were

observed in both types of mice; however, metastasis was reduced in the $CXCR4^{+/-}$ mice. In another study by Kim et al, they found that lymphatic vessels in metastatic tissues promoted CXCR4+/CD133+ cell metastasis to organs secreting CXCL12 (Kim, Koh et al. 2010). Previous clinical studies have also shown that increased expression of CXCR4 is correlated with poor prognosis, for example, in uveal melanoma (Franco, Botti et al. 2010). Supporting this, in primary cutaneous melanoma, a correlation between over-expression of CXCR4 with survival and prognosis has been observed (Kuhnelt-Leddihn, Muller et al. 2012)

Collectively, these studies have led to the development of small molecular inhibitors some of which have already been tested and used in the clinic and offer promise as a therapeutic modality. For example, the CXCR4 antagonists AMD3100 and the more recent development of AMD11070 have shown some promising results.

1.4.5 AMD3100 and AMD11070

AMD3100 is a small molecule inhibitor containing two cyclam rings connected by a phenylene linker (Fricker, Anastassov et al. 2006). In the presence of physiological pH, two nitrogens are protonated allowing charge-charge interactions with the carboxylate groups on the CXCR4 receptor, inhibiting the binding of CXCL12 and preventing downstream signalling (Fricker, Anastassov et al. 2006). Initially, it was identified as a highly selective inhibitor of HIV-1 and HIV-2 replication (Fricker, Anastassov et al. 2006). It is now used in patients with non-Hodgkin's lymphoma and multiple myeloma where it mobilises haematopoietic stem cells to the peripheral blood and is also used for autologous transplantation (Flomenberg, Comenzo et al. 2010). In the context of melanoma, experimental studies have shown that AMD3100 inhibits metastasis of these tumour cells to sites that secrete high levels of CXCL12 such as the lungs (Scala, Giuliano et al. 2006, D'Alterio, Barbieri et al. 2012, Takekoshi, Ziarek et al. 2012). However, AMD3100 exhibits poor bioavailability and has shown to cause adverse side effects, for example, the induction of fibrosis (Saiman 2012) and therefore has limited the potential of this inhibitor in cancers such as melanoma.

The novel CXCR4 inhibitor AMD11070 is a small non-cyclam which functions and binds with a similar mode of action to AMD3100 but with more favourable pharmacokinetic properties, for example, it is more stable within the cell (Mosi, Anastassova et al. 2012). When AMD11070 is administered (in fasted healthy individuals) plasma concentrations achieved at the maximum dose given (400mg/kg^{-1}) reach approximately 2µg/ml (6.6µM) (Stone, Dunaway et al. 2007). Furthermore, the Cmax occurs within 1-2 hours of oral dosing are sustained for longer. To date, AMD11070 has only demonstrated efficacy for HIV infection in which *in vitro* studies demonstrate its ability to inhibit replication of X4-tropic HIV (Moyle, DeJesus et al. 2009). However, given that it is more potent and has more sustainable properties, AMD11070 may prove valuable in the setting of a wide range of cancers including melanoma metastasis to the liver.

AMD3100

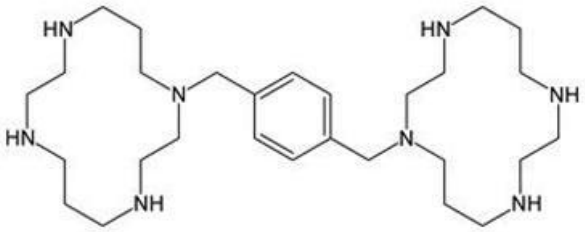

AMD11070

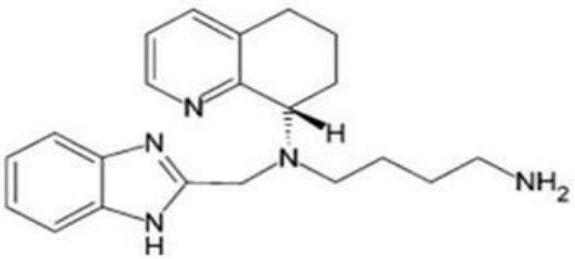

Figure 1.7: The chemical structure of AMD3100 and AMD11070.

1.5 Anatomy of the liver

The liver is the largest internal organ in the body which in adults weighs approximately 1.5kg, contributing up to 2.5% of the total body weight (Wallace, Burt et al. 2008). The liver is positioned in the right hypochondriac region of the abdominal cavity beneath the diaphragm and is situated to the right of the stomach. Apart from one area which is connected to the diaphragm, the liver is encased by the Glisson; a thin, double membrane capsule which helps to prevent friction against neighbouring organs and also serves to protect the hepatic blood vessels and bile duct. The liver is divided by the flaciform ligament and traditionally was designated four functional lobes; the left, right caudate and quadrate. More recently, it has been suggested that the liver can actually be divided into nine segments by the vascular and ductal branching patterns present on the left and right sides (MacSween 2002). These lobes are composed of lobules with a vein in the centre that passes through to connect to the hepatic vein in order to transport blood out of the liver. Additionally, there are many ducts, veins, arteries on the surface to allow materials to flow in and out.

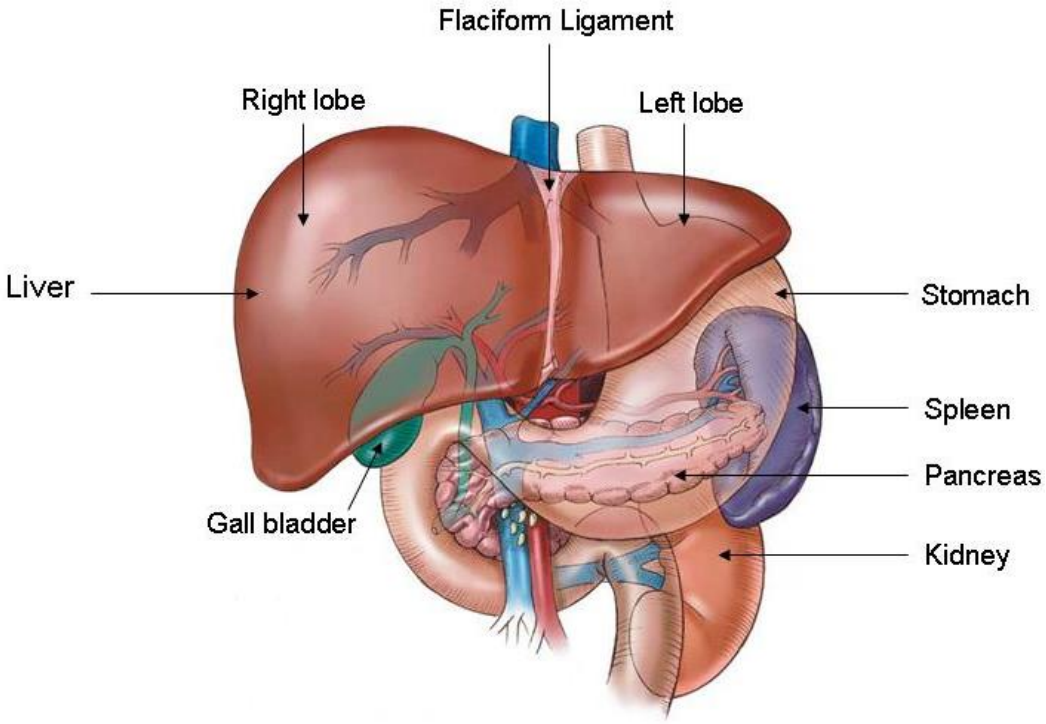

Figure 1.8: The anatomy of the liver.

The liver exhibits high metabolic activity and therefore requires an efficient blood supply. This is achieved by a dual blood supply; approximately one third of the blood is supplied by the hepatic-artery and the rest is received from the portal vein. The hepatic artery is a branch of the coeliac axis and the portal vein is composed of the superior mesenteric and splenic veins. The hepatic artery transports blood from the aorta, whereas the portal vein carries blood rich in nutrients from the gastrointestinal tract, spleen and pancreas. The two blood inputs are admixed within the sinusoids which are essentially the liver's capillaries which allow the exchange of materials from the space of Dissé to the hepatocytes and the endothelial cells. Blood travels through the sinusoids and into each lobule via the central veins. The exact volume from each blood source can vary considerably, for example, in cirrhosis, the volume received from the hepatic artery increases dramatically due to portal-systemic shunting of the venous blood (MacSween 2002).

1.5.1 Functional units

The liver exhibits a unique architecture of a number of functional units that contain specific cell types arranged around the portal and central veins where the blood enters and exits respectively. It is estimated that there are 1.0-1.5 million lobules in the liver which are not cylindrical or prismatic but hexagonal in shape and exhibit extensive branching which allows them each to have their own blood supply (Wallace, Burt et al. 2008). As there are no impermeable barriers between the liver units in either humans and rodents the actual structure of the liver has been debated.

Weppler was the first to describe the lobular architecture of the liver and following this many other models have been proposed; the portal lobule, the acinus and the primary lobule being the most commonly used. Kiernan described the classic hexagonal lobule structure with Mall later proposing the portal lobule model. The portal lobule describes the six portal tracts arranged around a central vein where it supplies the lobule and drains at the periphery. Rappaport later proposed the liver acinus, a smaller functional unit, separated into three zones. Zone 1 (periportal zone) and zone 2 (intermediate zone) being the nearest to the portal tract and central vein respectively. Zone 3 (perivenous zone) which is located between the intermediate and perivenous zones. The liver acinus is often

preferred by histopathologists because it is useful in describing both functional and structural units thus allowing lesions such as necrosis and fibrosis to be described (MacSween 2002). More recently the primary lobule proposed by Matsumoto et al (Matsumoto and Kawakami 1982) has become increasingly popular because it describes the vessel architecture, the classic lobule and includes the conducting and parenchymal portion of the portal venous tress.

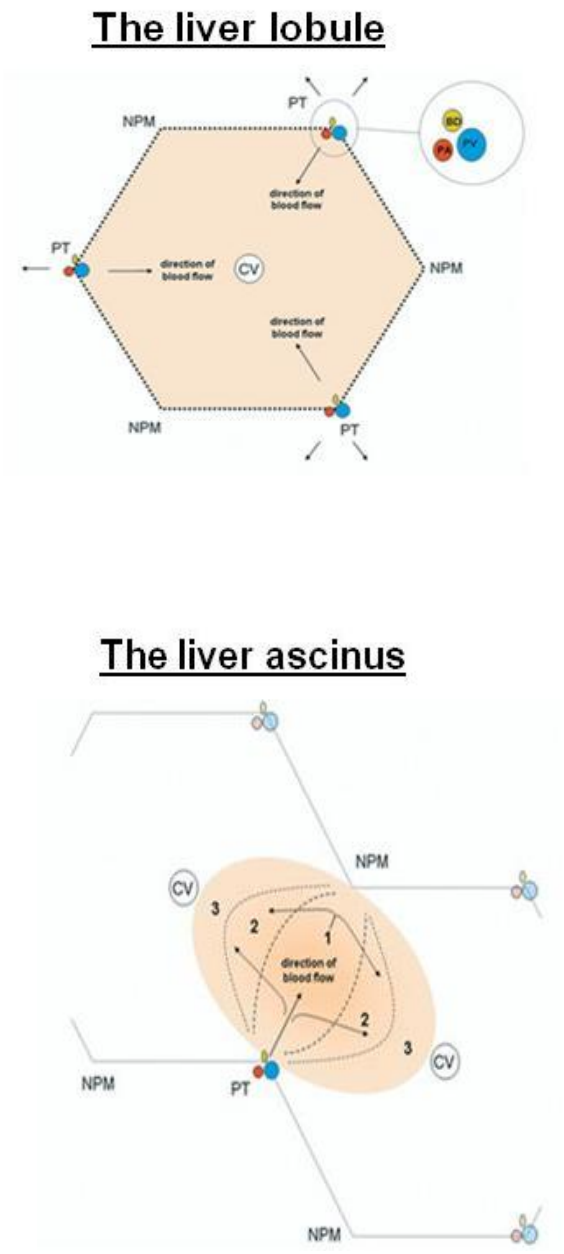

Figure 1.9: The liver lobules (Wallace, Burt et al. 2008).
Schematic diagrams of the hepatic lobule of Kiernan (upper) and liver acinus of Rappaport (lower).

1.5.2 The main liver cell types

There are at least 15 different cell types in the liver. The most abundant are the hepatocytes which contribute to over half of the total cell population and account for 80% of the total volume of the liver (Wallace, Burt et al. 2008). The other main cell types include the sinusoidal cells (SECS), Kupffer cells, quiescent stellate cells (qHSCs), biliary epithelial cells (BECs), oval cells and the pit cells. Each cell type plays a key role in maintaining homeostasis in the liver.

1.5.2.1 Hepatocytes

Heptocytes carry out most of the functions of the liver, for example, the production of bile and intermediary metabolism (Wallace, Burt et al. 2008). These cells are positioned along the sinusoids up to the centrilobular region (lobule) or zone 3 (acini) as polarized epithelial cells. The liver sinusoids behave as capillaries where they regulate the flow of materials going in and out of the space of Dissé. The sinusoids are also known to express heterogeneous genes for example, the expression of CYPs (cytochrome P450s) which are predominantly expressed by the hepatocytes around the central veins (Wallace, Burt et al. 2008).

1.5.2.2 Sinusoidal cells (SECs)

The sinusoidal cells (SECs) form the sinusoidal wall which serves as a barrier between the blood and the hepatocytes and plays a pivotal role in filtering and regulating the exchange of fluids, solutes and macromolecules. SECs are considered as being unique endothelial cells due to the presence of fenestrae (open pores) which act as dynamic filters. In addition, they do not have a basal lamina beneath the endothelium but exhibit a strong cytoskeletal support to withstand the pressure from the dynamic blood flow.

1.5.2.3 Biliary epithelial cells (BECs)

Biliary epithelial cells (BECs) also known as cholangiocytes form the bile duct epithelium and are therefore pivotal for the transport of bile. Initially, the bile is transported from the membrane of the hepatocytes and then exits the liver through the common bile duct and the type and size of the bile duct that they form will determine their structure.

1.5.2.4 Kupffer cells

Kupffer cells also known as liver macrophages, are derived from circulating monocytes and are located within the sinusoids. They vary in shape but have protrusions that extend into the sinusoids. They function in removing debris by the process of phagocytosis and also play an important role in stimulating the immune system by secreting various mediators of inflammation including cytokines.

1.5.2.5 Oval cells

Oval cells are intrahepatic 'stem cells' found in the periportal regions of the liver and are a potential source for both hepatocytes and bile duct epithelial cells. During liver injury, oval cells are able to migrate and replace damaged hepatocytes.

1.5.2.6 Pit cells

Pit cells are large granular lymphocytes which act as liver-specific natural killer (NK) cells and are found in the sinusoidal lumen. They secrete soluble factors that are able to induce death of tumour cells and infected liver cells.

1.5.2.7 Quiescent stellate cells (qHSCs)

Quiescent stellate cells (qHSCS) originally identified by Boll and von Kupffer in the 1870s were previously known as Ito cells. They reside in the perisinusoidal space of Dissé which is located between the sinusoidal endothelium and hepatocytes and has relatively low levels of extracellular matrix (ECM) proteins. In the normal liver, stellate cells exist in a quiescent state and contain small lipid droplets in the cytoplasm rich in vitamin A and esters. Upon liver injury, qHSCs undergo a process of 'activation' where they transdifferentiate to a myofibroblast-like phenotype (Kocabayoglu and Friedman 2013).

1.5.3 The extracellular matrix

The extracellular matrix (ECM) is essential for the regeneration and modulation of liver function. The ECM proteins consists of; collagens, glycoproteins and proteoglycans that provide a structural framework for the liver, cohesiveness between cells, cell polarization and intercellular communication (Wallace, Burt et al. 2008). ECM in the normal liver such as type IV collagen is located

predominantly in the portal tracts around the central veins and sometimes in the space of Dissé (Wallace, Burt et al. 2008). Additionally, the interstitial collagens type I and type III are found adjacent to the hepatocytes in the space of Dissé (Wallace, Burt et al. 2008).

1.5.4 The physiological roles of the liver

The liver plays a major role in intermediary metabolism and in the clearance of toxins and is the main site of metabolism for most drugs and xenobiotics. The liver is also responsible for bile acid metabolism, inducing bile flow in the biliary system and also for aiding absorption of dietary lipid in the intestine (MacSween, Burt et al. 2007). The bile is contained in the bile canaliculi which come together to form the intrahepatic and extrahepatic bile ducts (Wallace, Burt et al. 2008). It is an important site for protein and amino acid metabolism and for the synthesis of major proteins such as albumin, complement and clotting factors. The liver is also responsible for the synthesis of glycogen; derived from either glucose, lactic and pyruvic acids or glycerol. Furthermore, ammonia which is produced during catabolism of amino acids and needed by some nitrogenous compounds is removed by the liver due to its toxicity. Other principal functions of the liver include; the generation of urea, carbohydrate metabolism and the regulation of systemic and mucosal immunity (Wallace, Burt et al. 2008).

1.5.5 Regenerative capacity of the liver

The liver has a remarkable capacity to regenerate and can function normally even in cases where up to three-quarters of its own mass is lost (Wallace, Burt et al. 2008). Indeed, in partial hepatectomies where cell death is significant, the liver will regenerate to its original size (Wallace, Burt et al. 2008). Liver regeneration is thought to be carried out primarily by two mechanisms. The first is in response to moderate liver tissue loss where adult differentiated hepatocytes divide and replicate and the second is in response to extensive hepatocellular loss which stimulates the proliferation of progenitor cells (Grisham 1994, Sell 2001, Sell 2003).

The regeneration of the liver is a tightly controlled, non-autonomous process regulated by certain factors that maintain the correct ratio between liver mass and body size. Amongst these factors are the serum growth factors including

epidermal growth factor (EGF) and hepatocyte growth factor (HGF) which promote DNA synthesis in both hepatocytes and bile duct epithelial cells (Michalopoulos 1990). In addition, various regulatory growth factors expressed by hepatocytes are involved for example, the transforming growth factor-alpha (TGF-α) and acidic fibroblast growth factor (a-FGF) (Michalopoulos 1990). Other cell types including Kupffer cells and myofibroblasts also express these growth factors such as HGF and transforming growth factor-beta (TGF-β) (Hsia, Axiotis et al. 1992, Burr, Carpenter et al. 1993). Cytokines including tumour necrosis factor (TNF-α) (Zhu, Zhou et al. 2012), Interleukin-1 (IL-1) (Sgroi, Gonelle-Gispert et al. 2011) and Interleukin 6 (IL-6) (Galun and Rose-John 2013) are also important for liver regeneration

The growth factors and cytokines form complex loops causing both stimulatory/inhibitory and autocrine/paracrine responses. A good example of this is demonstrated by myofibroblasts when they secrete TGF-β, this cytokine behaves as an autocrine stimulus for myofibroblasts but conversely acts as a paracrine repressor of hepatocyte proliferation (Strain 1992). Regeneration of the liver also requires nutrients and these are supplied predominantly by the portal venous blood from intestinal digestion and absorption. Additionally, hormones including insulin, glucogen and the catecholamines are known to influence regeneration, for example in the absence of insulin the process of regeneration is much slower compared to when insulin is present (Barra and Hall 1977, Johnston, Johnson et al. 1986). One of the most fascinating observations of hepatic growth regulation is in human liver transplantation whereby if the liver is too small for the host it will grow until the organ is the correct size and conversely, if the liver is too large it will decrease in size (Kam, Lynch et al. 1987). This has led to an increase in living donor transplantation and also split transplants (Broelsch, Emond et al. 1990, Strong 2006). However, despite these advances there is still a shortage of liver organs and this is due to both the lack of organs and the rising incidence of chronic liver disease (Friedman 2000).

1.6 Liver fibrosis

Accidental or deliberate poisoning to the liver such as an adverse effect to a therapeutic drug or for example paracetamol (acetaminophen) overdose can cause substantial liver necrosis, liver failure and death (Wallace, Burt et al. 2008).

Nevertheless, chronic liver damage which often leads to liver fibrosis is by far a greater clinical problem (Wallace, Burt et al. 2008). Currently, liver cirrhosis (end stage of liver fibrosis) is in the top ten causes of death in the western world and is imposing a mounting economic burden.

Liver fibrosis is caused by the wound healing response of liver injury due to inflammation from a wide range of aetiologies including; viral infections, alcohol abuse, biliary disease, iron overload, inherited metabolic defects and more recently obesity and diabetes (Wallace, Burt et al. 2008). Cirrhosis is the most advanced stage of fibrosis and has been described by the World Health Organization as a *'diffuse process characterized by fibrosis and the conversion of the normal liver architecture into structurally abnormal nodules'* (Anthony, Ishak et al. 1977).

Due to the overcapacity of the liver some patients can still live a normal life for a long periods of time and certainly the 'injury-cirrhosis' period can differ considerably between patients. However, irrespective of the cause, chronic damage to the liver results in hepatocyte apoptosis and/or necrosis and an increase in other cell types including Kupffer cells, myofibroblasts, SECs and BECs (Wallace, Burt et al. 2008). A progressive accumulation of ECM for example, type I and type III collagens accumulate in the portal tracts and also in the lobules (Wallace, Burt et al. 2008). There is also an accumulation of non-collagen proteins including fibronectin, elastin, laminin and proteoglycans. As the quality and the quantity of the ECM changes it forms interstitial scar-type collagen rich matrix which makes degradation of the ECM difficult. Indeed, it has been determined that in severe cases of liver fibrosis, the liver contains six times more ECM compared to a normal liver (Wallace, Burt et al. 2008). Deposition of this excess ECM can have catastrophic effects; altering and distorting hepatic architecture and vascular structure and impeding hepatocyte regeneration which can lead to cirrhosis and eventually liver failure (Wallace, Burt et al. 2008). In end stage liver disease, the liver can no longer regenerate and therefore liver transplantation remains the only option.

1.6.1 Myofibroblasts and their role in liver fibrosis

Upon liver injury, quiescent stellate cells undergo a process of 'activation' to a myofibroblast-like phenotype expressing a variety of cytokines, chemokines and α-smooth muscle actin (α-sma) and go onto proliferate and produce ECM and proteases (Friedman 2000, Bataller 2001). The triggering of quiescent stellate cells to myofibroblasts is believed to be due to cytokines and reactive oxygen species (ROS) secreted by Kupffer cells and other leukocytes (Casini , Simeonova 2001, Bataller 2003). For example, Kupffer cells release many of the pro-inflammatory cytokines including IL-6, TNF-α and TNF-β which are known to promote liver myofibroblast activity (MacSween 2002). However, it has recently been found that these cells are not the only fibrogenic cell present in the liver. A study carried out recently found that where damage was present in the periportal regions of the liver lobule it was the portal tract fibroblasts not the stellate cells that were predominantly responsible for this (Knittel 1999).

Since myofibroblasts express vimentin, desmin, and α-sma it is believed that they are derived from a mesenchymal origin (Yokoi 1984, Burt 1986, Ballardini 1988). Indeed, several markers of neural/neuroectodermal differentiation have also been found to be expressed on these cells for example, the intermediate filament glial fibrillary acidic protein (GFAP) (Neubauer 1996). Furthermore, synaptophysin, a membrane protein is a marker of synaptic vesicles containing neurotransmitters (Cassiman 1999) and is present on the surface of both myofibroblasts and neural cells (Douglass 2008). This membrane protein has an external cellular location and cycling to intracellular location(s) and due to its restricted expression on cells means that it is an ideal target for anti-fibrotic therapeutics (Douglass 2008).

1.6.2 *In vitro* and *in vivo* models of liver fibrosis

There are three main groups of models for liver fibrosis; cell culture systems, human tissues taken at biopsy and animal models. In the cell culture models, primary cells are isolated and purified from either normal or injured livers and these systems have for example, enabled the functional role of different liver cells to be studied in response to different conditions. Human tissues obtained from biopsies can be used to generate vast amounts of information and validate findings from cell culture systems and animal models. Nevertheless, due to

ethical constraints it is difficult to obtain multiple liver biopsies thus; data is limited to a “snap shot” of information. However, animal models allow multiple sampling of tissue and also help to define the mechanisms and events that take place *in vivo*. Indeed, a number of rodent models exist for liver fibrosis but the most commonly used for modelling centrilobular fibrosis is the administration of carbon tetrachloride (CCl_4). For studying periportal fibrosis, ligation of the common bile duct (BDL) is normally performed, however due to limitations to this model such as high mortality rates, alternatives such as methapyrilene (MP) are being investigated (Probert, Ebrahimkhani et al. In press) (Probert, Ebrahimkhani et al. In press). Other models include specific diets for example, the choline-deficient diet and also the expression of hepatotropic viral proteins and genetically modified animals.

1.7 Liver fibrosis and cancer metastasis

Many cancers metastasize to the liver including melanoma suggesting that it provides an ideal microenvironment for cancer cells to migrate to and then reside and grow. Furthermore, studies have recently been carried out that show a role of myofibroblasts in the development of a wide range of cancers. A study published recently studied the role of myofibroblasts in the promotion of liver metastasis of colon cancer cells via the CXCR4-CXCL12 chemokine axis (Matsusue 2009). The results showed that myofibroblasts were located around the liver metastasis area and also secreted CXCL12 (Matsusue 2009). Furthermore, they demonstrated that the concentration of CXCL12 in media from quiescent stellate cells was significantly lower compared to the media obtained from myofibroblasts (Matsusue 2009). Another study by Hong and colleagues showed that CXCL12 expression is increased in cirrhotic livers and that CXCL12 binding to CXCR4 on stellate cells promoted proliferation and collagen production via the signalling pathways ERK 1/2 and P13K-Akt (Hong 2009).

In the context of melanoma, an experimental study demonstrated that melanoma cells migrate significantly greater to the cirrhotic liver (Qi, Qiu et al. 2004). However, studies investigating the role of melanoma metastasis towards the damaged and/or fibrotic liver are limited and furthermore, the specific cells involved has not been reported. However, since liver damage results in the proliferation of myofibroblasts chemokine levels such as CXCL12 may increase.

Thus, it was hypothesized that cells involved in fibrosis may promote the directional migration of CXCR4 expressing melanoma cells to the liver.

1.8 Aims

Thus, the central aim of this study was to examine the role of the CXCR4-CXCL12 chemokine axis in melanoma metastasis towards various liver cell types and to the normal and damaged liver. To achieve this aim, the specific objectives were to:

1. Confirm the expression of CXCR4 and CXCL12 in murine and human melanoma cell lines in *in vitro.*

2. Evaluate the expression of CXCR4 and CXCL12 in various liver cell types both *in vitro* and *in vivo.*

3. Test the hypothesis that inhibition of the CXCR4-CXCL12 chemokine axis by the novel CXCR4 inhibitor AMD11070 reduces migration of melanoma cells towards conditioned media containing CXCL12 in *in vitro*.

4. Determine the influence of chronic liver injury on the expression levels of CXCL12 in three different *in vivo* models; CCl_4, BDL and MP.

5. Examine murine and human melanoma metastasis to the normal and damaged liver in *in vivo* models.

Chapter 2:
Materials and Methods

2.0 Materials and Methods

2.1 Animals

2.1.1 Ethics

All animal procedures were performed in accordance to the UK Home Office regulations under the project licence (PPl 60/3907) and personal licence (PIL 60/12677) of Professor Matthew Wright. Prior to the commencement of each study, protocols were designed individually and the senior animal technician consulted. All animals were cared for under Home Office regulations.

2.1.2 Mice

Female C57BL/6 mice and female nude mice (20-30g body weight) were purchased from Charles River (Charles River, East Lothian, UK) and housed separately in the Comparative Biology Centre (CBC) at Newcastle University. Both sets of mice were incubated at 20 +/- 2^{o}C with a relative humidity of 50 +/- 10% with 12 hour light/dark cycles. Since nude mice are immune compromised these animals were kept in a sterile isolation unit and all equipment was sterilised prior to use (Fogh and Giovanella 1978).

2.1.3 Male Sprague-Dawley rats

Male Sprague-Dawley rats (230-250g body weight) were purchased from Charles River (Charles River, East Lothian, UK) and housed in the CBC at Newcastle University. The rats were kept in an incubated unit at 20 +/- 2^{o}C with a relative humidity of 50 +/- 10% with 12 hour light/dark cycles.

2.1.4 Modelling human melanoma metastasis to the liver *in vivo*

To examine human melanoma metastasis to the normal and damaged liver, female nude mice (6-8 weeks old) were injected intravenously (i.v) with 200µl of 1 x sterile phosphate buffered saline (PBS) containing 0.2 x 10^{7} of A375^{red} cells/ml. The number of cells injected were determined as described previously (Marshall 2010). The melanoma cells were transfected with a fluorescent protein; Dsred which is derived from Discosma (excitation/emission maxima of 558/583nm). PBS was prepared by dissolving one tablet of PBS (Sigma-Aldrich, Gillingham, UK) in 200ml of deionised water (dH_2O) (3.2 mM Na_2HPO_4, 0.5 mM

KH_2PO_4, 1.3 mM KCl, 135 mM NaCl, pH 7.4) and autoclaving before use. The cells were harvested during the exponential growth phase and prior to injection were washed twice in sterile 1 x PBS. Throughout the procedure, cells were kept on ice and cell viability was >95% as determined by trypan blue (0.4% w/v) (Sigma, Gillingham, UK) exclusion as described in section 2.2.7. Control animals received 200µl of 1 x sterile PBS alone. To establish liver damage, animals were injected with 100µl of paracetamol (20mg/ml) in 1 x sterile PBS via intraperitoneal injection (i.p) twice weekly for four weeks prior to injection of melanoma cells. Mice were identified by ear notching and treatment groups are given in Table 2.1.

Animals were imaged in the In Vivo Imaging System (IVIS) (Perkin Elmer, Massachusetts, USA) every two weeks and prior to imaging, were anaesthetized using isoflurane. After 6 weeks, mice were humanely culled by schedule 1 and the organs of interest were collected and snap frozen for protein and RNA and also fixed for immunohistochemistry.

Group	**Number of mice**	**Paracetamol injected i.p**	**$A375^{red}$ (0.2×10^7/ml) cells injected i.v**
1	2	-	-
2	1	Yes	-
2	4	-	Yes
3	4	Yes	Yes

Table 2.1: Treatment groups for modelling human melanoma metastasis to the liver *in vivo*.

2.1.5 B16-F10 as a murine *in vivo* model for human melanoma

A pilot study was set up to determine if B16-F10 murine melanoma cells (gift from Professor Antal Rot, University of Birmingham, UK) engrafted in the normal and/or fibrotic liver or in any other organ. Cells in exponential growth phase were harvested and prior to injection were washed twice in sterile 1 x PBS. Throughout the procedure, the cells were kept on ice and cell viability was >95% as determined by trypan blue (0.4% w/v) (Sigma, Gillingham, UK) exclusion as described in section 2.2.7. Animals were injected by subcutaneous injection (s.c) or via intravenous injection (i.v) with 1 x 10^5/ml B16-F10 cells suspended in 200µl 1 x PBS. To establish fibrosis, animals were treated bi-weekly with 25% (v/v) carbon tetrachloride (CCl_4) (Sigma-Aldrich, Gillingham, UK) dissolved in olive oil (Sigma-Aldrich, Gillingham, UK). After 3 weeks, mice were humanely culled by schedule 1 and the organs of interest were collected and snap frozen for protein and RNA and also fixed for immunohistochemistry. Treatment groups are given in Table 2.2. In order to reduce animal numbers, archived tissue was used for Group 1.

Group (3 mice per group)	Treatment	B16-F10 cells injected (1 x 10^5/ml) cells injected
1	Olive oil	-
2	Olive oil	Yes (i.v)
3	CCl_4	Yes (i.v)
4	-	Yes (s.c)

Table 2.2: Treatment groups for the B16-F10 as a murine model for human melanoma.

2.1.6 Generation of CXCL12 specific stellate cell knockout mice.

In an attempt to delete the CXCL12 gene specifically in hepatic stellate cells in CB57BL/6 mice, the Cre-Lox technology system was utilised (Niesner and Maheshri 2013). The Cre protein is a site-specific DNA recombinase which is able to catalyse the recombination of DNA between specific sites (Niesner and Maheshri 2013). The principle behind this system is simplified in Figure 2.1.

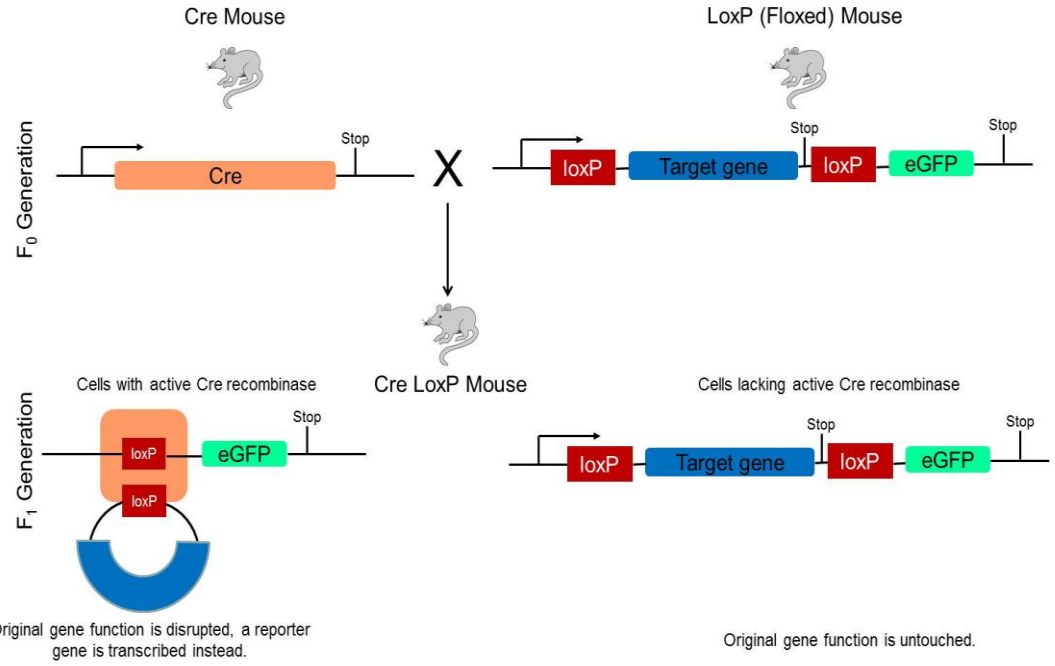

Figure 2.1: Mechanism of the Cre-Lox system for generating knockout animals adapted from Zepper (Zepper 2008) .

In brief, heterozygotic mice (C57BL/6) carrying 2 loxP sites flanking exon 2 of the CXCL12 gene (gift from Professor Nagasa, Kyoto University, Japan) were housed in the East Building animal house at Mount Sinai School of Medicine, New York. Recombination at these sites deletes a ~500 base pair region including exon 2. To generate a conditional-knockout (KO) the mice were bred with transgenic mice carrying the Cre-recombinase under the control of the murine GFAP promoter (The Jackson Laboratories, New York USA) since it is known to be expressed by hepatic stellate cells (Apte, Haber et al. 1998). Animals were used with the approval of the Institutional Animal Care and Use Committee (IACUC) and cared for under the National Institutes of Health (NIH) guidelines. To identify Cre^{+} mice on the F_1 population (for the potential to

knockout CXCL12 expression in GFAP expressing cell types) PCR was performed as described in section 2.3 to amplify the Cre gene.

2.1.7 Bile Duct Ligation (BDL) and Methapyrilene (MP) treatment

Periportal liver damage was established in rats either by bile duct ligation (BDL) (performed by Dr Fiona Oakley) or by the treatment of Methapyrilene (MP) (performed by Philip Probert) as described previously (Probert, Ebrahimkhani et al. In press). BDL was carried out by exposing the bile duct and double-ligating it. The areas between the two ligations were then cut and rats were allowed to develop cholestatic disease for three weeks. Sham control rats underwent the same procedure, however, the bile duct was not ligated. In the MP model, rats were treated with 150mg of MP hydrochloride/kg body weight in 1 x PBS (Sigma-Aldrich, Gillingham, UK) by oral gavage tri-weekly for three weeks. Control animals received 1 x sterile PBS alone.

2.2 Routine cell culture

2.2.1 Chemicals and reagents

All chemicals and reagents used were of molecular or analytical grade unless otherwise stated. All routine culture reagents and plastic ware were supplied by Sigma-Aldrich (Gillingham, UK) and Corning-Costar, VWR International Ltd. (Leicestershire, UK) respectively unless otherwise specified. All cell culture techniques were performed inside a class II microbiological safety cabinet (BIOMAT-2, Medical Air Technology Ltd., Oldham, UK) and sterilised alongside reagents and plastic ware with 70% (v/v) ethanol prepared in dH_2O. All PBS was prepared as described in section 2.1.4 and was sterile unless otherwise stated.

2.2.2 Culture of adherent cell lines

Adherent cell lines were maintained in appropriate media as summarised in Table 2.3. All cell lines were incubated at 37°C in a humidified atmosphere of 95% air and 5% CO_2 in 75cm^2 flasks or 6 well plates. In order to maintain cells in exponential phase of growth, cells were sub-cultured twice weekly. Culture media was aspirated from the flask or plate and cells were washed with pre-warmed (37^oC) 1 x PBS to ensure all media was removed. The cells were then incubated with 1 x Trypsin- Ethylenediaminetetraacetic acid (EDTA) (flask: 4mL,

each well of plate: 0.5ml) and incubated at 37^{o}C until cells had detached. To neutralize trypsin, an equal volume of serum-containing culture media was added. The cell suspension was then transferred to a 50ml falcon tube and centrifuged for 4 minutes at 2000 x rpm. The supernatant was removed carefully and the pellet re-suspended in fresh media (Table 2.3) before being transferred to either 75cm^2 flasks or 6 well plates. Cell lines were used up to a maximum passage number of 30 prior to new stocks being revived.

Cell Line	Morphology	Culture Media
B16-F10	Murine melanoma	DMEM (glucose 1000mg/l),10% (v/v) FCS, 1 % (v/v) P/S, 1% (v/v) Glut.
JS-1	Murine stellate	DMEM (glucose 1000mg/l),10% (v/v) FCS, 1 % (v/v) P/S, 1% (v/v) Glut.
603B	Murine biliary epithelial	DMEM (glucose 1000mg/l), 10% (v/v) FCS, 1 % (v/v) P/S, 1% (v/v) Glut.
TSEC	Murine sinusoidal endothelial	DMEM (glucose 1000mg/l),5% (v/v) FCS, 1 % (v/v) P/S, 1% (v/v) Glut., 5% (v/v) EGS.
A375, CHL-1, Wm2664	Human melanoma	DMEM (glucose 4500mg/l),10% (v/v) FCS, 1 % (v/v) P/S, 1% (v/v) Glut.
LX-2	Human stellate	DMEM (glucose 4500mg/l), 10% (v/v) FCS, 1 % (v/v) P/S, 1% (v/v) Glut.
H69	Human biliary epithelial	DMEM (glucose 1000mg/l), 10% (v/v) FCS, 1 % (v/v) P/S, 1% (v/v) Glut , 240ng/ml adenine, 27ng/ml triodothyronine, 10 µg/ml ephinepherine, 1x insulin-transferring-selenium solution (ITS-solution), and 1µM hydrocortisone.

Table 2.3: Cell line media and specific supplements.
DMEM = Dulbecco's Modified Eagle Medium, **FCS**= Foetal calf serum, **Glut** =Glutamine, **EGS** = Endothelial Growth Supplement, **P/S**= penicillian/ streptomycin.

2.2.3. Isolation of primary human and murine liver cells.

Primary human liver cells were isolated from re-sected liver tissue with informed donor consent and ethical approval from the Newcastle & North Tyneside Research Ethics Committee. For the isolation of primary murine liver cells, livers were extracted from CB57BL/6 mice according to the Home Office Regulations.

2.2.3.1 Isolation of primary human and murine hepatic stellate cells (HSC).

In brief, the human liver resections were perfused with calcium free Hanks Balanced Salt Solution ($HBSS^-$) (1L = 900ml sterile H_20, 100ml 10X HBSS without Ca^{2+} Mg^{2+}, 80g/l NaCl, , 4g/L KCl, 10g/l glucose, 600mg/l KH_2PO_4, 475mg/l Na_2HPO_4 and 170mg/l phenol red supplemented with 6mls of 1M sterile (4-(2-hydroxyethyl)-1-piperazineethanesulfonic acid) (HEPES), 4.6mls of 7.5% (w/v) $NaHCO_3$ and 1 ml of 1 M$CaCl_2$, pH 7.4). Following this, the liver was perfused with HBSS+ (prepared the same as $HBSS^-$ but with the addition of 1mM $CaCl_2$). In order to facilitate digestion, the Glisson's capsule of the liver was removed and the liver cut into small pieces. The dissected liver was transferred into a sterile sterilin and digested with HBSS+ supplemented with 235mg pronase (Roche, Burgess Hill, UK), 30mg of Collgenase B (Roche, Burgess Hill, UK), 10mg DNase (Sigma-Aldrich, Gillingham,UK) and incubated at 37^{o}C**,** 250 x rpm for 30 minutes. The liver digest was then filtered through a 125µm nybolt mesh with HBSS+ and transferred to a 50ml falcon with the addition of 1mg of DNase and centrifuged at 2000 x rpm for 7 minutes. The supernatant was removed and the cell pellet washed by re-suspending in 50ml of $HBSS^+$ containing 1mg of DNase and centrifuging at 2000 x rpm for 7 minutes and this was repeated twice. After the final wash, the stellate cells were isolated by density centrifugation by re-suspending the pellet in 13ml of Optiprep (Sigma-Aldrich, Gillingham, UK), 2mg DNase and 60ml of HBSS+. To prevent the stellate cells from floating to the top, 2ml of HBSS+ was carefully layered above this. The cells were centrifuged at 1500 x rpm for 20 minutes and then the stellate cell phase removed and re-suspended in HBSS+. The cell suspension was centrifuged at 2000 x rpm for 7 minutes, HBSS+ was then removed and the cells were then re-suspended in culture medium and seeded out into 6 well plates.

For the isolation of murine stellate cells, the portal veins of between two and six C57BL/6 mice were cannulated *in situ*. The same method was then used as

described for human stellate cells, however the livers were pooled together and the pronase and collagenase scaled down as necessary.

Both human and murine HSCs were maintained in DMEM containing 4500mg/l glucose and supplemented with 20% (v/v) foetal calf serum (FCS), 1% (v/v) penicillin streptomycin and 1% (v/v) glutamine. The cells were maintained at 37°C in a humidified atmosphere of 95% air and 5% CO_2 in 75cm^2 flasks and passaged as described in section 2.2.2.

2.2.3.2 Isolation of primary human and murine hepatocytes

Primary human and murine hepatocytes were isolated by collagenase perfusion. A cannula was inserted into the hepatic portal vein and the liver was perfused with Earle's balanced salt solution without $Ca^{2+}Mg^{2+}$ ($EBSS^-$) supplemented with 500μM ethylene glycol tetraacetic acid (EGTA) (Sigma-Aldrich, Gillingham, UK). The liver was then perfused with $EBSS^+$ (with Ca^{2+} and Mg^{2+}) supplemented with 10mg/ml of collagenase A. Once digested, the liver was filtered through a blotting cloth with $EBSS^+$. The cell suspension was then centrifuged at 50 x rpm for 4 minutes at 4°C and the pellet snap frozen and stored at -80^{o}C.

2.2.3.3 Isolation of primary human and murine biliary epithelial cells

The liver was perfused and cut up into small pieces as described in section 2.2.3.1. The liver was then transferred to a sterilin and 5ml of 10mg/ml collagenase A and 2ml of 2mg/ml DNase I was added and made up to 50ml with 1 x sterile PBS and then incubated at 37^{o}C for 30-45 minutes. The digested liver was then sieved through the nybolt mesh into a beaker and mashed further with 1 x PBS to facilitate cell passage. The mesh was carefully removed and 5ml of 2mg/ml DNase I was added and made up to a total volume of 400ml. This was then transferred to 8 x 50ml centrifuge tubes and spun at 600g for 5 minutes. Supernatant was removed and pellets were re-suspended in 20ml 1 x PBS and then 0.5ml of DNase I to each tube was added. Tubes were centrifuged at 600g for 5 minutes, supernatant was discarded and the previous step was repeated. The pellets were then re-suspended in the two centrifuge tubes in 10 ml of 1 x PBS, mixed and then combined into one tube. 1 ml of DNase I was then added and made up to a total of 24ml with 1 x sterile PBS.

In order to semi purify the BECs, density gradient using Percoll (Sigma-Aldrich, Gillingham, UK) was performed. Percoll gradients were prepared as following:

- Percoll stock solution: Add 11ml of sterile 10x PBS to 1 litre Percoll medium.
- 33% Percoll: Add 33ml Percoll stock solution to 67ml 1 x PBS
- 77% Percoll: Add 77ml Percoll stock solution to 23ml 1 x PBS

Into 8 x 15ml centrifuge tubes 3ml of 33% percoll was added and then 3ml of 77% percoll was slowly pipetted under this layer using a 5ml plastic pipette. 3ml of the cell suspension was pipetted on top and then centrifuged at 2000rpm for 30 minutes at 80% acceleration and 0% deceleration. Once centrifuged, two rings were observed-the top ring which contained the hepatic stellate cells (HSC) and hepatocytes and the bottom ring containing the biliary epithelial cells (BECS) (Figure 2.1.2).

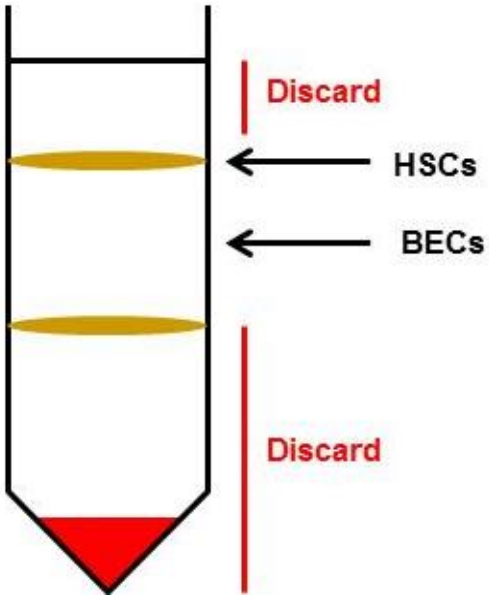

Figure 2.2: Isolation of biliary epithelial cells by Percoll gradient centrifugation.

The HSCs were isolated as described in section 2.2.3.1 (from the Optiprep stage). The bottom ring containing the BECs and the overlying aqueous layer was carefully extracted using a Pasteur pipette and then transferred to a 50ml centrifuge tube. To wash the extracted BECs, 3 volumes of 1 x PBS was added and centrifuged at 600g for 5 minutes. After centrifugation, the supernatant was discarded and re-suspended in 9ml of 0.1% BSA in 1 x PBS. This was then

mixed and transferred to a 15ml centrifuge tube (without DNase) and immune-magnetic purification of the BECs was performed.

HEA-125 Dynabeads (Invitrogen, Paisley, UK) were transferred to a roller to ensure that they were adequately mixed. Next, 50-100µl was pipetted into a microcentrifuge tube with 1ml of 0.1% BSA in 1 x sterile PBS and then placed in the magnet (Invitrogen, Paisley, UK) for 1 minute. The supernatant was then removed and a further 1ml of 0.1% BSA in 1 x PBS was added, the tube was removed from the magnet and re-suspended in the Dynabeads. The re-suspended Dynabeads were then added to the semi-purified BEC suspension in a 15ml centrifuge tube and placed on the roller in the cold room for 30 minutes. The tube was then transferred to the magnet for 5 minutes, and then the supernatant was removed. The tube was then removed from the magnet and a further 10ml of 0.1% BSA in PBS was added and re-suspended in the Dynabead-bound BECs. The tube was placed back into the magnet for 2 minutes and then the supernatant was removed. To ensure that any non-binding cells were removed, this step was repeated. Finally, the re-suspended Dynabead-bound BECs were re-suspended in 10ml of BEC media and transferred to a 25cm^2 flask and placed in the incubator. The BEC media consisted of; 1:1 DMEM:Hams F12 medium (Sigma-Aldrich, Gillingham, UK), 10% FCS (v/v) 1 % (v/v) P/S, 10 ng/ml epidermal growth factor (EGF) (Calibiochem, Darmstadt, Germany), 0.248 IU/ml Insulin (Sigma-Aldrich, Gillingham, UK), 2 µg/ml hydrocortisone (Sigma-Aldrich, Gillingham, UK), 10 ng/ml cholera toxin (Sigma-Aldrich, Gillingham, UK), 2nM tri-iodo-L-thyronine (Sigma-Aldrich, Gillingham, UK) and 5 ng/ml hepatocyte growth factor (HGF) (Calibiochem, Darmstadt, Germany).

2.2.4 Isolation of primary melanocytes

Primary melanocytes were isolated from adult abdominal and foreskin with informed donor consent and ethical approval from the Newcastle & North Tyneside Research Ethics Committee.

The blood vessels and connective tissue were removed from the skin samples and then dissected into small pieces. These were then digested by incubating in 10ml 1 x sterile PBS supplemented with 20mg of dispase and 10% penicillin/streptomycin/fungizone (PSA) (Lonza Biologics, Slough, UK) overnight

at 4ºC. All the samples were rinsed in PBS containing 1% PSA. The epidermis was then removed with sterilised forceps and incubated in 5ml of 1% trypsin EDTA (TE). After incubation, 500µl of FCS was added and the solution was centrifuged at 1200rpm for five minutes. After centrifugation, the pellet was re-suspended in fresh Epilife ® medium (Invitrogen, Paisley, UK) supplemented with PSA and Human Keratinocyte Growth Serum (HKGS) (Invitrogen, Paisley, UK). The medium was transferred to a tissue culture flask and then after 24 hours, the media was removed and changed so that cells that had not adhered were removed. The cells were maintained in DMEM supplemented with 5% (v/v) FCS and 1 % (v/v) PSA. Once the dermal fibroblasts had adhered the melanocytes were isolated by removing the media and washing once in 1 x PBS and then adding trypsin for 30-60 seconds. The cells were then centrifuged for 5 minutes at 1200 x rpm, the supernatant was removed and protein was extracted as described in section 2.4.1.

2.2.5 Long term storage of cells

Cell lines and primary cells were routinely frozen down and stored long-term in liquid nitrogen. Cells were detached (as described in section 2.2.2), transferred into a 50ml falcon (containing pre-warmed media) and then centrifuged at 1500 x rpm, for 5 minutes. The media was removed and the pellet re-suspended in freezing medium (90% (v/v) FCS and 10% (v/v) dimethyl sulphoxide (DMSO)). Typically, 3mls per pellet was harvested from each confluent 75cm^2 tissue culture flask and then aliquoted into sterile 1.8ml cryovials (1.5ml/cryovial). The cryovials were immediately placed in an isopropyl alcohol filled freezing container (Mr Frosty, Nalgene ®) and placed overnight at -80ºC to gradually cool (1ºC per minute cooling rate). The next day, the vials were transferred to the liquid nitrogen until needed.

2.2.6 Revival of cell line stocks

Cells were removed from liquid nitrogen and quickly thawed at 37ºC (until approximately 80% had thawed). Cell suspensions were then transferred to a 50ml falcon containing pre-warmed medium and centrifuged for 5 minutes at 1500 x rpm. To remove residual DMSO, supernatant was discarded and the cell pellet re-suspended in fresh media and transferred to a 25cm^2 culture flask. After 24 hours, once cells had attached, the culture media was changed and the cells

were then cultured as described in section 2.2.2. Cells were not used for experimental purposes until they had been passaged at least twice.

2.2.7 Measurement of cell number and viability using a haemocytometer

Measurement of cell viability was assessed by the ability of a cell to exclude trypan blue (dead cells are stained blue because the dye traverses through the membrane and cannot be pumped out). Cell suspensions were diluted 1:1 with 0.4% (v/v) trypan blue (final concentration 0.1% (w/v)) and a small volume of the cell suspension: trypan blue mix (10µl) was loaded via capillary action onto a haemocytometer (VWR International Limited., Leicestershire, UK). Duplicate cell counts were performed and cell viability was determined by counting both viable and non-viable cells.

2.2.8 Collection of conditioned media

For conditioned media, $2x10^4$/ml cells were seeded into 24 well plates and after 24 hours the media was replaced with 300µl of either 10% (v/v) FCS or serum free DMEM media. At 24, 48 and 72 hours the conditioned media was collected and centrifuged at 2000 x rpm to remove particulate debris. The media was then aliquoted into 15 ml falcons and stored at -80°C until needed.

2.2.9 Cell viability assay

Cell viability was measured using a commercially available MTS kit-CellTiter 96 Aqueous Non-Radioactive Cell Proliferation Assay (Promega, Southampton, UK) according to the manufacturer's instructions. MTS 3-(4,5-dimethylthiazol-2-yl)-5-(3-carboxymethoxyphenyl)-2-(4-sulfophenyl)-2H-tetrazolium) is a tetrazolium compound which in the presence of phenazine methosulfate (PMS) produces a soluble formazan product which turns indigo in colour. The compound (MTS) measures the mitochondrial dehydrogenase activity within the cells and therefore can be used as a measure of cell viability. Hence, an increase in viability results in an increase in mitochondrial dehydrogenase, which is correlated with the absorbance of the sample due to the formazan dye produced.

Cells were seeded into 96 well plates at a density of $1x10^4$ cells per well and were allowed to attach overnight. On the day of treatment, the culture medium in each well was replaced with either 10% FCS (v/v) or serum free DMEM media

containing the recombinant CXCL12 (PeproTech Inc, Rocky Hill, NJ) at varying concentrations or the conditioned media previously collected (section 2.2.8). After 24, 48 and 72 hours, 10µl of the MTS reagent was added to each well (without mixing) followed by incubation at 37^{o}C, 5% CO_2 in air for 4 hours. The plates were then read using a SpectraMax 250 plate reader (Molecular Devices Ltd, Wokingham, UK) at an optical density of 490nm. Results were normalized to the control value and the percentage cell viability was calculated.

2.3 Polymerase Chain Reaction (PCR) analysis

2.3.1 RNA purification with Trizol

Cell culture media was removed from each well of a 6 well plate and the cells were then washed with ice-cold 1 X PBS. To each well, 1ml of Trizol (Invitrogen, Paisley, UK) was added and the cells were then scraped (using an ice cold scraper) and then transferred to an RNase/DNase free eppendorf. For tissue samples, these were excised using sterile tools and a small piece was cut using a clean scalpel and transferred into an RNase/DNase free eppendorf containing 1 ml of Trizol. The tissue was initially mashed and was then broken down further by sonication using a Soniprep 150 Plus (MSE, London, UK). To each of the samples, 200µl of chloroform (Sigma-Aldrich, Gillingham, UK) was added, mixed then centrifuged for 15 minutes at 12000 x rpm at 4°C. The upper aqueous layer was transferred into a new eppendorf followed by the addition of 500µl of chilled isopropanol (Fisher Scientific UK Ltd, Loughbrough,UK) and then incubated on ice. After 10 minutes, samples were centrifuged at 12000 x rpm for 10 minutes at 4°C. The supernatant was removed carefully and the pellet dislodged and washed in 70% (v/v) sterile ethanol. The samples were then centrifuged at 12000 x rpm at 4°C and then the supernatant was removed. The pellet was air dried, re-suspended in 15 µl of sterile H_2O and then quantified using a Nanodrop ® (Thermo Scientific, Denver, USA).

The principles of this instrument are based upon the Beer Lambert Law whereby the concentration (ng/µl) is measured by the absorbance of UV light at 260nm and 280nm in 1µl of sample. The ratio of these absorbances, are also used to assess both quality and purity of the RNA where values between 1.8 and 2.0 are deemed acceptable for analysis.

2.3.2 DNAse treatment of RNA

To minimise genomic DNA contamination, RNA was DNAse treated prior to the PCR (Promega, Sounthampton, UK). Briefly, RNA was diluted in 50µl of sterile water and to this 5µl of both RQI 10x DNase I Reaction Buffer and 5µl of DNase I were added. This was mixed gently and then incubated at 37°C for 30 minutes. To stop the reaction, 5 µl of DNase stop solution was then added and incubated at 65°C for 10 minutes. RNA samples were stored at -20°C until needed.

2.3.3 Reverse transcription-polymerase chain reaction (RT-PCR)-production of cDNA from RNA

To produce 1st strand cDNA, RNA was diluted with sterile H_2O to a final concentration of 200ng/µl. 4µl of RNA (800ng) was then incubated with 1µl (50ng/µl) of random primers (Promega, Southampton, UK) for 3 minutes at 90°C and then afterwards immediately placed on ice. 15µl of RT master mix (per tube: 4µl x5 RT buffer, 0.5µl RNasin, 7.5µl H_20, 2µl of 10mM dNTP's and 1µl of MMLV) was added to each sample and then to synthesize DNA was incubated for 1 hour at 42°C. 2µl of cDNA was then used for PCR and the remaining RNA was stored at -20°C or -80°C for long term storage.

2.3.4 Polymerase chain reaction (PCR)

18µl of PCR master mix (per tube:10µl 2 x Go-Taq Green master mix, 6µl dH_20, 2µl 10pmol/µl of upstream and downstream primers) was prepared and 2µl (80ng) of the appropriate cDNA or sterile water was added to each tube and mixed gently. PCR reactions were performed on a programmable bench top thermocyclar and the standard PCR programme was used as shown below.

Step	Temperature	Time (minutes)	Cycles
Denature	95	1	1
Denature	95	1	35
Annealing*	55	1	35
Elongation	73	1.5	35
Elongation	73	8	1
Hold	4	-	-

* Annealing temperature was dependent upon the primers used (Table 2.4)

2.3.5 Primer design

Primer sequences were designed to amplify specific DNA sequences of interest. DNA sequences were obtained from the NCBI database (www.ncbi.nlm.nih.gov) and the Primer-BLAST programme was used to check the specificity of the primer sequences and also the likelihood of primer dimer formation. Ideally, primers were designed to have a GC content between 40% and 60% and be approximately 18-30 base pairs in length so that each set of primers had similar melting temperatures (Tm) where Tm = 2 C x (A + T) + 4 C x (G + C). An annealing temperature of generally 55^{o}C was used to start with and then optimized by +/- 2^{o}C if necessary (Table 2.4).

Primer	5'-3' Sequence	Annealing Temperature (°C)	Amplicon size (bp)
mCXCL12-α	US CGCTCTGCATCAGTGACGGTA DS TGTCAGCCTTCCTCGGGGGTC	55	276
mCXCL12-β	US CCACATCGCCAGAGCCAACGT DS ACACCTCTCACATCTTGAGCC	55	179
mCXCL12-γ	US CCCTTCAGATTGTTGCACGGC DS TCGGCAGGAAGCGGGGAACT	55	212
mCXCR4	US CACCACGGCTGTAGAGGCGAGT DS GCCGGTACTTGTCCGTCATGC	57	264
rCXCL12-α	US GCATCAGTGACGGTAAGCCA DS CTCAGCATGACCCCAGTCAG	55	362
rCXCL12-β	US GCATCAGTGACGGTAAGCCA DS GGCCCTTCCCTAACACTGAC	55	304
rCXCL12-γ	US TGCATCAGTGACGGTAAGCC DS CCATCTGCAGGAAGCACGTA	55	333
rCXCR4	US TGCCATGGAAATATACACTTCGGA DS CACCCACATAGACGGCCTTT	57	473
hCXCL12-α	US GCTCTGCCTCAGCGACGACGGGAA DS CGAGTGGGTCTAGCGGAAAGT	55	265
hCXCL12-β	US TTCAGATTGTAGCCCGGCTGA DSTGTGGCAGGCCCTTCCCTAAC	55	188
hCXCL12-γ	US GCCCTTCAGATTGTAGCCCGG DS GAGCAAATTTACAAAGCGCCGAGAG	55	256
hCXCR4	US TAGTGGGCGGGGCAGAGGAGT DS AACAAAAGGGCACTGAGACGCTGAG	57	70
GAPDH	US TGACATCAAGAAGGTGGTGAAG DS TCTTACTCCTTGGAGGCCATGT	55	243
18s	US CCCGAAGCGTTTACTTTGAA DS CCCTCTTAATCATGGCCTCA	55	189
Cre	US GCG GTC TGG CAG TAA AAA CTA TC DS GTG AAA CAG CAT TGC TGT CAC TT	55	389

Table 2.4: DNA oligonucleotide sequences employed in RT-PCR.

2.3.6 Agarose gel electrophoresis

Agarose gel electrophoresis was performed to separate and identify nucleic acids according to their length. PCR products migrate at different rates depending upon their size towards a positive charge when an electric field is applied.

Typically, 1.5% (w/v) agarose gels were prepared by adding 6g of ultrapure agarose powder (Sigma-Aldrich, Gillingham, UK) to 400ml 1 x tris-acetate-EDTA acid solution (TAE) (40mM tris, 20mM acetic acid, 1mM EDTA, pH 8.0) buffer and heated in the microwave. Once the agarose granules had all melted, 5µl of Ethidium Bromide (EtBr) (10µl/100ml, final concentration 0.5µg/ml) was added and mixed by gentle swirling. The liquid was cooled to approximately 60^{o}C and then poured into a cassette and a comb inserted to form the wells. Once set, the gel was placed into an agarose gel electrophoresis system (Bio-Rad Labs Ltd, Hertfordshire, UK) containing TAE buffer. The comb was removed and 6µl of 100bp ladder (New England Biolabs, Hertfordshire, UK) was added to the first well followed by 20µl of each sample. The system was then connected to a power pack and run at 90V for approximately 45 minutes or until sufficient migration had occurred. The gel was then removed carefully and placed in a Gel Doc and visualised under UV light.

EtBr intercalates with the DNA and upon exposure to UV excitation emits a fluorescent signal at 610nm. Due to the intercalation, emitted light is increased by at least 20 x which means the bands can be visualised. Furthermore, by comparing their base pair (bp) sizes with a DNA ladder made up of known fragment sizes, samples can be identified.

2.3.7 SYBR-Green quantitative RT-PCR (qRT-PCR)

SYBR-Green quantitative RT-PCR (qRT-PCR) was used to determine the expression of different genes of interest. SYBR green is able to bind to double stranded DNA (dsDNA) and will absorb blue light at λmax = 488nm and emits green light at λmax = 522nm. The amount of excited light emitted is proportional to the amount of DNA synthesized. Thus, quantification of the dsDNA can be measured and the quantity of target gene determined. For each gene of interest, samples were tested in triplicate and a non-template control (cDNA replaced by

sterile H_2O) was used to control for DNA contamination. Master mixes were prepared for each set of primers (Table 2.5).

Reaction component	Per reaction
Primers-forward and reverse mixture (250nM)	0.3 µl
SYBR Green ™ Master Mix (2x)	5.0 µl
Nuclease-free H2O	2.7 µl
cDNA (5ng/µl)	2.0 µl
Total Volume	**10 µl**

Table 2.5: The components for a single PCR reaction.

To each well of a 96 well PCR plate, 8µl of the appropriate master mix and then 2µl of each pre-prepared cDNA sample (5ng) or for controls sterile water was added. The plate was then carefully sealed with an optical film. Briefly, the plates were centrifuged at 250 x rpm for 1 minute to remove bubbles and to ensure all reagents were collected at the bottom of each well. Plates were then placed into an Applied Biosystems 7500 fast thermocycler and the conditions were optimized for each primer, the standard programme is given below.

Standard PCR programme:

Temperature	Time	Cycles
50	2 minutes	1x
95	10 minutes	1 x
95	15 seconds	40x
60	1 minute	40x

Once the run had complete, cycle threshold (CT) values for each reaction were calculated and an average for each sample was taken to determine gene expression. The transcript expression was normalized to the gene 18s rRNA. Fold change in gene expression was then calculated using the the $2^{-\Delta\Delta Ct}$ where ddCt is the change in Ct relative to 18s and experimental control as described previously (Livak and Schmittgen 2001).

2.4 Western Blotting

Western blotting was used to quantify protein expression. The proteins were extracted, separated on a polyacylamide gel and then transferred to a nitrocellulose membrane and the proteins of interest were then identified using labelled antibodies.

2.4.1 Protein preparation from whole cell extracts

Cell pellets were prepared by centrifuging cell culture media at 13000 x rpm for 10 minutes. Gently, the supernatant was discarded and the cell pellet was washed twice with sterile 1 x PBS. Total protein was extracted from the cell pellets into an appropriate volume of lysis buffer (50-100µl) (20mM Tris pH 7.4) containing 1 x protease inhibitors (Sigma-Aldrich,Gillingham, UK).

2.4.2 Protein preparation from primary tissue

Primary tissues of interest were dissected with sterile tools and then transferred into clean eppendorfs and snap frozen by immersing in liquid nitrogen. Samples were stored at -80^{o}C for future use or for immediate use, were homogenized. Lysis buffer containing protease inhibitor was added, the volume being dependent upon amount of tissue present (~5mg tissue ~300µl lysis buffer added) and then tissues were homogenised by firstly mashing and then by sonication as described in section 2.3.1. The samples were then centrifuged at 16000 x rpm for 20 minutes at 4^{o}C after which the supernatant was transferred to a clean eppendorf on ice and the pellet discarded.

2.4.3 Quantification of protein by Lowry assay and sample preparation

To determine protein concentrations of cell and tissue lysates a Lowry assay using BSA standards (0-20ug/ml) (Table 2.6) was performed. ABC buffer was prepared by adding 500µl of Lowry B (2% w/v sodium tartrate) and 500µl of Lowry C (1% w/v copper sulphate) to 50ml of Lowry A (2% w/v Na2CO3, 4% w/v NaOH,). To each eppendorf, 50µl of dH_20, 1ml of Lowry A and 5µl of sample was added and incubated at room temperature for 10 minutes. 100µl of Folin and Ciocalteau's phenol reagent (Sigma-Aldrich, Gillingham, UK) diluted 1:1 in dH_20 was added and incubated for a further 20-30 minutes at room temperature. Each sample was then read at an absorbance of 750nm. A calibration curve was generated using the absorbance of the standards and from this the concentration

in the samples was determined. The protein samples were diluted to 1µg/µl in reducing loading buffer (62.5mM Tris Buffer pH 6.8, 10% (v/v) glycerol, 2% (w/v) SDS 100mM Dithiothreitol (DTT) and 0.02% (w/v) bromophenol blue) and then denatured at 90°C-100°C for 5-10 minutes on a heat block. Once cool, samples were loaded onto an SDS-page gel as described in the following section.

Standard	BSA stock (20mg/ml) to add (µl)	dH_20 to add (µl)
0	0	100
1	5	95
2	10	90
4	20	80
5	25	75
8	40	60
10	50	50
12	60	40
15	75	25
20	100	0

Table 2.6: Preparation of BSA standards.

2.4.4 SDS-page gel electrophoresis

SDS (sodium dodecyl sulphate) is an amphipillic 12 carbon alkyl sulphate molecule which denatures proteins and imparts a negative charge around the polypeptide chains. In SDS page gel electrophoresis, samples are loaded onto the gel and an electric field is applied and the negatively charged proteins separate and migrate through the gel towards the anode. The speed of migration is dependent upon their molecular weight; larger proteins travel more slowly through the gel compared to smaller proteins.

Typically gels were prepared 9/12/14% (w/v) bis-acrylamide, 375mM Tris buffer pH 8.8, 0.1% (w/v) SDS, 0.05% (w/v) ammonium persulphate and 0.05% (v/v) Tetramethylethylenediamine (TEMED) and in order to remove air bubbles and to achieve a straight gel a layer of 100% isopropanol (200µl) was added. Once the gels had set (~30 minutes) isopropanol was removed and the gels were washed with dH_20. A 4% stacking gel (4% (w/v) acrylamide, 125mM Tris buffer pH 6.8, 0.1% (w/v) SDS, 0.05% (w/v) ammonium persulphate and 0.1% (v/v) TEMED)

was then cast on top of the separating gel and a comb was inserted to create wells for the samples. Once the stacking gel had polymerised, the combs were removed and the wells were washed with dH_20 and placed into the electrophoresis tank filled with electrode running buffer (ERB) (20mM Tris, 160mM glycine, 0.08% (w/v) SDS, pH 8.3). 15-30µg of total protein was then loaded into each well alongside 6µl of Colour burst molecular weight size marker (Sigma-Aldrich, Gillingham, UK) and the gel was connected to a power pack and run at 100V. As soon as the samples had reached the bottom of the gel it was removed and equilibrated by immersing in cold transfer buffer (25mM Tris, 192 mM glycine and 20% (v/v) methanol, pH 8.3) to ensure that gel shrinkage did not occur whilst transferring.

2.4.5 Electro-transfer of proteins

After separation, the proteins were transferred onto nitrocellulose membranes. During this transfer process, the negatively-charged proteins migrate towards the positively-charged cathode.

The gel and the nitrocellulose membrane were sandwiched together between transfer sponges and 3mm filter paper (pre-soaked with cold transfer buffer) and then clamped together, making sure no air bubbles were present.
This was then placed into the tank containing transfer buffer and an electric field was applied at 100V for 1-2 hours. A magnetic stirrer and an ice block were also in the tank to prevent over-heating. The membranes were then removed and washed briefly in TBS-T (Tris-Buffered Saline Tween;0.2M NaCl, 20mM Tris, pH 7.4 and 0.05% (v/v) tween) to remove traces of methanol and were then cut carefully into sections if necessary. To inhibit non-specific binding, membranes were blocked for one hour at room temperature or overnight at 4°C in TBS-T containing 3% non-fat milk and then washed 3 x 5 minutes in TBS-T.

2.4.6 Immunodetection of proteins

Membranes were probed with primary antibodies (Table 2.7) at either room temperature or overnight at 4^oC in incubation buffer (0.03% non-fat milk in TBS-T) on a roller mixer. Membranes were then washed 3 x 5 minutes in TBS-T followed by incubation for 1 hour at room temperature with an appropriate secondary HRP conjugated antibody (Table 2.7) in incubation buffer. The

membranes were then washed up to an hour with 4-6 changes of 1 x TBS-T. If re-probing membranes for proteins of similar size, the membranes were stripped using western blotting stripping buffer (eBiosciences, Hatfield, UK) which removes the antibodies, preferentially without affecting the proteins. Once the membrane was stripped it was washed thrice in TBS-T, blocked and re-probed as described above.

Antibody	Dilution	Molecular Weight (kDa)	Supplier (Product Code)
CXCR4 (Mouse monoclonal)	WB-1/1000 IHC-1/500	39	R and D MAB172
CXCR4 (Rabbit polyclonal)	WB-1/1000 IHC-1/500	39	Abcam Ab2074
CXCL12 (Mouse monoclonal)	WB-1/1000 IHC-1/500	11	R and D MAB350
CXCL12 (Rabbit polyclonal)	WB-1/500 IHC-1/500	11	Santa Cruz Sc-28876
CXCL12 (Rabbit polyclonal)	WB-1/1000 IHC-1/500	11	Abcam Ab9797
CXCL12 (Rabbit polyclonal)	WB-1/1000 IHC-1/500	11	Abcam Ab25117
B-actin (Mouse monoclonal)	WB-1/3000 IHC N/A	43	Sigma-Aldrich A5441
CK-19 (Mouse monoclonal)	WB N/A IHC-1/500	N/A	Abcam Ab8591
CK-19 (Rabbit monoclonal)	WB N/A IHC-1/500	N/A	Abcam Ab52625
Anti-vimentin (Mouse monoclonal)	WB/N/A IHC-1/1000	N/A	Sigma V6300
Anti-vimentin (Mouse monoclonal)	WB/N/A IHC-1/1000	N/A	Abcam Ab8978
α-SMA-FITC (Mouse monoclonal)	WB N/A IF-1/1000	N/A	Sigma-Aldrich F3777

anti-mouse-HRP 2º (goat)	WB – 1/6000 IHC – 1/200	N/A	Dako P0447
anti-rabbit-HRP 2º (goat)	WB – 1/3000 IHC – 1/200	N/A	Dako P0448
anti-mouse FITC-HRP 2º (rabbit)	WB N/A IF – 1/200	N/A	Dako P5100
anti-rabbit-FITC 2º (sheep)	WB N/A IF – 1/200	N/A	Sigma-Aldrich F7512
anti-rabbit-TRITC 2º (swine)	WB N/A IF – 1/400	N/A	Dako R0156

Table 2.7: Antibodies specifications.

The proteins were visualized using the ECL kit (GE Healthcare Life Sciences, Buckinghamshire, UK) which works on the principle that the reagents bind to the HRP conjugated on the secondary antibody which catalyses the formation of $2H_2O + O_2$ from peracid. Consequently, resulting in degradation of Luminol via peroxidise catalysed degradation and therefore chemiluminscence is produced (Figure 2.3).

In brief, reagent 1 and 2 were mixed at a ratio 1:1 and applied to the membranes for 30 seconds. Any excess reagent was removed and then the membranes were carefully covered in a saran wrap and taped into a developing cassette. The membranes were developed in the dark room by placing a photographic film (CL-Xposure^{Tm} film) (Fisher Scientific, Loughbrough, UK) on top of the wrapped nitrocellulose, sealed into the cassette for a pre-determined time and then was developed by placing the film into the developer. To determine protein expression levels, quantitative densitometry of signal intensity was carried out using Image J and all values were normalized to the housekeeping protein β-actin

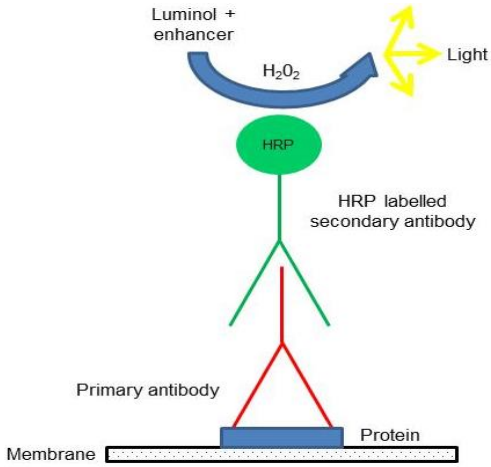

Figure 2.3: The production of luminescence via ECL.

2.4.7 Coomassie blue gel staining

Gels were removed from the electrophoresis apparatus and rinsed in dH_2O and then transferred into GelCode Blue Stain reagent (Fisher Scientific UK Ltd, Loughbrough,UK) at 1 hour at room temperature. To destain the gels they were placed in water for at least one hour and then visualised on an Alpha Innotech flurorescent imaging system and processed using Fluorchem software.

2.4.8 Ponceau staining

Ponceau S is a sodium salt of a diazo dye that can be used to check for the efficiency of the transfer of proteins. Membranes were incubated in ponceau S solution for 2 minutes on a rocker at room temperature and then to visualise the proteins, the membranes were transferred into dH_20.

2.5 Immunohistochemistry

2.5.1 Immunohistochemistry

Archival human liver tissue was obtained with full ethical approval and written informed consent from the Newcastle & North Tyneside Research Ethics Committee.

Tissues were fixed in 10% (v/v) formalin (Fisher Scientific, Loughborough, UK) diluted in 1 x PBS for 24 hours and then processed through increasing concentrations of ethanol. Tissues were embedded in paraffin and sections were

cut (4-8µm) and mounted onto super frost microscope slides and incubated overnight at 37ºC.

Tissue sections were de-waxed in xylene (Fisher Scientific, Loughborough, UK) for 10 minutes and then rehydrated in 100% and then 95% ethanol (Fisher Scientific, Loughborough, UK) for 3 minutes each and then placed into water. To break the protein cross-links formed by formalin fixation and to reveal antigenic sites an antigen retrieval process was carried out. Antigen retrieval was performed by immersing sections into 0.01M citrate buffer pH6 in a pressure cooker and timing for 1 minute once pressure of the system was reached. Tissue sections were then cooled with water, outlined with a hydrophobic pen and then incubated in 3% (v/v) hydrogen peroxide H_2O_2 prepared in methanol for 10 minutes to ensure endogenous peroxide activity was quenched. Tissue sections were then washed in 1 x PBS prior to blocking non-specific binding of antibodies with 20% FCS (v/v) in 1 x PBS for 30 minutes. Primary rabbit antibodies were diluted in 1 x PBS containing 0.05% (v/v) FCS (Table 2.7), added to each section and then incubated overnight at 4ºC. Following overnight incubation, sections were washed 2 x for 5 minutes in 1 x PBS before being incubated for 1 hour at room temperature with the appropriate secondary HRP antibody (Table 2.7). Following a final 2 washes x 5 minutes in 1 x PBS, staining was developed using diaminobenzidine (DAB) (Dako UK Ltd, Cambridgeshire, UK) which is oxidized by hydrogen peroxide and a dark brown colour is observed. The DAB was added to each section (~200µl) and incubated for 1 minute and then washed in water prior to haematoxylin staining. Sections were counterstained with haematoxylin for 2 minutes, washed with water and then stained with Scotts tap water (Fisher Scientific, Loughborough, UK) for 30 seconds. Finally, sections were dehydrated briefly through a series of ethanols (50%, 75%, 95%, 100%) and then cleared in xylene for 10 minutes prior to mounting in Depex (DPX) (Sigma-Aldrich, Gillingham, UK).

2.5.2 Haematoxylin and Eosin (H & E) staining

Haematoxylin (stains the nuclei blue) and eosin (stains the cytoplasm red) is the most common staining method used in histology. Tissue sections were de-waxed and rehydrated as described in section 2.5.1. They were then stained in haematoxylin for 2 minutes, washed with normal tap water and then immersed in

Scott's tap water for 30 seconds. Tissue sections were then counter stained in eosin (Fisher Scientific, Loughborough, UK) for 30 seconds, washed in water and then dehydrated and mounted as described in section 2.5.1.

2.5.3 Sirius red staining

Picro-sirius red binds to collagen due to its sulphonic groups reacting with the basic groups found in collagens and so is ideal for determining levels of fibrosis in tissue (Wallace, Burt et al. 2008). Tissue sections were de-waxed and rehydrated as described in section 2.5.1. They were then immersed in picro-sirius red for 2-3 hours and then washed in 2 x 0.5% (v/v) acetic acid prepared in dH_2O. Finally, sections were dehydrated and mounted as described in section 2.5.1. Sirius red staining was quantified by using the Leica software programme.

2.5.4 Double immunofluorescence staining

Tissue sections were de-waxed and rehydrated and antigen retrieval carried out as described in section 2.5.1. Tissue sections were then washed in 1 x PBS prior to blocking non-specific binding of antibodies with 20% FCS (v/v) in 1 x PBS for 30 minutes. Primary rabbit antibodies were diluted in 1 x PBS containing 0.05% (v/v) FCS (Table 2.7), added to each section and then incubated overnight at 4^{o}C. Antibodies were added together if raised against different species for example, rabbit against target-1 and mouse against target 2. No primary antibody controls were incubated with blocking buffer alone. Following overnight incubation, sections were washed 2 x for 5 minutes in 1 x PBS before being incubated in the dark for 1 hour at room temperature with the appropriate flurochrome secondary antibody (Table 2.7). Sections were then counterstained with DAPI (4',6-diamidino-2-phenylindole) for 10 minutes and then rinsed in 1 x PBS for 5 minutes. DAPI is a fluorescent probe that binds to AT regions of double stranded DNA, thus cell nuclei can be visualized. To quench auto-fluorescence, sections were immersed in Sudan Black (Sigma-Aldrich, Gillingham, UK) (0.3% (w/v) made up in 100% ethanol and filtered before use) and placed on a rocker for 30-45 minutes. After rinsing in 1 x PBS 4 x 10 minutes, sections were mounted with a cover slip with a small drop of fluorescence mounting medium (Dako UK Ltd, Cambridgeshire, UK) and the cover slip edges sealed with nail varnish to prevent drying and movement under the microscope.

Sections were observed under confocal microscopy using a Leica TCS SP II laser-scanning confocal microscope and LCS Lite 2.61 software. The basic principle behind confocal microscopy is that it uses point illumination in order to eliminate out-of focus signal. This is achieved by the pinhole being located in front of the detector thus, allowing only fluorescence to be detected when close to the focal plane.

2.5.5 Immunocytochemistry

For fluorescence microscopy, cells were grown in 6 well plates. The media was removed from the 6 well plates and washed twice in 1 x PBS. Cells were permeabilized with 100% methanol (Fisher Scientific, Loughborough, UK) for 10 minutes and fixed with fixation buffer (2% (v/v) formaldehyde, 0.2% (v/v) glutaraldehyde in PBS, pH7.4) for 20 minutes at -20^{o}C. If cells were not stained immediately they were stored with 2mls of 1 x PBS in each well at 4^{o}C. For staining, cells were blocked with 2mls of 20% FCS (v/v) in 1 x PBS for 30 minutes. Cells were then incubated in the presence or absence of a primary antibody (Table 2.7) at room temperature for 1 hour or overnight at 4^{o}C. After incubation, cells were washed 2 x 5 minutes with 1 x PBS with gentle agitation and detected with the appropriate secondary antibody (Table 2.7) in the dark to prevent quenching of fluorescence signal. They were then washed a further 4 times in 1 x PBS for 5 minutes each. The PBS was removed and cells were counterstained with DAPI for 10 minutes, the cells were washed in 1 x PBS for 2 x 5 minutes and images were captured by fluorescence microscopy.

2.6 ELISA

2.6.1 ELISA for secreted CXCL12

To measure CXCL12 secretion in conditioned media, an Enzyme-linked immunosorbent assay (ELISA) kit (Quantikine® Colorometric ELISA) was performed according to the manufacturer's instructions (R&D Systems, Inc., Minneapolis, USA). In brief, samples and standards were pipetted into the wells of a 96 well plate pre-coated with a CXCL12 specific antibody. CXCL12 present (if any) bound to the immobilised antibody whereas the unbound materials were removed by washing the plate thrice. A monoclonal antibody specific to CXCL12 was added and the plate was washed thrice in wash buffer provided. Following

this, the secondary antibody was added to the wells and the plate was washed thrice. The substrate solution was added and incubated in the dark for 30 minutes prior to the stop solution and was then measured at an optical density at 450nm within 30 minutes on a Bio Rad 680 Microplate Reader (Bio Rad, California, USA) and wavelength correction was set at 570nm. A reference curve generated from standards using purified recombinant murine CXCL12 was used to determine the secreted CXCL12 concentration.

2.7 Transwell chemotaxis assays

Migration assays were utilised to investigate the chemotaxis properties of cells *in vitro*. Chemotaxis was assayed using specialised 24 culture insert companion plates (VWR International, Leicestershire, UK).

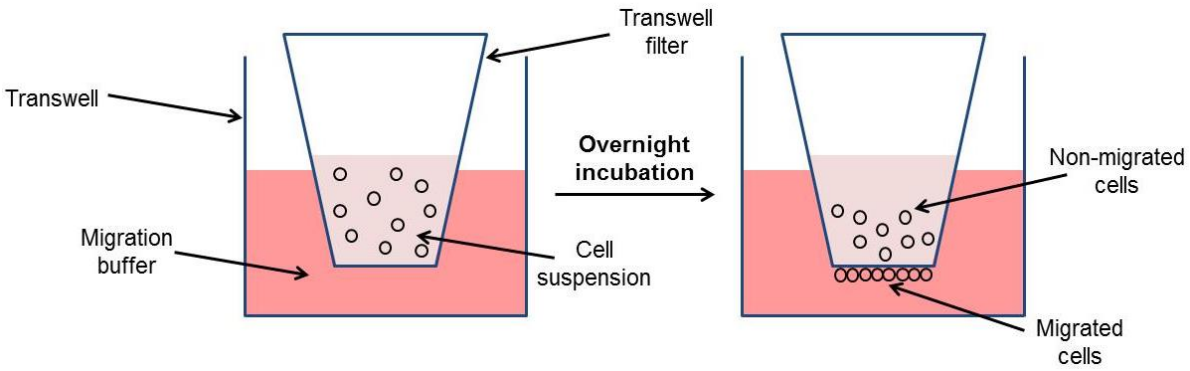

Figure 2.4: Set up of the transwell migration assay.

To prepare these plates for use, each well was blocked with 1% (w/v) BSA (Sigma-Aldrich, Gillingham, UK) diluted in RPMI (Roswell Park Memorial Institute)-1640 medium for 1 hour at room temperature. Prior to the addition of the cell culture filter insert (8µm diameter pore size), each insert was also pre-coated on the under-side with 150µl of 2.5µg/ml fibronectin (Sigma-Aldrich, Gillingham, UK) prepared diluted in RPMI-1640 medium for 1 hour at room temperature. Following 1 hour incubation, the excess fluid was removed from all of the wells and filter inserts allowed to air dry at room temperature for 2 hours. 800µl of RPMI-1640 medium containing 0.1% (w/v) BSA was then added to each well in the presence or absence of recombinant human CXCL12 ligand (100ng/ml) or conditioned media. 200,000 of cells (serum starved overnight)

were then added to each pre-coated cell culture filter before insertion into the corresponding well +/- AMD11070/AMD3100.

The chemokine inhibitors AMD3100 and AMD11070 (Genzyme Drug Discovery and Development, Waltham, MA, USA) were prepared as 1mg/ml stock solutions in normal saline solution and citric acid/normal saline solution respectively, according to the manufacturers specifications (Genzyme Ltd, 2010) and were kept at 4^{o}C, shielded from light and used within one week of preparation. AMD3100 was further diluted and added to cell cultures in normal saline solution and AMD11070 in citric acid/normal saline and again. Both AMD3100 and AMD11070 were used at clinically achievable concentrations as described previously (Mosi, Anastassova et al. 2012) and an equal volume of vehicle was used to treat control cells which in all assays did not exceed 0.01% of the total culture volumes.

To prevent evaporation, surrounding wells were filled with sterile 1 x PBS and the lid was placed carefully on top. The plates were then incubated for overnight at 37°C. The inserts were removed from the 24 well plates with sterile forceps and the inserts were swabbed gently with a cotton bud to remove the non-migrating cells. The cells were then fixed through the addition of 1 ml of 100% ice cold methanol (Fisher Scientific, Loughborough, UK) and incubated overnight (or for at least 3 hours) at -20^{o}C before washing three times in dH_20. To visualise cells which had migrated through the pores of the cell culture inserts, each insert was stained with haematoxylin for 10 minutes at room temperature before washing once for 10 minutes with Scott's tap water and final dehydration through 50, 75, 90 and 100% ethanol each for 1 minute. Once dry, the filter membrane from each insert was then cut out carefully with a scalpel blade and mounted with a cover-slip and DPX onto glass microscope slides. The number of migrated cells were counted blindly under a Leica light microscope using a 10x objective and normalized to controls.

2.8 Adhesion assays

To assess adhesion of B16-F10 cells adhesion assays were carried out. Transwell inserts (3µm pore size) were coated on both sides with 4µg/mL bovine collagen (type 1) (Sigma-Aldrich, Gillingham, UK). 4 x 10^4/ml of murine stellate

cells (JS-1) were seeded on the bottom of the insert and allowed to adhere for 1 hour and then placed in 24 wells plates in normal media and incubated. After 24 hours, 3 x 10^4/ml transformed sinusoidal endothelial cells (TSECs), were plated in the inner chamber of the insert and incubated for 48 hours. After 48 hours, murine melanoma cells (B16-F10) were labelled by incubating with 2µM Carboxyfluorescein Diacetate Succinimidyl Ester CFSE (Invitrogen, Paisley, UK) for 30 minutes at 37°C. The cells were then washed in 1 x PBS and then re-suspended at 4 x 10^5/ml in serum free RPMI and 500µl added inside the insert. After 1 hour of incubation, non-adherent cells were removed by gently washing 3 x in 1 x PBS. Cells were fixed and then mounted onto slides with Vectashield containing DAPI (Vector Laboratories, Burlingame, USA). Cells were counted blindly in 10 random fields of view at x 10 magnification and normalized to controls.

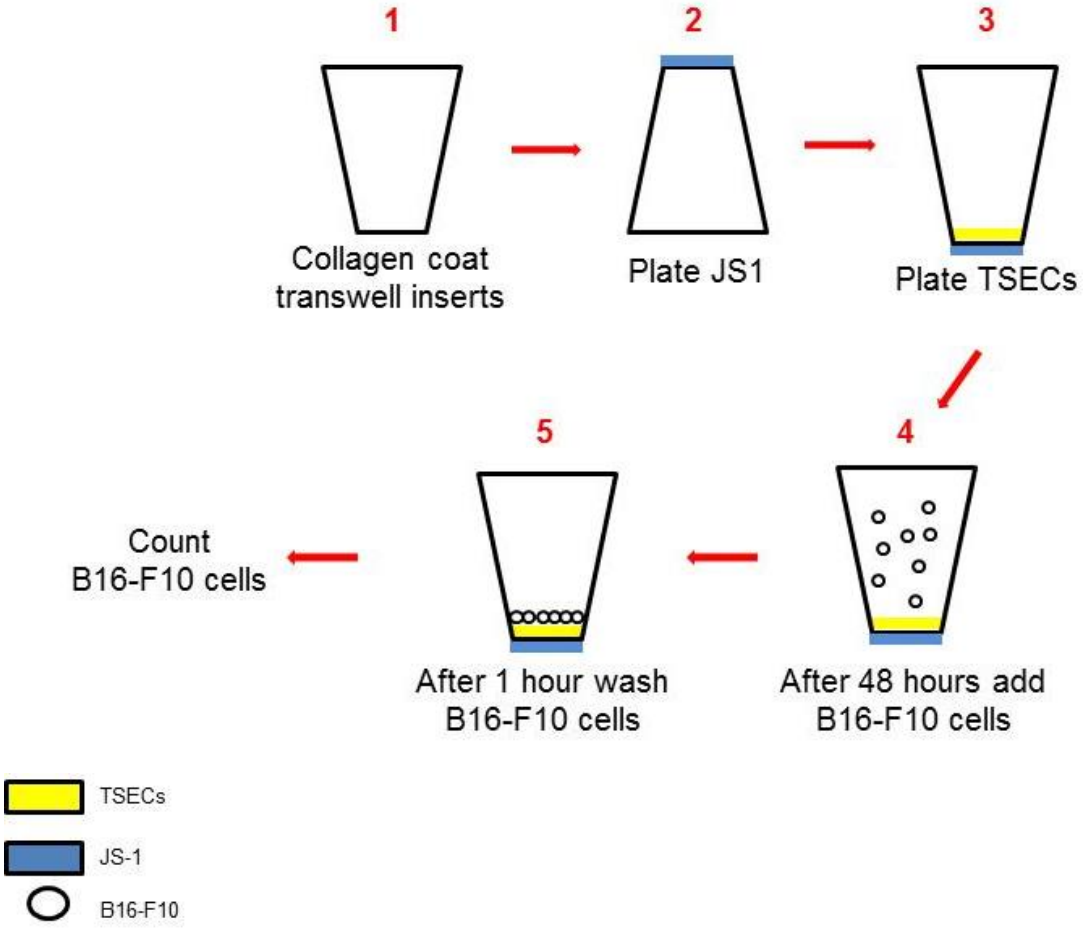

Figure 2.5: Adhesion assay set up adapted from (Saiman 2012).

2.9 Cytokine array

A cytokine array was performed using the R and D Systems Human Cytokine Array, Panel A (R&D Systems, Inc., Minneapolis, USA). This kit simultaneously detects the relative levels of 36 different cytokines and chemokines (Table 2.9.1) in a single sample. In brief, the cell extract was mixed with a cocktail of biotinylated detection antibodies and then incubated with the nitrocellulose membranes which were spotted with capture antibodies. The cytokines/chemokines present in the sample bound to the cognate immobilized antibody present on the membranes. Streptavidin-Horseradish Peroxidase and chemiluminescent detection reagents were then added and then developed in the same way as a Western blot (section 2.4.6). A signal was produced in proportion to the amount of cytokine/chemokine bound. After detection, the array data was analysed by determining the average signal (pixel density) of the pair of duplicate spots representing each cytokine by using Image J analysis.

2.10 Statistical analysis

Results were analysed using Excel 2003 (Microsoft) and Prism version 5 (Graph pad, San Diego, USA) and expressed as the mean ± standard deviation (SD). The statistical significance of each experiment was analysed using Prism and compared by one way Analysis of Variance (ANOVA) with Dunnett's or Bonferroni's post-hoc correction or Student t-tests and significance was indicated by the P value * $P < 0.05$, ** $P < 0.001$, *** $P < 0.0001$.

Chapter 3: Results 1

CXCR4 expression in melanoma mediates migration of tumour cells towards CXCL12 secreting liver cells *in vitro.*

3.1 Introduction and Aims

Over the past decade, substantial evidence has highlighted an important role for the CXCR4-CXCL12 chemokine axis in melanoma progression (Kim, Mori et al. 2006, Lee, Kakinuma et al. 2006, Scala, Giuliano et al. 2006, Di Cesare, Marshall et al. 2007, Schutyser, Su et al. 2007, Bartolome, Ferreiro et al. 2009, Li, Yang et al. 2009, Franco, Botti et al. 2010, D'Alterio, Barbieri et al. 2012, Takekoshi, Ziarek et al. 2012). Indeed, studies have demonstrated that inhibition of this axis reduces melanoma metastasis to organs secreting high levels of CXCL12 such as the lungs (Lee, Kakinuma et al. 2006, D'Alterio, Barbieri et al. 2012). It has also been reported that factors including hypoxia increase CXCR4 expression (Schioppa, Uranchimeg et al. 2003) in tumour cells and that CXCL12 may act as a survival factor (Teicher and Fricker 2010). Thus, the development of small molecule chemokine antagonists and neutralizing antibodies may prove to be an effective novel treatment strategy for melanoma.

Although studies have demonstrated that melanoma cells migrate to the liver, they have not shown which liver cells are involved specifically. Furthermore, although it has been shown that AMD3100 inhibits melanoma migration both *in vitro* and *in vivo* (D'Alterio, Barbieri et al. 2012), the novel CXCR4 inhibitor AMD11070, which has already been tested in HIV (Mosi, Anastassova et al. 2012) has not been assessed in the context of melanoma. Therefore, the aims of this chapter were to confirm the expression of both CXCR4 and CXCL12 in melanoma cell lines and liver cell types employed in these studies *in vitro* and examine the effect of hypoxia on expression levels of these proteins. Furthermore, an additional aim was to establish the potential of AMD11070 to inhibit the CXCR4-CXCL12 chemokine axis in melanoma towards conditioned media from two main liver cell types; myofibroblasts and biliary epithelial cells.

3.2 Results

3.2.1: Both CXCR4 and CXCL12 are expressed by murine and human melanoma cell lines.

The protein expression of CXCR4 and CXCL12 was examined by Western blotting in whole cell extracts from exponentially growing murine B16-F10 melanoma cells and the house-keeping gene β-actin was used as a loading control. Since cells were to be cultured in serum free media for up to 24 hours in chemotaxis assays, expression was determined in both 10% FCS and serum free media conditions. The results demonstrated that the B16-F10 cells survived in serum free conditions (Figure 3.1A) and both CXCR4 (Figure 3.1B) and CXCL12 (Figure 3.1C) were expressed. Immunofluorescence staining was also performed since Western blot analysis does not give an indication of cellular localisation. The results illustrated that CXCR4 expression was located in both the nucleus and cellular membrane (Figure 3.1D) whereas CXCL12 was predominantly located in the cytoplasm (Figure 3.1D), 4',6-diamidino-2-phenylindole (DAPI) was used to stain the nuclei.

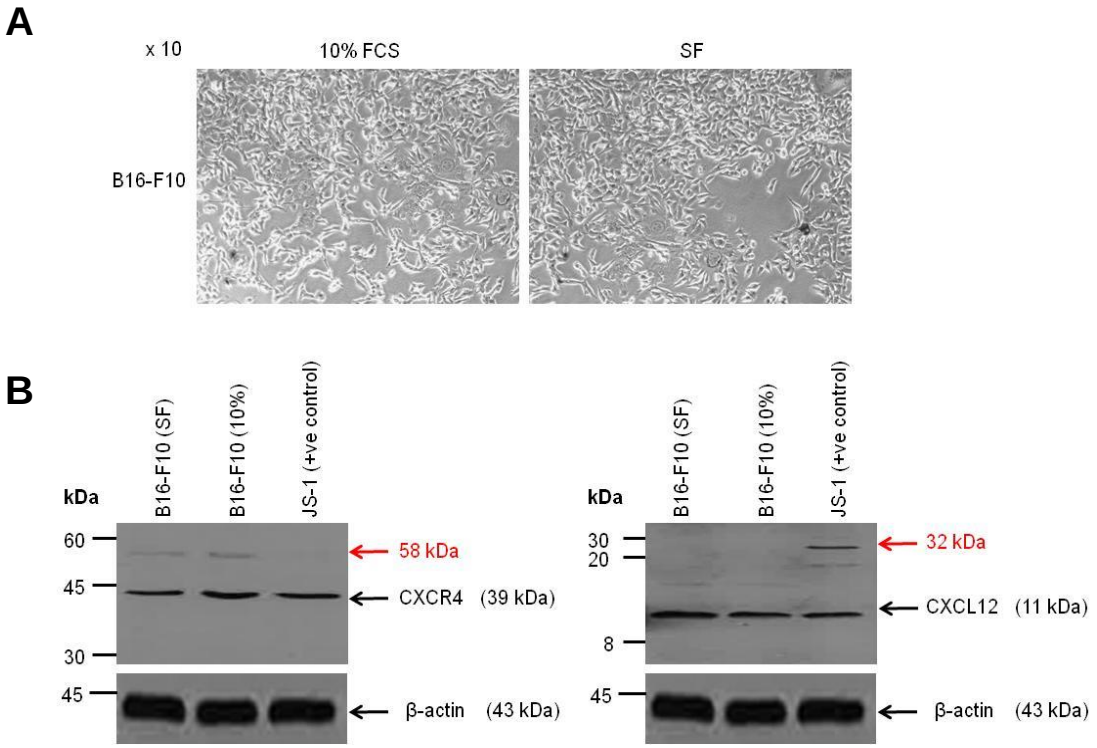

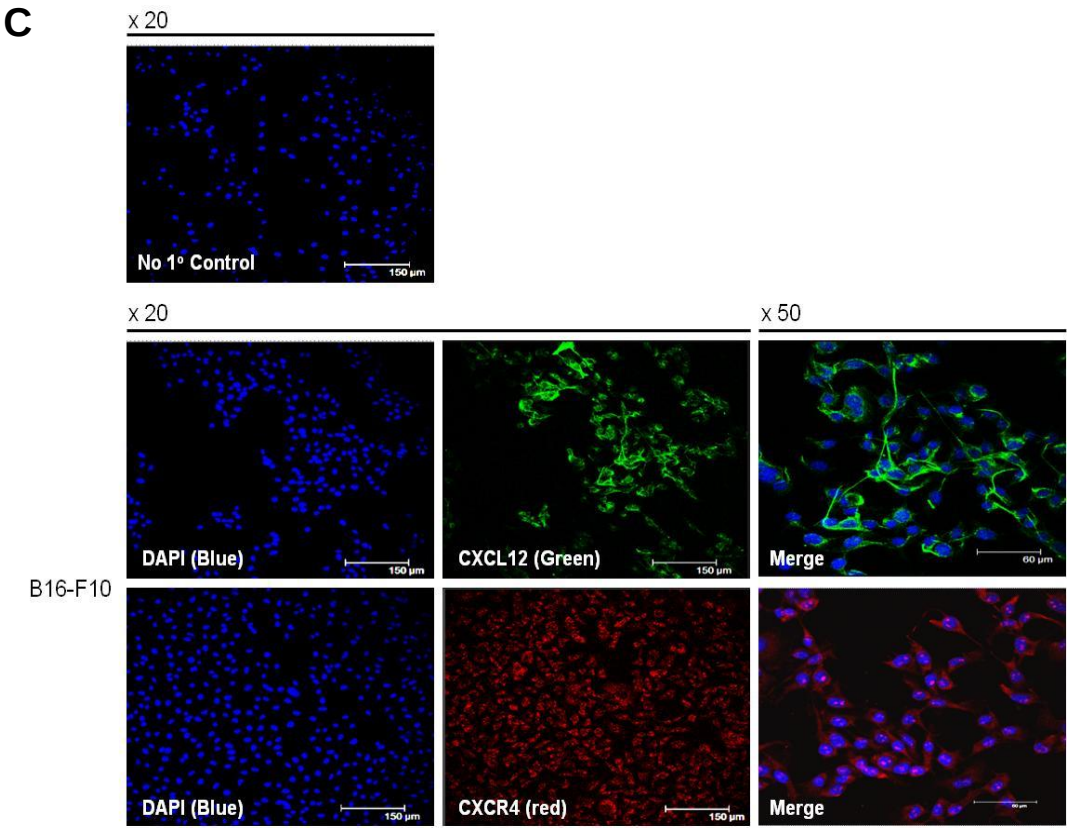

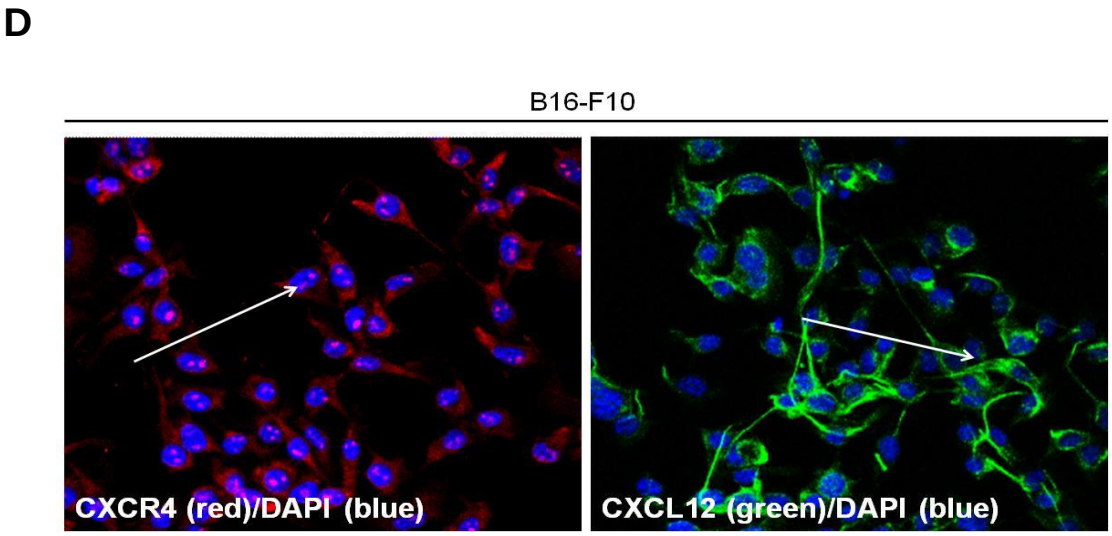

Figure 3.1: B16-F10 murine melanoma cell line expresses both CXCR4 and CXCL12.
A) Bright field images of B16-F10 cells in serum free and 10% FCS media conditions taken at x 10 magnification. **B)** Representative Western blot for the expression of CXCR4 and CXCL12 in the B16-F10 cell line. For all Western blots 20µg of protein was loaded per lane and β-actin was used as a loading control. **C)** The expression of CXCR4 (red) and CXCL12 (green) was determined in B16-F10 cells by confocal microscopy and background levels were set against the no primary control. DAPI was used to stain the nuclei. **D)** Zoomed in images. Representative images were acquired at x 20 and x 50 magnification. Scale bars = 150µm Staining is typical of three separate experiments.

Expression of CXCR4 and CXCL12 was also determined in three human melanoma cell lines (A375, CHL-1 and Wm2664) cultured in both serum free media and media supplemented with 10% FCS. Results demonstrated that all three cell lines survived in serum free conditions (Figure 3.2A) and expressed CXCR4 and CXCL12 in both conditions (Figure 3.2B). An additional band was also observed at ~58 kDa in the CXCR4 blot (Figure 3.2B). Immunofluorescence staining suggests that CXCR4 was expressed in both the nucleus and membrane (Figure 3.3C and E) while CXCL12 was observed in the cytoplasm (Figure 3.3D and E).

A

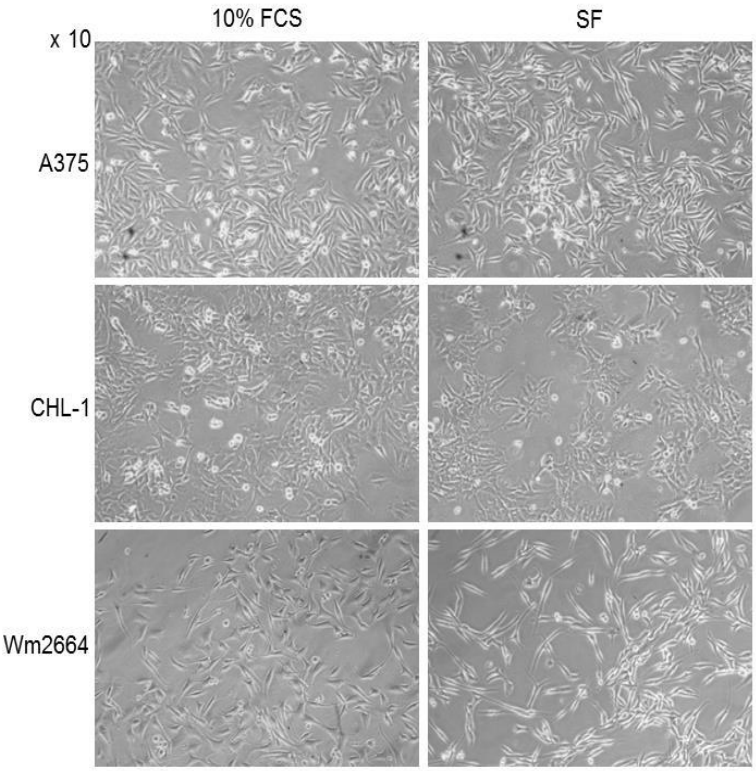

B

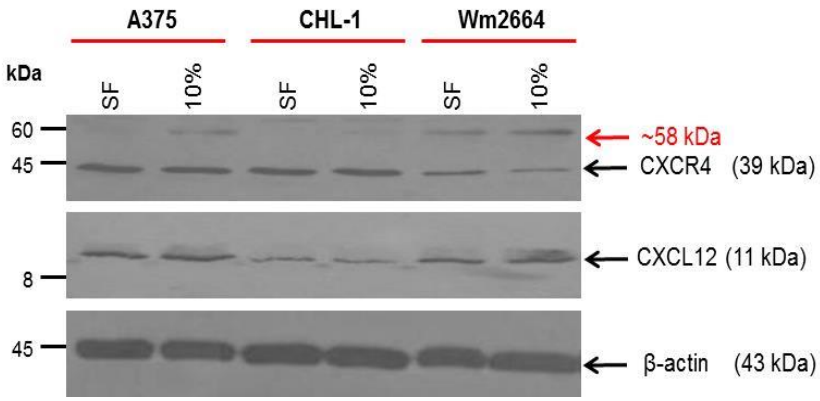

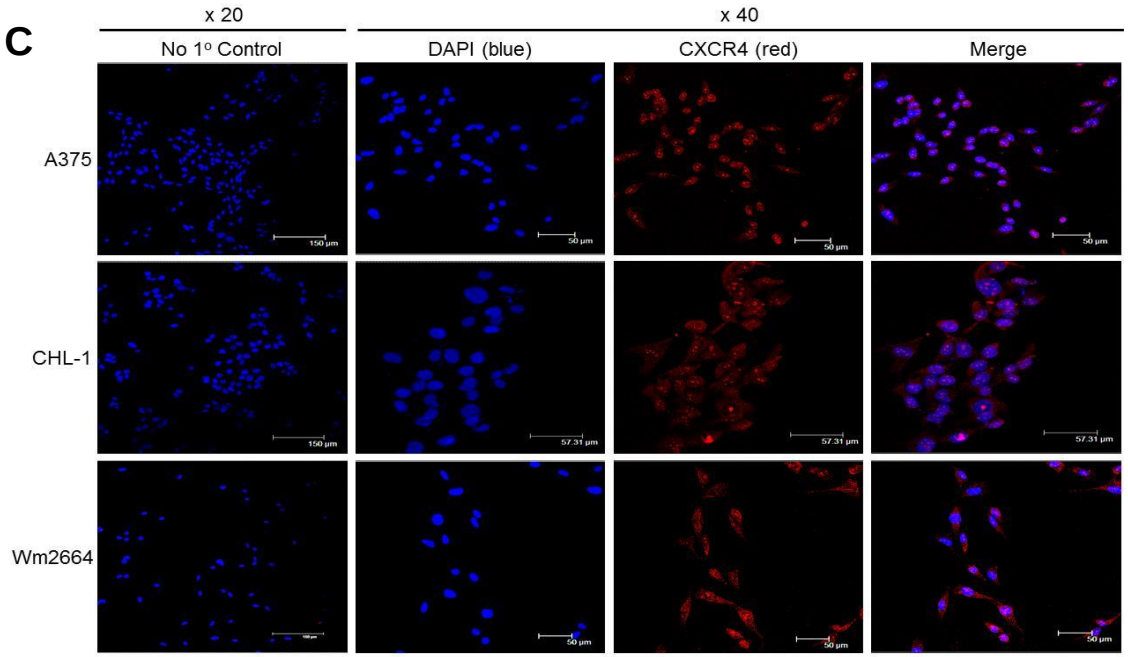
C
x 20
x 40
No 1º Control
DAPI (blue)
CXCR4 (red)
Merge
A375
CHL-1
Wm2664

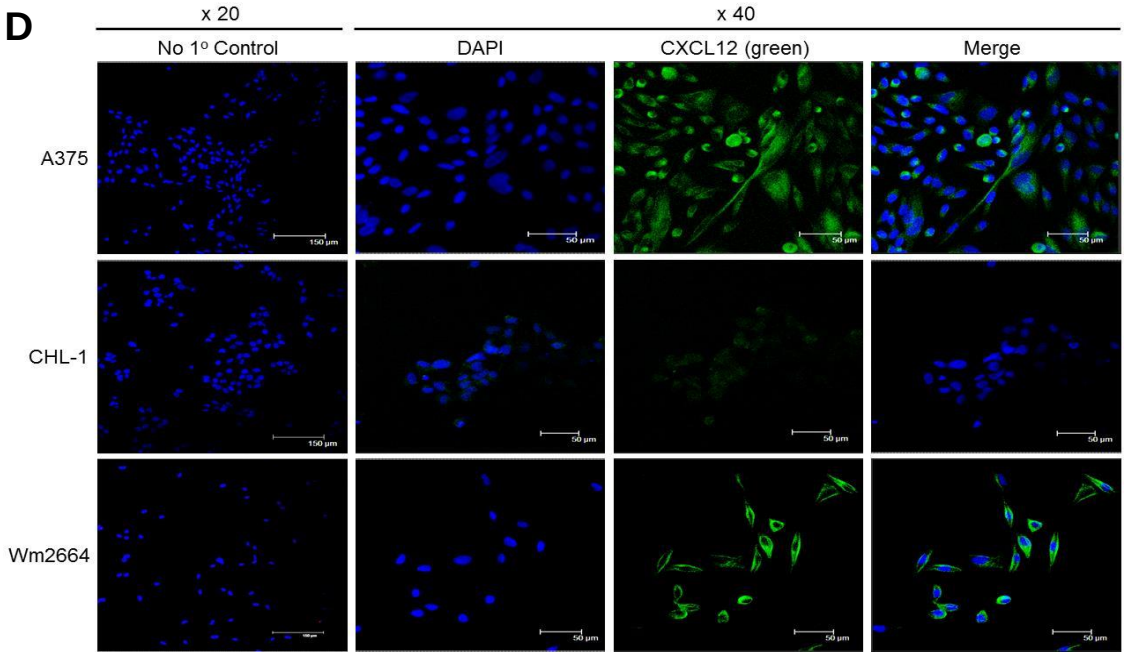
D
x 20
x 40
No 1º Control
DAPI
CXCL12 (green)
Merge
A375
CHL-1
Wm2664

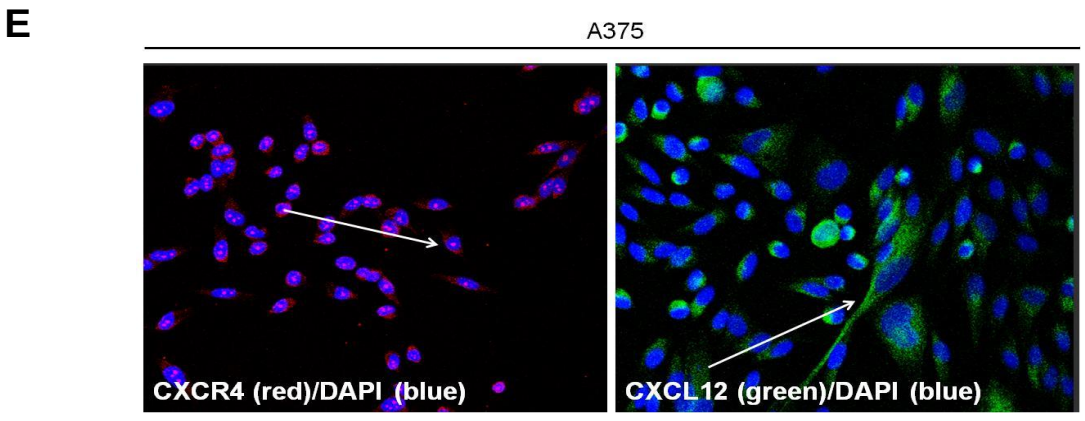
E
A375
CXCR4 (red)/DAPI (blue)
CXCL12 (green)/DAPI (blue)

Figure 3.2: Human melanoma cell lines (A375, CHL-1 and Wm2664) express both CXCR4 and CXCL12.
A) Bright field images of human melanoma cell lines in serum free and 10% FCS media conditions taken at x 10 magnification. **B)** Representative Western blot for the expression of CXCR4 and CXCL12 in the human melanoma cell lines. For all Western blots 20µg of protein was loaded per lane and β-actin was used as a loading control. **C)** The expression of CXCR4 (red) and **D)** CXCL12 (green) was determined in melanoma cells by confocal microscopy and background levels were set against the no primary control. DAPI was used to stain the nuclei. **D)** Zoomed in images. Representative images were acquired at x 20 and x 40 magnification. Scale bars = 150µm (x 20) and 50µm (x 40). Staining is typical of three separate experiments.

3.2.2: Expression of CXCR4 and CXCL12 is not detected in primary human melanocytes.

Primary human melanocytes were isolated as described in section 2.2.4 (Figure 3.3A) and Western blotting results demonstrated that at the protein level, neither CXCR4 or CXCL12 was expressed (Figure 3.3B).

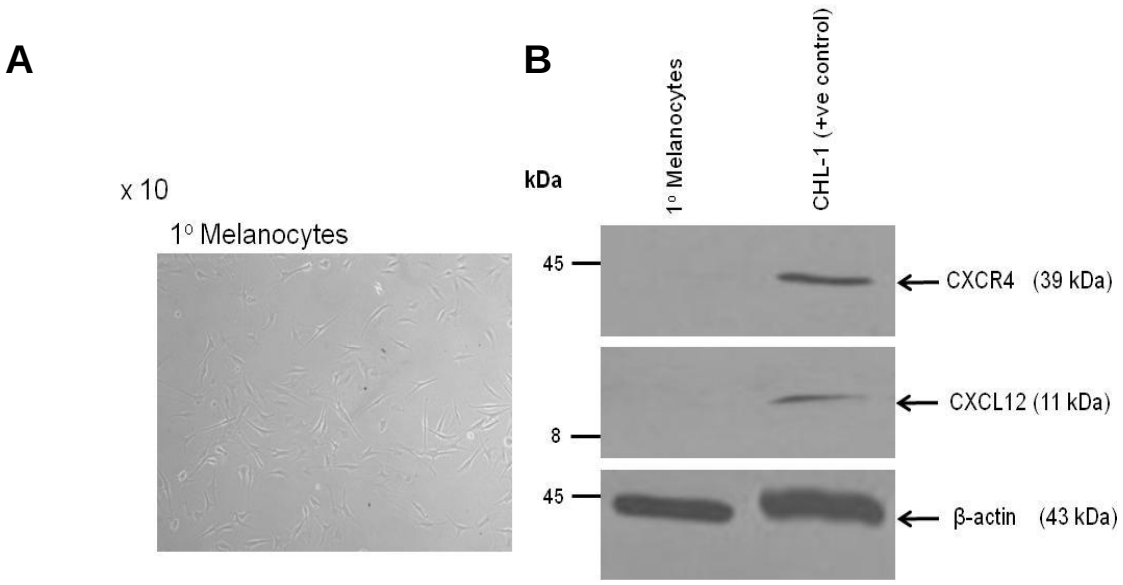

Figure 3.3: Expression of CXCR4 and CXCL12 is not detected in primary human melanocytes.
A) Bright field image of primary human melanocytes taken at x 10 magnification. **B)** Representative Western blots for the expression of CXCR4 and CXCL12 in the melanocytes. For all Western blots 20µg of protein was loaded per lane and β-actin was used as a loading control.

3.2.3 Hypoxic conditions increases expression of a protein with a higher molecular weight for both CXCR4 and CXCL12.

A375 and CHL-1 melanoma cells were incubated under normal (5 % oxygen) and hypoxic (1% oxygen) conditions for 72 hours in 10% FCS media (Figure 3.4A). Western blotting demonstrated that CXCR4 (Figure 3.4A) and CXCL12 (Figure 3.4B) expression levels remained constant when A375 and CHL-1 cell lines were cultured in hypoxic and non-hypoxic conditions. In addition to the bands observed, another band for CXCR4 at ~58 kDa size (Figure 3.4B) and for CXCL12 at ~43 kDa (Figure 3.4C) was observed. Furthermore, the expression increased for both of these bands when the cell lines were cultured in hypoxic conditions (Figure 3.4A and B).

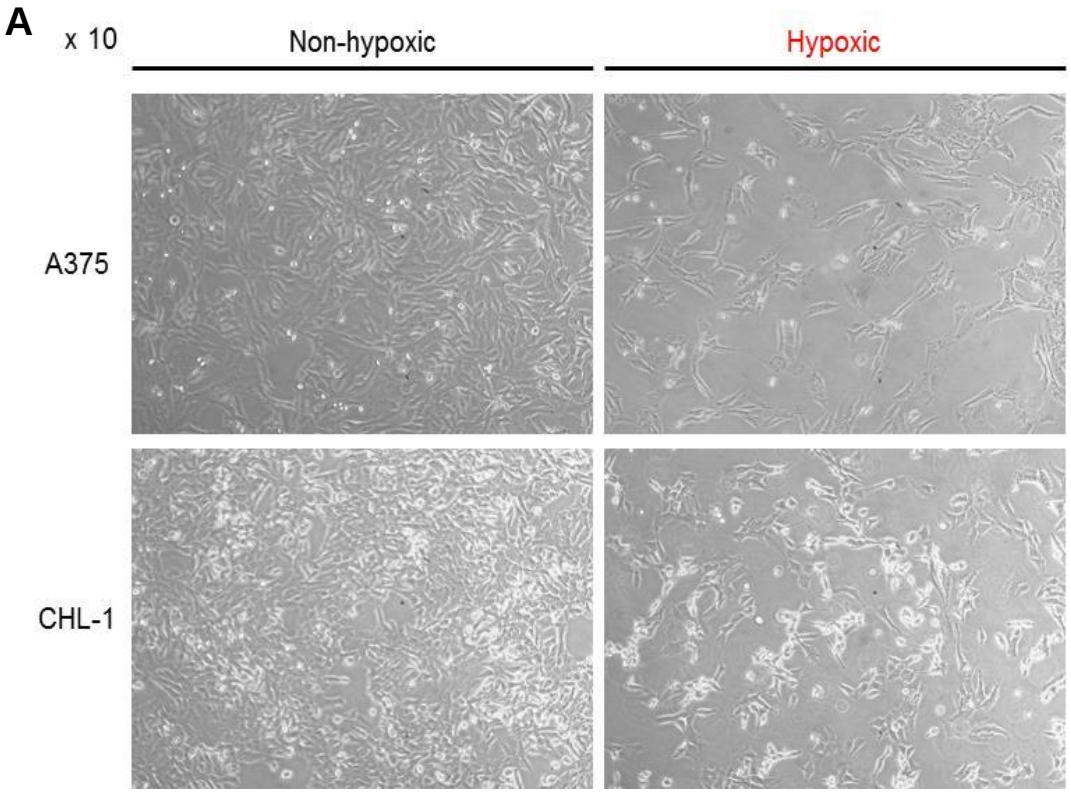

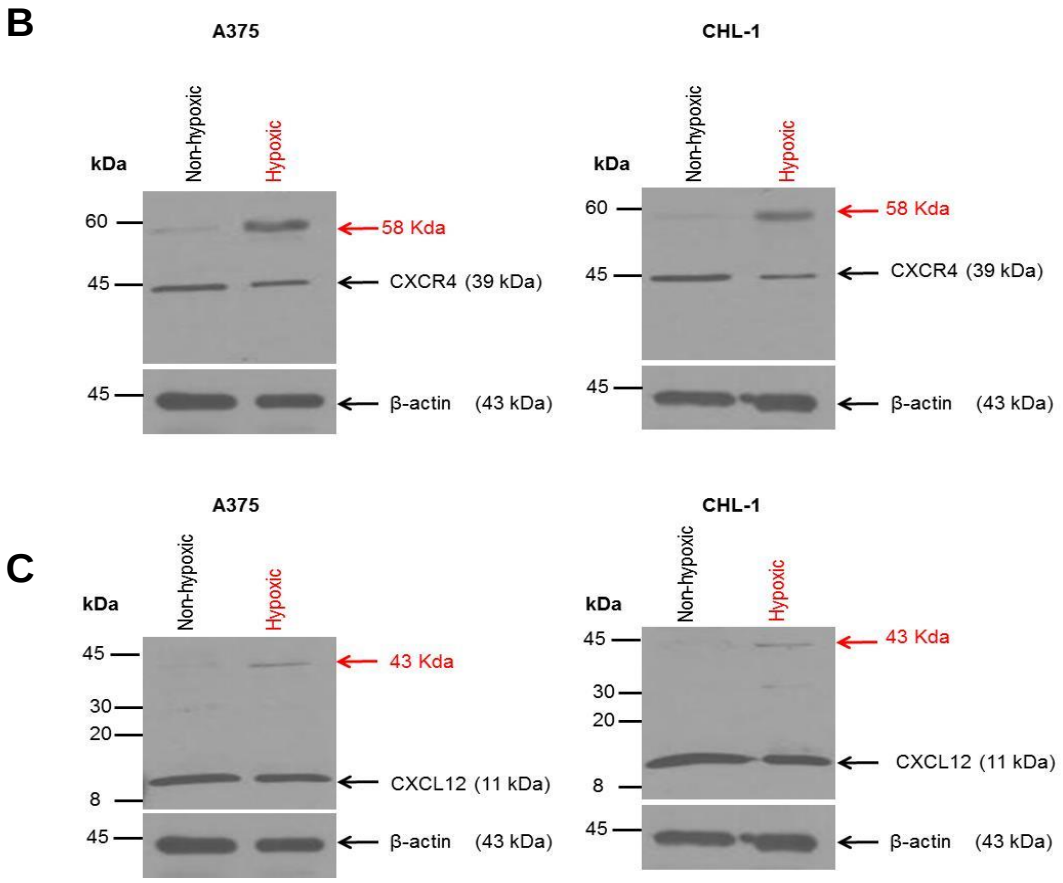

Figure 3.4: Hypoxic conditions increases expression of a protein with a higher molecular weight for both CXCR4 and CXCL12.
A) Bright field images of A375 and CHL-1 cell lines incubated in hypoxic and non-hypoxic conditions taken at x 10 magnification. **B)** Representative Western blot for the expression of CXCR4 and CXCL12 cells incubated in both conditions. For all Western blots 20µg of protein was loaded per lane and β-actin was used as a loading control.

3.2.4: CXCR4 and CXCL12 are expressed by murine stellate (JS-1) and biliary epithelial (603b) cell lines.

The protein expression of CXCR4 and CXCL12 was examined in the JS-1 stellate and 603b biliary epithelial murine cell lines (gift from Dr Yedidya Saiman, Mount Sinai School of Medicine, New York). Western blotting confirmed expression of both CXCR4 and CXCL12 (Figure 3.5A) and immunofluorescence studies illustrated CXCR4 expression in both the cell membrane and nucleus of the JS-1 (Figure 3.5C) and 603b (Figure 3.5D) cell lines while CXCL12 expression was confined to the cytoplasm in both cell lines (Figure 3.5E and F).

A x 10

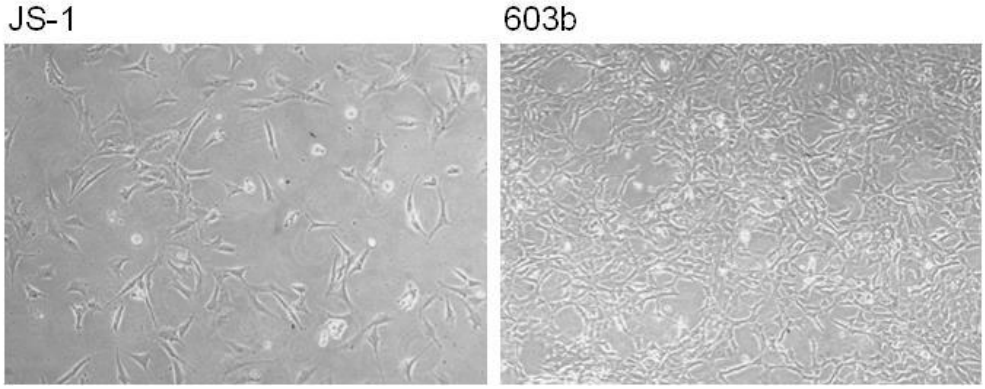
JS-1
603b

B

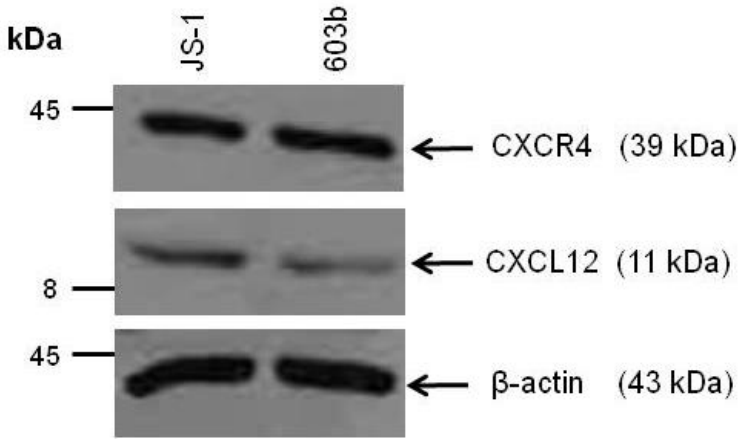
kDa
JS-1
603b
45
CXCR4 (39 kDa)
8
CXCL12 (11 kDa)
45
β-actin (43 kDa)

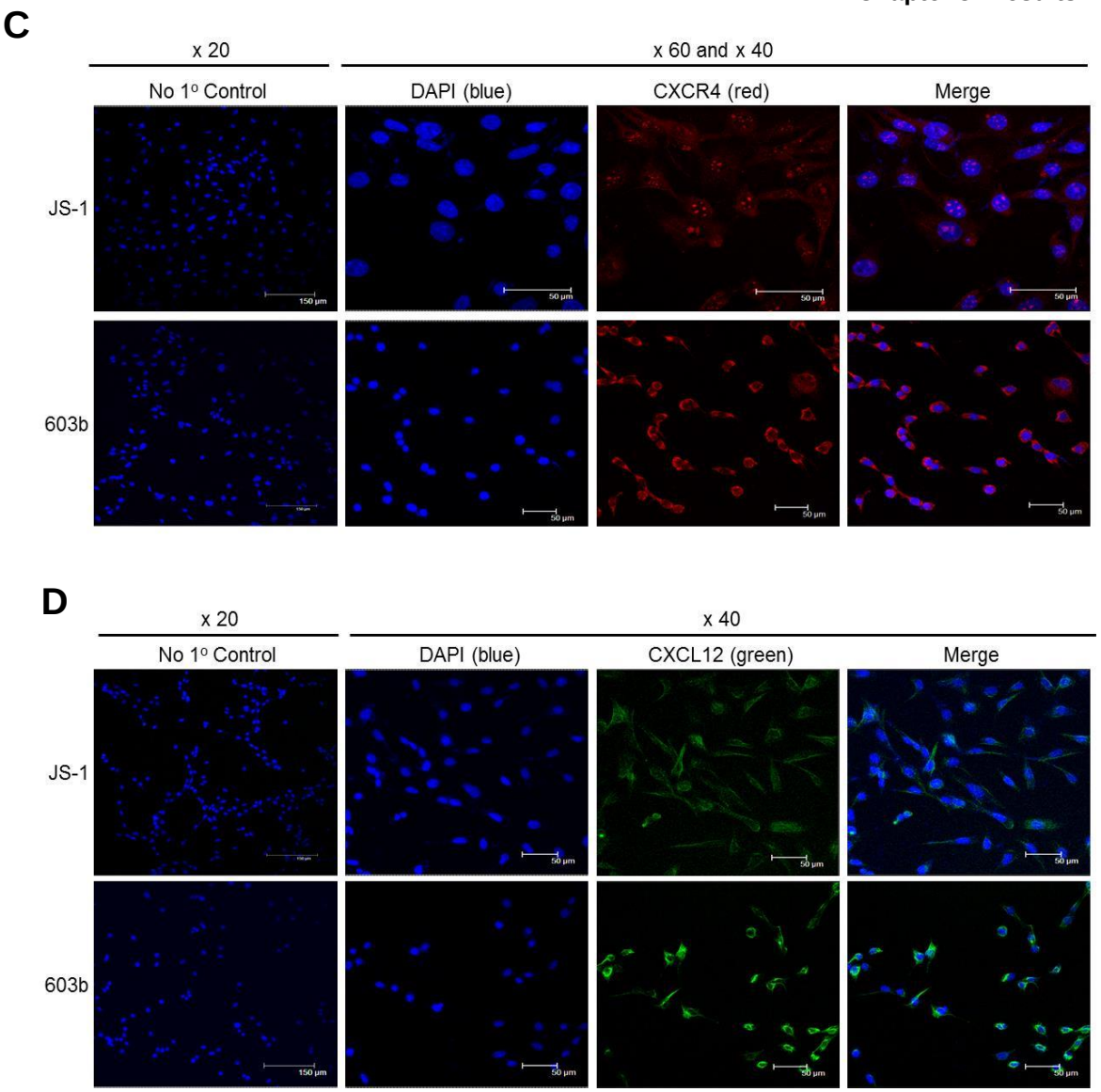

Figure 3.5: CXCR4 and CXCL12 are expressed by murine stellate and biliary epithelial cell lines.
A) Bright field images of murine stellate (JS-1) and bilary epithelial (603b) cell lines taken at x 10 magnification. **B)** Representative Western blot for the expression of CXCR4 and CXCL12 in the JS-1 and 603b cell lines. For all Western blots 20µg of protein was loaded per lane and β-actin was used as a loading control. **C)** The expression of CXCR4 (red) and **D)** CXCL12 (green) was determined in JS-1 and 603b cells by confocal microscopy and background levels were set against the no primary control. DAPI was used to stain the nuclei. Scale bars = 150µm (x 20) and 50µm (x 40). Staining is typical of three separate experiments.

3.2.5: The human stellate (LX-2) and biliary epithelial (H69) cell lines express both CXCR4 and CXCL12.

CXCR4 and CXCL12 protein expression was determined in the LX-2 stellate and H69 biliary epithelial human cell lines (Figure 3.6A) by Western blotting, confirming expression of each in both cell types (Figure 3.6B). Immunofluorescence studies also revealed expression of CXCR4 in the nucleus and membrane (Figure 3.6C) whereas CXCL12 was expressed only in the cytoplasm (Figure 3.6D).

A

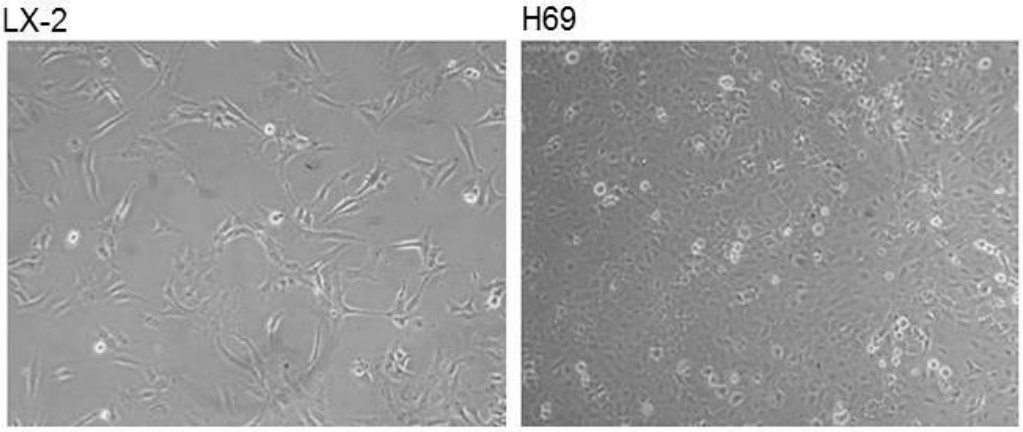

B

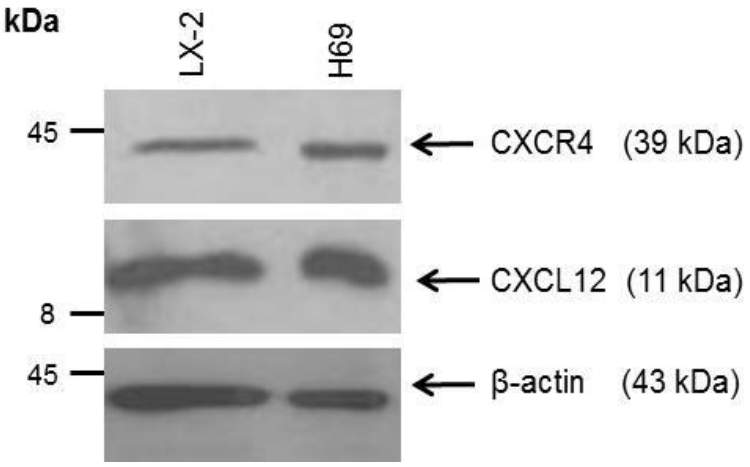

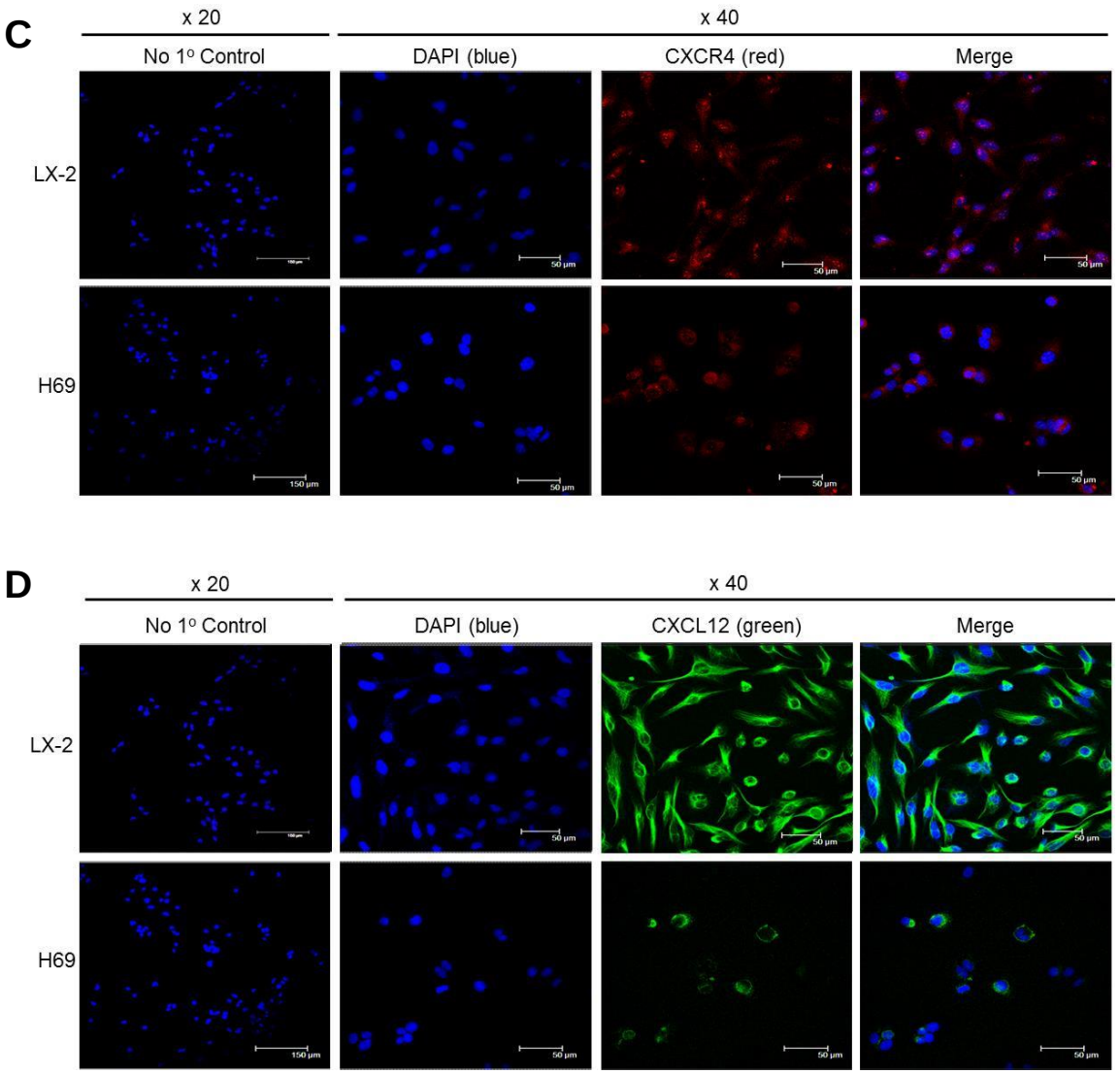

Figure 3.6: The human stellate (LX-2) and biliary epithelial (H69) cell lines express both CXCR4 and CXCL12.
A) Bright field images of the human stellate (LX-2) and biliary epithelial (H69) cell lines taken at x 10 magnification. **B)** Representative Western blot for the expression of CXCR4 and CXCL12 in the LX-2 and H69 cell lines. For all Western blots 20µg of protein was loaded per lane and β-actin was used as a loading control. **C)** The expression of CXCR4 (red) and **D)** CXCL12 (green) was determined in JS-1 and 603b cells by confocal microscopy and background levels were set against the no primary control. DAPI was used to stain the nuclei. Scale bars = 150µm (x 20) and 50µm (x 40). Staining is typical of three separate experiments.

3.2.6: Primary murine myofibroblasts express CXCR4 and CXCL12.

To examine CXCR4 and/or CXCL12 protein expression by primary murine myofibroblasts (passage 3), cells were isolated from murine livers as described in section 2.2.3. The results demonstrated that primary murine myofibroblasts expressed CXCR4 and CXCL12 (Figure 3.7A) and secreted CXCL12 in both serum free and 10% FCS conditions (Figure 3.7B). Furthermore, secretion levels increased over time (Figure 3.7B).

A

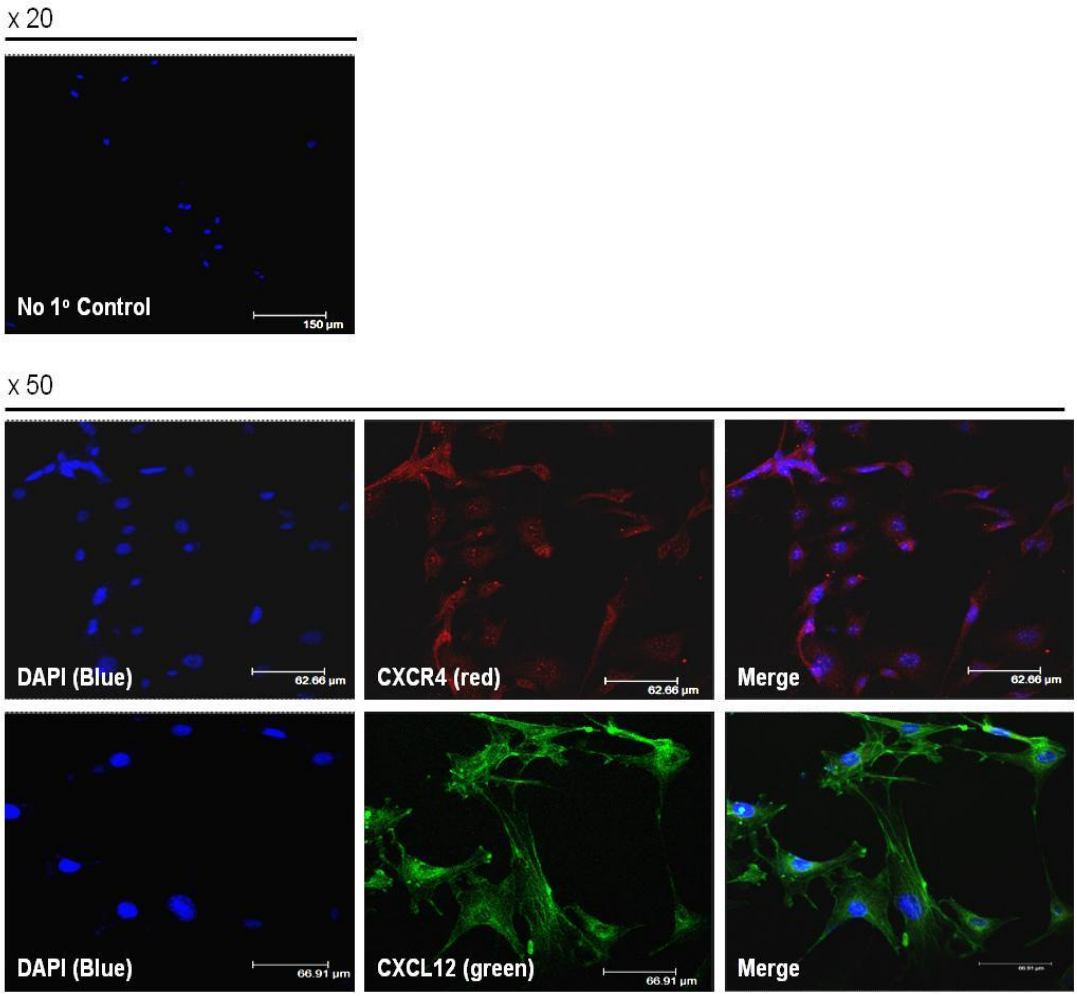

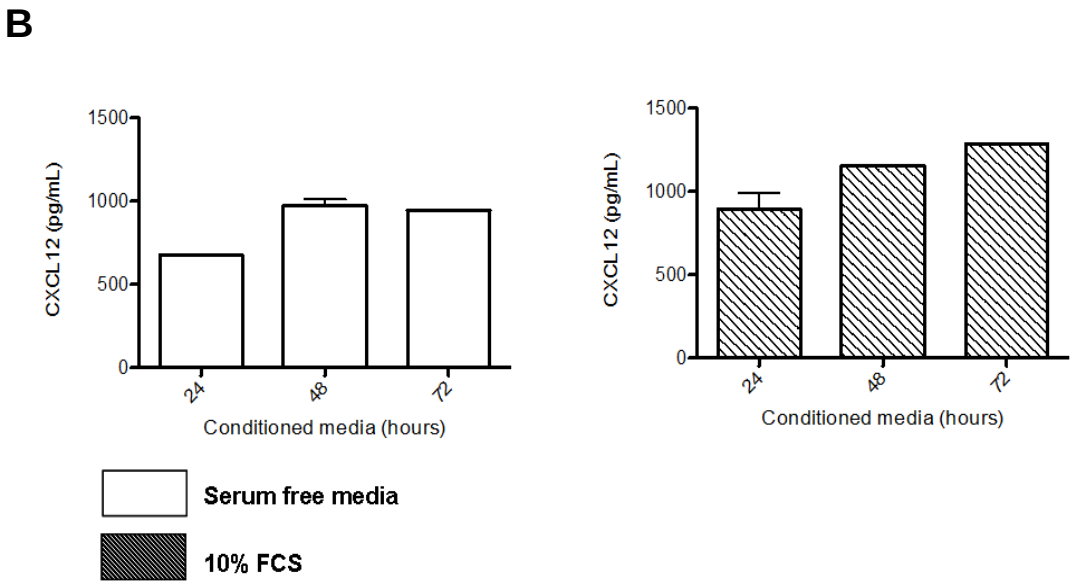

Figure 3.7: Primary murine myofibroblasts express CXCR4 and CXCL12.
A) The expression of CXCR4 (red) and CXCL12 (green) was determined in primary murine stellate cells by confocal microscopy and background levels were set against the no primary control. DAPI was used to stain the nuclei. Scale bars = 150µm (x 20) and 60µm (x 50). Staining is typical of three separate experiments. **B)** ELISA for the secretion of CXCL12 (pg/ml) in conditioned murine stellate media (10% FCS and SF) collected at 24, 48 and 72 hours. DAPI was used to stain the nuclei. Scale bars = 150µm (x 20) and 50µm (x 50). Results are typical of three separate experiments.

3.2.7 Primary human myofibroblasts and biliary epithelial cells express CXCR4 and CXCL12 and hepatocytes express CXCR4.

To examine CXCR4 and/or CXCL12 protein expression by primary liver cells (myofibroblasts (passage 3), biliary epithelial cells (passage 0) and hepatocytes (passage 0)) cells were isolated from human re-sected livers as described in section 2.2.3. Immunofluorescence studies demonstrated that human myofibroblasts expressed both CXCR4 and CXCL12 and also a marker of these cell types; α-SMA (Figure 3.8A). Biliary epithelial cells also expressed both of these proteins as well as CK-19, a marker of these cell types (Figure 3.8B). Western blotting results confirmed the immunofluorescence data showing that both human myofibroblasts and biliary epithelial cells express these proteins (Figure 3.8C). The results also demonstrated that primary human hepatocytes express CXCR4 but do not express CXCL12 (Figure 3.8C). Furthermore, Western blotting results revealed bands above the predicted molecular weight (Figure 3.8C).

A

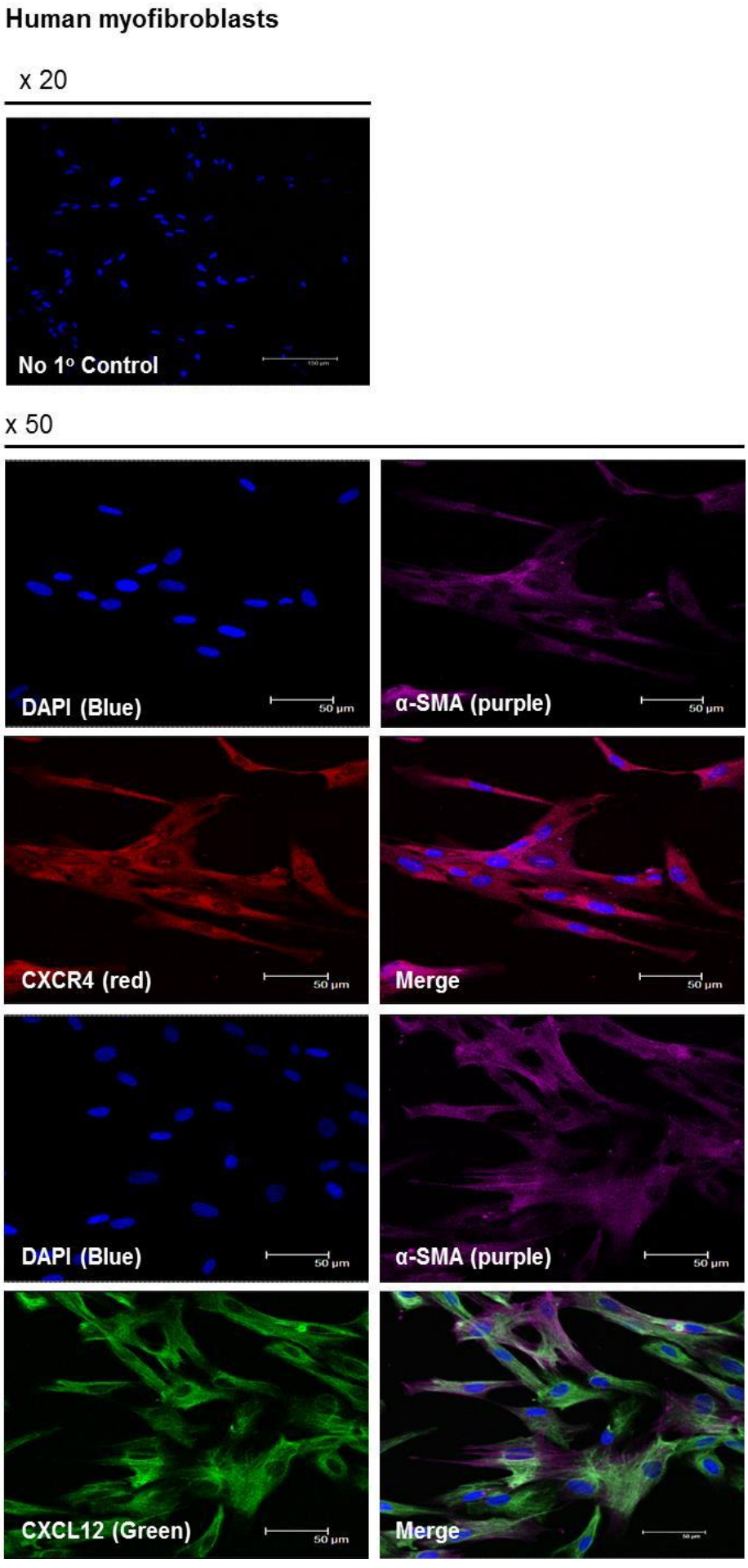
Human myofibroblasts
x 20
No 1° Control
x 50
DAPI (Blue)
α-SMA (purple)
CXCR4 (red)
Merge
DAPI (Blue)
α-SMA (purple)
CXCL12 (Green)
Merge

B

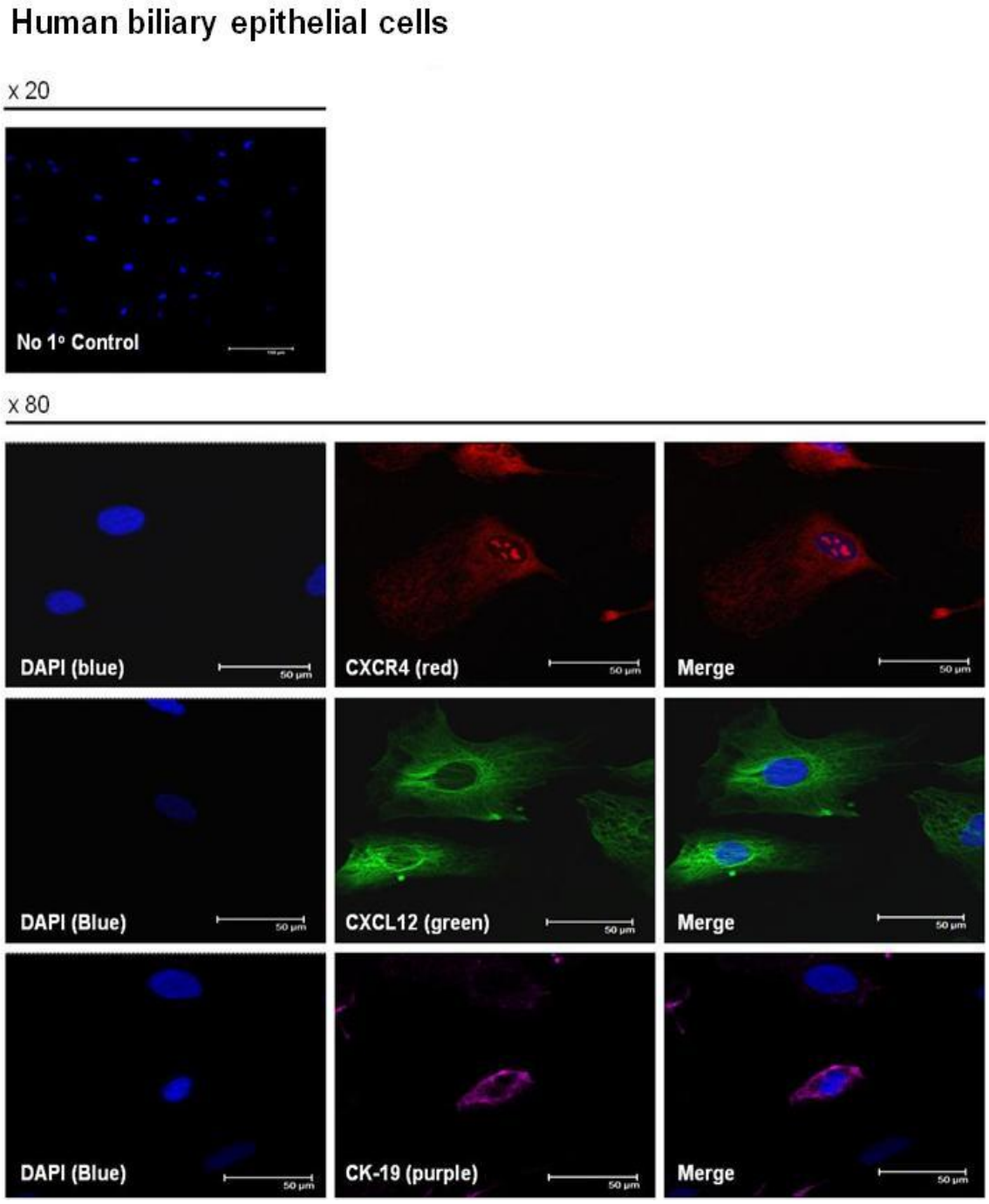
Human biliary epithelial cells
x 20
No 1° Control
x 80
DAPI (blue)
CXCR4 (red)
Merge
DAPI (Blue)
CXCL12 (green)
Merge
DAPI (Blue)
CK-19 (purple)
Merge

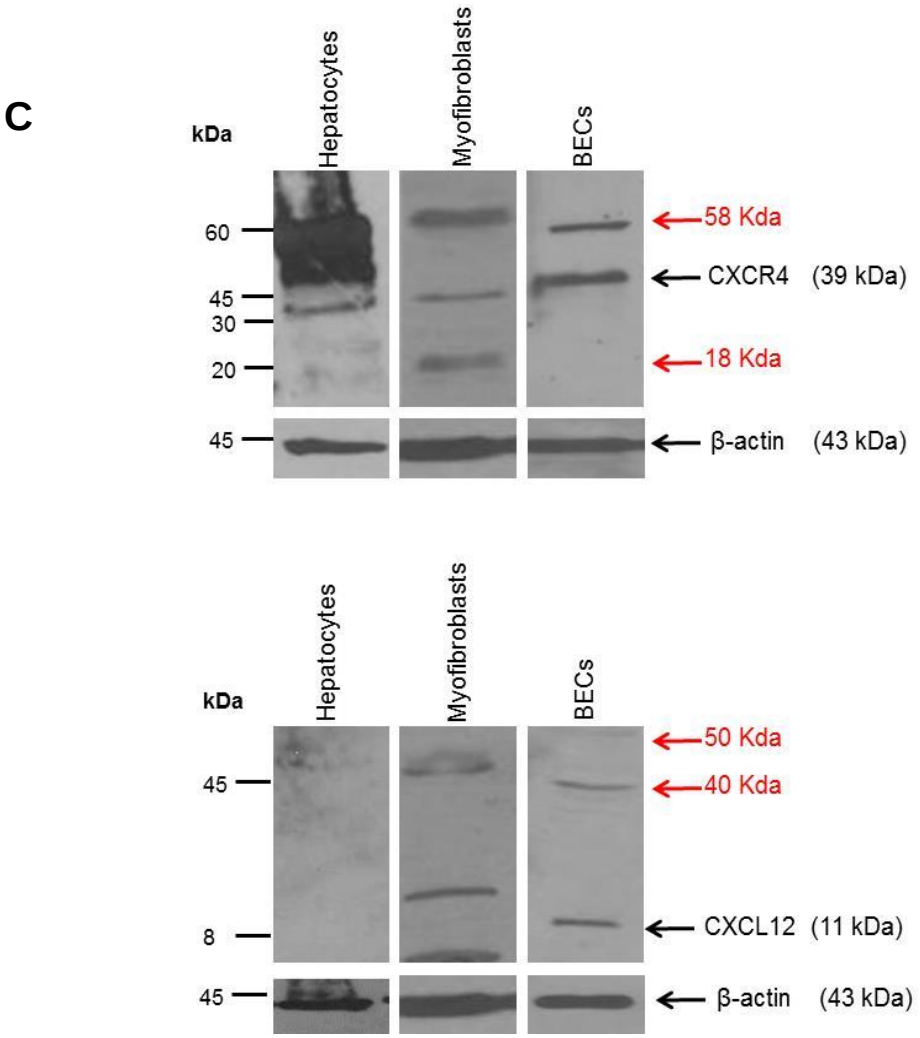

Figure 3.8: Primary human stellate and biliary epithelial cells express CXCR4 and CXCL12 and hepatocytes express CXCR4.
A) The expression of CXCR4 (red), CXCL12 (green) and α-SMA (purple) was determined in primary human myofibroblasts by confocal microscopy and background levels were set against the no primary control. DAPI was used to stain the nuclei. Scale bars = 150µm (x 20) and 50µm (x 50). Staining is typical of three separate experiments. **B)** The expression of CXCR4 (red), CXCL12 (green) and CK-19 (purple) was determined in primary human biliary epithelial cells by confocal microscopy and background levels were set against the no primary control. DAPI was used to stain the nuclei. Scale bars = 150µm (x 20) and 50µm (x 50). Staining is typical of three separate experiments. **C)** Representative Western blots for the expression of CXCR4 and CXCL12 in primary liver cells. For all Western blots 20µg of protein was loaded per lane and β-actin was used as a loading control.

3.2.8: Recombinant CXCL12 promotes cell viability in a B16-F10 melanoma and JS-1 stellate cell line.

To determine if recombinant CXCL12 promoted cell viability *in vitro*, B16-F10 murine melanoma and JS-1 stellate cells were incubated with various concentrations of murine recombinant CXCL12 ranging from 0-500ng/ml in both serum free and 10% FCS media conditions and an MTS assay was performed. Results demonstrated that for both cell lines in serum free and 10% FCS conditions cell viability was not affected (Figure 3.9A and B).

A

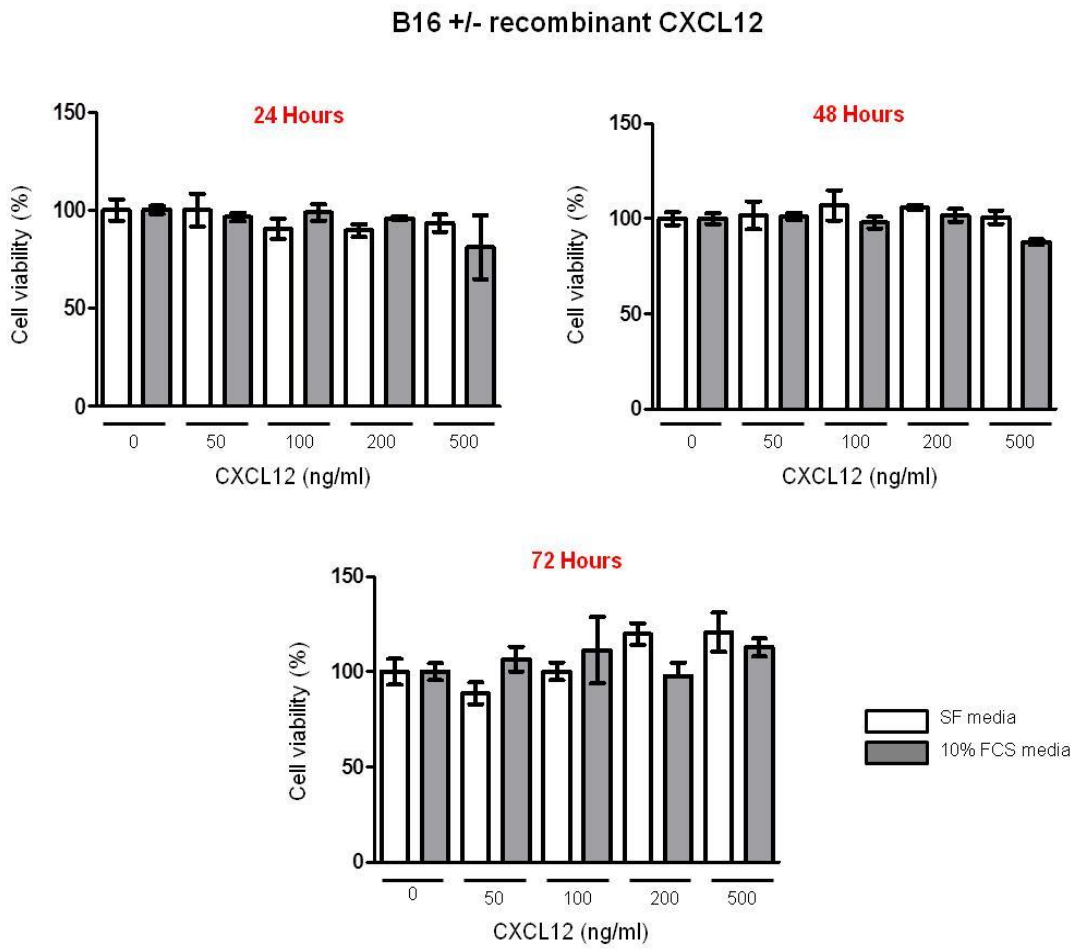

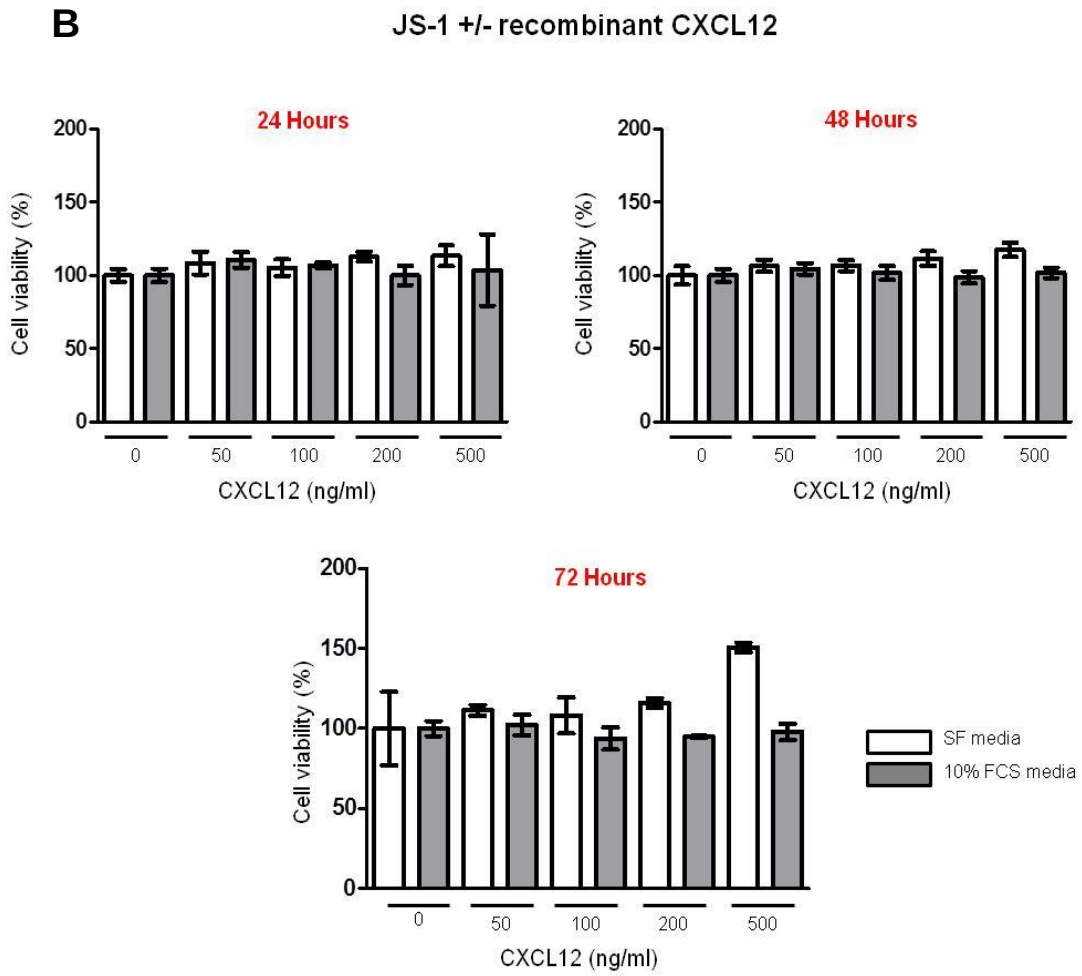

Figure 3.9: Recombinant CXCL12 promotes cell viability in a B16-F10 melanoma and JS-1 stellate cell line.
A) B16-F10 cells and **B)** JS-1 cells were cultured in the presence of murine recombinant CXCL12 at concentrations ranging from 0-500ng/ml in both 10% FCS and serum free conditions and cell viability was determined by the MTS assay as described in section 2.2.9. Each bar is the mean +/- SD (n=3). Statistical analyses were compared by one way ANOVA with Bonferroni's post hoc correction.

3.2.9: Conditioned JS-1 media significantly reduces cell viability of B16-F10 murine melanoma cells at 72 hours of treatment.

JS-1 conditioned media (serum free and 10% FCS) was collected at 24, 48 and 72 hours and an ELISA was performed in order to quantify secretion levels as described in section 2.6. The results demonstrated that secretion levels were greater in 10% FCS conditions compared to the serum free media and furthermore, levels increased over time (Figure 3.10A). To determine if JS-1 conditioned media promoted the viability of the B16-F10 cells they were incubated with this media for 24, 48 and 72 hours and an MTS assay was performed as described in section 2.2.9. The results demonstrated that at 72 hours cell viability was significantly decreased compared to serum free media alone (Figure 3.10B).

A

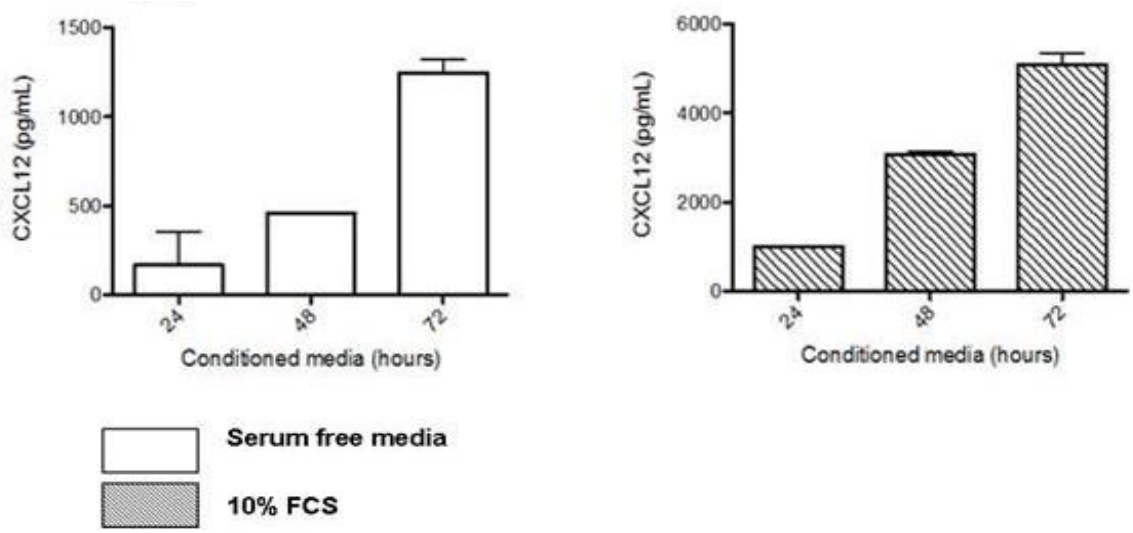

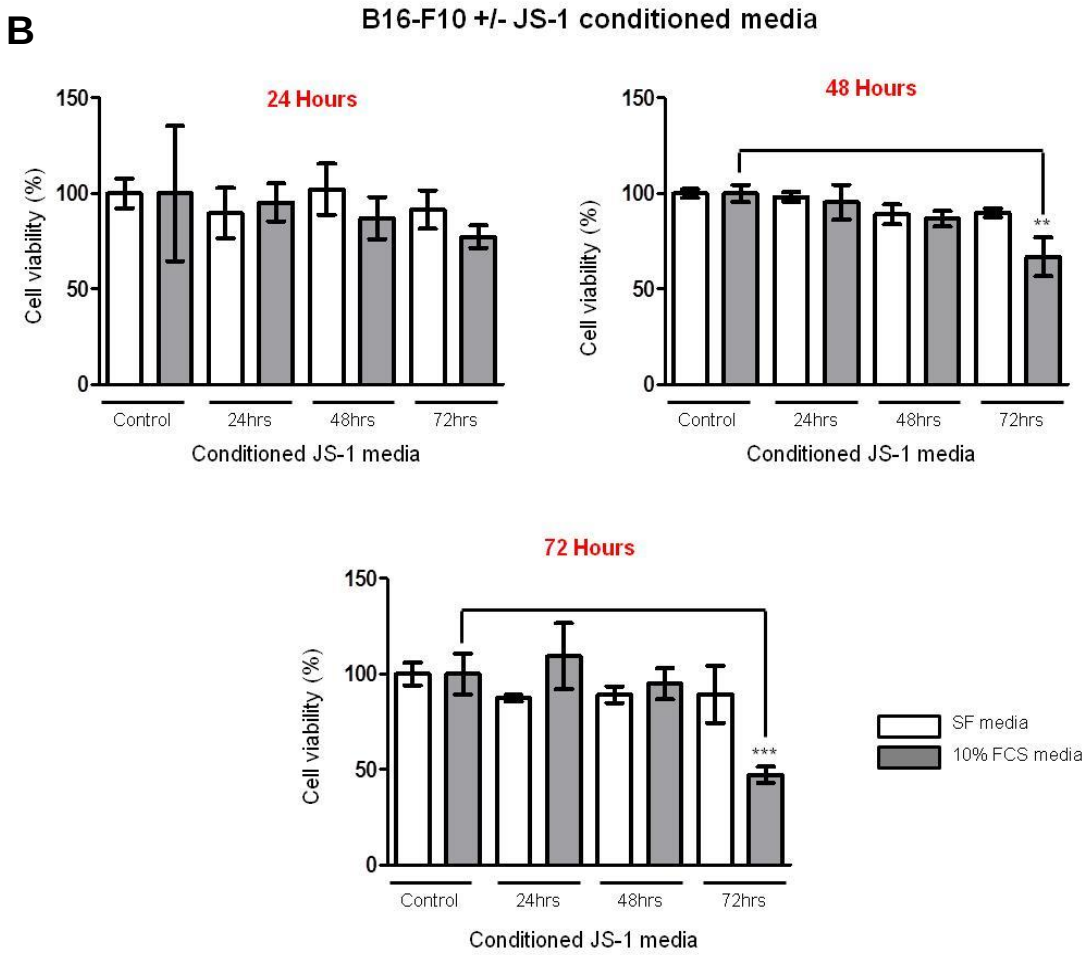

Figure 3.10: Conditioned JS-1 media significantly reduces cell viability of B16-F10 murine melanoma cells.
A) ELISA for the secretion of CXCL12 (pg/ml) in conditioned JS-1 stellate media (10% FCS and SF) collected at 24, 48 and 72 hours. **B)** B16-F10 cells were cultured in the presence of the conditioned media and cell viability was determined by the MTS assay as described in section 2.2.10. Each bar is the mean +/- SD (n=3). Statistical analyses were compared by one way ANOVA with Bonferroni's post hoc correction. ***P <0.001.

3.2.10: CXCL12 secretion by primary murine liver cells (myofibroblasts and biliary epithelial cells) promotes chemotaxis of B16-F10 melanoma cells.

ELISA assays were performed to assess the concentration of CXCL12 in conditioned media collected from primary rat biliary epithelial cells and murine myofibroblasts. The results demonstrated that CXCL12 secretion was significantly greater in the rat biliary epithelial media compared to the myofibroblast media (Figure 3.11A). Chemotaxis assays were then performed to assess the migration of the B16-F10 murine melanoma cells towards this conditioned media. The results demonstrated that more cells significantly migrated towards both the myofibroblast media (Figure 3.11B) and also the biliary epithelial cell media (Figure 3.11C) compared to the controls.

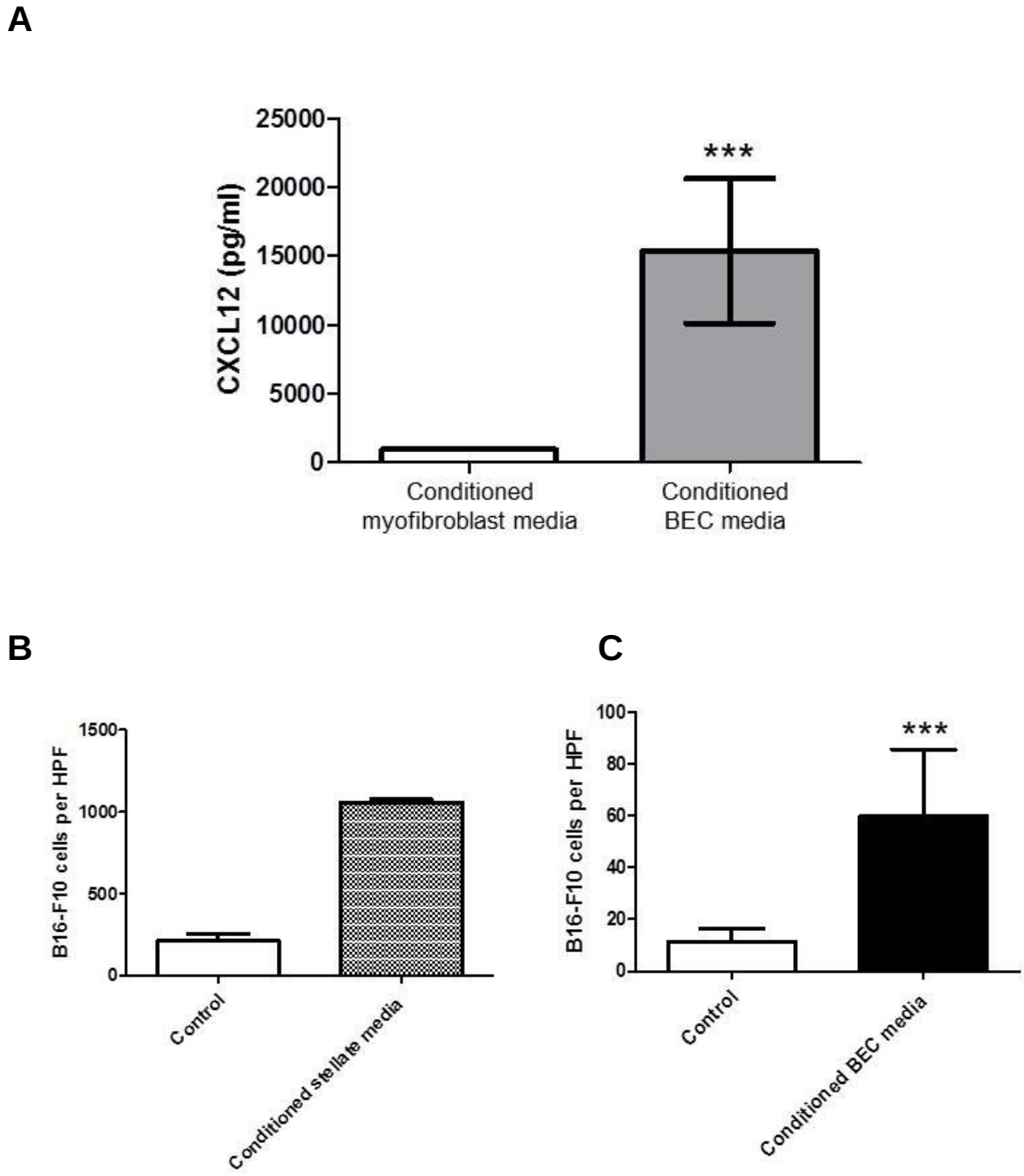

Figure 3.11: B16-F10 cells migrate significantly towards conditioned media from primary activated stellate and biliary epithelial cells.
A) ELISA for the secretion of CXCL12 (pg/ml) in conditioned murine stellate and biliary epithelial cell media collected at 48 hours. Chemotaxis assay using B16-F10 cells migrated overnight towards conditioned media from **B)** activated stellate cell media and **C)** biliary epithelial cell media. HPF = high power field. Each bar is the mean +/- SD (n=3). Statistical analyses were compared by the Student's unpaired t-test.. ***P <0.0001.

In collaboration with Dr Graeme O'Boyle (Institute of Cellular Medicine, Newcastle University, UK) chemotaxis assays were performed in order to assess the ability of AMD3100 and AMD11070 to inhibit migration towards human recombinant CXCL12 and conditioned human activated stellate media. The compounds and conditioned media were prepared by myself and chemotaxis assays were performed and analysed by Dr Graeme O'Boyle.

3.2.11: Inhibition of the CXCR4-CXCL12 chemokine axis in melanoma by AMD3100 and AMD11070 (O'Boyle, Swidenbank et al. 2013).

Firstly, chemotaxis assays were performed using AMD3100 and AMD11070 to test their ability to inhibit A375 and CHL-1 melanoma migration towards human recombinant CXCL12. Results demonstrated that both inhibitors significantly blocked migration of CHL-1 cells (Figure 3.12A). However, when tested in the A375 cell line, AMD11070 was more effective at inhibiting migration compared to AMD3100 (Figure 3.12A). In addition, a greater number of A375 cells (BRAF ^{V600E}) in the absence of CXCL12 migrated compared to the CHL-1 cell line (Figure 3.12A).

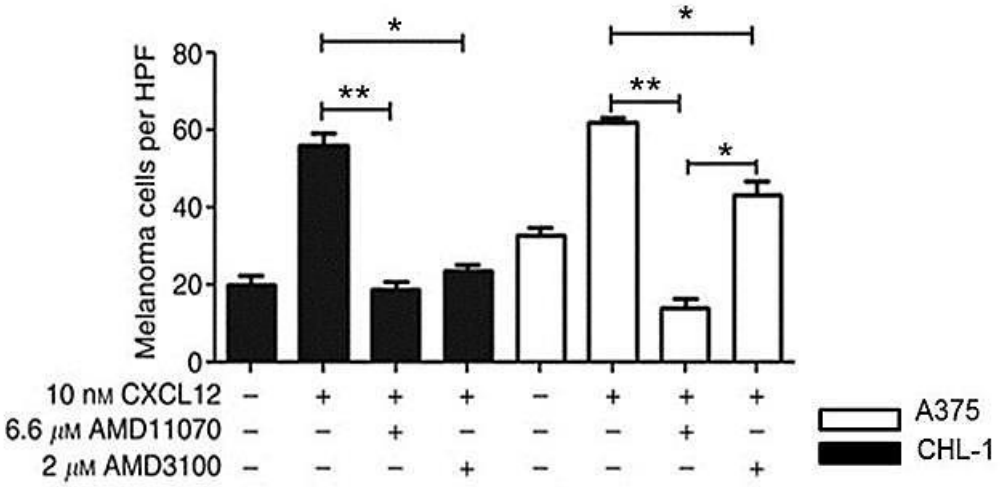

Figure 3.12: Inhibition of the CXCR4-CXCL12 chemokine axis in melanoma by AMD3100 and AMD11070.

Chemotaxis assay using CHL-1 and A375 cells migrated for 16 hours towards 10nM CXCL12. across an 8-μm pore size filter in the presence of 2 μM AMD3100 or 6.6 μM AMD11070. HPF = high power field. Each bar is the mean +/- SD (n=3). Statistical analyses were compared by one way ANOVA with Bonferroni's post hoc correction. * P<0.05, ** P<0.001.

3.2.12: Effect of B-RAF-V600E on melanoma migration (O'Boyle, Swidenbank et al. 2013).

The role of B-RAF in melanoma migration was then assessed towards human recombinant CXCL12 +/- AMD3100/AMD11070. Western blotting results demonstrated that both A375 and CHL-1 cells displayed similar levels of total BRAF expression (Figure 3.13A) indicating that the increased migration of the A375 cells observed previously (Figure 3.12A) was not dependent on the over-expression of $BRAF^{V600E}$. CHL-1 cells were then transfected with vectors encoding WT and V600E BRAF (performed by Dr Jane Armstrong, Dermatological Sciences, Newcastle University) which subsequently increased ERK activation in these cells (data not shown). The transfected cells were then used in the chemotaxis assay and interestingly, results demonstrated that compared to WT control cells over-expression of V600E increased the migration of the cells (Figure 3.13B)

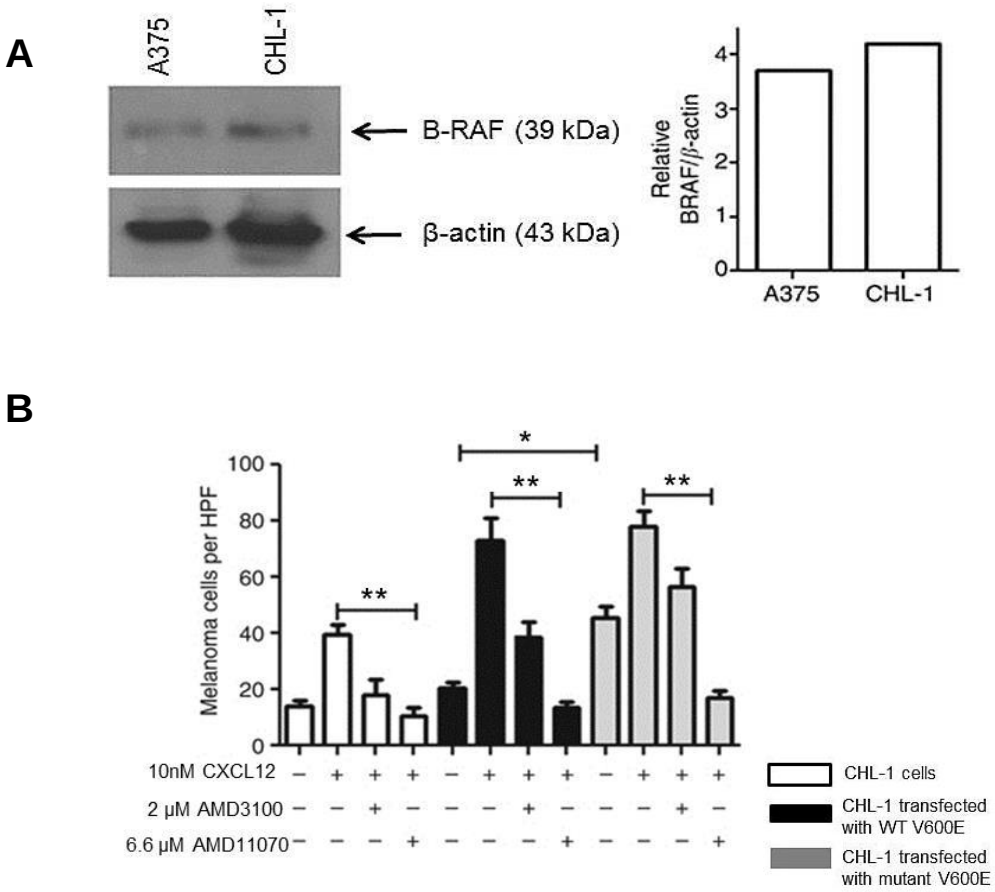

Figure 3.13: Effect of B-RAF-V600E on melanoma migration.
A) Representative Western blot for the expression of BRAF in A375 and CHL-1 melanoma cell lines and densitometry quantification. 20μg of protein was loaded per lane and β-actin was used as a loading control. **B)** A375 (white bars), CHL-1 cells transfected with WT (black bars) or mutant

(V600E) (grey bars). B-RAF migrated for 16h towards 10nM CXCL12 in the presence of 2 μM AMD3100 or 6.6 μM AMD11070. HPF = high power field. Each bar is the mean +/- SD (n=3). Statistical analyses were compared by one way ANOVA with Bonferroni's post hoc correction. * P<0.05, ** P<0.001, ***P <0.0001.

3.2.13: Effect of B-RAF-V600E on melanoma migration towards conditioned human myofibroblast media (O'Boyle, Swidenbank et al. 2013).

The ability of AMD3100 and AMD11070 to inhibit migration of A375 and CHL-1 cells towards conditioned myofibroblast media was then tested. A CXCL12-neutralising antibody was also used since the conditioned media may have contained other factors that promote migration. The results demonstrated that migration of A375 and CHL-1 melanoma cells was blocked by CXCL12 neutralisation (Figure 3.14). The migration response of CH-1 cells was significantly inhibited by AMD3100 and AMD11070 however, only AMD11070 inhibited the migration of the A375 cells (Figure 3.14).

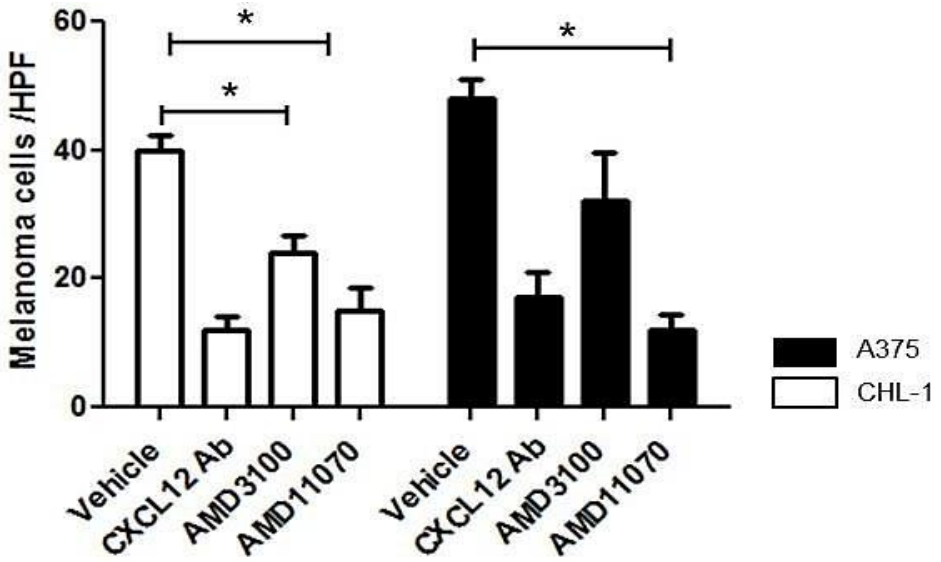

Figure 3.14: Effect of B-RAF-V600E on melanoma migration towards conditioned primary human myofibroblast media.
Chemotaxis assay using A375 (white bars) and CHL-1 (black bars) migrated for 16hr towards conditioned media from human myofibroblasts in the presence of 100µg/ml CXCL12 neutralizing antibody, 2µM AMD3100 or 6.6µM AMD11070. HPF = high power field. Each bar is the mean +/- SD (n=3). Statistical analyses were compared by one way ANOVA with Bonferroni's post hoc correction. * P<0.05, ** P<0.001, ***P <0.0001.

3.2.14: Migration of melanoma cells towards conditioned human biliary epithelial cell media.

An ELISA was performed on conditioned media collected from primary human myofibroblasts and biliary epithelial cell media (48 hours serum free) to determine the concentration levels of secreted CXCL12. The results demonstrated that the levels of CXCL12 secreted by the biliary epithelial cells was low (35 pg/ml) compared to the positive control (myofibroblasts) where secretion levels were above 1500pg/ml (Figure 3.15A). This biliary epithelial media was used to assess the migration of the A375 and CHL-1 melanoma cell lines. The results demonstrated that both cell lines migrated towards the conditioned media significantly and interestingly, A375 cells migrated more compared to the CHL-1 cell line (Figure 3.15B). In the presence of AMD11070, migration of both the melanoma cells was inhibited significantly (Figure 3.15B).

A

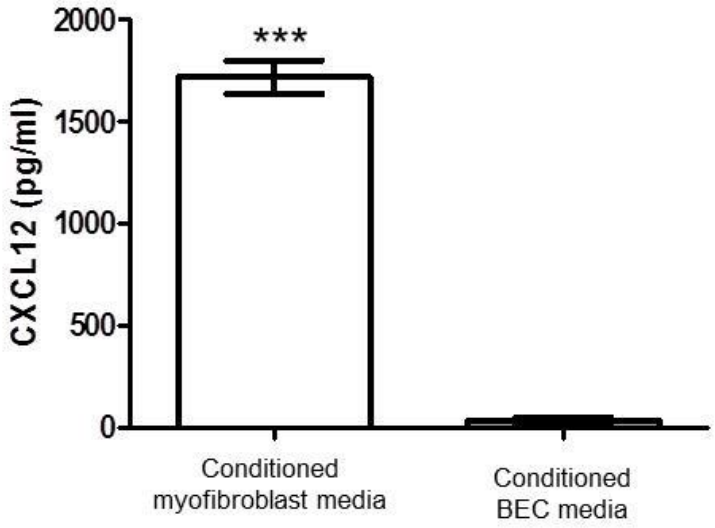

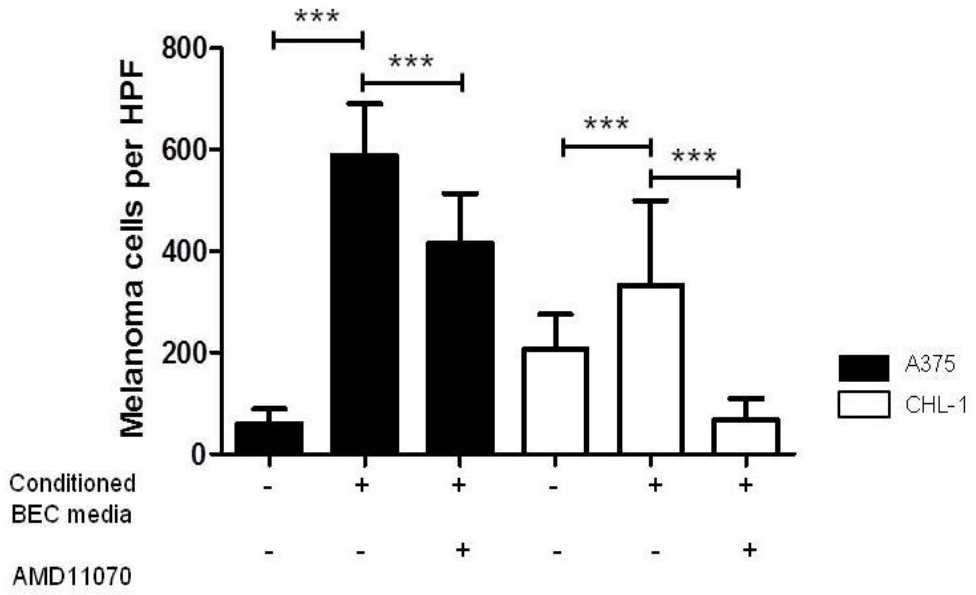

Figure 3.15: Melanoma cells significantly migrate towards conditioned human BEC media. **A)** ELISA for the secretion of CXCL12 (pg/ml) in conditioned human stellate and biliary epithelial cell media collected at 48 hours. **B)** Chemotaxis assay using A375 (black bars) and CHL-1 (white bars) migrated for 16hr towards conditioned media from biliary epithelial cells in the presence of vehicle control or AMD11070 (6.6µM). HPF = high power field. Each bar is the mean +/- SD (n=3). Statistical analyses were compared by one way ANOVA with Bonferroni's post hoc correction. * P<0.05, ** P<0.001, ***P <0.0001.

3.2.15 Adhesion of murine melanoma cells increases towards murine stellate cells.

The adhesion of B16-F10 cells towards murine JS-1 cells was assessed in an adhesion assay as described in section 2.8. The results demonstrated that a greater number of B16-F10 cells adhered in the presence of JS-1 cells when coated on the filter and even more so when they were present in the wells, however, results were not significant (Figure 3.16).

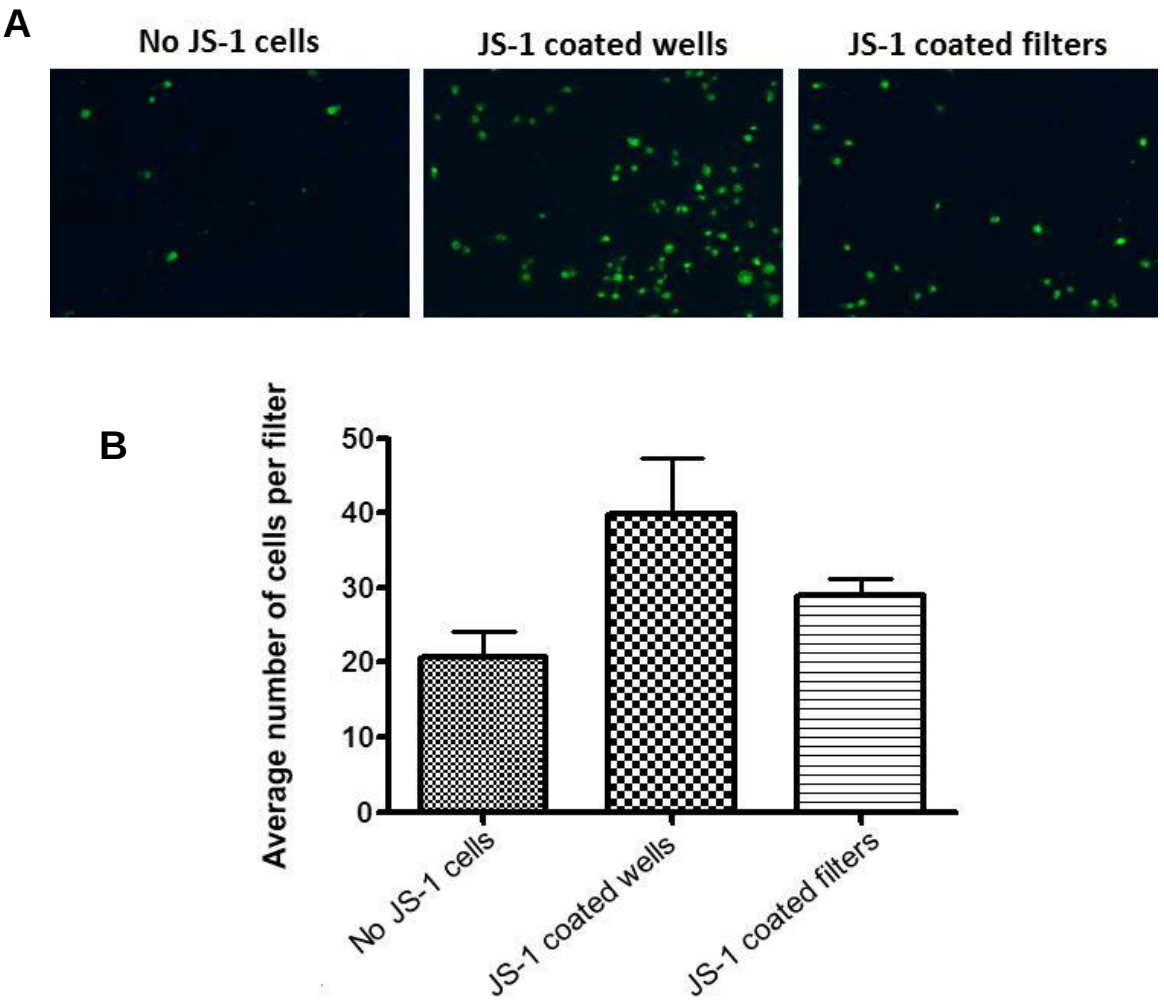

Figure 3.16: Adhesion of murine melanoma cells increases towards murine stellate cells. B16-F10 cells labelled with CFSE were incubated on endothelial cell monolayers +/- JS-1 cells. **A)** Images were acquired at x 10 magnification using fluorescence microscopy. B) B16-F10 cells adhered more in the presence of JS-1 cells. Each bar is the mean +/- SD (n=3).

3.3 Chapter Discussion

The results in this chapter demonstrated that murine and human melanoma cell lines express CXCR4 and CXCL12 *in vitro* and furthermore, CXCR4 was expressed in the nucleus and membrane whereas CXCL12 was concentrated in the cytoplasm. This was to be expected since CXCR4 is a G-protein coupled receptor and therefore would be located on the cellular membrane and as a result of intracellular sequestration upon binding of CXCL12, nuclear expression would also be observed (Teicher and Fricker 2010). As CXCL12 is a secreted chemokine this would explain the reason for expression being predominantly in the cytoplasm. Although these observations were not novel, it was important to confirm expression of these proteins prior to the commencement of other assays. Hypoxic conditions did not affect expression of either of these proteins, however, a band at a higher molecular was observed and interestingly this was increased in hypoxic conditions. Since it has been reported that hypoxia promotes CXCR4 expression (Teicher and Fricker 2010) it would be interesting to carry out further analysis to determine whether or not this is an isoform of CXCR4 that is being up-regulated. Furthermore, since total protein expression was measured it would be beneficial to separate both nuclei and membrane expression by using for example, flow cytometry.

Consistent with previous studies, murine and human stellate and biliary epithelial cell lines and primary cells expressed CXCR4 and CXCL12 and hepatocytes expressed CXCR4 (Hong, Tuyama et al. 2009) *in vitro*. However, bands were also observed in the primary cells above the predicted molecular weights and this has not been reported. This may have been due to non-specific proteins being detected or alternatively, it could mean that CXCR4 and CXCL12 are post translationally modified and this is discussed in more detail in the next chapter. Additionally, it would have been beneficial to use recombinant CXCL12 in the Western blotting rather than a cell line in these studies to help to determine if the antibody was specific. Recombinant CXCL12 promoted cell viability of both B16-F10 cells and JS-1 cells in serum free media suggesting that CXCL12 may act as a survival factor. Indeed, it has been reported that CXCL12 can promote survival of cells via the PI3-kinase-MAP-kinase pathway (Teicher and Fricker 2010). On the contrary, conditioned media rich in CXCL12 from JS-1 cells

reduced the viability of B16-F10 cells at 72 hours of treatment suggesting that the media contained a soluble factor that induced cell death. In the adhesion assay, a greater number of B16-F10 cells adhered in the presence of the JS-1 cell line suggesting that the JS-1 cell line secretes a factor that promotes adhesion and it would be interesting to study this further using the human melanoma cell lines.

The chemotaxis assay results demonstrated that B16-F10 cells migrate significantly towards both conditioned primary myofibroblast and rat biliary epithelial cell media and currently, there are no published scientific studies which have investigated this. However, the ELISA results demonstrated that the myofibroblast media contained high levels of CXCL12 compared to the bilary epithelial media suggesting that the latter contained other factors that promoted the migration of the cells. Thus, it would be interesting to perform further analysis, for example a cytokine array on the conditioned media from these cells.

In accordance with previous studies (Chen, Tardell et al. 2012), transfection of V600E into CHL-1 cells (WT BRAF) up-regulated ERK activation (O'Boyle, Swidenbank et al. 2013) and furthermore, expression of V600E did not affect the ability of AMD11070 to inhibit migration (O'Boyle, Swidenbank et al. 2013). This is clinically important as it would enable patients with both WT and BRAF mutations to be treated. The results also suggest that the total expression levels of BRAF may influence the chemotactic ability of the melanoma cells since the majority of BRAF in the cells was as a result of the transfected plasmid (O'Boyle, Swidenbank et al. 2013). Furthermore, migration of the human melanoma cell lines towards conditioned myofibroblast and biliary epithelial media demonstrated that CXCR4 expression in melanoma mediates migration of tumour cells towards CXCL12 secreting liver cells *in vitro.* However, since the secretion levels of CXCL12 were relatively low in the biliary epithelial cell media this suggests that another isoform of CXCL12 is being secreted.

Collectively, these data suggest that AMD11070 may provide a promising new therapy for preventing melanoma metastasis to the liver. However, whilst the data provides proof of concept that this inhibitor may reduce migration of melanoma cells, additional preclinical studies are required to investigate its potential clinical use. Such efforts would require the validation of a suitable model of human

metastatic melanoma, lack of which represents a significant barrier to translational research in metastatic disease. Nevertheless, the benefits of AMD11070 may not be limited only to melanoma patients as CXCR4 is highly expressed by many other cancers, including breast cancer, lung cancer, neuroblastoma, colorectal cancer and ovarian cancer.

Chapter 4: Results 2

Differential CXCR4 and CXCL12 expression in normal mouse organs and human liver tissue.

4.1 Introduction and Aims

CXCL12 was initially cloned from a murine bone marrow-derived stromal cell line and was shown to function as a pre-B-cell growth stimulating factor (PBSF) (Tashiro, Tada et al. 1993). The two main splicing variants of the CXCL12 gene are CXCL12-α (alpha) and CXCL12-β (beta) with the former being the predominant variant (Davis, Singer et al. 2005). It has been reported that CXCL12-α undergoes rapid proteolysis in blood (Janowski 2009) and is found to be expressed in most organs including the brain, heart, bone marrow, lung and the liver (Teicher and Fricker 2010). On the contrary, CXCL12-β is more resistant to this degradation and is known to promote angiogenesis and is therefore found in highly vascularized organs for example, spleen, kidneys and the liver (Janowski 2009). More recently, other human isoforms of CXCL12 derived from alternative splicing have been identified including CXCL12-γ (gamma), CXCL12-δ (delta), CXCL12-ε (epsilon) and CXCL12-φ (phi) (Yu, Cecil et al. 2006). CXCL12-γ has found to be expressed in less vascularized organs such as, the brain and the heart (Janowski 2009) whereas CXCL12-δ (delta), CXCL12-ε (epsilon) and CXCL12φ (phi) have been detected in numerous human tissues including the liver, kidney and pancreas (Janowski 2009). The chemokine receptor CXCR4 is also known to be expressed in a broad range of tissues including the brain, lung, heart, kidney and liver (Teicher and Fricker 2010).

Therefore the aims of this chapter were firstly to confirm the mRNA expression of three of the main CXCL12 variants (α, β and γ) as well as CXCR4 in various normal mouse organs and human liver tissue samples. In conjunction, to determine protein expression levels of both CXCL12 and CXCR4. The data presented in the previous chapter demonstrated that in *in vitro*, myofibroblasts and biliary epithelial cells express both CXCR4 and CXCL12 with hepatocytes expressing only CXCR4. Therefore, an additional aim of the present chapter was to establish a correlation between *in vitro* and *in vivo* expression as well as to determine whether or not other cell types in the liver expressed these proteins.

4.2 Results

4.2.1 Both CXCR4 and CXCL12 variants are expressed in normal mouse organs and human liver.

Since liver damage and fibrosis are reported to affect the expression levels and profiles of chemokines and chemokine receptors (Saiman and Friedman 2012), a histological examination of male mouse liver tissue was performed in paraffin embedded tissue to ensure that the tissue was normal i.e. that there were no signs of damage and/or fibrosis. Sirius red and haematoxylin and eosin (H and E) staining was carried out to examine collagen levels and tissue morphology respectively. As myofibroblasts and fibroblasts are known to be involved in fibrosis progression and matrix deposition (Wallace, Burt et al. 2008), tissue was also stained with markers for myofibroblasts (α-SMA) and fibroblasts (vimentin). As shown by the representative sirius red and H and E images in Figure 4.1A low levels of collagen deposition were observed with a morphology typical of normal liver tissue. The α-SMA and vimentin staining (Figure 4.1B) showed some expression of both markers around the periportal regions (as denoted by the arrows), but at a level consistent with healthy tissue while a significant increase in positively stained cells would have been observed if the tissue had been fibrotic.

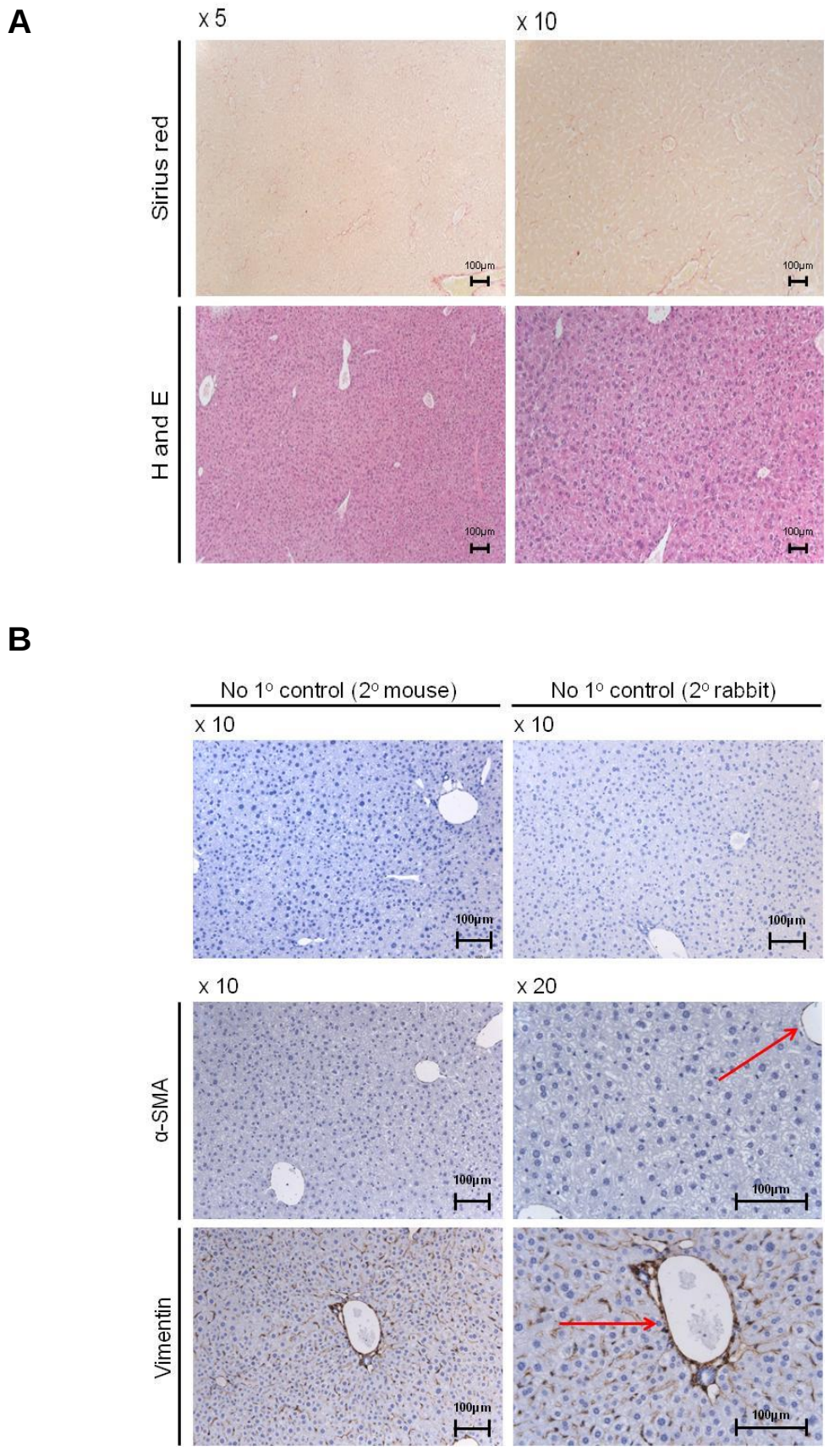

Figure 4.1: Assessment of fibrosis and damage in normal mouse liver tissue.
C57BL/6 mice were culled and livers were harvested and fixed for 24 hours in 10% formalin made up in 1 x PBS. Samples were then processed, embedded in paraffin and sectioned (5µm). Sections were then de-waxed and stained using **A)** sirius red or Haematoxylin and Eosin (H and E). **B)** Sections were stained with antibodies to either α-SMA or vimentin. No primary antibody controls were included and were stained with the secondary anti-mouse IgG (for α-SMA) or anti-

rabbit IgG (for vimentin) antibody alone. As indicated by the arrows positive staining was observed around the periportal regions. Representative images were acquired at x 5 and x 10 (sirius red and H and E) and x 10 and x 20 (α-SMA and vimentin) magnification. Staining is typical of three separate experiments. Scale bars = 100µm.

Once the morphology of the mouse liver tissue was confirmed, mRNA and protein levels of both CXCR4 and CXCL12 variants were determined. For RT-PCR analysis, mRNA expression was confirmed relative to the expression of the housekeeping gene GAPDH, while protein levels determined by Western blotting were quantified and expressed relative to the house-keeping protein, ß-actin.

As shown in Figure 4.2A, at the transcript level, CXCR4 and CXCL12-α and β were expressed in the three mouse liver tissue samples (M1, M2 and M3) however, CXCL12-γ was not detectable. Western blotting (Figure 4.2B) demonstrated low protein expression levels of CXCR4 in all three samples (M1, M2 and M3) compared to the positive control (Figure 4.2C). However, bands of greater intensity in all three samples (M1, M2 and M3) were present at both ~58 kDa and ~38 kDa and fainter bands at ~80 kDa and ~55 kDa (Figure 4.2B). In addition, Western blotting (Figure 4.2D) demonstrated no expression of CXCL12 (Figure 4.2E) in all three samples, however, prominent bands were observed at ~62 kDa (Figure 4.2D).

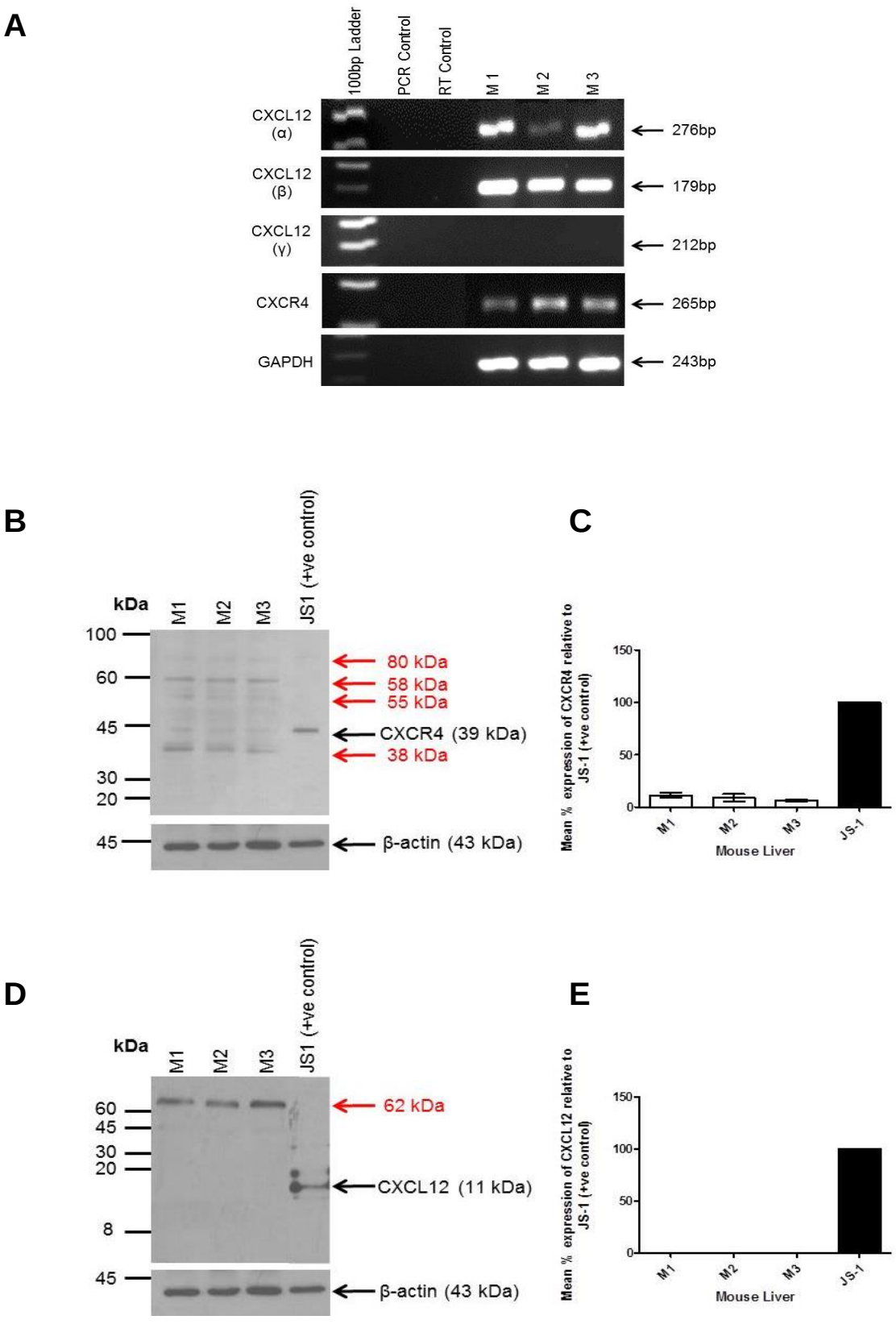

Figure 4.2: Both CXCR4 and CXCL12 variants are expressed in normal mouse liver tissue.

A) Representative RT-PCR for the expression of CXCR4 and CXCL12 variants in normal mouse liver tissue. Total RNA was isolated using Trizol, as per manufacturer's instructions from whole mouse liver tissue. RT-PCR and RT controls were carried out in the absence of template RNA and reverse transcriptase respectively. RT-PCR products were electrophoresed in 1.5% agarose gels containing ethidium bromide with a 100bp ladder to establish the size of the RT-PCR

products and visualized by UV light. **B)** Representative Western blot for the expression of CXCR4 in mouse liver tissue and **C)** Quantitative densitometry analysis of three typical western blots was performed using the Image J software. **D)** Representative Western blot for the expression of CXCL12 in mouse live tissue and **E)** Quantitative densitometry analysis of three typical western blots was performed using the Image J software. For all Western blots whole liver tissue was homogenised followed by sonication and prepared for protein analysis by Western blot. 20µg of protein was loaded per lane and β-actin was used as a loading control. M = Mouse liver. Error bars represent +/- SD.

mRNA and protein expression of CXCR4 and CXCL12 variants were also assessed in control normal mouse organs; brain, lungs, kidney and spleen and liver. RT-PCR analysis demonstrated that at the mRNA level all organs expressed CXCL12-α and CXCR4 (Figure 4.3A) while CXCL12-β was only expressed in the liver, kidney and spleen and CXCL12-γ in the brain and lungs (Figure 4.3A). At the protein level, CXCR4 was detected in the lungs, liver and spleen (Figure 4.3B) and as shown by densitometry analysis (Figure 4.3C) compared to β-actin loading control, was most abundant in the spleen. Bands of varying sizes were also observed at ~90 kDa (lungs, liver, kidney, spleen and CHL-1), ~75 kDa (liver and kidney), ~63 kDa (lungs, liver, kidney and CHL-1) and at ~35 kDa (brain, liver and CHL-1) (Figure 4.3B). As shown in Figure 4.3D, CXCL12 was observed in the lungs and spleen, while very faint bands were evident in the liver and kidney. Quantitative densitometry analysis (Figure 4.3E) demonstrated highest levels of CXCL12 expression in the spleen. In addition, bands were also observed at ~18 kDa (brain, lungs, liver and kidney), ~45 kDa (brain) and in all organs a distinct increase in molecular weight could be seen at ~62 kDa (Figure 4.3D).

A

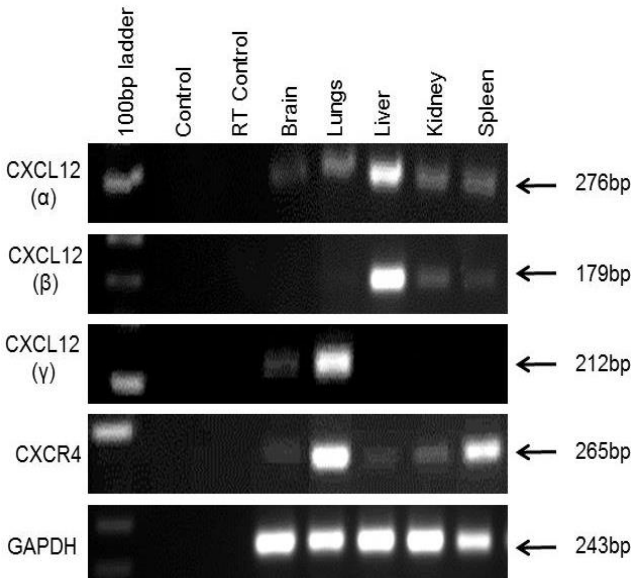

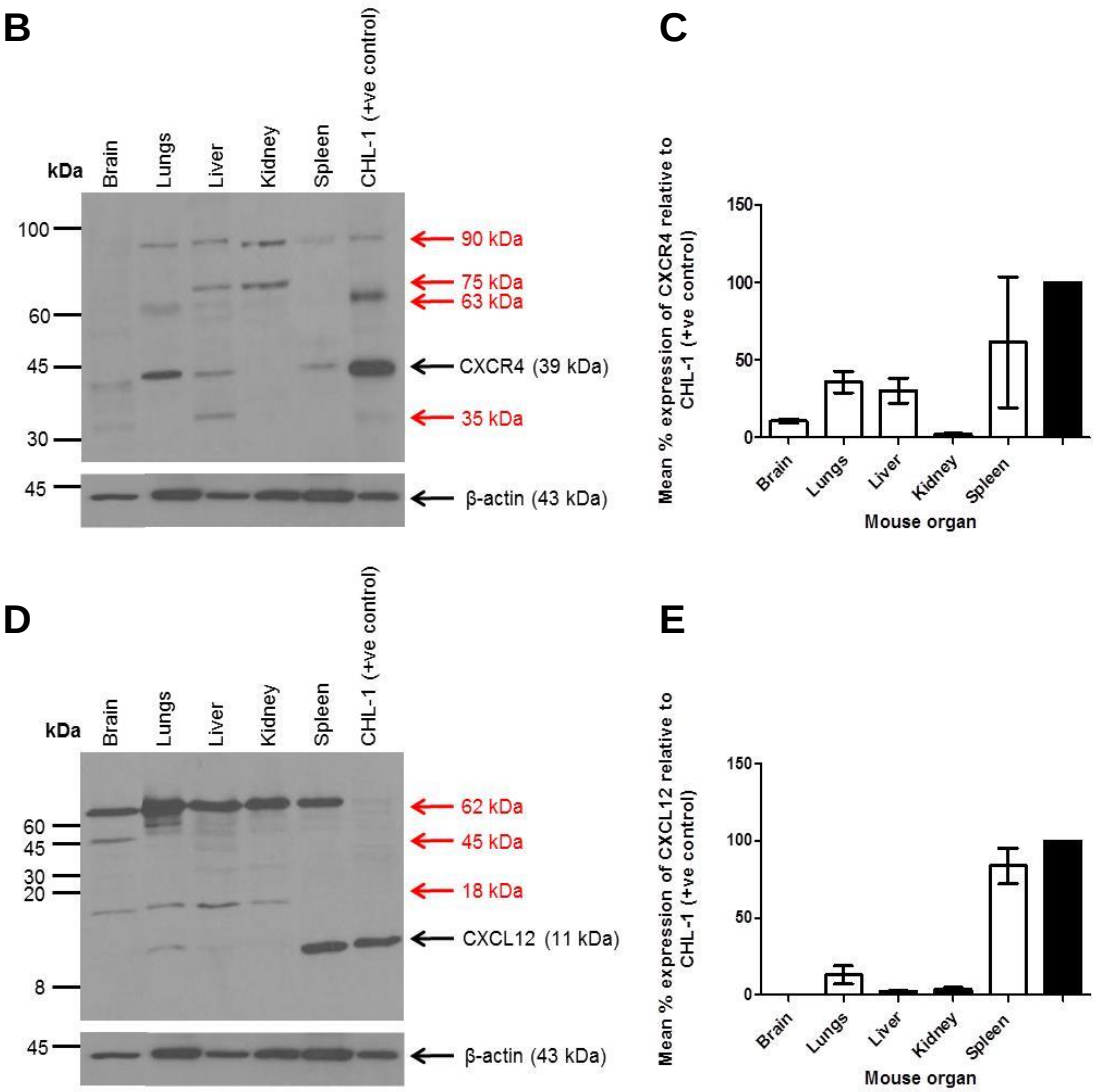

Figure 4.3: Both CXCR4 and CXCL12 variants are expressed in normal mouse organs.
A) Representative RT-PCR for the expression of CXCR4 and CXCL12 variants in normal mouse liver tissue. Total RNA was isolated using Trizol, as per manufacturer's instructions from whole mouse liver tissue. RT-PCR and RT controls were carried out in the absence of template RNA and reverse transcriptase respectively. RT-PCR products were electrophoresed in 1.5% agarose gels containing ethidium bromide with a 100bp ladder to establish the size of the RT-PCR products and visualized by UV light. **B)** Representative Western blot for the expression of CXCR4 in mouse organs and **C)** densitometry analysis of three typical western blots was performed using the Image J software. **D)** Representative Western blot for the expression of CXCL12 in mouse organs and **E)** densitometry analysis of three typical western blots was performed using the Image J software. For all Western blots whole mouse organs were homogenised followed by sonication and prepared for protein analysis by Western blot. 20µg of protein was loaded per lane and β-actin was used as a loading control. Error bars represent +/- SD.

4.2.2 In human liver patient samples CXCR4 and CXCL12 variants are expressed.

To examine collagen levels and tissue morphology in formalin fixed paraffin embedded human liver tissue (obtained during surgical resection at a minimum of 5 cm from the tumour) sirius red and H and E staining were carried out respectively. As shown by Figure 4.4A collagen deposition in all human liver samples indicated low levels of fibrosis. However, differences in the morphology were observed between differing samples for example, sample NHL14 showed signs of fat accumulation as revealed by the spongy appearance indicated by the arrows (Figure 4.4B).

A

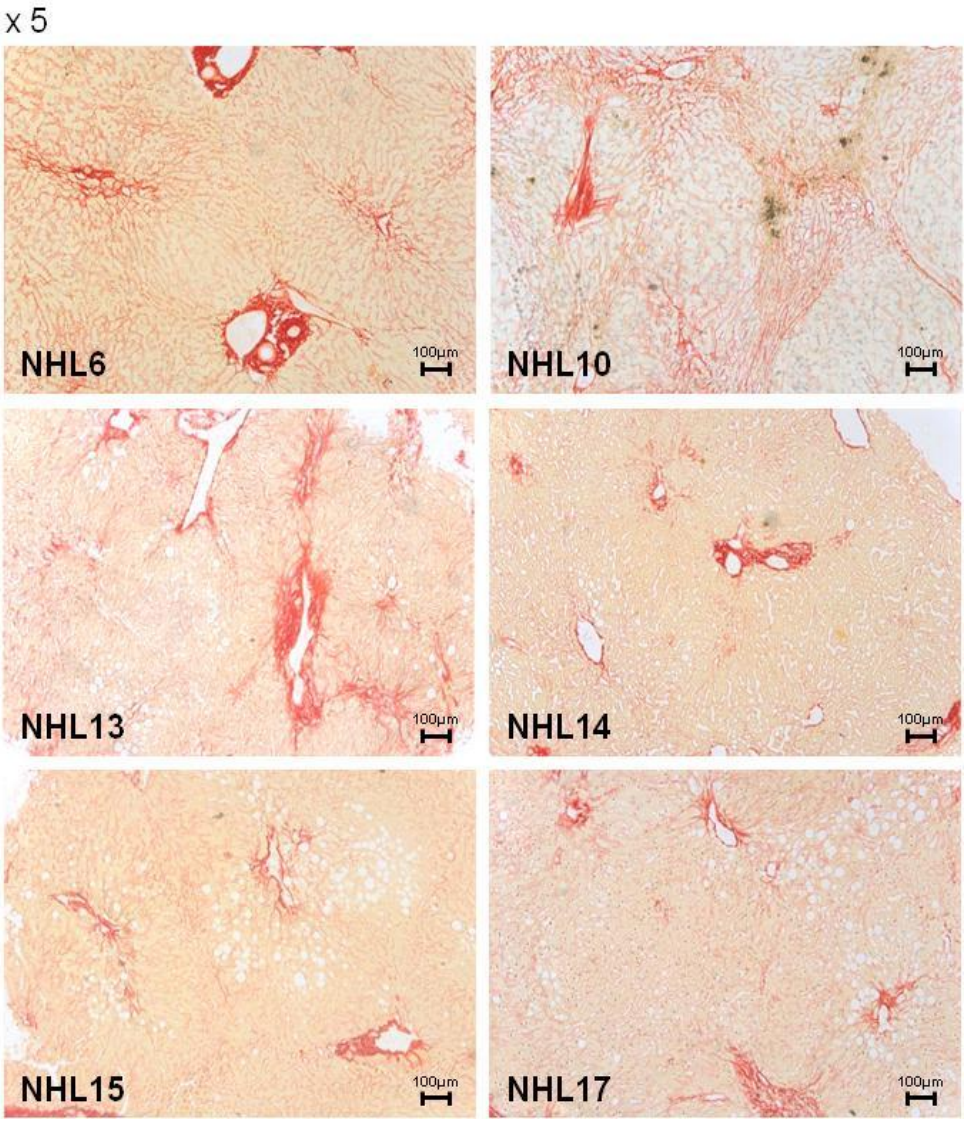

B

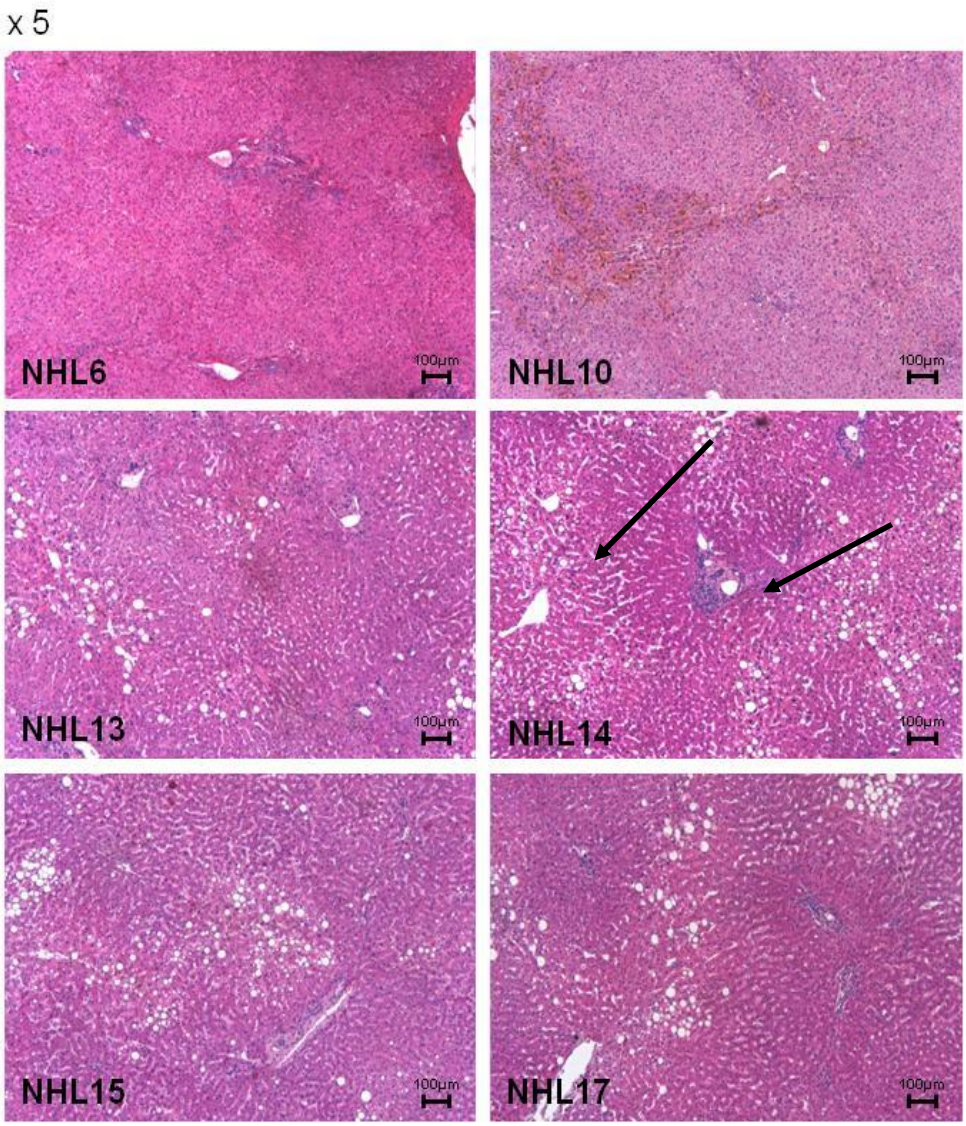

Figure 4.4: Human liver tissue demonstrated low levels of collagen deposition and differences in morphology.
Six different human liver samples were fixed for 24 hours in 10% formalin made up in 1 x PBS. Samples were then processed, embedded in paraffin and sectioned (5µm). Sections were then de-waxed and stained using **A)** sirius red or **B)** Haematoxylin and Eosin (H and E). Representative images were acquired at x 5 magnification. Staining is typical of three separate experiments. Scale bars = 100µm.

To further investigate damage in the differing human liver samples, each patient liver section were stained for α-SMA (Figure 4.5A) and vimentin (Figure 4.5B). As shown by the representative images, all samples displayed positive staining for both markers.

A

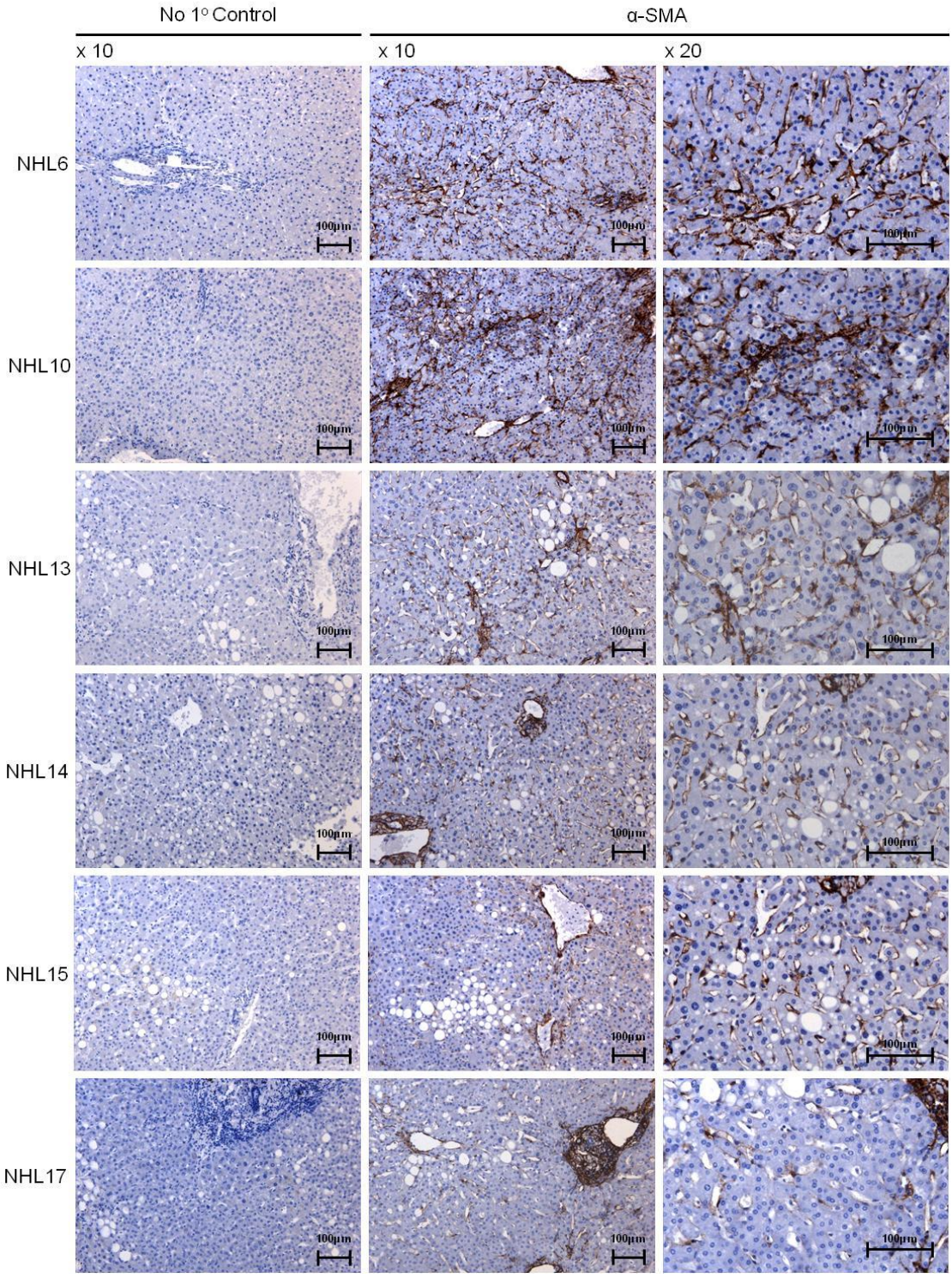

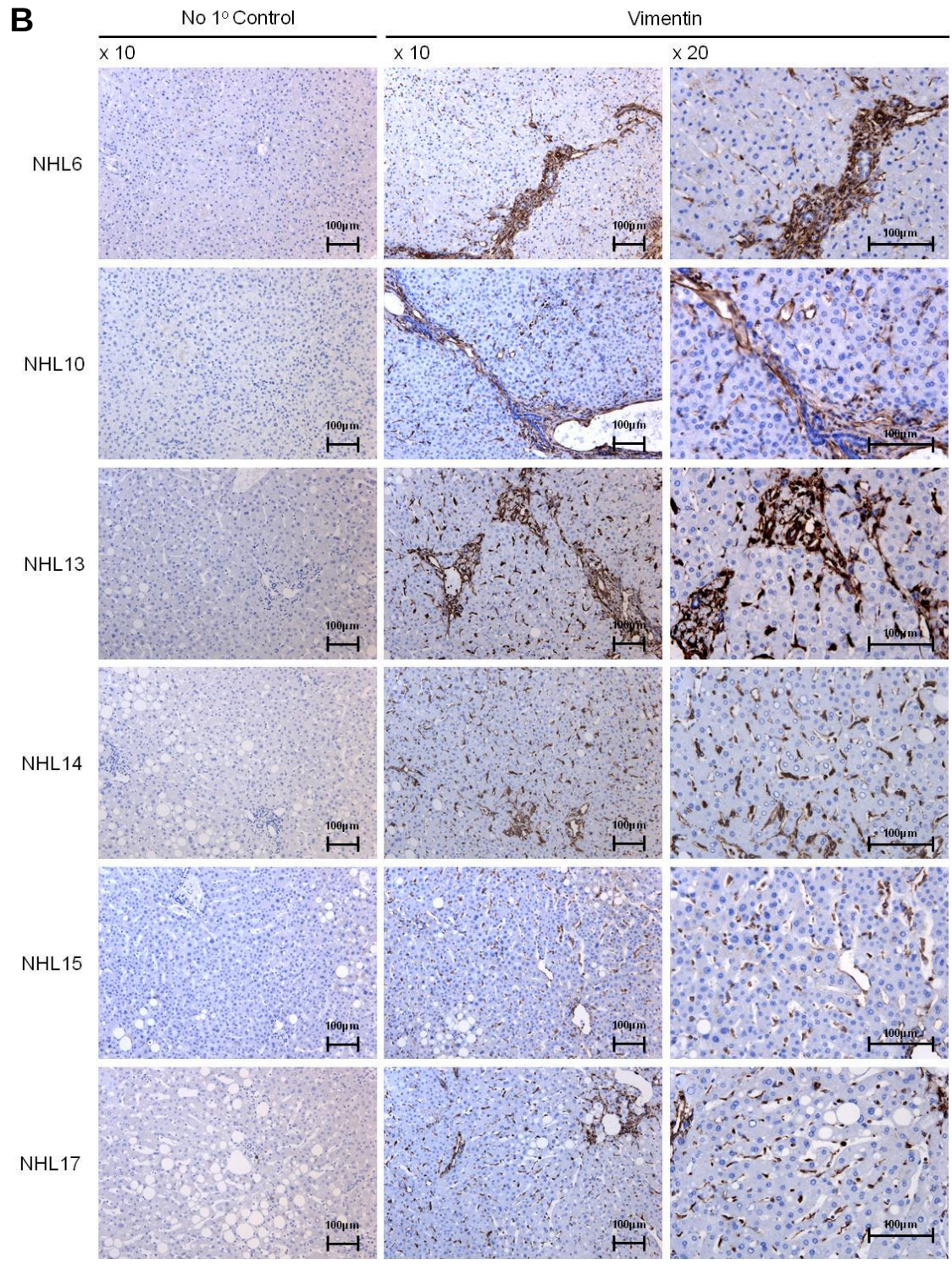

Figure 4.5: Human liver tissue demonstrated low levels of damage.
Six different human liver samples were fixed for 24 hours in 10% formalin made up in 1 x PBS. Samples were then processed, embedded in paraffin and sectioned (5µm). Sections were then de-waxed and stained using **A)** α-SMA and **B)** vimentin. No primary antibody controls were included and were stained with the secondary anti-mouse IgG (for α-SMA) or anti-rabbit IgG (for vimentin) antibody alone. Representative images were acquired at x 10 and x 20 magnification. Staining is typical of three separate experiments. Scale bars = 100µm.

To determine if biliary fibrosis in the human liver samples was evident, sections were also immunohistochemically stained using a marker for biliary epithelial cells (CK-19). As illustrated by Figure 4.6 positive staining was present in all of the six samples, however, biliary injury was not evident.

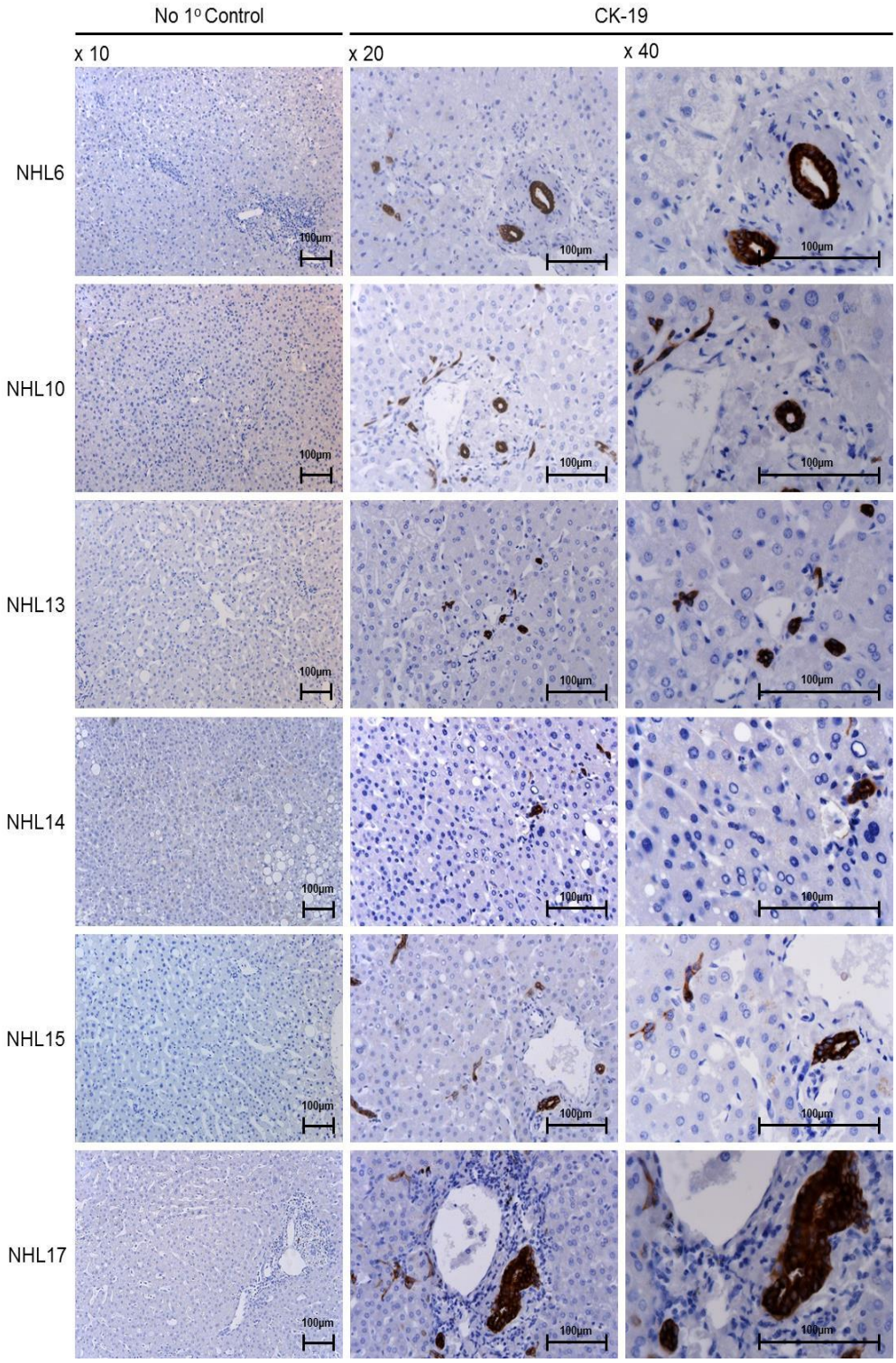

Figure 4.6: Assessment of biliary fibrosis in human liver tissue.
Six different human liver samples were fixed for 24 hours in 10% formalin made up in 1 x PBS. Samples were then processed, embedded in paraffin and sectioned (5µm). Sections were then de-waxed and stained using **A)** CK19. No primary antibody controls were included and were

stained with the secondary anti-mouse IgG antibody alone. Representative images were acquired at x 10 and x 20 magnification. Staining is typical of three separate experiments. Scale bars = 100µm.

The mRNA and protein expression of CXCR4 and CXCL12 variants in the human liver samples was examined by using RT-PCR and Western blot analysis respectively. RT-PCR analysis demonstrated that all liver samples expressed CXCR4 and CXCL12 mRNA variants (α β γ) apart from NHL14 which did not express CXCR4 mRNA (Figure 4.7A). At the protein level, CXCR4 was present in patients NHL15 and NHL17 (Figure 4.7B) but expression levels were low compared to the positive control (Figure 4.5C). Bands were also observed at ~80 kDa (NHL-17 and CHL-1), ~70 kDa (CHL-1), ~53 kDa (NHL-6), ~47 kDa (NHL10, 13, 14, 15 and 17) and at ~38 kDa (NHL13, 14, 15 and 17) (Figure 4.7B). Expression of CXCL12 was not observed in any of the patient samples (Figure 4.5D and E), however, prominent bands were observed in all of the patient samples at ~62 kDa and bands at ~60 kDa (NHL6, 10 and 13) (Figure 4.7D). Fainter bands were observed at ~43 kDa in all of the patient samples except NHL14 (Figure 4.7D).

A

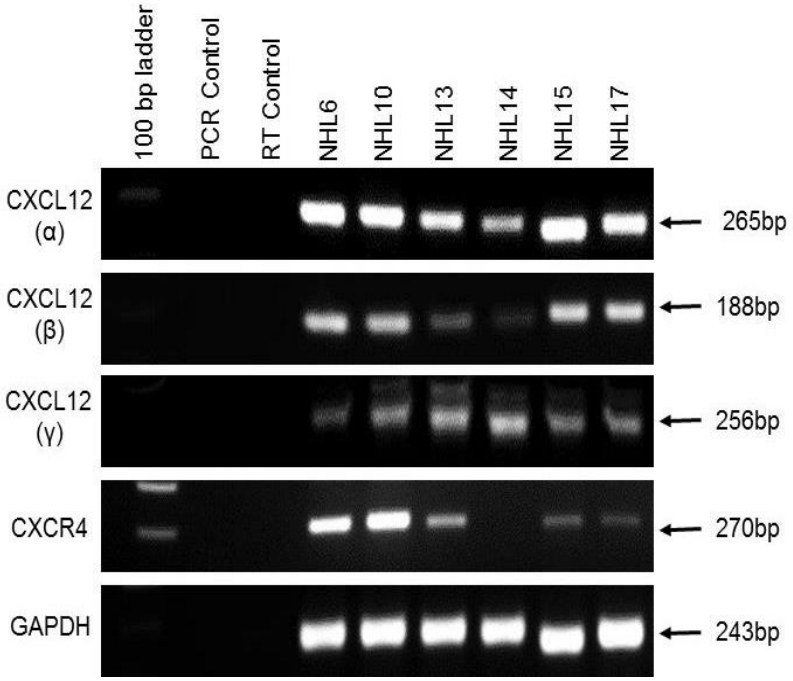

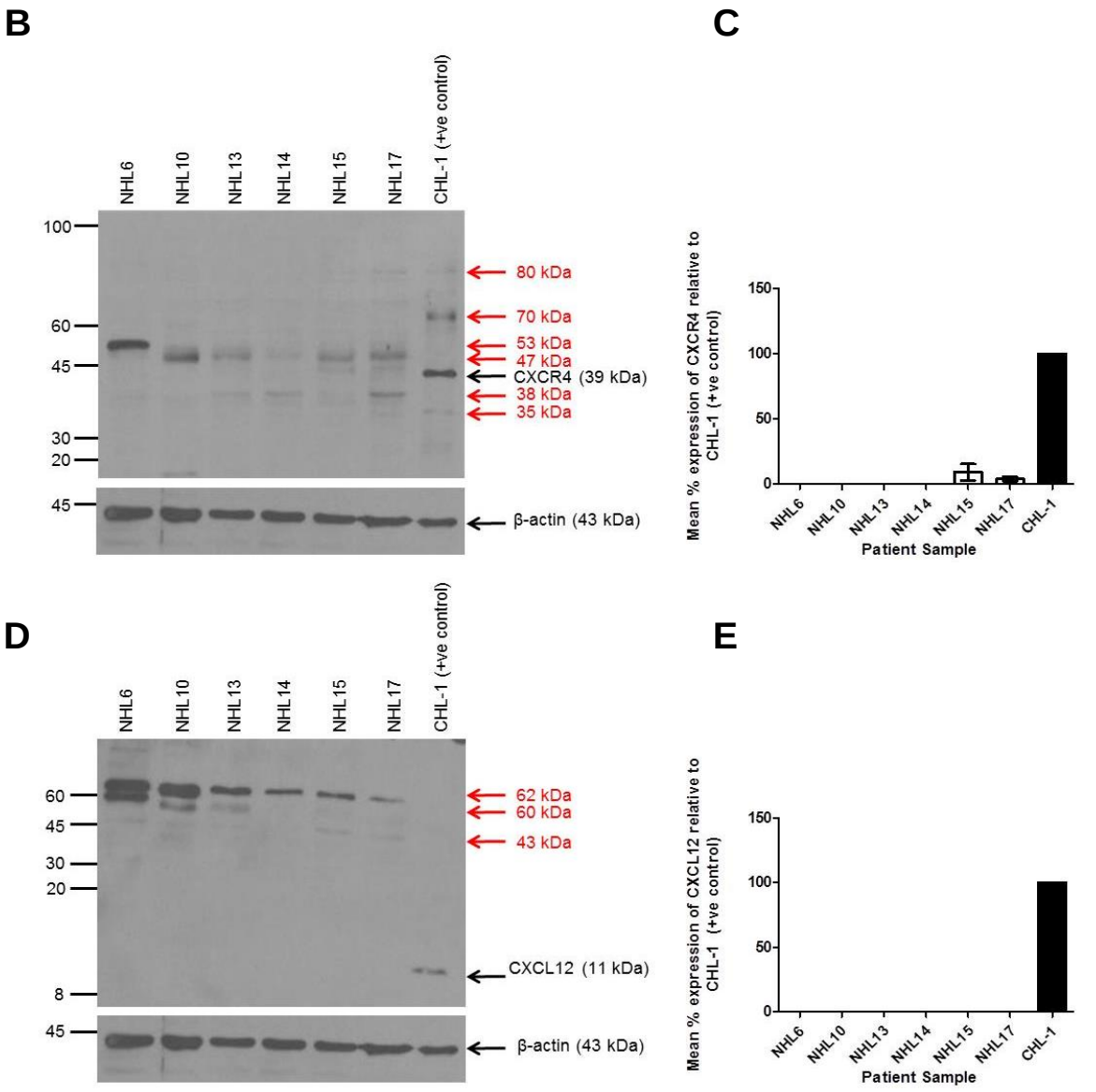

Figure 4.7: Both CXCR4 and CXCL12 variants are expressed in human liver tissue.
A) Representative RT-PCR for the expression of CXCR4 and CXCL12 variants in human liver tissue. Total RNA was isolated using Trizol, as per manufacturer's instructions from whole human liver tissue. RT-PCR and RT controls were carried out in the absence of template RNA and reverse transcriptase respectively. RT-PCR products were electrophoresed in 1.5% agarose gels containing ethidium bromide with a 100bp ladder to establish the size of the RT-PCR products and visualized by UV light. **B)** Representative Western blot for the expression of CXCR4 in human liver tissue and **C)** Quantitative densitometry analysis of three typical western blots was performed using the Image J software. **D)** Representative Western blot for the expression of CXCL12 in human liver tissue and **E)** Quantitative densitometry analysis of three typical western blots was performed using the Image J software. For all Western blots whole liver tissue was homogenised followed by sonication and prepared for protein analysis by Western blot. 20µg of protein was loaded per lane and β-actin was used as a loading control. Error bars represent +/- SD.

4.2.3: Murine biliary epithelial cells and hepatocytes express CXCR4 in normal mouse liver tissue.

Subsequent studies of CXCR4 expression in specific cell types within normal mouse liver was determined in paraffin embedded tissue by immunohistochemistry. As shown by the representative images in Figure 4.8A and B CXCR4 was expressed by the hepatocytes and biliary epithelial cells and on closer viewing was seen to be concentrated in the nucleus and nuclear membrane (Figure 4.8B). Immunofluorescence staining was also performed on the mouse liver sections with the addition of α-SMA. The results supported the immunohistochemistry results in section 4.2.1, demonstrating that fibrosis was not evident (Figure 4.8A) and in addition showed that the hepatocytes and biliary epithelial cells express CXCR4 (Figure 4.8C and D).

A

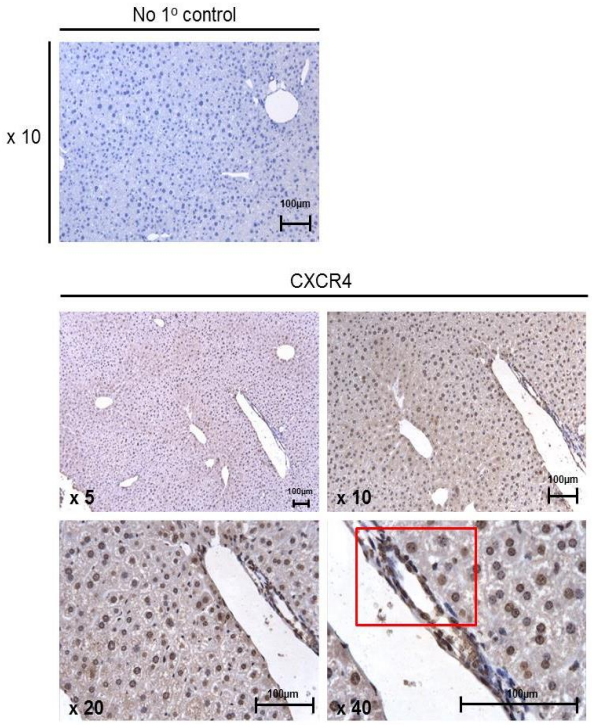

B

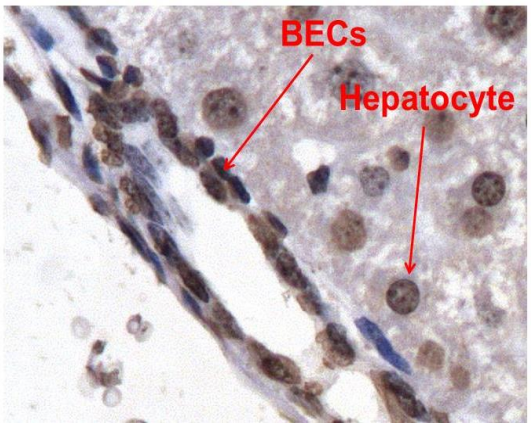

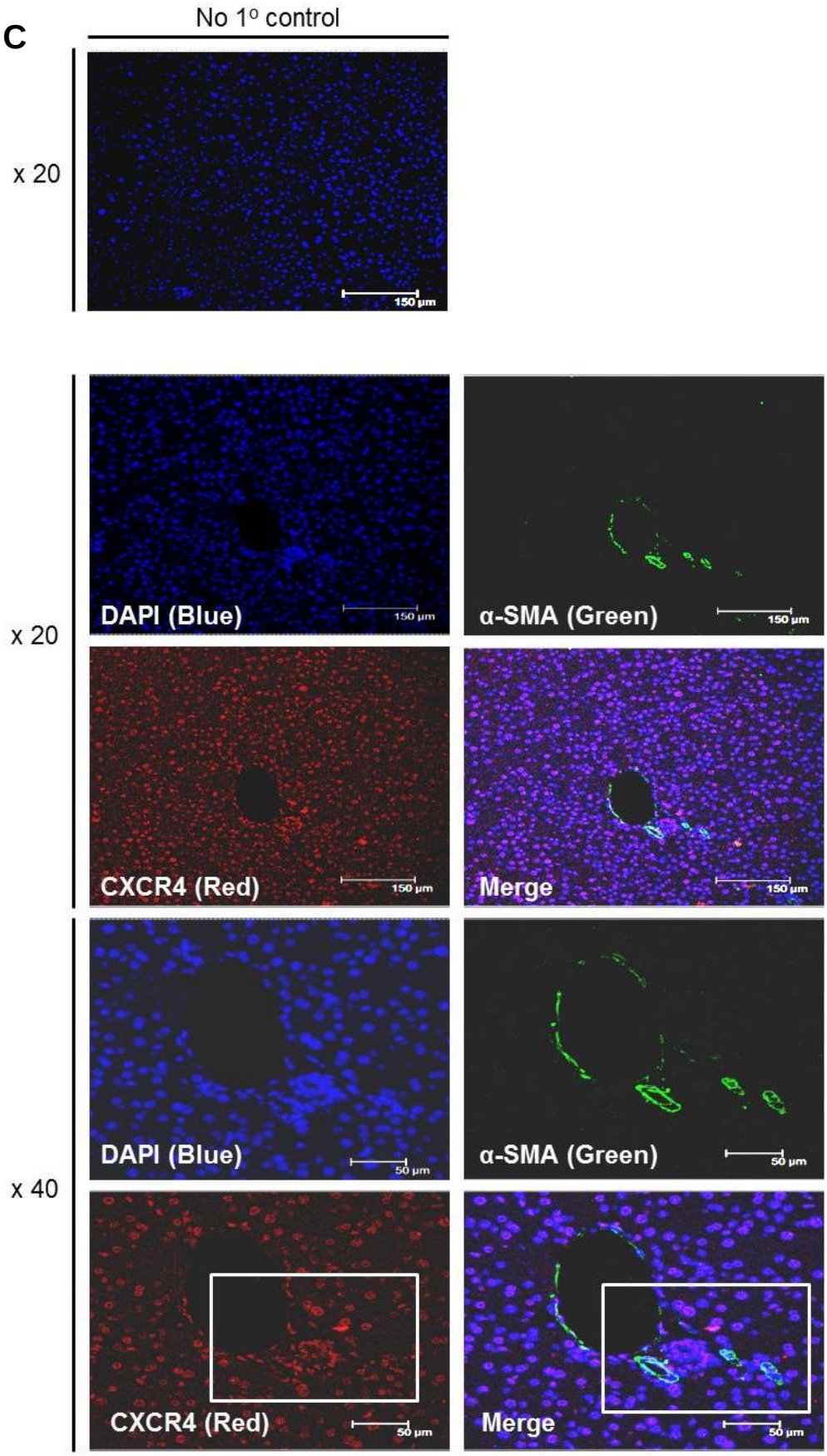
C
No 1º control
x 20
150 µm
x 20
DAPI (Blue)
150 µm
α-SMA (Green)
150 µm
CXCR4 (Red)
150 µm
Merge
150 µm
x 40
DAPI (Blue)
50 µm
α-SMA (Green)
50 µm
CXCR4 (Red)
50 µm
Merge
50 µm

D

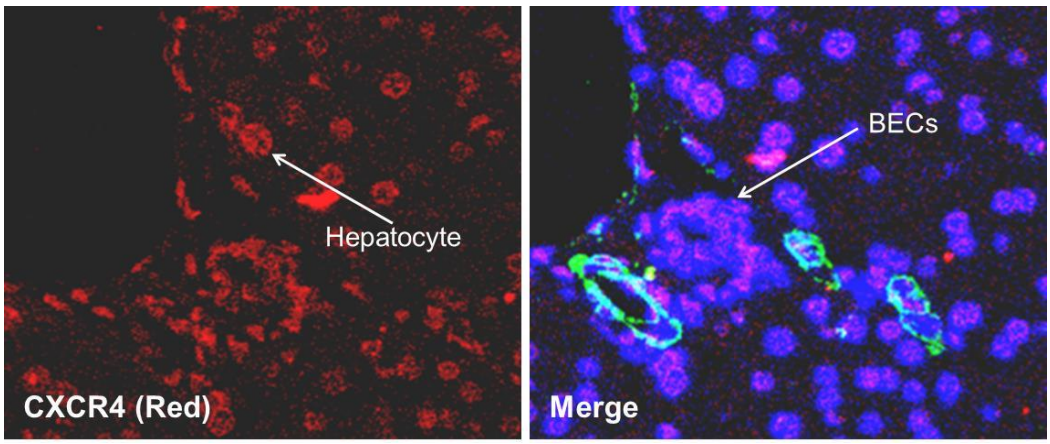

Figure 4.8: CXCR4 is expressed by biliary epithelial cells and hepatocytes in the normal mouse liver.
C57BL/6 mice were culled and livers were harvested and fixed for 24 hour in 10% formalin made up in 1 x PBS. Samples were then processed, embedded in paraffin and sectioned (5µm). Sections were then de-waxed and immunochemically stained. **A)** No primary antibody controls were included and were stained with the secondary anti-mouse IgG alone. Sections were stained with the antibody to CXCR4. Representative images were acquired at x 5, x 10, x 20 and x 40 magnification. Scale bars = 100µm **B)** A closer view of the x 40 image shows the expression of CXCR4 concentrated in the nucleus and nuclear membrane. **C)** The expression of CXCR4 (red) and α-SMA (green) was determined by confocal microscopy and background levels were set against the no primary control. DAPI was used to stain the nuclei. CXCR4 was expressed by the hepatocytes and the biliary epithelial cells also shown by **D)** zoomed in images. Representative images were acquired at x 20 and x 40 magnification. Scale bars = 150µm (x 20) and 50µM (x 40). Staining is typical of three separate experiments.

4.2.4: CXCL12 is expressed by murine biliary epithelial cells in normal mouse liver tissue.

CXCL12 expression was determined in the normal mouse liver tissue sections by immunohistochemistry and immunofluorescence. Representative immunohistochemistry images (Figure 4.9A-B), supported by the immunofluorescence studies (Figure 4.9C and D) demonstrated that CXCL12 was expressed by mouse biliary epithelial cells.

A

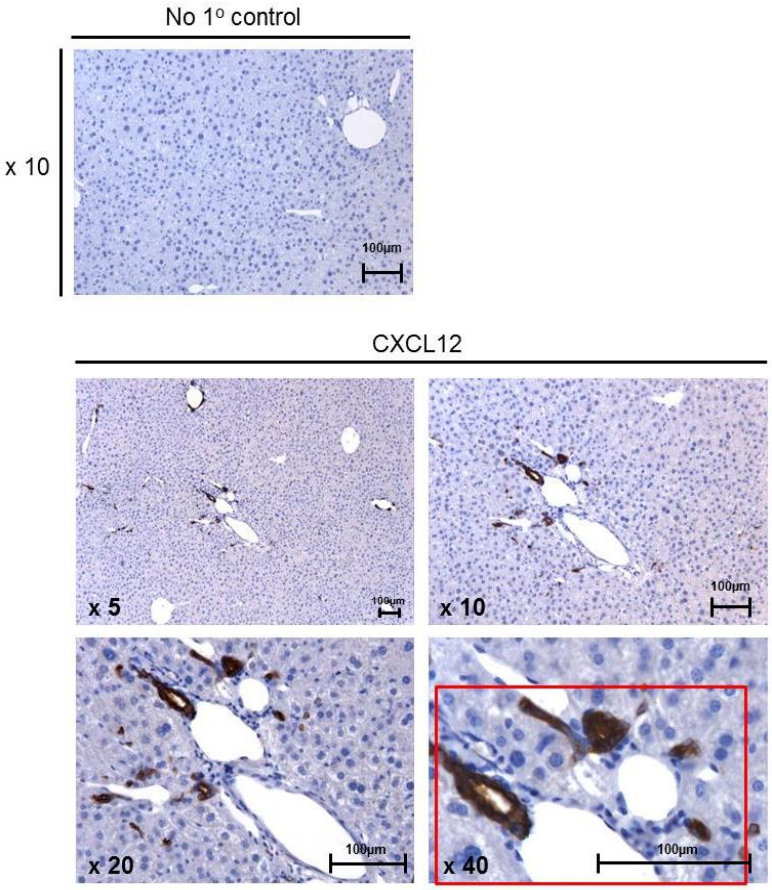
No 1º control
x 10
100µm
CXCL12
x 5
100µm
x 10
100µm
x 20
100µm
x 40
100µm

B

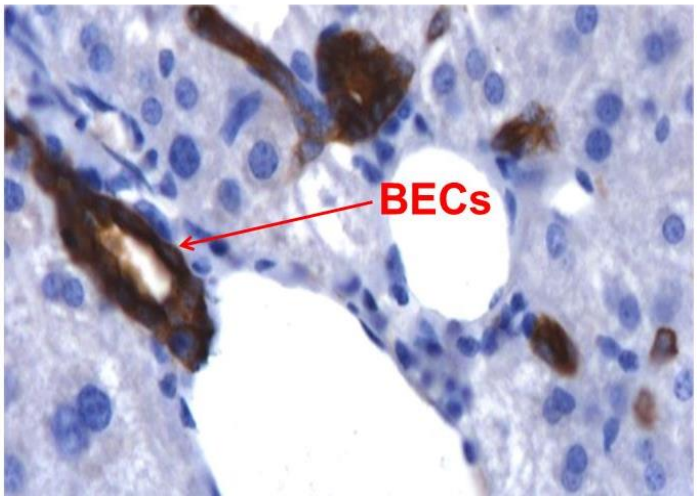
BECs

C

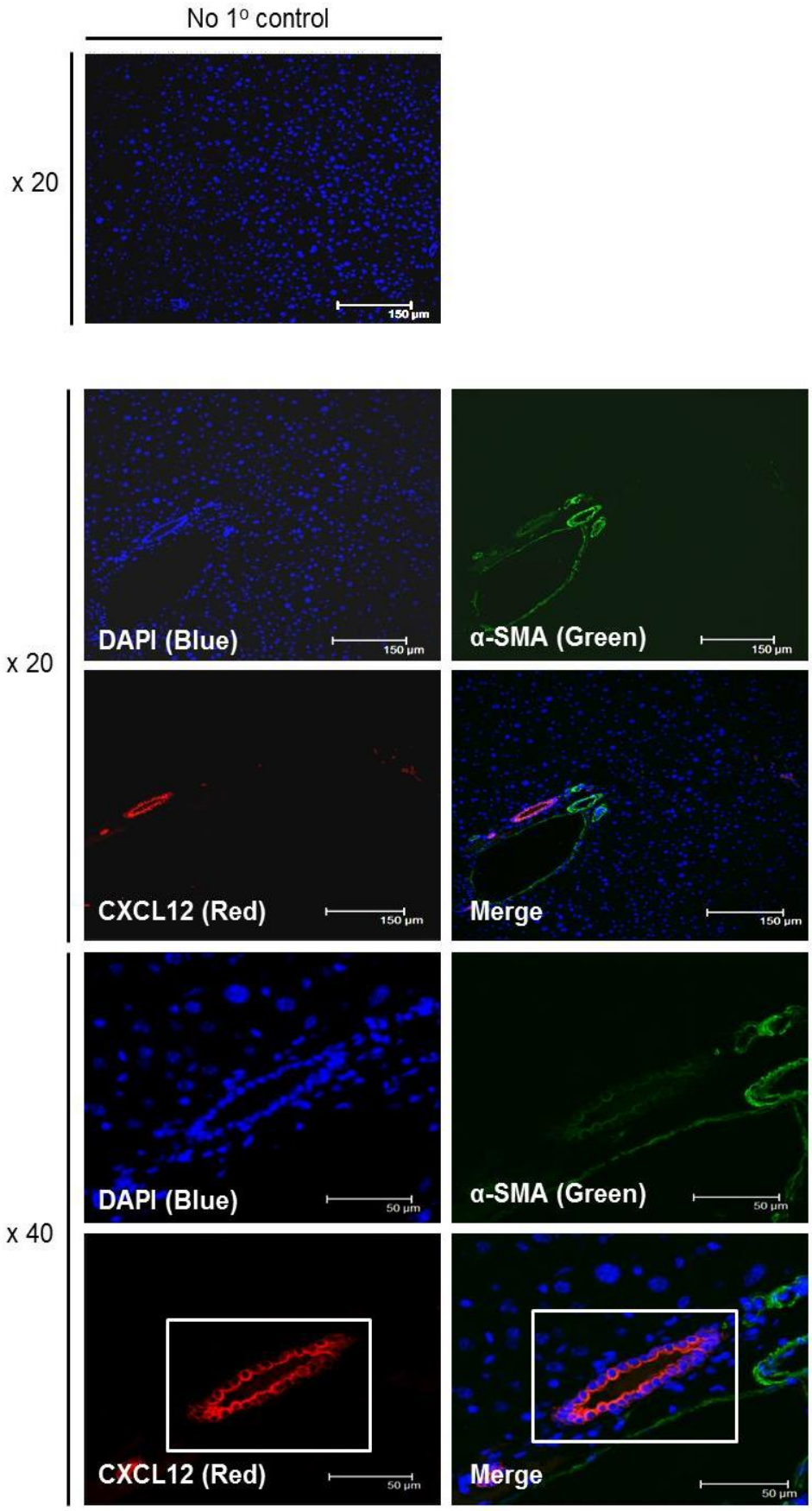
No 1º control
x 20
150 µm
x 20
DAPI (Blue)
150 µm
α-SMA (Green)
150 µm
CXCL12 (Red)
150 µm
Merge
150 µm
x 40
DAPI (Blue)
50 µm
α-SMA (Green)
50 µm
CXCL12 (Red)
50 µm
Merge
50 µm

D

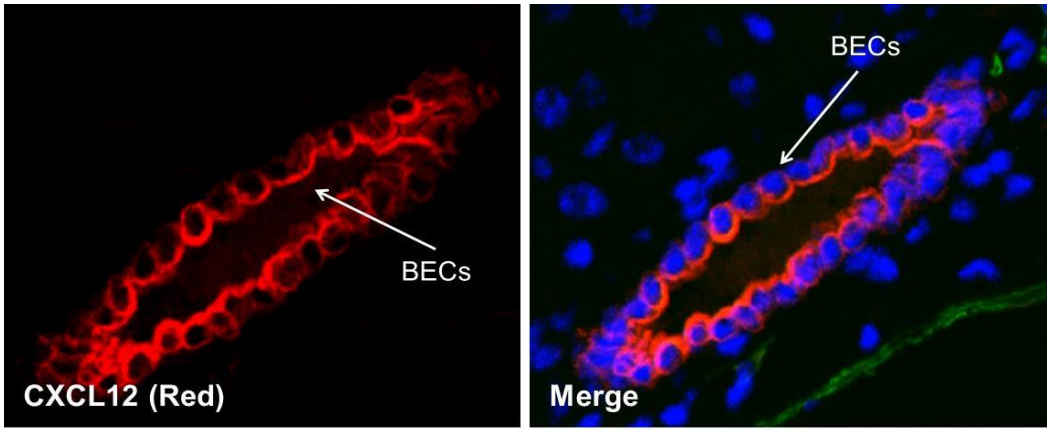

Figure 4.9: CXCL12 is expressed by biliary epithelial cells in the normal mouse liver. C57BL/6 mice were culled and livers were harvested and fixed for 24 hour in 10% formalin made up in 1 x PBS. Samples were then processed, embedded in paraffin and sectioned (5µm). Sections were then de-waxed and immunochemically stained. **A)** No primary antibody controls were included and were stained with the secondary anti-mouse IgG alone. Sections were stained with the antibody to CXCL12. Representative images were acquired at x 5, x 10, x 20 and x 40 magnification. Scale bars = 100µm **B)** A closer view of the x 40 image shows the expression of CXCL12 concentrated inside the biliary duct. **C)** The expression of CXCR4 (red) and α-SMA (green) was determined by confocal microscopy and background levels were set against the no primary control. DAPI was used to stain the nuclei. CXCL12 was expressed by the biliary epithelial cells also shown by **D)** zoomed in images. Representative images were acquired at x 20 and x 40 magnification. Scale bars = 150µm (x 20) and 50µM (x 40). Staining is typical of three separate experiments.

4.2.5: In human liver tissue, biliary epithelial cells and hepatocytes express CXCR4.

As in studies of CXCR4 expression in mouse liver, expression was also determined by both immunohistochemistry and immunofluorescence in human liver tissue. In three representative patient samples, results demonstrated that CXCR4 was expressed by both hepatocytes and biliary epithelial cells. In addition, expression of CXCR4 was concentrated in the nucleus and the nuclear membrane (Figure 4.10A-E).

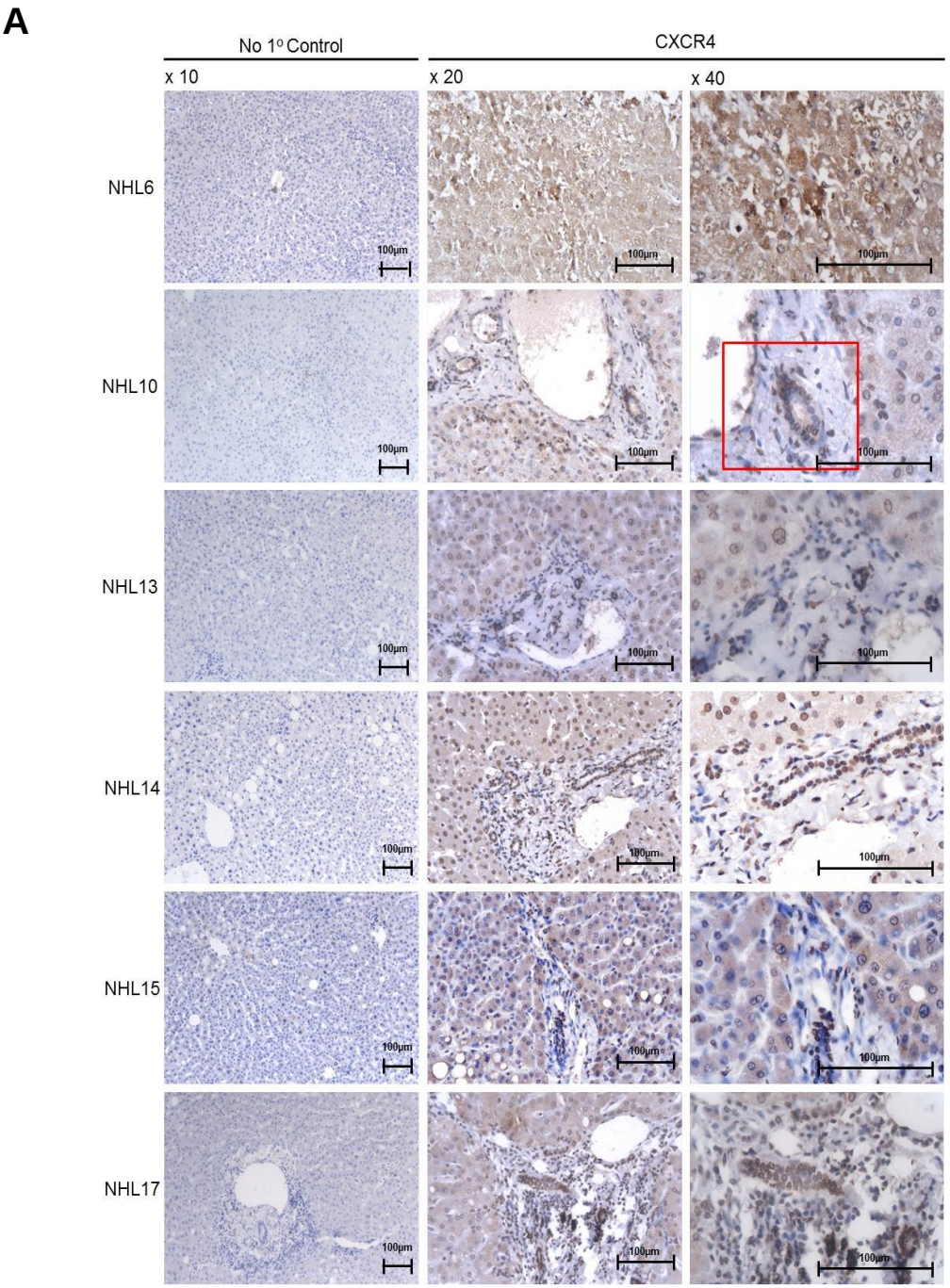

B

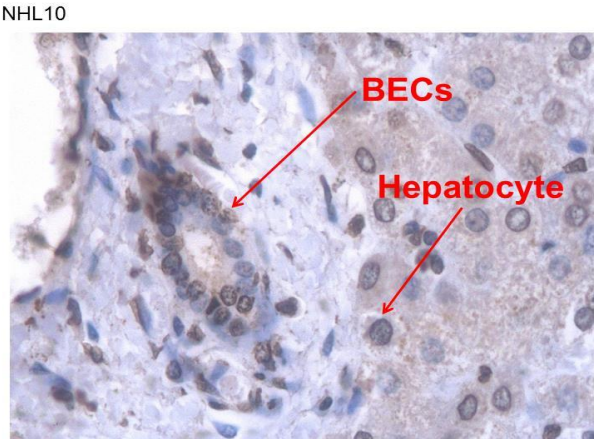
NHL10
BECs
Hepatocyte

C

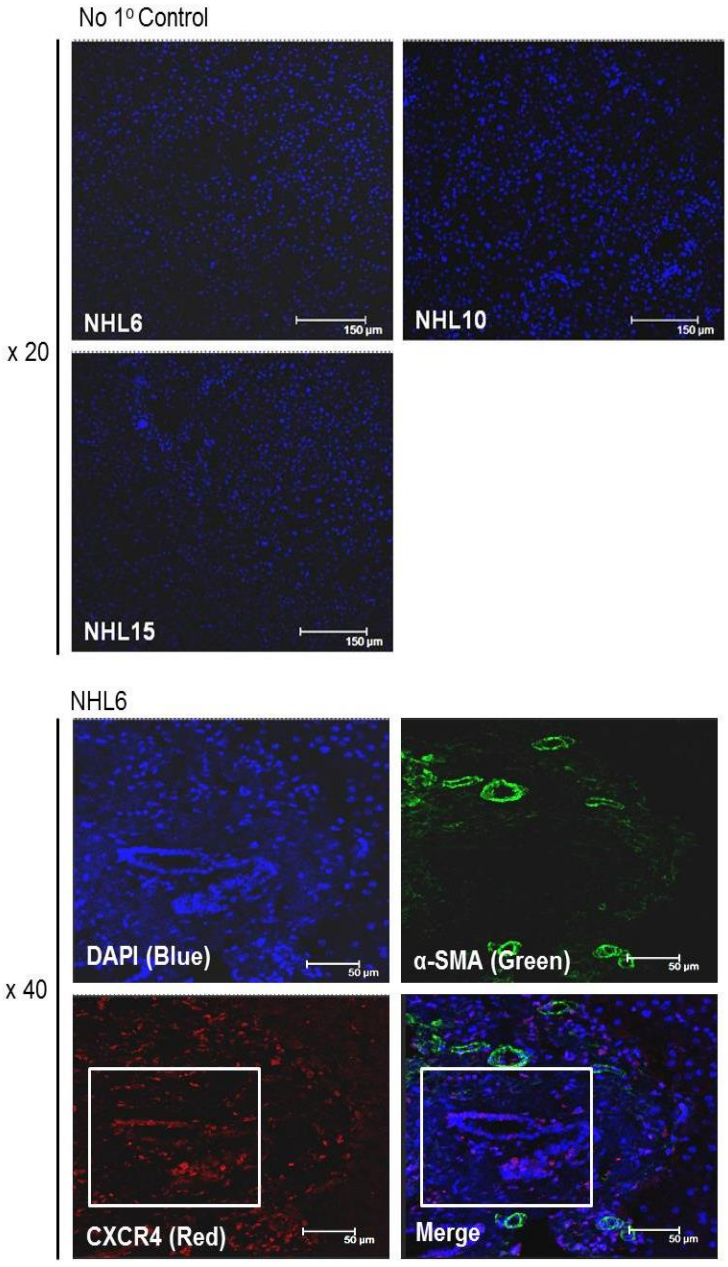
No 1° Control
x 20
NHL6
150 µm
NHL10
150 µm
NHL15
150 µm
NHL6
x 40
DAPI (Blue)
50 µm
α-SMA (Green)
50 µm
CXCR4 (Red)
50 µm
Merge
50 µm

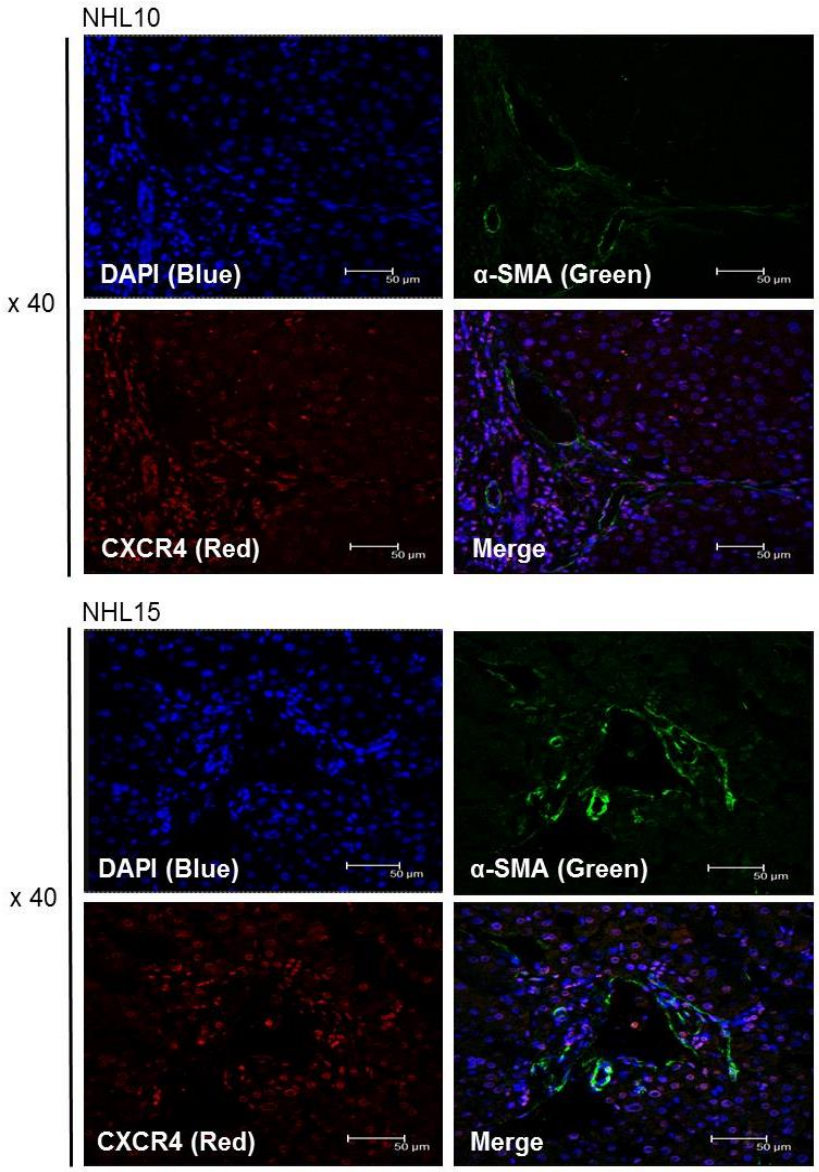

D

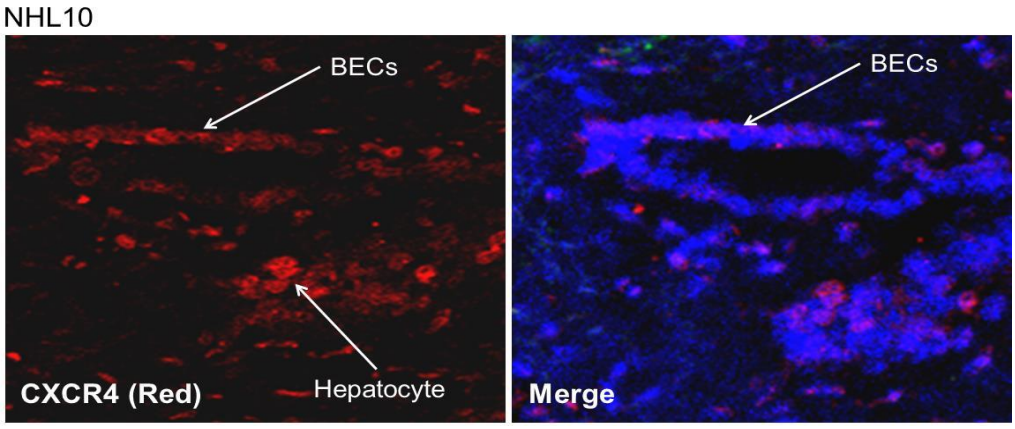

Figure 4.10: CXCR4 is expressed by biliary epithelial cells and hepatocytes in human liver. Six different human liver samples were fixed for 24 hours in 10% formalin made up in 1 x PBS. Samples were then processed, embedded in paraffin and sectioned (5µm). Sections were then de-waxed and immunochemically stained. **A)** No primary antibody controls were included and

were stained with the secondary anti-mouse IgG alone. Sections were stained with the antibody to CXCR4. Representative images were acquired at x 5, x 10, x 20 and x 40 magnification. Scale bars = 100µm **B)** A closer view of the x 40 image shows the expression of CXCR4 by biliary epithelial cells (BECs) and hepatocytes. **C)** The expression of CXCR4 (red) and α-SMA (green) was determined by confocal microscopy and background levels were set against the no primary control. DAPI was used to stain the nuclei. CXCR4 was expressed by the hepatocytes and the biliary epithelial cells also shown by the **D)** zoomed in images. Representative images were acquired at x 20 and x 40 magnification. Scale bars = 150µm (x 20) and 50µM (x 40). Staining is typical of three separate experiments.

4.2.6: Human biliary epithelial cells express CXCL12 *in vivo*.

Immunohistochemistry and immunofluorescence was performed on the human liver sections and CXCL12 was observed in the biliary epithelial cells (Figure 4.11A-E) but detection of CXCL12 in sinusoidal cells was not evident. The α-SMA staining also demonstrated low levels of damage in the three representative patient samples (Figure 4.11C).

A

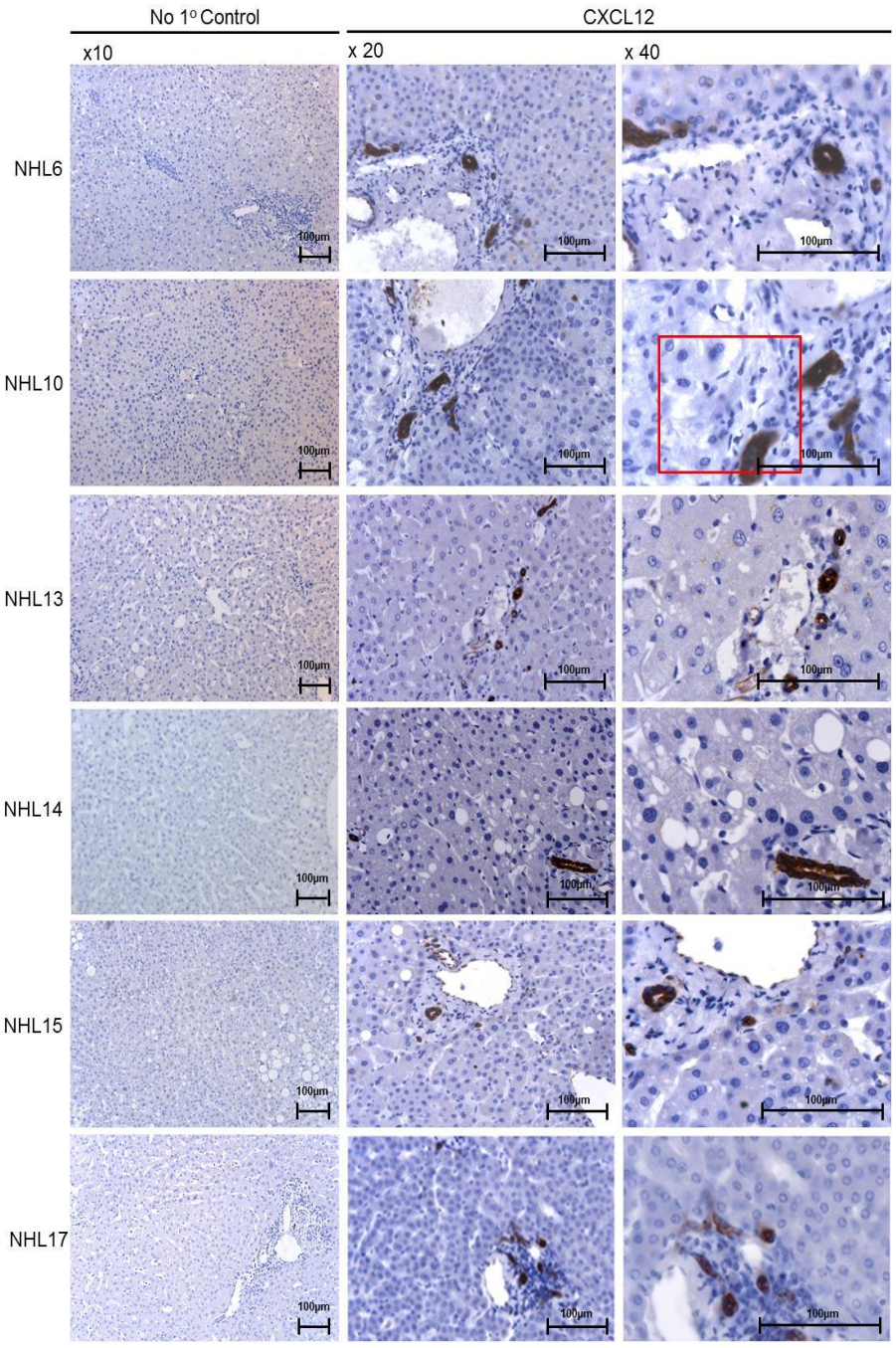

B

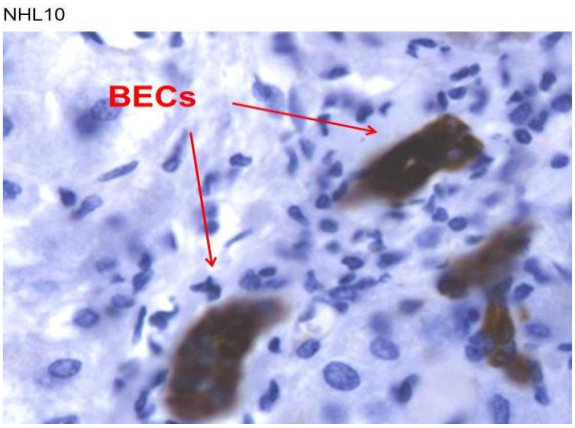
NHL10
BECs

C

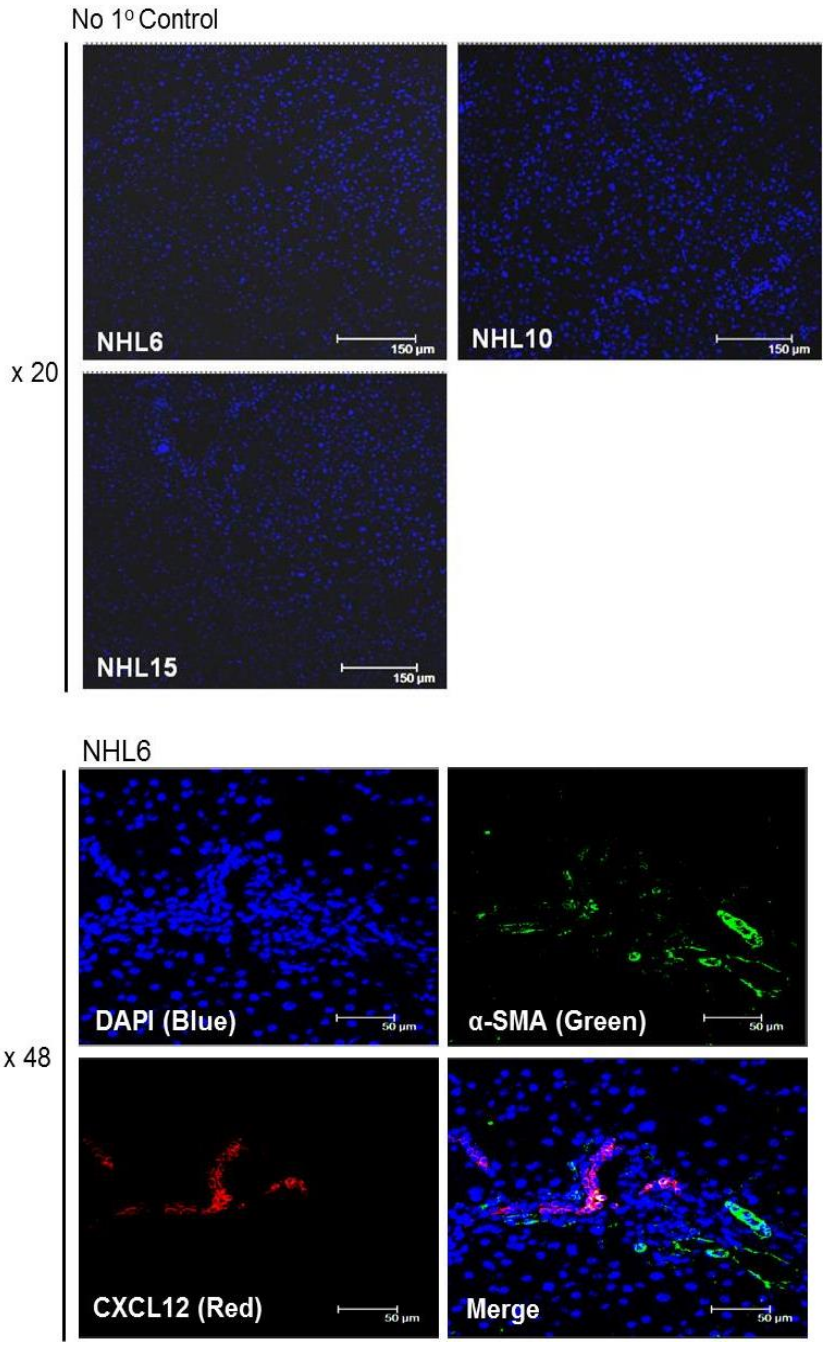
No 1º Control
x 20
NHL6
150 µm
NHL10
150 µm
NHL15
150 µm
NHL6
x 48
DAPI (Blue)
50 µm
α-SMA (Green)
50 µm
CXCL12 (Red)
50 µm
Merge
50 µm

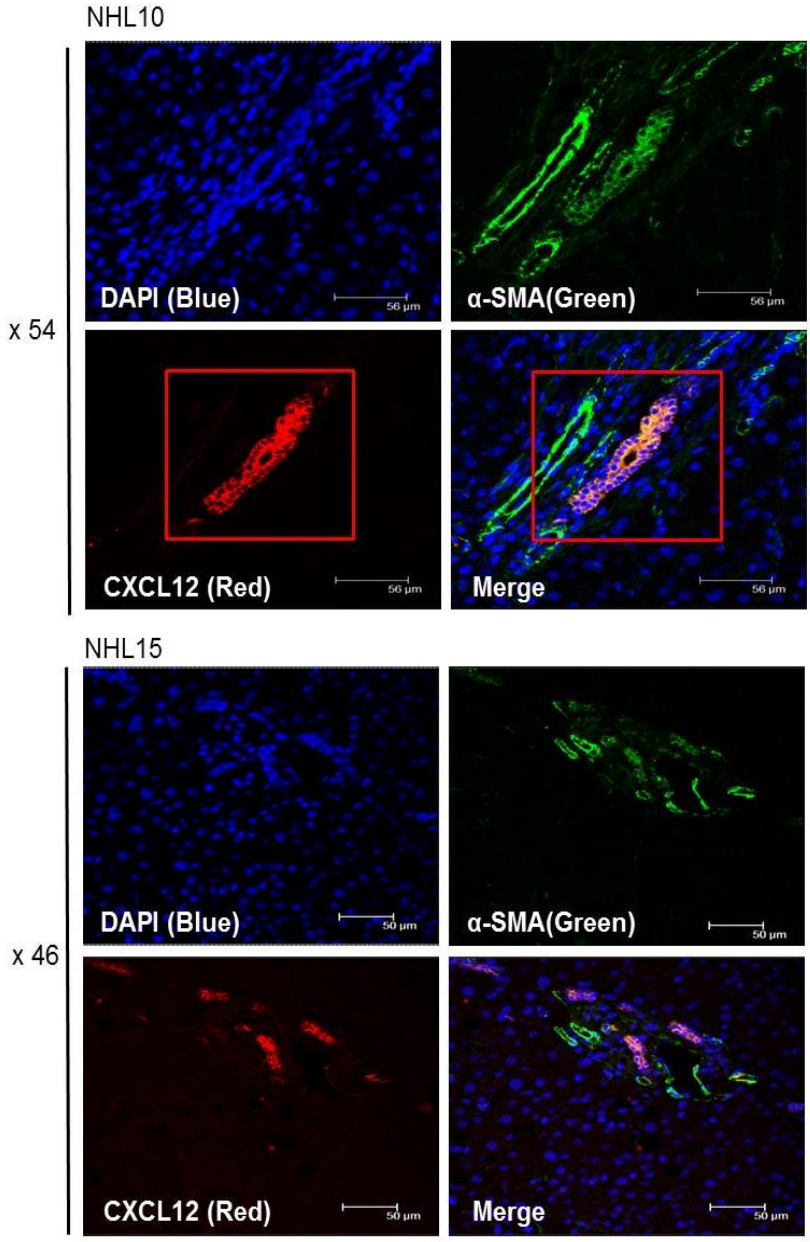

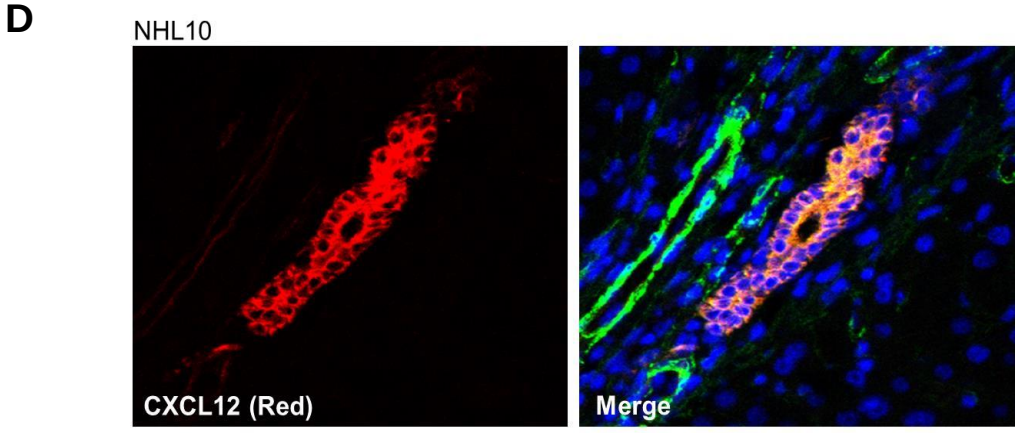

Figure 4.11: CXCL12 is expressed by biliary epithelial cells in the human liver.
Six different human liver samples were fixed for 24 hours in 10% formalin made up in 1 x PBS. Samples were then processed, embedded in paraffin and sectioned (5µm). Sections were then

de-waxed and immunochemically stained. **A)** No primary antibody controls were included and were stained with the secondary anti-mouse IgG alone. Sections were stained with the antibody to CXCL12. Representative images were acquired at x 5, x 10, x 20 and x 40 magnification. **B)** A closer view of the x 40 image shows the expression of CXCL12 by biliary epithelial cells (BECs). **C)** The expression of CXCL12 (red) and α-SMA (green) was determined by confocal microscopy and background levels were set against the no primary control. DAPI was used to stain the nuclei. CXCL12 was expressed by the biliary epithelial cells also shown by the **D)** zoomed in images of NHL10. Representative images were acquired at x 20 and x 40 magnification. Scale bars = 150µm (x 20) and 50µM (x 40). Staining is typical of three separate experiments.

4.3: Chapter Discussion

Results from this chapter demonstrated that in normal mouse organs and human liver tissue, CXCR4 and variants of CXCL12 mRNA were expressed. In addition to this, CXCR4 protein was present in the murine brain, lungs, liver, kidney and spleen but was only detected in two of the human liver tissue samples (NHL 15 and NHL17). While CXCL12 was not detected in the murine or human liver tissue, it was expressed in the murine lungs and spleen. However, interestingly, for each protein, bands of differing sizes in both murine and human tissue were observed. As these bands were absent in the positive controls, they could be non-specific i.e. binding to another protein. Alternatively, they could be post-translationally modified proteins which will be discussed later in more detail. Results also confirmed that both murine and human biliary epithelial cells expressed CXCR4 and CXCL12 while hepatocytes expressed CXCR4. Furthermore, CXCR4 expression appeared to be concentrated in the nucleus and the nuclear membrane and CXCL12 in the cytoplasm, supporting the data observed in *in vitro* in the previous chapter.

Consistent with previous findings, results from the present study demonstrated CXCL12-α was the most abundantly expressed splicing variant where it is known to be found in highly vascularised organs such as the liver (Teicher and Fricker 2010). The data from murine studies also confirmed previous observations that CXCL12-β is not detected in the brain (Janowski 2009). However, it was surprising this variant was not detected in the lungs as this has been reported previously (Janowski 2009). However, since the PCR carried out was semi-quantitative expression levels may have been too low to be detected. Therefore it would be beneficial to perform qRT-PCR to confirm this finding.

In previous studies, in humans (Yu, Cecil et al. 2006) CXCL12-γ was expressed at low levels in vascularized organs such as the liver and the data presented here is consistent with this. At the protein level, CXCR4 was expressed in various organs supporting previous literature (Teicher and Fricker 2010). It has been reported that CXCL12 is present in most organs (Teicher and Fricker 2010) however, in these studies it was only abundant in the lungs and spleen. In the human liver tissue, CXCR4 was observed in patients NHL15 and NHL17 but

CXCL12 expression was not detected. Despite this, Western blotting data revealed bands for both CXCR4 and CXCL12 of varying sizes which has not been reported previously. It is known that chemokines and chemokine receptors form dimers *in vivo* (Janowski 2009). However, it is unlikely that this would be the reason for observing bands above the predicted sizes since disulphide bonds should be broken during sample preparation as they are prepared in DTT and then heated at 90^{o}C. One possible explanation which may account for this is that the antibodies used may be detecting another protein, so although specific *in vitro* they may be non-specific *in vivo*. An alternative explanation to these findings is that the proteins are post translationally modified *in vivo* and this has recently been reviewed for other chemokines in detail (Yoshimura, Robinson et al. 1989, Shirozu, Nakano et al. 1995).

Post translational modifications (PTMs) may include an addition of a functional group such as acetates, phosphates, lipids and carbohydrates, alternatively they may be modified via proteolytic processing by specific enzymes including proteases and peptidylargine deminases (Moelants, Mortier et al. 2013). There have been numerous studies that have already detected PTMs *in vivo* (Furutani, Nomura et al. 1989, Robinson, Yoshimura et al. 1989, Van Damme, Van Beeumen et al. 1989, Jiang, Tabak et al. 1991, Shirozu, Nakano et al. 1995, Van Coillie, Van Damme et al. 1999, Loos, Mortier et al. 2008, Proost, Loos et al. 2008). For example, natural truncated and glycosylated chemokines have been identified (Furutani, Nomura et al. 1989, Robinson, Yoshimura et al. 1989, Van Damme, Van Beeumen et al. 1989, Yoshimura, Robinson et al. 1989, Schroder, Sticherling et al. 1990, Jiang, Tabak et al. 1991) and in the chemokines; CCL2, CCL7, CCL8 and CCL13 the NH_2-terminal glutamine residue is converted in pyroglutamic acid (Van Coillie, Van Damme et al. 1999). The chemokines CXCL8 and CXCL10 modifications of arginine residues into citrulline have also been identified (Van Coillie, Proost et al. 1998, Loos, Mortier et al. 2008, Proost, Loos et al. 2008). More recently, nitration/nitrosylation was identified as another process by which chemokines are modified whereby tyrosine is converted into nitrotyrosine by reactive oxygen species including peroxynitrate anion and nitrogen dioxide (Murphy, Cho et al. 2007). PTMs are known to influence chemokine activity (Moelants, Mortier et al. 2013) for example, matrix metalloproteinase-9 on CXCL18 promotes its activity (Van den Steen, Proost et

al. 2000) whilst, matrix metalloproteinase-1-gelatinase A reduces the activity of CCL7 (McQuibban, Gong et al. 2000).

In the context of CXCL12 and CXCR4 PTMs have been identified (Caruz, Samsom et al. 1998). For example, phosphorylation on serine and threonine residues in the C terminal on CXCR4 occurs on agonist stimulation and phosphorylation at Ser-324 and Ser-325 which results in ubiquitination and protein degradation (Caruz, Samsom et al. 1998). Furthermore, sulfation on Tyr-21 is needed in order to achieve efficient binding of CXCL12, which in turn promotes dimerization (Caruz, Samsom et al. 1998). Tyr-12 have been found to be sulphated in a sequential manner once Tyr-21 is sulphated and interestingly, the binding affinity for CXCL12 is correlated with the number of sulfotyrosines (Caruz, Samsom et al. 1998). Furthermore, O and N glyocosylations have been observed and the N glyocosylations have shown to inhibit co-receptor function in HIV-strains by preventing the interaction with their Env glycoproteins (Caruz, Samsom et al. 1998). CXCL12-α is initially cleaved at the C-terminus and is then processed at the N-terminus (Shirozu, Nakano et al. 1995). As a result of binding to heparin and cell surface proteoglycans the C-terminal processing of CXCL12-α is reduced (Shirozu, Nakano et al. 1995). However, the reason as to why proteins are observed above the predicted sizes (CXCR4 (39 Kda) and CXCL12 (11 Kda)) is yet to be determined.

The detection of PTMs of chemokines *in vivo* has been extremely challenging firstly since the concentration of chemokine secretion is generally low and secondly that the assays used such as ELISAs are unable to discriminate between the different isoforms (Moelants, Mortier et al. 2013). Furthermore, PTMs by NH_2 or COOH-terminal truncation, citrullination or nitration cause structural and chemical changes and therefore the antibodies may not be able to identify isoforms present (Moelants, Mortier et al. 2013). Additionally, detection in clinical samples may be further complicated due to the presence of chemokine degrading enzymes active still after sampling (Moelants, Mortier et al. 2013). Moreover, in order to identify the modifications complex techniques such as mass spectrometry and Edman degradation are required. However, one possible investigation which could be performed would be to knockdown CXCR4 and

CXCL12 in the different liver cell types that express these proteins and then see whether or not bands above the predicted molecular weights are observed.

Results demonstrating expression of CXCL12 and CXCR4 by bilary epithelial cells and CXCR4 by hepatocytes supports previously published studies (Coulomb-L'Hermin, Amara et al. 1999, Terada, Yamamoto et al. 2003, Vlahakis, Villasis-Keever et al. 2003) and unpublished studies by the Bansal laboratory. In addition, the data supports the *in vitro* results observed in the previous chapter. Other studies have reported that murine and human sinusoidal cells express CXCL12 on their cell surface (Mendt and Cardier 2012, Saiman and Friedman 2012) but expression in these cells was not observed and therefore this would warrant further investigation. Furthermore, in section 3.2.7 it was shown that myofibroblasts secrete CXCL12 and this has also been reported *in vivo* (Hong, Tuyama et al. 2009). However, very few myofibroblasts would have been present since the tissues used were deemed to be healthy.

Collectively, the data presented here demonstrates that CXCR4 and variants of CXCL12 are present in a wide range of tissues. More specifically that they are expressed by biliary epithelial cells and hepatocytes in liver tissue. Furthermore, the data suggests that in *in vivo* PTMs to these two proteins may occur. Since modified chemokines have been shown to influence their activity under certain physiological and pathological conditions (Moelants, Mortier et al. 2013) it will be essential to identify the modified chemokines present and also their specific biological functions.

Chapter 5: Results 3

Influence of liver fibrosis on CXCL12 levels in chronic liver injury models.

5.1: Introduction and Aims

Liver damage causes hepatic fibrosis characterized by an accumulation of scarring proteins leading to the development of cirrhosis, hepatocellular carcinoma and eventually liver failure (Wallace, Burt et al. 2008). Ultimately, the localisation and distribution of fibrosis within the lobule is determined by the type of liver injury (Wallace, Burt et al. 2008). For example, in animal models of chronic liver injury, fibrosis induced by carbon tetrachloride (CCl_4) results in centrilobular necrosis and fibrosis emerging from the central vein (Wallace, Burt et al. 2008). Whereas bile duct ligation (BDL) and methapyrilene (MP) treatment causes damage to the periportal regions of the lobules and fibrosis emerging from the portal tracts. In humans, alcohol abuse, can lead to centrilobular necrosis whereas in viral hepatitis, fibrosis surrounding the portal tracts is observed (Wallace, Burt et al. 2008). Irrespective of the type of damage, in both acute and chronic liver injury, cell infiltration, angiogenesis and the secretion of chemokines from various liver cell types occurs (Saiman and Friedman 2012).

Several studies have demonstrated that chemokine production is dependent upon both the type and the duration of the injury (Goddard, Williams et al. 2001, Ajuebor, Hogaboam et al. 2003, Ajuebor, Hogaboam et al. 2004, Ajuebor, Carey et al. 2006, Ajuebor, Wondimu et al. 2007, Hokeness, Deweerd et al. 2007, Ajuebor, Chen et al. 2010, Aoyama, Inokuchi et al. 2010). For example, injury induced by the toxicity of paracetamol promotes the secretion of CCL2 by various liver cells including hepatocytes, resulting in the recruitment of cells expressing CCR2 to the site of injury such as monocytes and macrophages (Saiman and Friedman 2012). In ischemia reperfusion, as a consequence of reactive oxygen species production, an up regulation of pro-inflammatory chemokines including CCL5 is apparent (Friedman, Wolf et al. 2012). In the context of CXCL12, this chemokine is predominantly expressed by the biliary epithelial cells in both the normal and injured liver tissue (Hong, Tuyama et al. 2009). However, more recently, researchers have identified an additional source of CXCL12 secretion in the damaged liver; myofibroblasts (Hong, Tuyama et al. 2009). Indeed, it has been found that this protein is up regulated in patients with chronic liver injury and furthermore, expression levels have been shown to be correlated with fibrosis severity (Wald, Pappo et al. 2004).

However, expression levels of CXCL12 in models of periportal fibrosis have received little attention. Thus, the aims of this chapter were to investigate the influence of different fibrosis models of liver injury on CXCL12 expression; CCl_4 (centrilobular), BDL and MP treatment (periportal). Given that biliary epithelial cells are one of the main sources of CXCL12 secretion and myofibroblasts have been shown to express this chemokine, it was hypothesized that expression levels would increase in each of the individual models. A further aim was to establish the specific liver cell types in the various fibrosis models that express this chemokine.

5.2: Results

5.2.1: CCl_4 mediated fibrosis increases levels of CXCL12 *in vivo*.

To determine levels of fibrosis in olive oil control and CCl_4 treated (4, 8 and 12wks) male mice, sirius red and H and E staining were performed on the paraffin embedded liver tissue sections. Sirius red staining was quantified in pictures taken around 10 central lobular veins (CLV) at x 10 magnification as described in section 2.5.3. As shown by the representative images (Figure 5.1A) fibrosis was established in animals that received CCl_4 as illustrated by the bridging effect between the central veins (denoted by the arrows). Furthermore, compared to the olive oil control, collagen deposition increased in the CCl_4 treated animals and significantly increased with treatment time (Figure 5.1B).

A

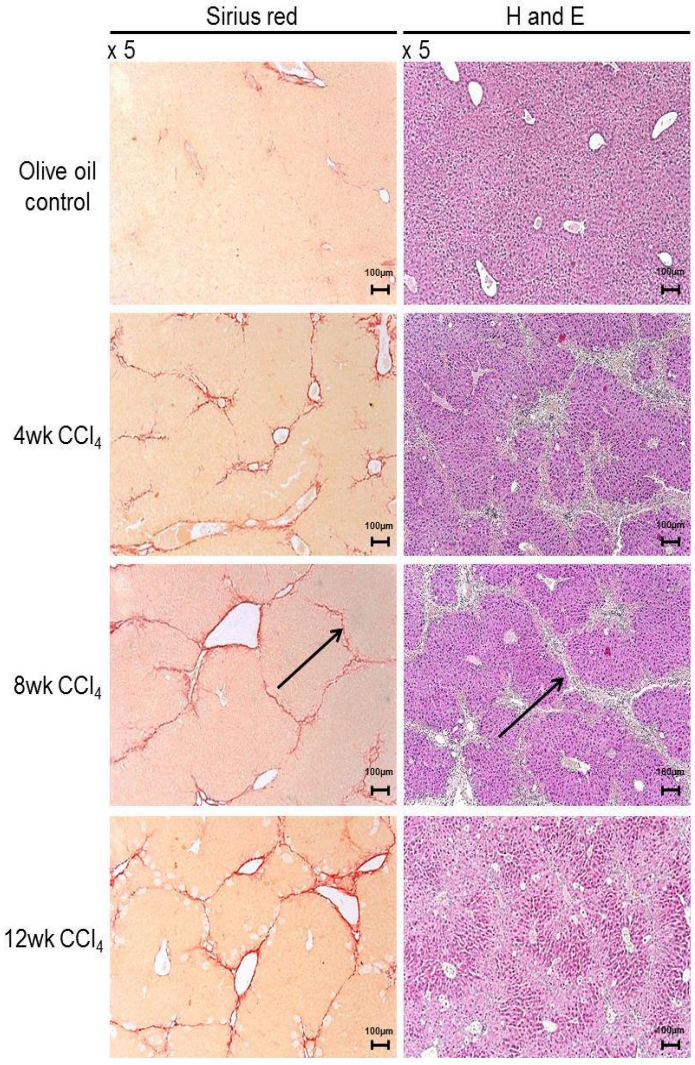

B

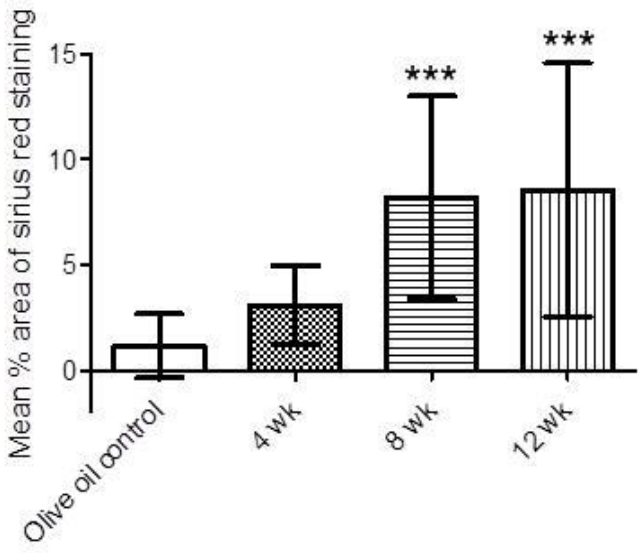

Figure 5.1: CCl_4 treatment leads to significant central lobular fibrosis.
C57BL/6 mice treated with olive oil or CCl_4 (4, 8 and 12 wks) were culled and livers were harvested and fixed for 24 hours in 10% formalin in 1 x PBS. Samples were then processed, embedded in paraffin and sectioned (5µm). Sections were then de-waxed and stained using **A)** sirius red and H and E. As indicated by the arrows, fibrosis was established in all animals treated with CCl_4. Representative images were acquired at x 5 magnification. Scale bars = 100µm. **B)** For quantification of sirius red staining, pictures were taken around 10 random CLV at x 10 magnification and the percentage area of the staining was quantified using the Leica software. Data are the mean and SD of percentage area of the sirius red stain for each treatment group and were tested for statistical significance using the one way ANOVA test with Dunnetts's multiple comparison test. *** Represent significant between 8wk and 12wk CCl_4 against olive oil control ($p<0.0001$). $n \geq 3$ for all groups.

The liver tissue sections were also stained with anti-α-SMA (Figure 5.2A) and anti-vimentin (Figure 5.2C) antibodies since these proteins are known to be expressed by myofibroblasts and portal tract fibroblasts respectively (Wallace, Burt et al. 2008). Results demonstrated that in the olive oil control, positive staining was only observed surrounding the portal arterioles, however, in mice treated with CCl_4, a significant percentage of cells expressing α-SMA was observed (Figure 5.2A and B). Vimentin staining results demonstrated that in the olive oil control, there were few positive cells, however, after CCl_4 treatment the percentage of cells expressing this protein significantly increased around the central veins (Figure 5.2C and D).

A

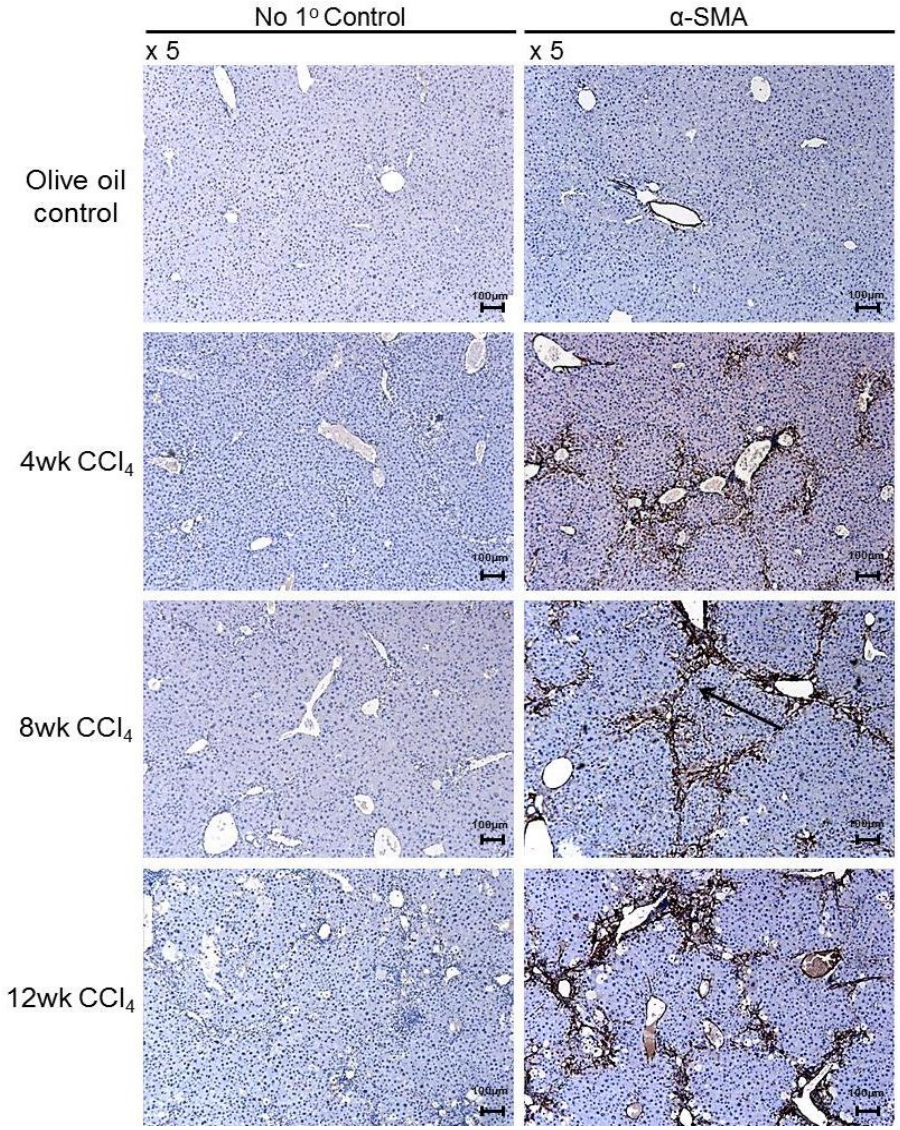
No 1° Control
α-SMA
x 5
x 5
Olive oil control
4wk CCl_4
8wk CCl_4
12wk CCl_4
100µm

B

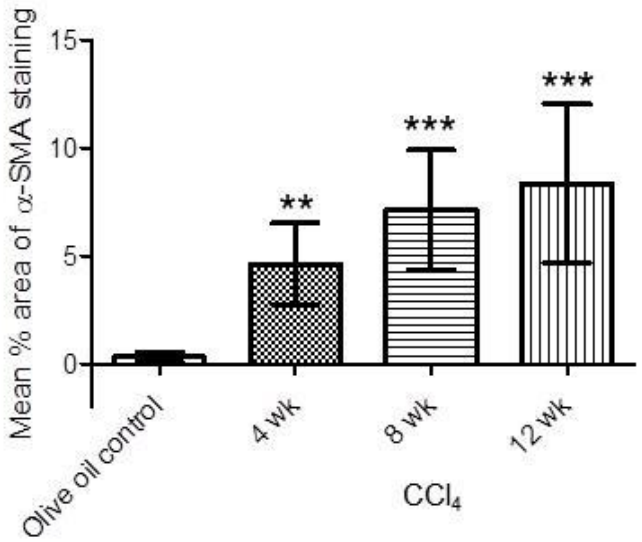
Mean % area of α-SMA staining
15
10
5
0
**
***
***
Olive oil control
4 wk
8 wk
12 wk
CCl_4

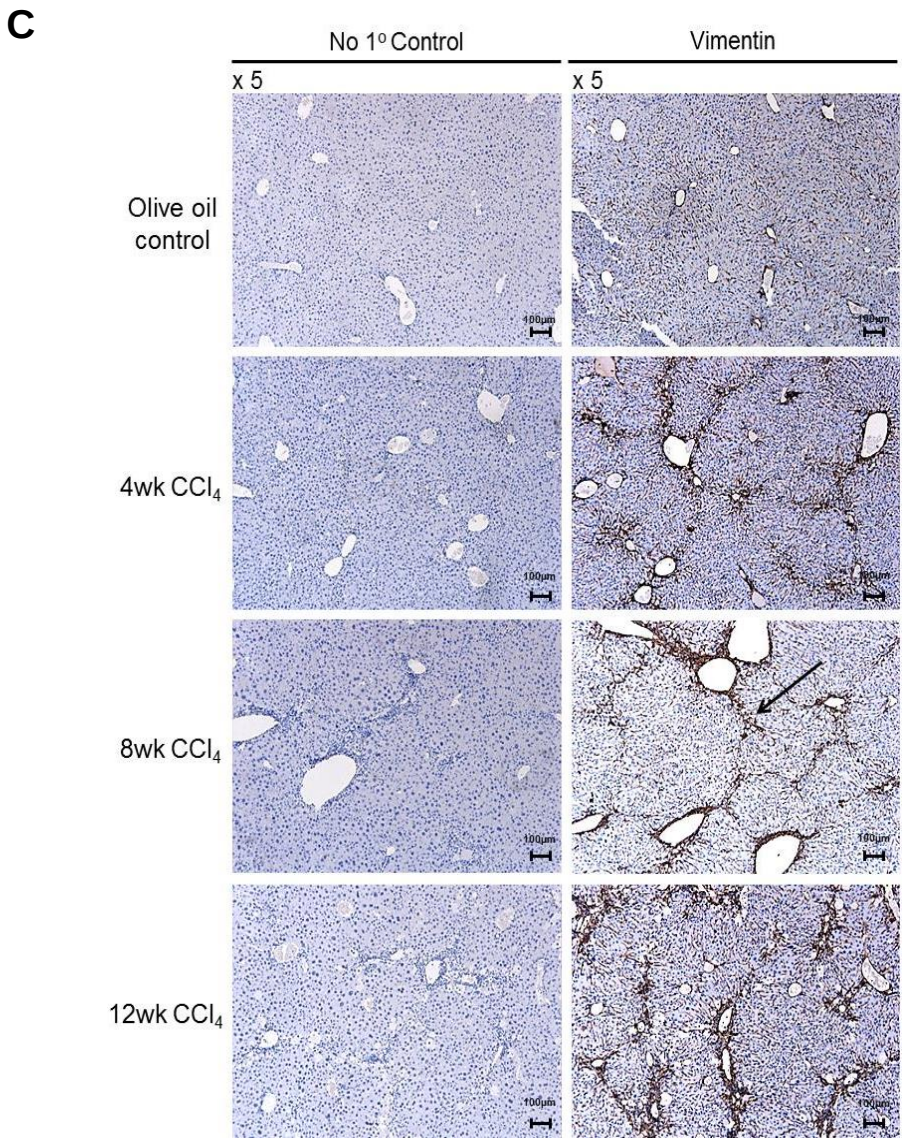

Figure 5.2: α-SMA and vimentin positive stained cells increase significantly in CCl_4 treated mice compared to olive oil controls.

C57BL/6 mice treated with olive oil or CCl_4 (4, 8 and 12 wks) were culled and livers were harvested and fixed for 24 hours in 10% formalin in 1 x PBS. Samples were then processed, embedded in paraffin and sectioned (5µm). Sections were then de-waxed and immunostained for **A)** α-SMA and **C)** vimentin. No primary antibody controls were included and were stained with the secondary anti-mouse IgG (for α-SMA) or anti-rabbit IgG (for vimentin) antibody alone. Representative images were acquired at x 5 magnification Scale bars = 100µm. For quantification of **B)** α-SMA and **D)** vimentin, pictures were taken around 10 random CLV at x 10 magnification and the percentage area of the staining was quantified using the Leica software. Data are the mean and SD of percentage area of the α-SMA or vimentin stain for each treatment group and were tested for statistical significance using the one way ANOVA test with Dunnetts's multiple comparison test. *** Represent significant between 4wk, 8wk and 12wk CCl_4 against olive oil control ($p<0.0001$). $n \geq 3$ for all groups.

To determine mRNA and protein CXCL12 expression levels of the control and fibrotic liver tissue, qRT-PCR and Western blotting were performed respectively. For qRT-PCR analysis, mRNA expression was normalised to the expression of 18S rRNA and for Western blot analysis, the house-keeping protein, ß-actin was used as a loading control. The mRNA levels of the CXCL12 variants α and β increased in the CCl_4 treated liver compared to the olive oil control (Figure 5.3A). Moreover, mRNA CXCL12-α levels significantly increased in the 8wk CCl_4 treated mice compared to the olive oil control. However, mRNA CXCL12-γ was not detected (data not shown). At the protein level, CXCL12 was not expressed (Figure 5.3B), however, an intense band at higher molecular weight of ~58 kDa in all treatment groups was observed (Figure 5.3B).

A

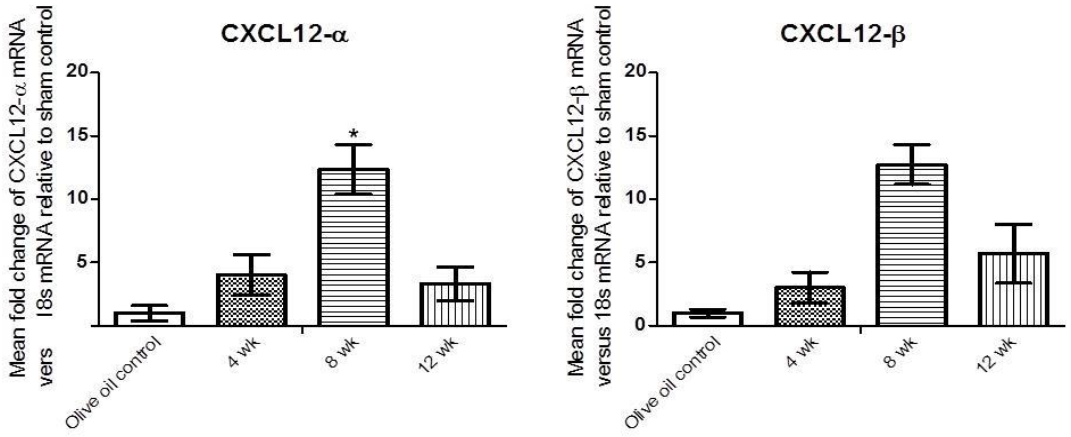

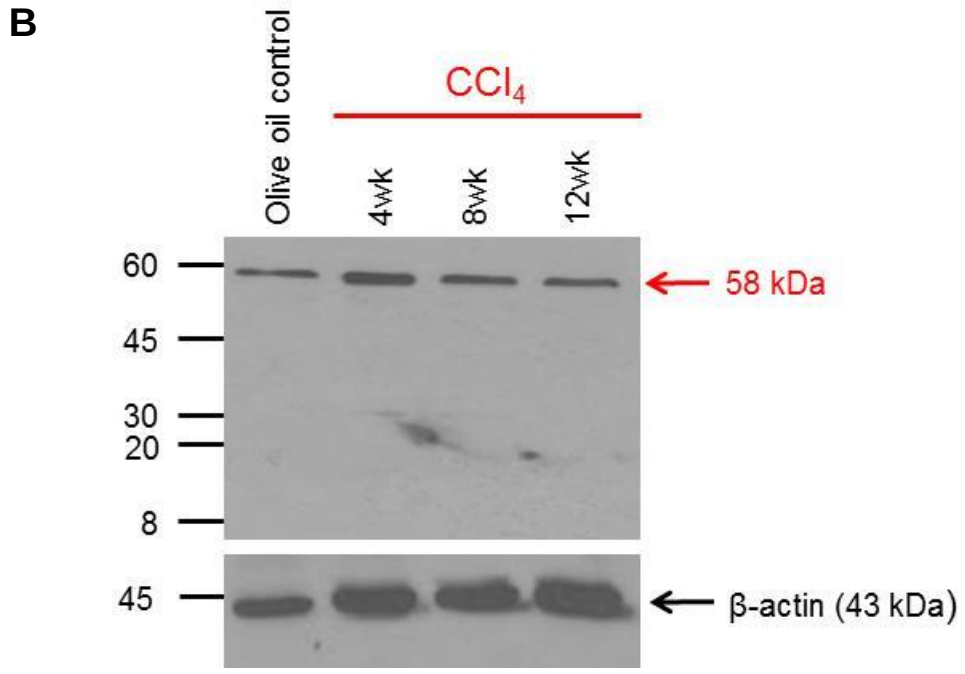

Figure 5.3: mRNA CXCL12 increases in CCl_4 treated liver but was not expressed at the protein level.
A) Representative qRT-PCR for the expression of CXCL12 variants in normal and fibrotic mouse liver tissue. Total RNA was isolated using Trizol, as per manufacturer's instructions from whole mouse liver tissue. PCR controls were carried out in the absence of template RNA. Error bars represent +/- SD. Results were tested for statistical significance using the one way ANOVA test with Dunnetts's multiple comparison test. * Represent significant between 8wk, against olive oil control ($p<0.05$). $n \geq 3$ for all groups. **B)** Representative Western blot for the expression of CXCL12. Whole liver tissue was homogenised followed by sonication and prepared for protein analysis by Western blot. 20µg of protein was loaded per lane and β-actin was used as a loading control.

To determine expression levels of CXCL12 and to establish which cells were positive for this chemokine, immunohistochemical staining was examined on the olive oil control and CCl_4 liver sections. As shown in figure 5.4A, biliary epithelial cells in all treatment groups were positive for CXCL12 and also cells resembling myofibroblasts were observed in the 12wk CCl_4 group (as denoted by the arrows) (Figure 5.4B). Additionally, CXCL12 expression was significantly increased in the 12wk treatment group compared to the olive oil control (Figure 5.4C).

A

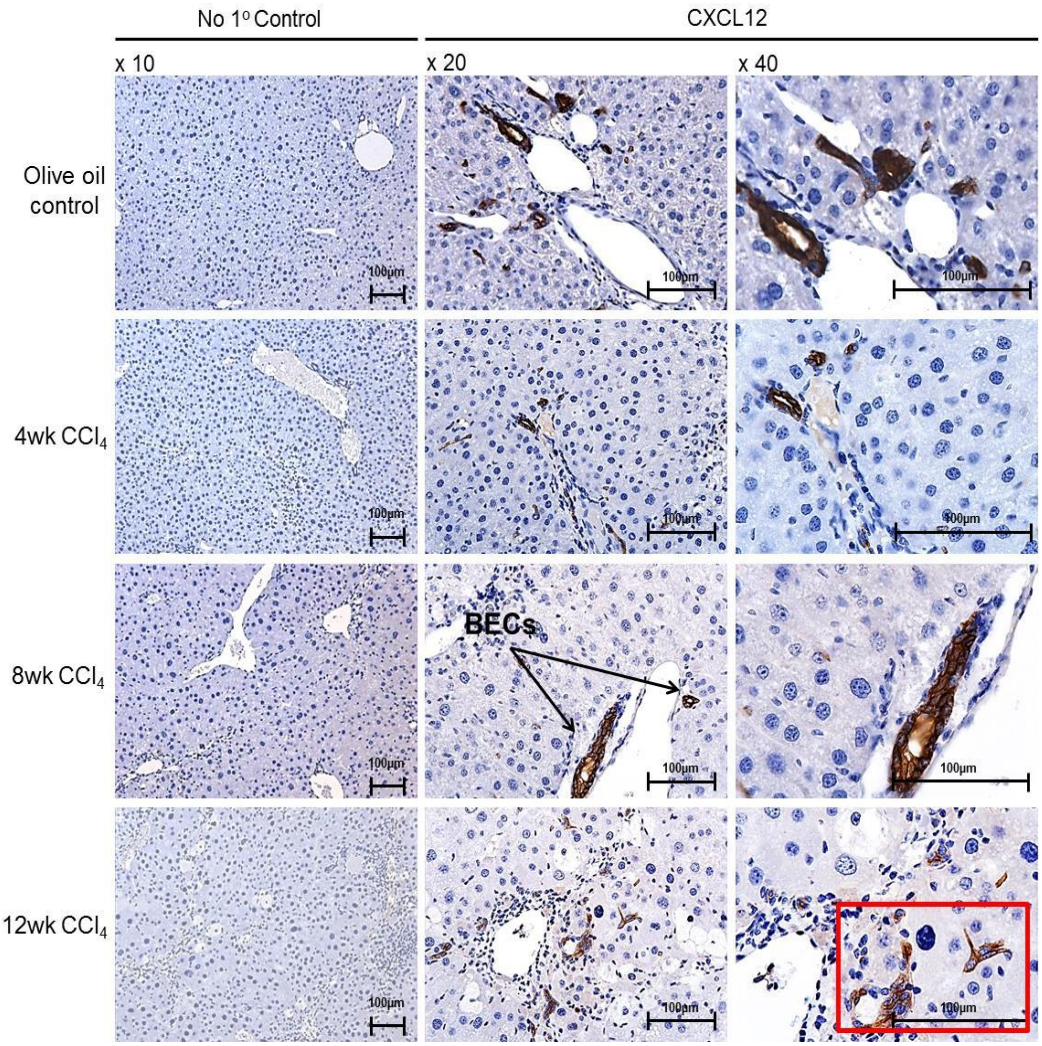
No 1° Control
CXCL12
x 10
x 20
x 40
Olive oil control
4wk CCl_4
8wk CCl_4
12wk CCl_4
BECs
100µm

B

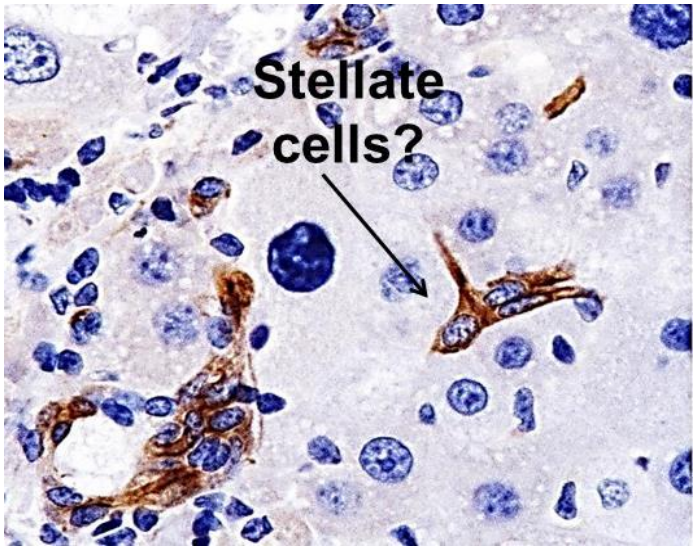
Stellate cells?

C

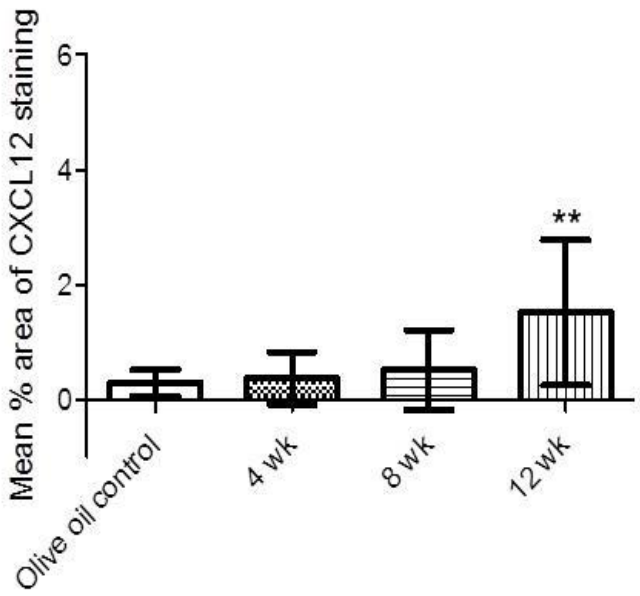

Figure 5.4: CXCL12 positive stained cells increase significantly in 12wk CCl_4 treated mouse liver tissue compared to olive oil control and biliary epithelial and stellate cells express CXCL12 in *in vivo*.
C57BL/6 mice treated with olive oil or CCl_4 (4, 8 and 12 wks) were culled and livers were harvested and fixed for 24 hours in 10% formalin made up in 1 x PBS. Samples were then processed, embedded in paraffin and sectioned (5µm). Sections were then de-waxed and stained using **A)** CXCL12. No primary antibody controls were included and were stained with the secondary anti-mouse IgG antibody alone. Representative images were acquired at x 20 and x 40 magnification Scale bars = 100µm. For quantification of **B)** CXCL12, pictures were taken around 10 random CLV at x 10 magnification and the percentage area of the staining was quantified using the Leica software. Data are the mean and SD of percentage area of CXCL12 stain for each treatment group and were tested for statistical significance using the one way ANOVA test with Dunnetts's multiple comparison test. ** Represent significant between 12wk, against olive oil control ($p<0.001$). $n \geq 3$ for all groups.

To confirm if myofibroblasts expressed CXCL12, immunofluorescence double staining was performed using a common marker for these cells (α-SMA) and co-localisation plots were generated. The results demonstrated that there was some co-localisation with CXCL12 and α-SMA (Figure 5.5C). However, biliary epithelial cells were also positive for α-SMA (Figure 5.5B) and therefore it was difficult to distinguish between the two different cell types.

A

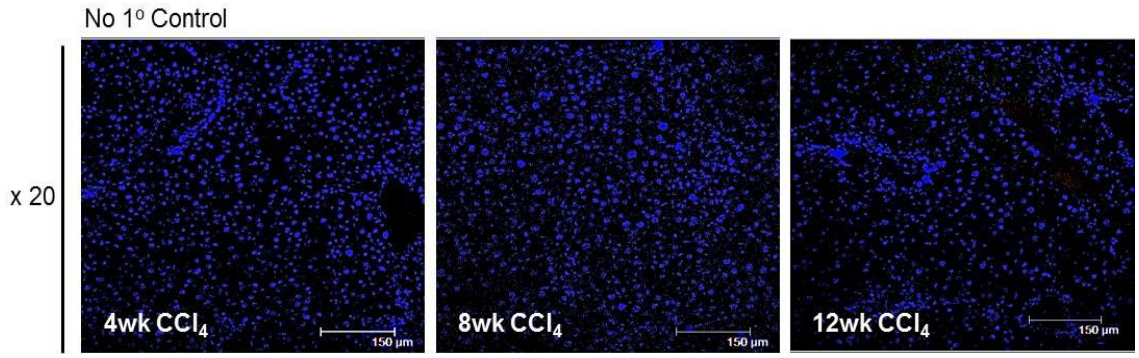

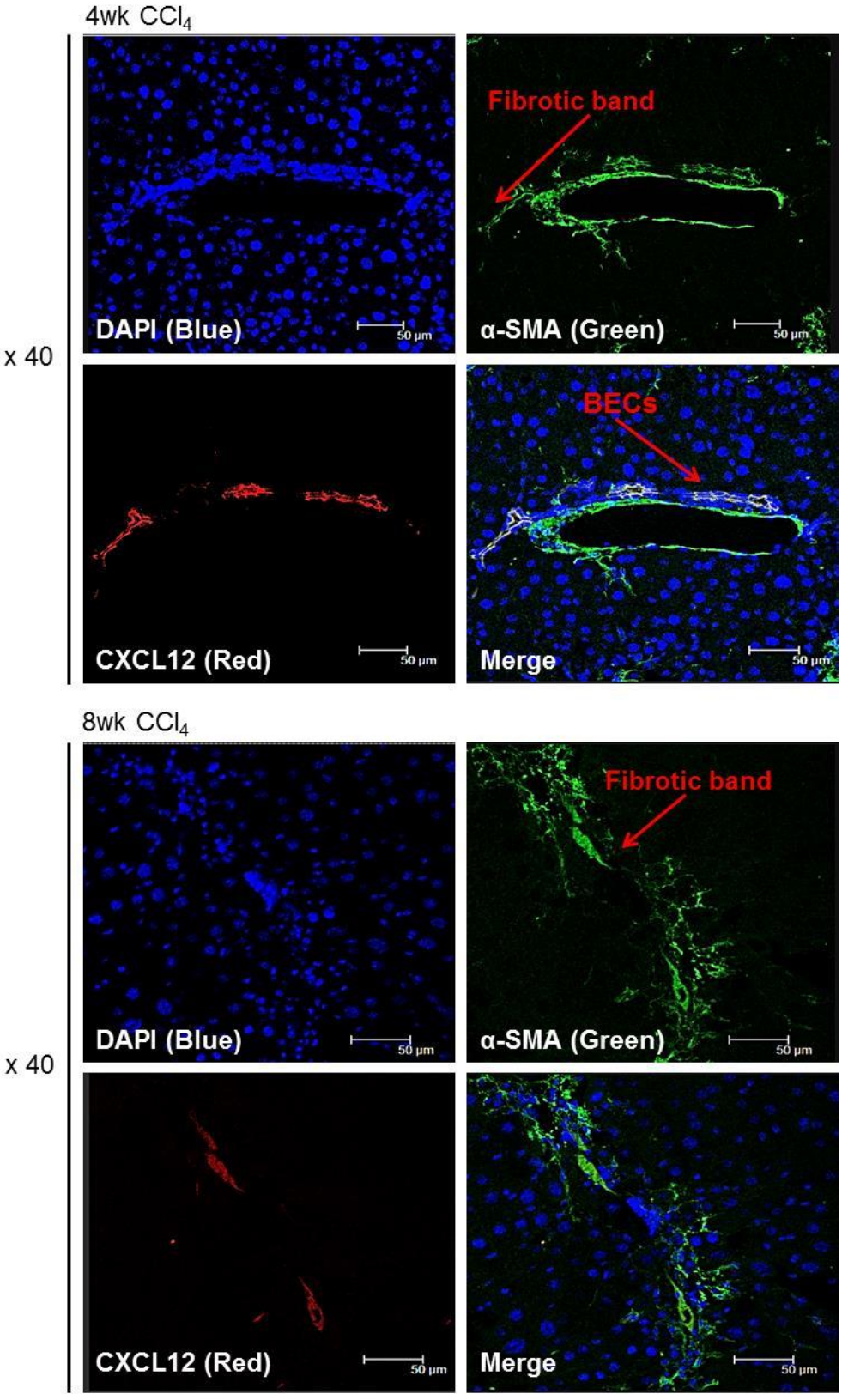
4wk CCl_4
x 40
DAPI (Blue)
50 μm
Fibrotic band
α-SMA (Green)
50 μm
CXCL12 (Red)
50 μm
BECs
Merge
50 μm
8wk CCl_4
x 40
DAPI (Blue)
50 μm
Fibrotic band
α-SMA (Green)
50 μm
CXCL12 (Red)
50 μm
Merge
50 μm

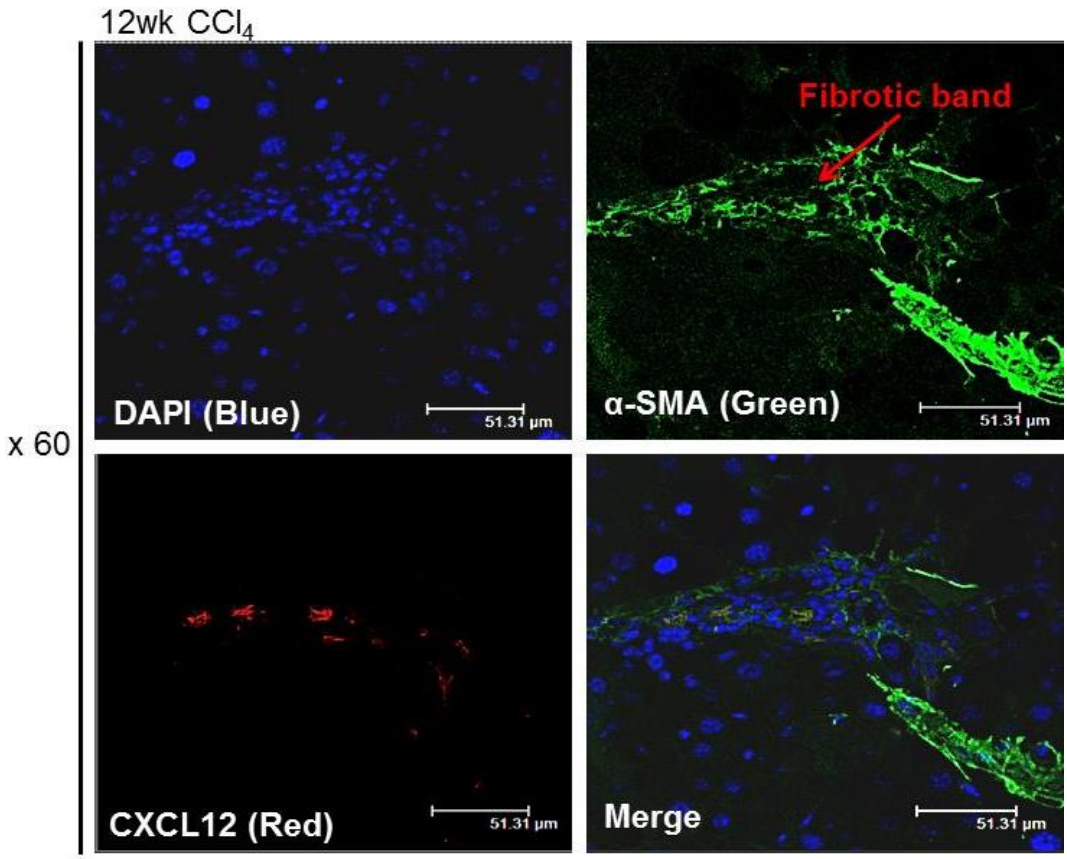

B

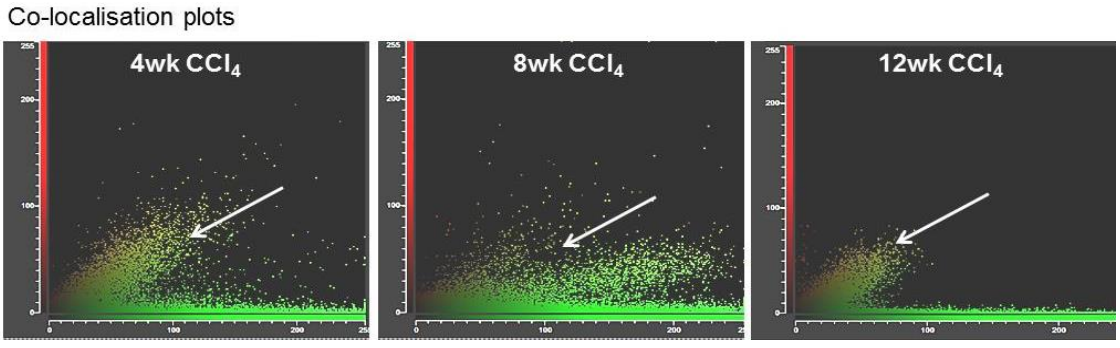

Figure 5.5: CXCL12 is expressed by biliary epithelial cells and activated stellate in the CCl_4 treated mice.
C57BL/6 mice treated with olive oil or CCl_4 (4, 8 and 12 wks) were culled and livers were harvested and fixed for 24 hours in 10% formalin made up in 1 x PBS. Samples were then processed, embedded in paraffin and sectioned (5µm). Sections were then de-waxed and stained for the expression of **A)** CXCL12 (red) and α-SMA (green) was determined by confocal microscopy and background levels were set against the no primary control. DAPI was used to stain the nuclei. **B)** co-localisation plots demonstrated co-localisation of CXCL12 with α-SMA. Scale bars = 50µm (x 40 and x 60).

5.2.2: ICAM1, IL-1 and CXCL9 are up regulated in CCl_4 (12wk) mouse liver tissue.

To examine the expression of other cytokines/chemokines (Table 5.1) in both normal and fibrotic liver, a cytokine array was performed on cell extracts collected from olive oil control and 12wk CCl_4 (fibrotic) liver tissue. The results demonstrated that ICAM-1, IL-1 and CXCL9 were up-regulated in the fibrotic tissue compared to the control liver tissue and C5/C5a expression levels were greater in the control liver (Figure 5.6A and B).

CXCL13/BLC/BCA-1	IL-5	M-CSF
C5a	IL-6	CCL2/JE/MCP-1
G-CSF	IL-7	CCL12/MCP-5
GM-CSF	IL-10	CXCL9/MIG
CCL1/I-309	IL-12 p70	CCL3/MIP-1 alpha
CCL11/Eotaxin	IL-13	CCL4/MIP-1 beta
ICAM-1	IL-16	CXCL2/MIP-2
IFN-gamma	IL-17	CCL5/RANTES
IL-1 alpha	IL-23	CXCL12/SDF-1
IL-1 beta	IL-27	CCL17/TARC
IL-1ra	CXCL10/IP-10	TIMP-1
IL-2	CXCL11/I-TAC	TNF-alpha
IL-3	CXCL1/KC	TREM-1
IL-4		

Table 5.1: Cytokines/chemokines analysed in array assay.

A

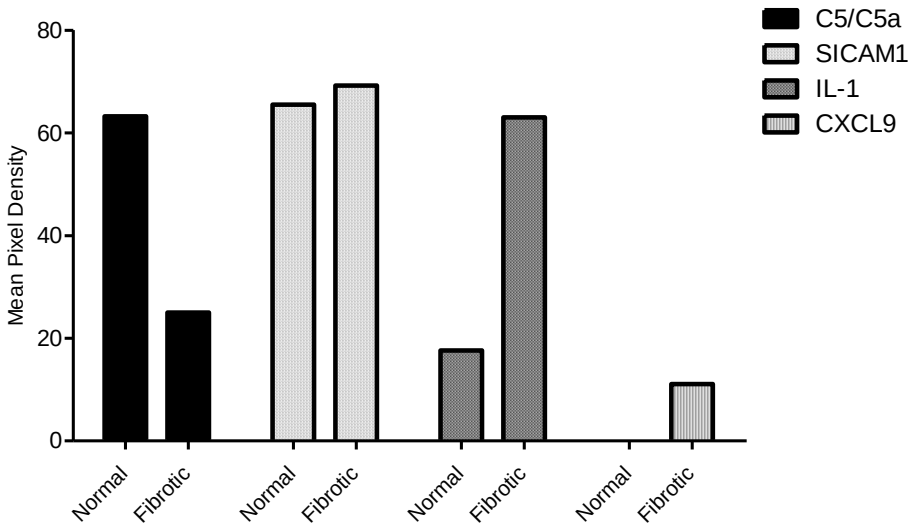

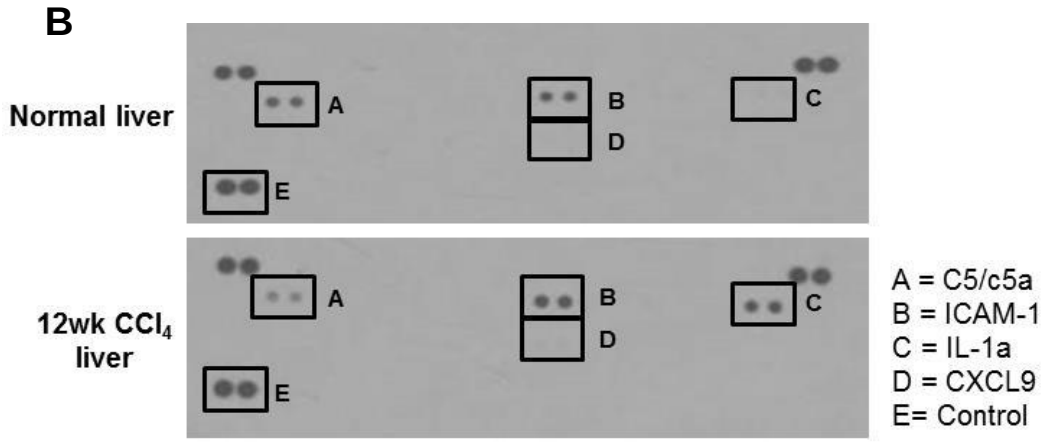

Figure 5.6: ICAM-1, IL-1 and CXCL9 are up regulated in CCl_4 (12wk) mouse liver tissue.
A cytokine array was performed as described in section 2.9. Mouse liver (normal and 12wk CCl_4) supernatant was mixed with a cocktail of biotinylated detection antibodies, and then incubated with the Mouse Cytokine Array. The array was then incubated with streptavidin-horseradish peroxidase followed by chemiluminescent detection. After detection, the array data were quantitated to generate a protein profile (histogram). The table shows the analytes detected and their location on the membrane.

5.2.3: Bile duct ligation (BDL) in rats mediated fibrosis modulates mRNA CXCL12 expression *in vivo*.

BDL was performed on male rats and cholestatic disease was allowed to develop for 3 weeks, sham control animals underwent the same procedure but without ligating the common bile duct as described in section 2.1.7. To examine establishment of cholestatic fibrosis, liver sections from the control and BDL animals were stained with H and E and sirius red staining. BDL animals showed a marked significant increase in periportal inflammatory cells (as denoted by the arrows) (Figure 5.7A) and sirius red staining significantly increased in this group compared to the control animals (Figure 5.7B).

A

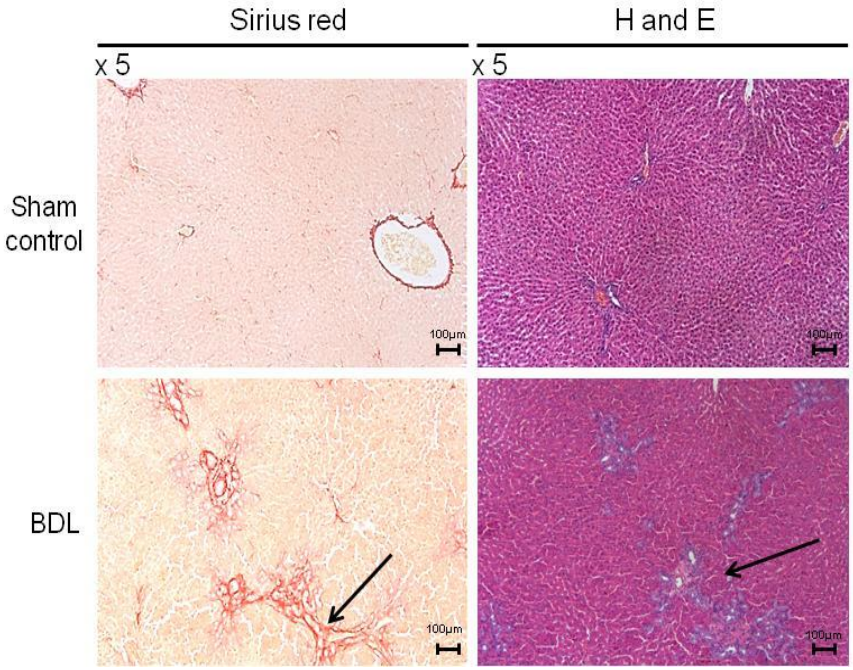

B

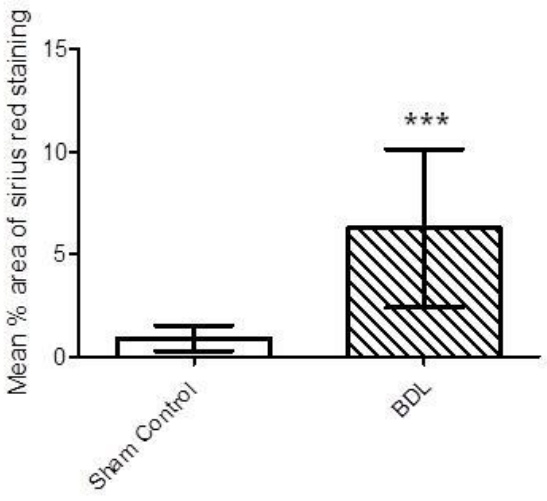

Figure 5.7: BDL causes a significant increase in periportal fibrosis.
Sham control and BDL rats were culled and livers were harvested and fixed for 24 hours in 10% formalin 1 x PBS. Samples were then processed, embedded in paraffin and sectioned (5µm). Sections were then de-waxed and stained using **A)** sirius red or H and E. Representative images were acquired at x 5 magnification. Scale bars = 100µm. B) Pictures were taken around 10 random periportal regions at x 10 magnification and the percentage area of the sirius red staining was quantified using the Leica software. Data are the mean and SD of percentage area for each treatment group and were tested for statistical significance using the Student's unpaired t-test. *** Represent significant between BDL and sham control ($p<0.0001$). $n \geq 3$ for all groups.

The BDL and control liver tissue sections were also stained with anti-α-SMA and anti-vimentin. The results illustrated that in control animals, α-SMA and vimentin positive cells were evenly spread around the lobules (Figure 5.8A). However, after BDL treatment, the percentage of cells expressing α-SMA (Figure 5.8B) and vimentin (Figure 5.8C) significantly increased.

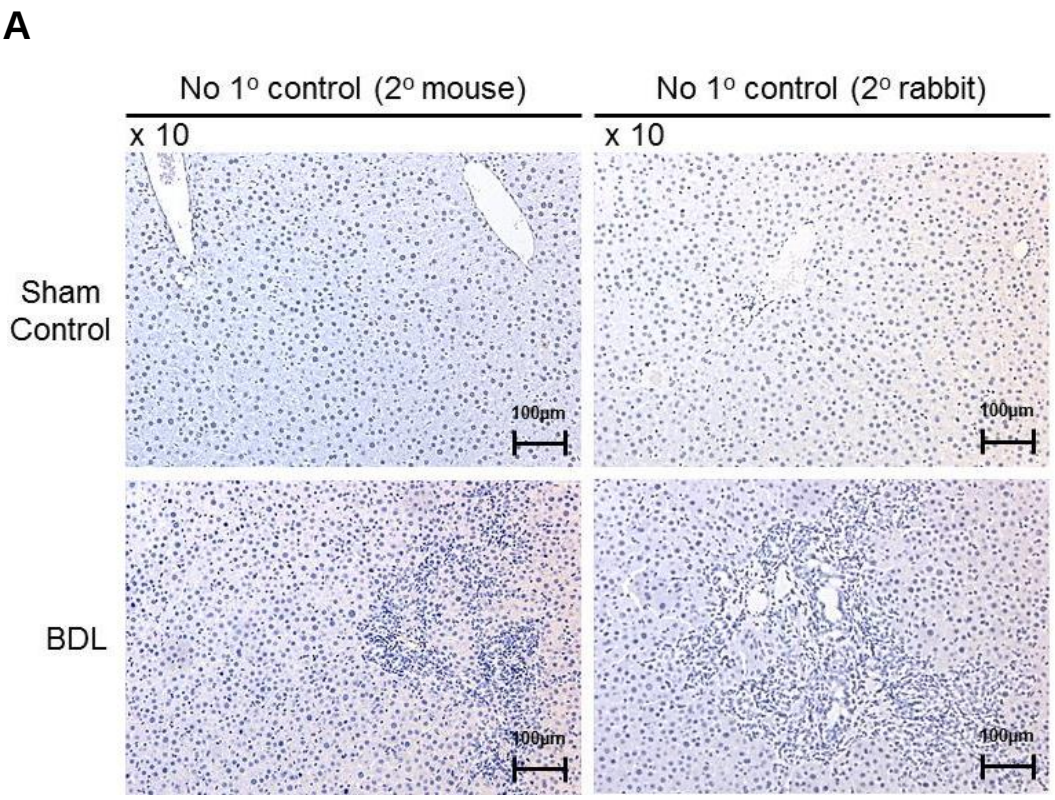

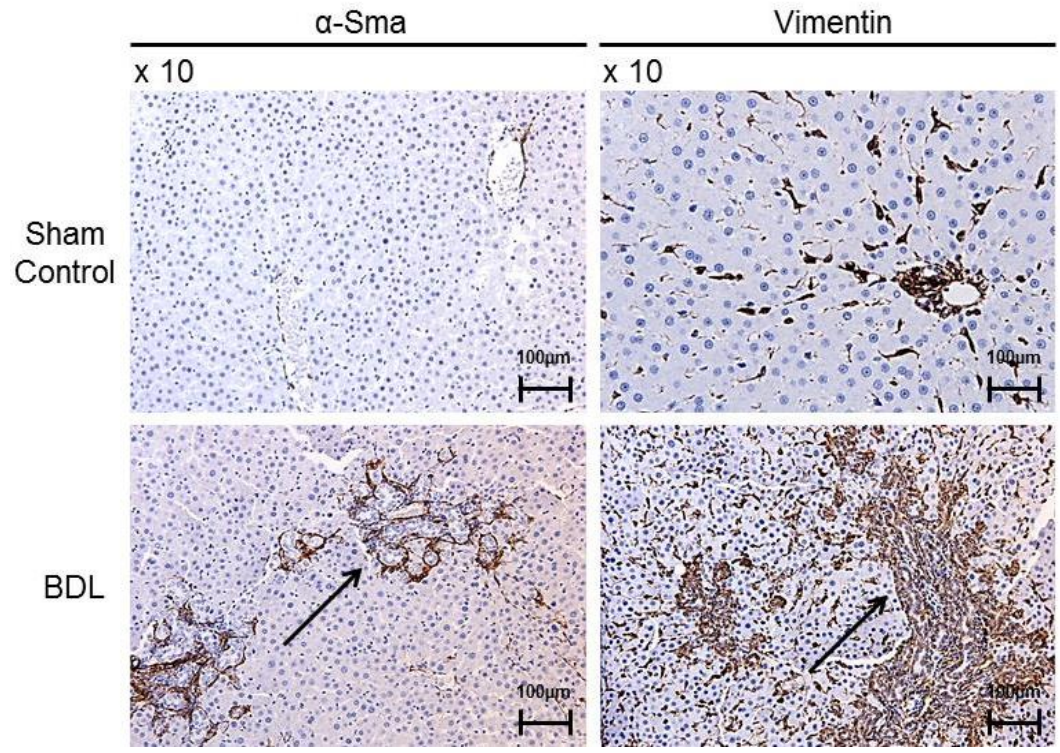
α-Sma
Vimentin
x 10
x 10
Sham Control
BDL
100µm
100µm
100µm
100µm

B

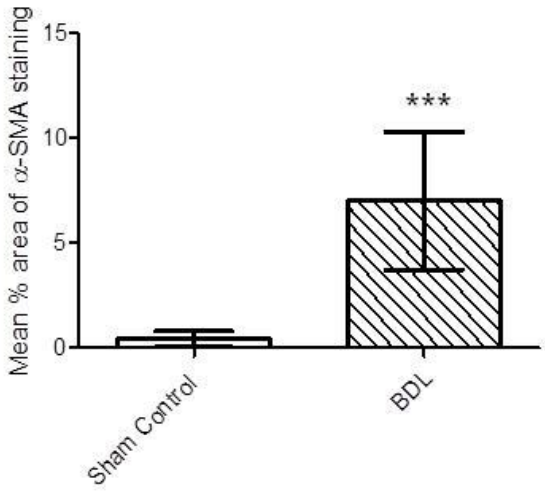
Mean % area of α-SMA staining
15
10
5
0
***
Sham Control
BDL

C

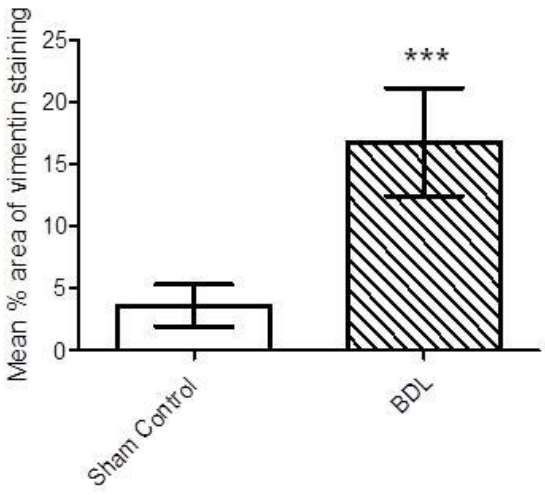
Mean % area of vimentin staining
25
20
15
10
5
0
***
Sham Control
BDL

Figure 5.8: BDL causes a significant increase in α-SMA and vimentin staining.
Sham control and BDL rats were culled and livers were harvested and fixed for 24 hours in 10% formalin in 1 x PBS. Samples were then processed, embedded in paraffin and sectioned (5µm). Sections were then de-waxed and stained using **A)** α-SMA and vimentin. No primary antibody controls were included and were stained with the secondary anti-mouse IgG (for α-SMA) or anti-rabbit IgG (for vimentin) antibody alone. Representative images were acquired at x 10 magnification Scale bars = 100µm. For quantification of **B)** α-SMA and **C)** vimentin pictures were taken around 10 random periportal regions at x 10 magnification and the percentage area of the staining was quantified using the Leica software. Data are the mean and SD of percentage area of α-SMA/vimentin stain for each treatment group and were tested for statistical significance using the Student's unpaired t-test. *** Represent significant between BDL and sham control ($p<0.0001$). $n \geq 3$ for all groups.

To unequivocally identify biliary epithelial cells in the control and BDL liver sections, sections were also stained for CK-19 (a marker of biliary epithelial cells (Chatzipantelis, Lazaris et al. 2006)) (Figure 5.9A). In the BDL rats, the percentage of CK-19 positive cells increased significantly compared to the control animals (Figure 5.9B).

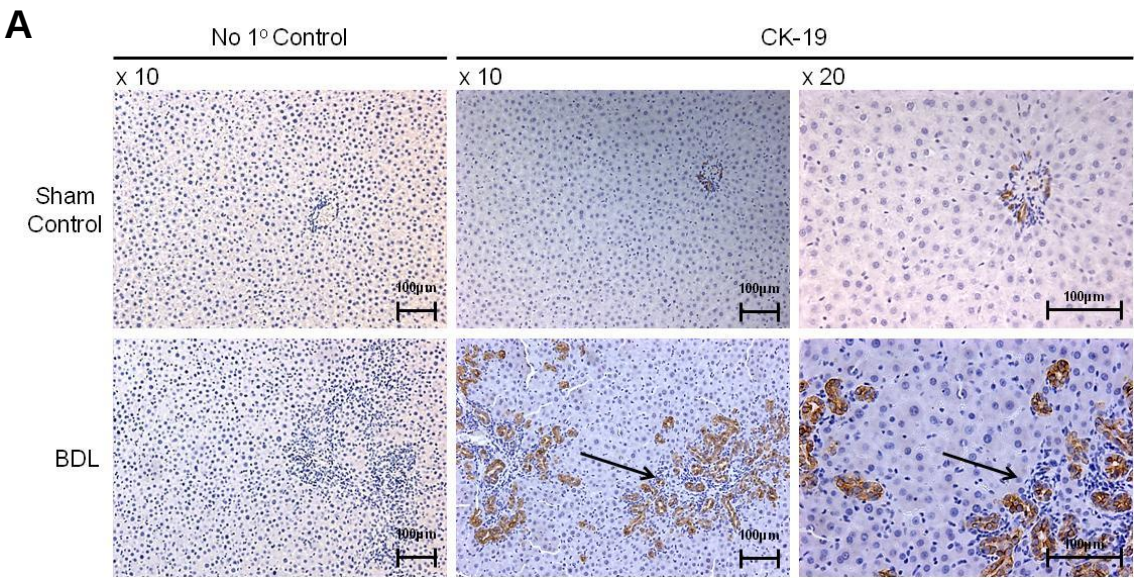

B

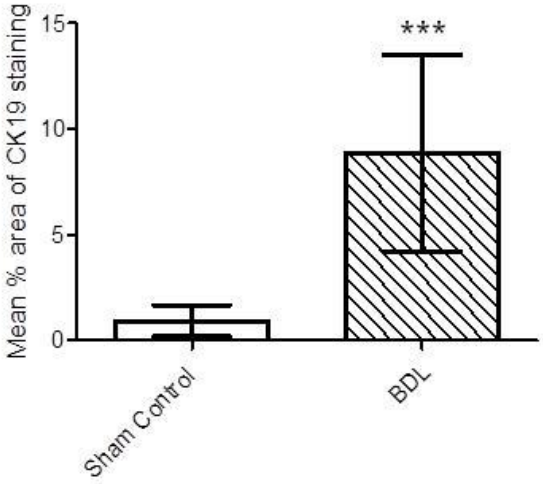

Figure 5.9: BDL causes a significant increase in CK-19 staining.
Sham control and BDL rats were culled and livers were harvested and fixed for 24 hours in 10% formalin in 1 x PBS.. Samples were then processed, embedded in paraffin and sectioned (5µm). Sections were then de-waxed and stained using **A)** CK-19. No primary antibody controls were included and were stained with the secondary anti-mouse IgG antibody alone. Representative images were acquired at x 10 and x20 magnification Scale bars = 100µm. For quantification of **A)** CK19 pictures were taken around 10 random periportal regions at x 10 magnification and the percentage area of the staining was quantified using the Leica software. Data are the mean and SD of percentage area of CK-19 stain for each treatment group and were tested for statistical significance using the Student's unpaired t-test. *** Represent significant between BDL and sham control ($p<0.0001$). $n \geq 3$ for all groups.

To determine the specific cells in this model that expressed CXCL12, immunohistochemical staining was performed on both the control and BDL liver sections. The results demonstrated that CXCL12 was expressed by the biliary epithelial cells (Figure 5.10A) and furthermore, the percentage of expression was significantly greater in these animals compared to the controls (Figure 5.10B).

A

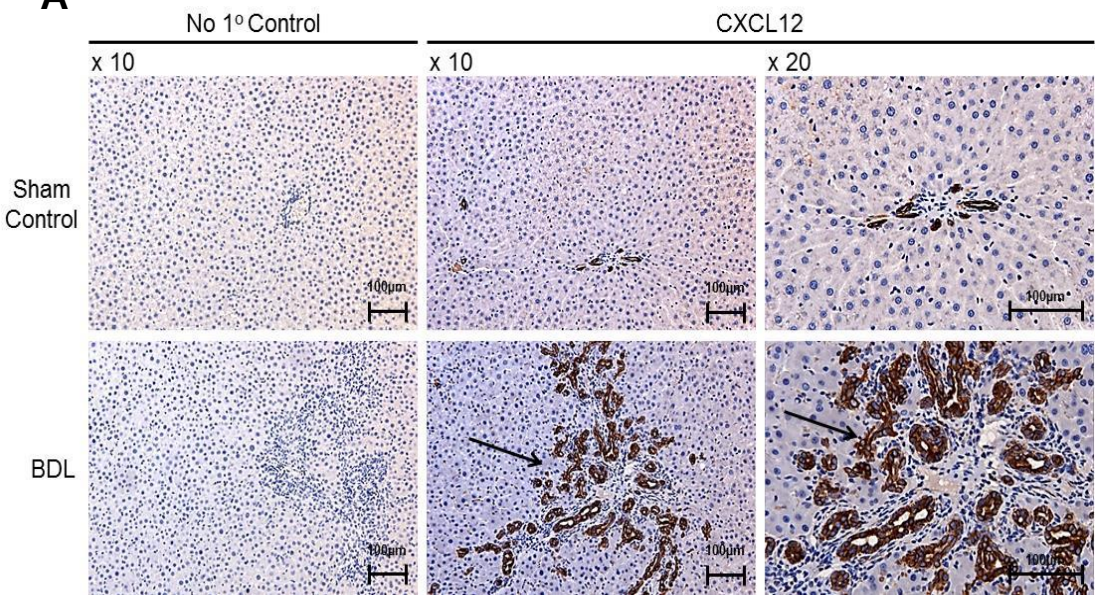

B

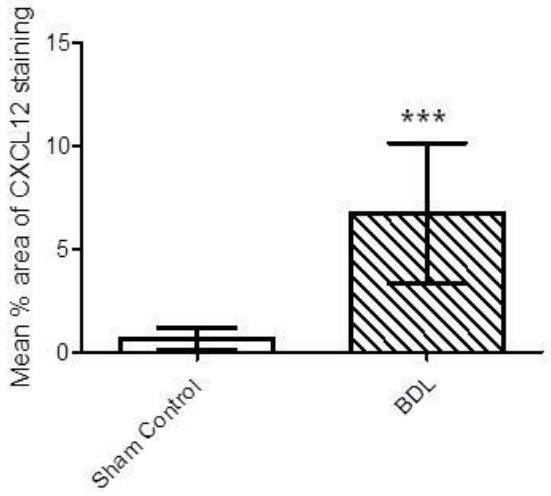

Figure 5.10: BDL causes a significant increase in CXCL12 staining.
Sham control and BDL rats were culled and livers were harvested and fixed for 24 hours in 10% formalin made up in 1 x PBS.. Samples were then processed, embedded in paraffin and sectioned (5µm). Sections were then de-waxed and stained using **A)** CXCL12. No primary antibody controls were included and were stained with the secondary anti-mouse IgG antibody alone. Representative images were acquired at x 10 and x20 magnification Scale bars = 100µm. For quantification of **B)** CXCL12 pictures were taken around 10 random periportal regions at x 10 magnification and the percentage area of the staining was quantified using the Leica software. Data are the mean and SD of percentage area of CK-19 stain for each treatment group and were tested for statistical significance using the Student's unpaired t-test. *** Represent significant between BDL and sham control ($p<0.0001$). $n \geq 3$ for all groups.

The mRNA and protein levels of CXCL12 in the control and BDL livers were determined by qRT-PCR and Western blotting respectively. The mRNA levels of the CXCL12 increased for all variants and significantly for CXCL12-α and β (Figure 5.11A) compared to the control. At the protein level, a faint band was only observed for CXCL12 in one control and one BDL animal (Figure 5.11B). However, an intense band of greater molecular weight was observed at ~62 kDa and fainter bands at 58, 47 and 18 kDa in all treatment groups (Figure 5.11B).

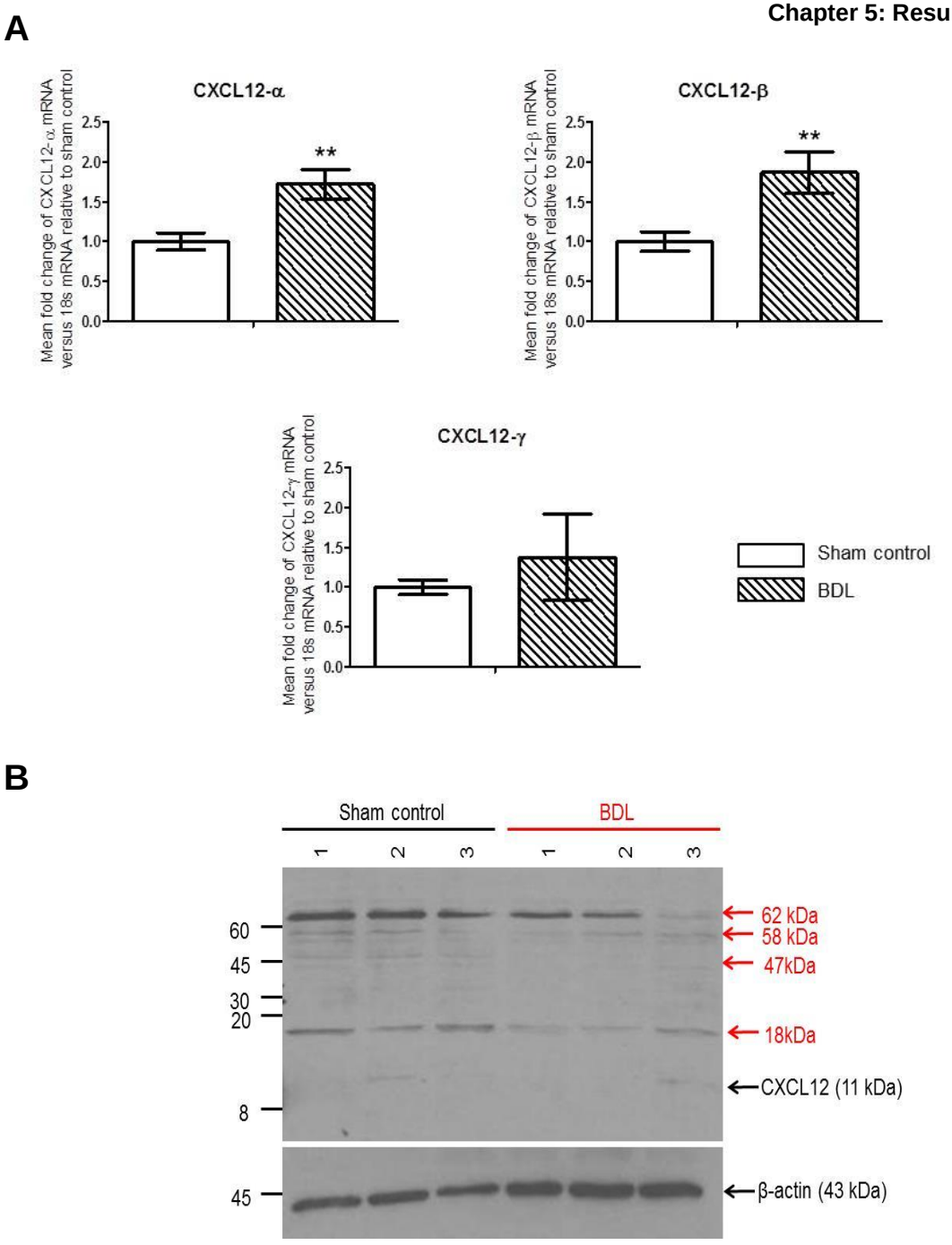

Figure 5.11: mRNA CXCL12 increases in BDL liver but is not increased at the protein level.

A) Representative qRT-PCR for the expression of CXCL12 variants in control and BDL liver tissue. Total RNA was isolated using Trizol, as per manufacturer's instructions from whole mouse liver tissue. PCR controls were carried out in the absence of template RNA. Data are the mean and SD of mRNA CXCL12 variants for each treatment group and were tested for statistical significance using the Student's unpaired t-test. ** Represent significant between BDL and sham control ($p<0.001$). n≥ 3 for all groups. **B)** Representative Western blot for the expression of CXCL12. Whole liver tissue was homogenised followed by sonication and prepared for protein analysis by Western blot. 20µg of protein was loaded per lane and β-actin was used as a loading control. n≥ 3 for all groups.

5.2.4: A novel model of periportal fibrosis induced by methapyriline (MP) increases CXCL12 expression *in vivo*.

Male rats were administered MP and control animals PBS for three weeks as described in section 2.1.7. The liver sections from each animal were stained with H and E and sirius red. MP treated rats showed a significant increase in periportal inflammatory cells (Figure 5.12A) and collagen deposition was significantly increased (Figure 5.12B) demonstrating that periportal fibrosis had been induced.

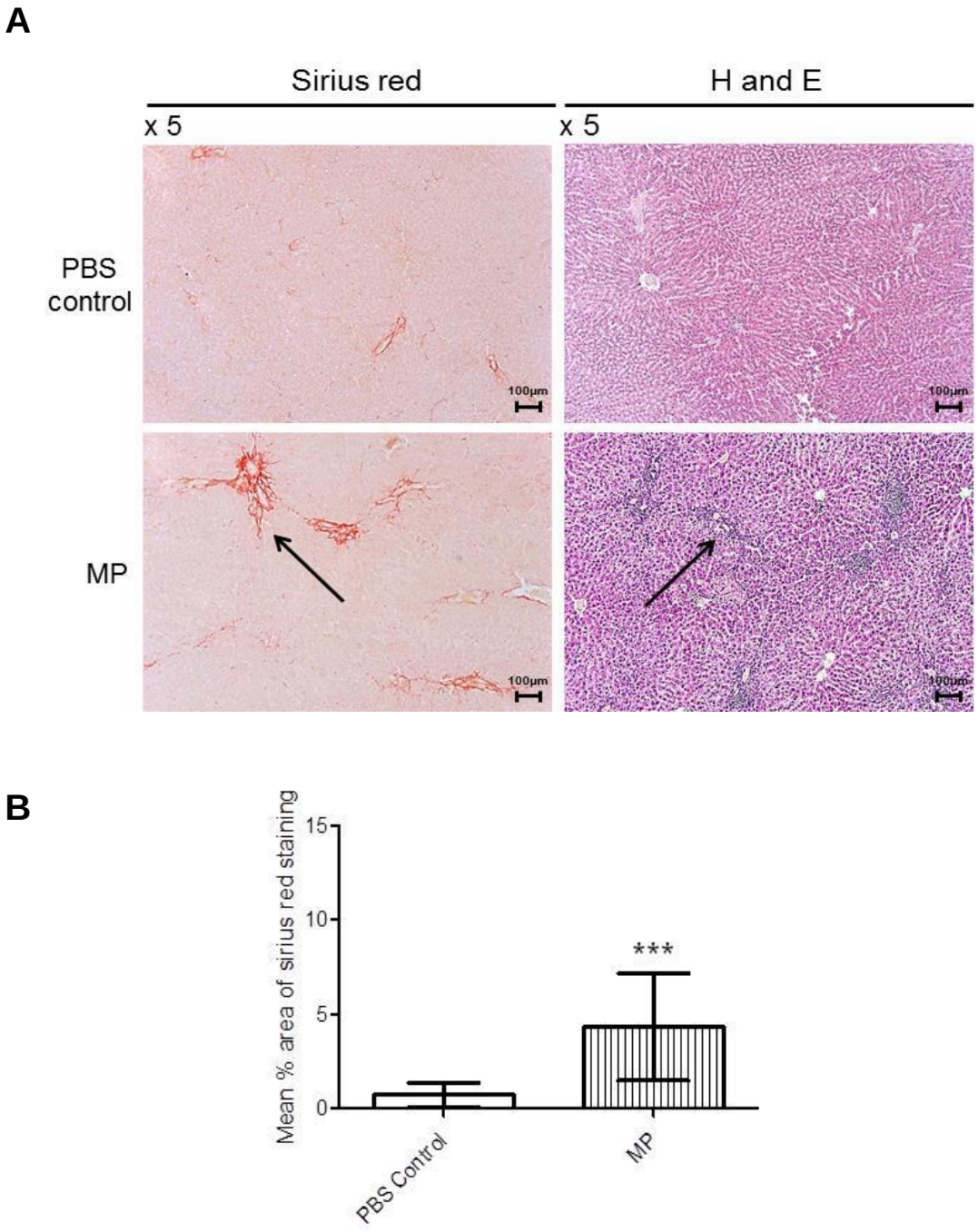

Figure 5.12: Fibrosis levels increase in the MP chronic liver injury tissue.
PBS control and MP treated rats were culled and livers were harvested and fixed for 24 hours in 10% formalin made up in 1 x PBS. Samples were then processed, embedded in paraffin and sectioned (5µm). Sections were then de-waxed and stained using **A)** sirius red or Haematoxylin and Eosin (H and E). Representative images were acquired at x 5 magnification. Scale bars = 100µm. B) Pictures were taken around 10 random periportal regions at x 10 magnification and the percentage area of the sirius red staining was quantified using the Leica software. Data are

the mean and SD of percentage area for each treatment group and were tested for statistical significance using the Student's unpaired t-test. *** Represent significant between MP and PBS control ($p<0.0001$). $n \geq 3$ for all groups.

α-SMA and vimentin expression in the control and MP treated liver sections was examined by immunohistochemistry. In control animals, α-SMA and vimentin positive cells were evenly spread around the lobules (Figure 5.13A) however, after MP treatment, the percentage of cells expressing these markers increased significantly (Figure 5.13B and C).

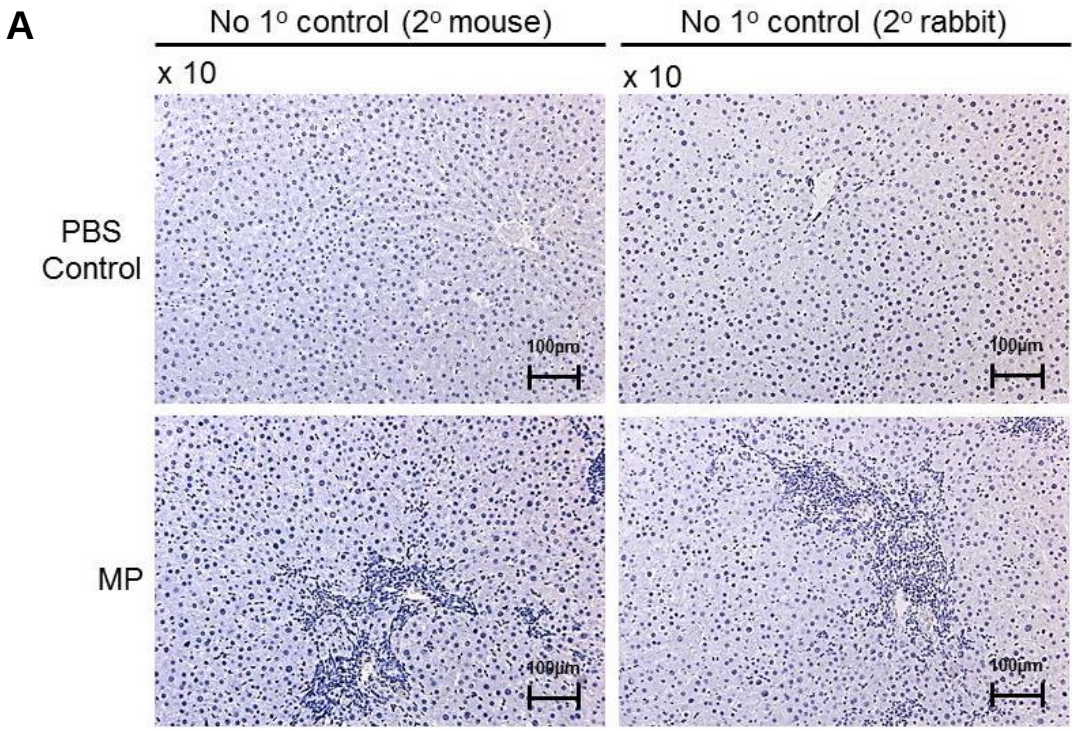

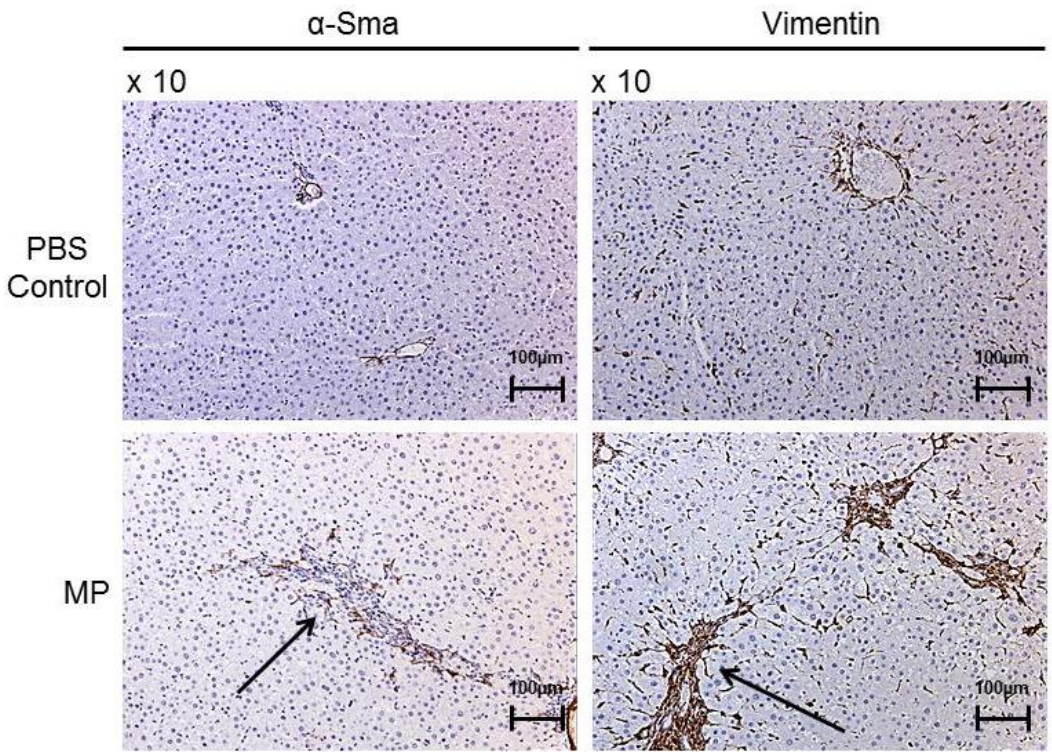
α-Sma
Vimentin
x 10
x 10
PBS Control
MP
100µm
100µm
100µm
100µm

B

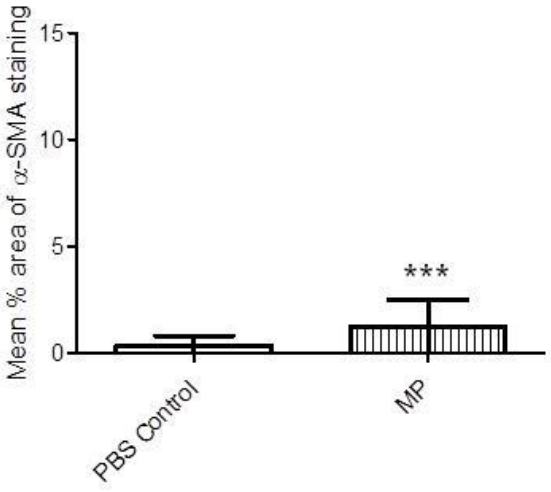
Mean % area of α-SMA staining
15
10
5
0
***
PBS Control
MP

C

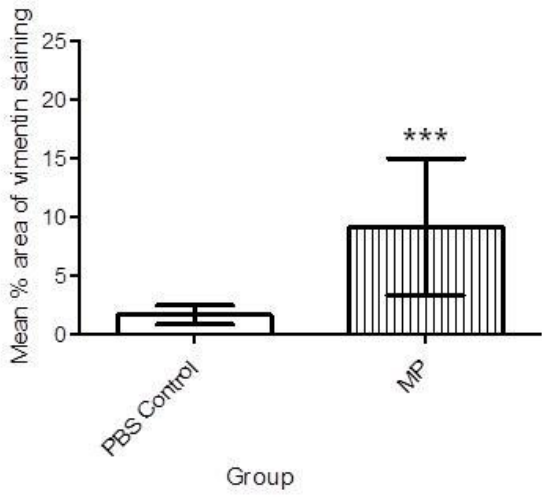
Mean % area of vimentin staining
25
20
15
10
5
0
***
PBS Control
MP
Group

Figure 5.13: MP treatment causes a significant increase in α-SMA and vimentin staining. PBS control and MP treated rats were culled and livers were harvested and fixed for 24 hours in 10% formalin made up in 1 x PBS.. Samples were then processed, embedded in paraffin and sectioned (5µm). Sections were then de-waxed and stained using **A)** α-SMA and vimentin. No primary antibody controls were included and were stained with the secondary anti-mouse IgG (for α-SMA) or anti-rabbit IgG (for vimentin) antibody alone. Representative images were acquired at x 10 magnification Scale bars = 100µm. For quantification of **B)** α-SMA and **C)** vimentin, pictures were taken around 10 random periportal regions at x 10 magnification and the percentage area of the staining was quantified using the Leica software. Data are the mean and SD of percentage area of the α-SMA/vimentin stain for each treatment group. Data are the mean and SD of percentage area for each treatment group and were tested for statistical significance using the Student's unpaired t-test. *** Represent significant between MP and PBS control ($p<0.0001$). $n \geq 3$ for all groups.

CK-19 staining (Figure 5.14A) was also performed on both the MP and demonstrated a significant increase in positive cells in the MP treated animals compared to the controls (Figure 5.14B).

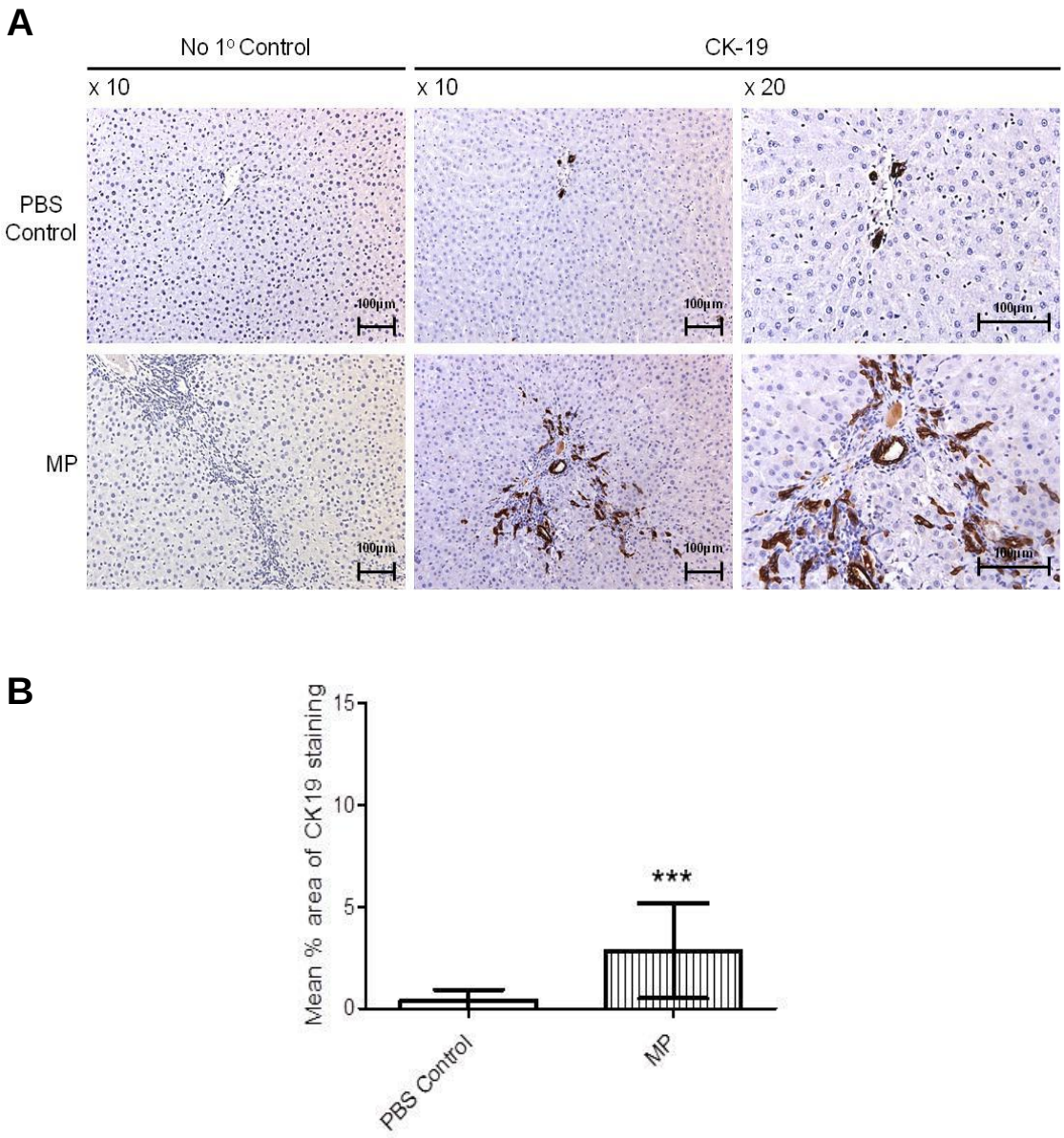

Figure 5.14: MP treatment causes a significant increase in CK-19 staining.
PBS control and MP treated rats were culled and livers were harvested and fixed for 24 hours in 10% formalin made up in 1 x PBS.. Samples were then processed, embedded in paraffin and sectioned (5µm). Sections were then de-waxed and stained using **A)** CK-19. No primary antibody controls were included and were stained with the secondary anti-mouse IgG antibody alone. Representative images were acquired at x 10 and x20 magnification Scale bars = 100µm. For quantification of **B)** CK-19, pictures were taken around 10 random periportal regions at x 10 magnification and the percentage area of the staining was quantified using the Leica software. Data are the mean and SD of percentage area of the α-SMA/vimentin stain for each treatment group. Data are the mean and SD of percentage area of the α-SMA/vimentin stain for each treatment group. Data are the mean and SD of percentage area for each treatment group and were tested for statistical significance using the Student's unpaired t-test. *** Represent significant between MP and PBS control ($p<0.0001$). $n \geq 3$ for all groups.

Both the PBS and MP liver sections were immunohistochemically stained for CXCL12 staining and the results demonstrated a significant percentage increase in positive cells in the MP treated group (Figure 5.15A and B).

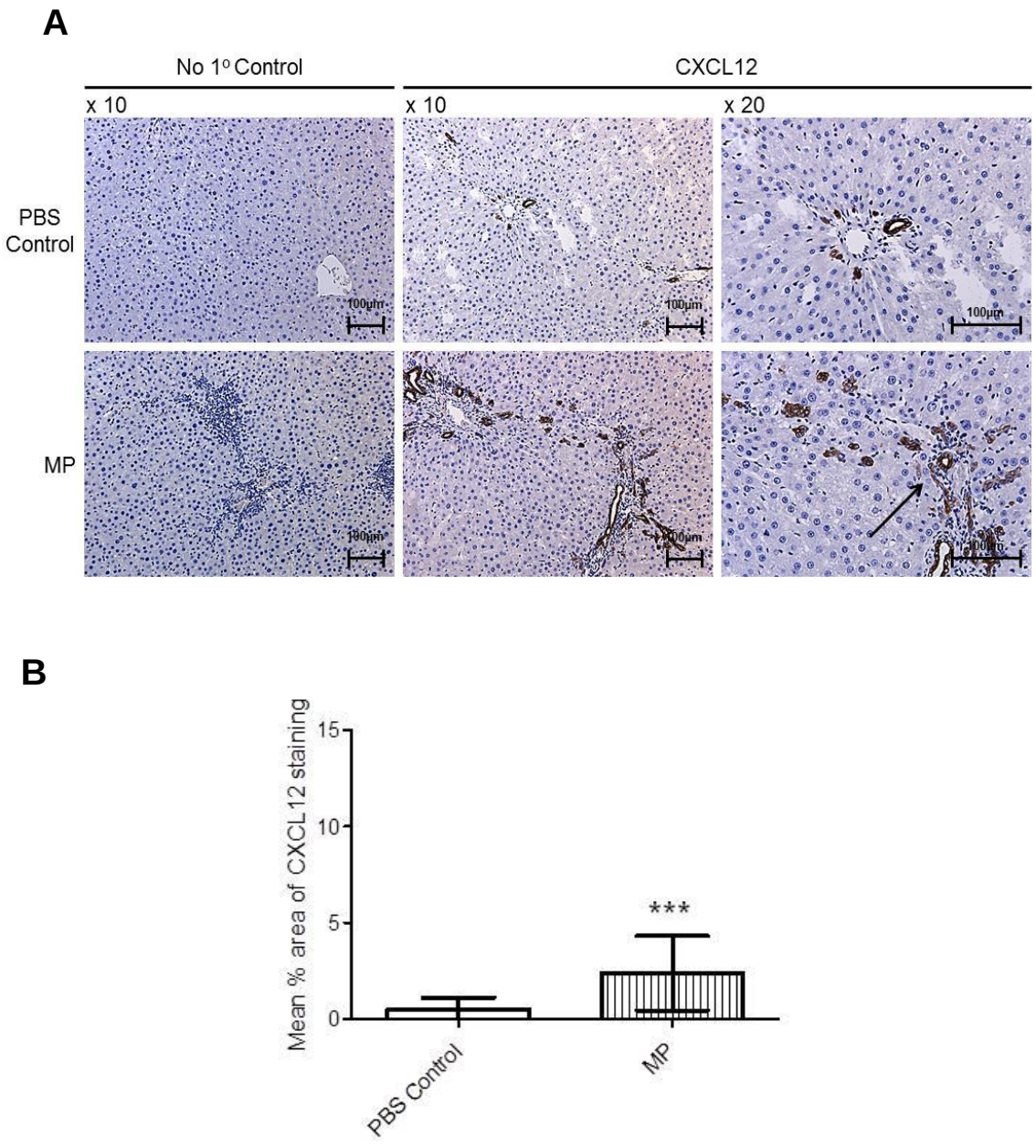

Figure 5.15: MP treatment causes a significant increase in CXCL12 staining.

PBS control and MP treated rats were culledand livers were harvested and fixed for 24 hours in 10% formalin made up in 1 x PBS.. Samples were then processed, embedded in paraffin and sectioned (5µm). Sections were then de-waxed and stained using **A)** CXCL12. No primary antibody controls were included and were stained with the secondary anti-mouse IgG antibody alone. Representative images were acquired at x 10 and x20 magnification Scale bars = 100µm. For quantification of **B)** CK-19, pictures were taken around 10 random periportal regions at x 10 magnification and the percentage area of the staining was quantified using the Leica software. Data are the mean and SD of percentage area of CK-19 staining for each treatment group and were tested for statistical significance using the Student's unpaired t-test. *** Represent significant between MP and PBS control ($p<0.0001$). $n \geq 3$ for all groups.

To determine mRNA and protein levels of CXCL12 in the PBS control and MP treated tissue qRT-PCR and Western blotting was performed respectively. The mRNA levels of the CXCL12 increased for all variants and significantly for CXCL12-α (Figure 5.16A) compared to the control animals. At the protein level, CXCL12 was not detected (Figure 5.16B) however, bands of greater intensity at ~58 and 50 kDa were observed.

A

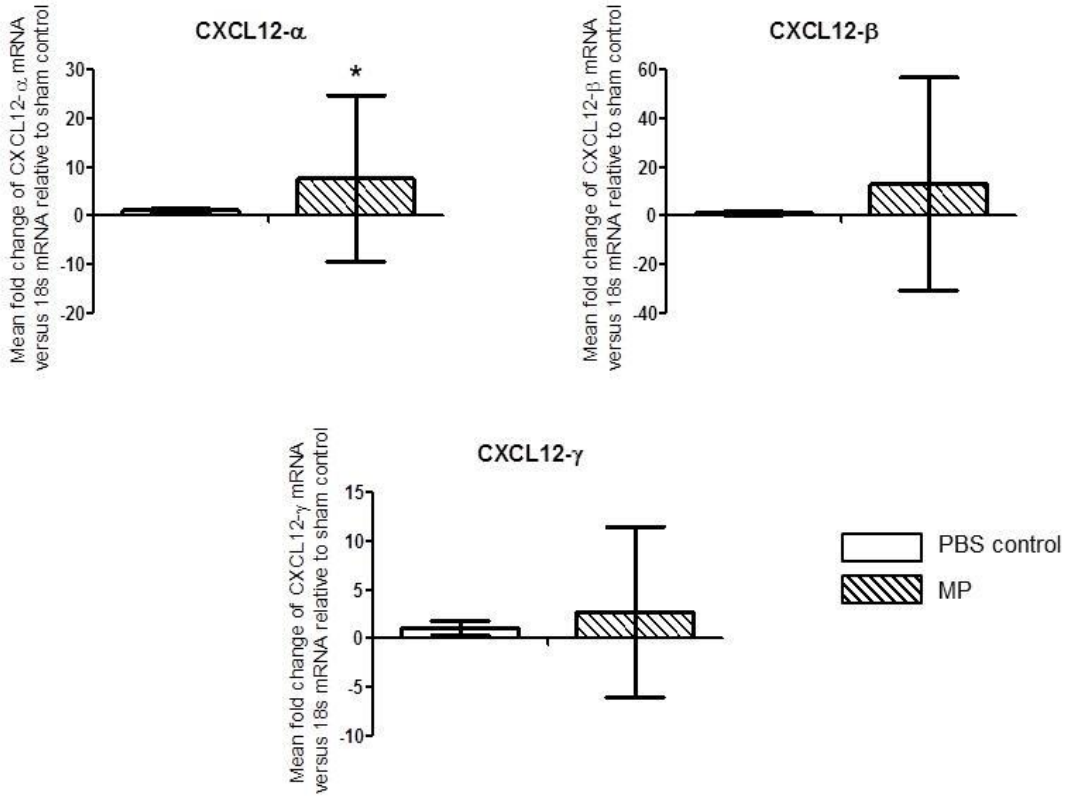

B

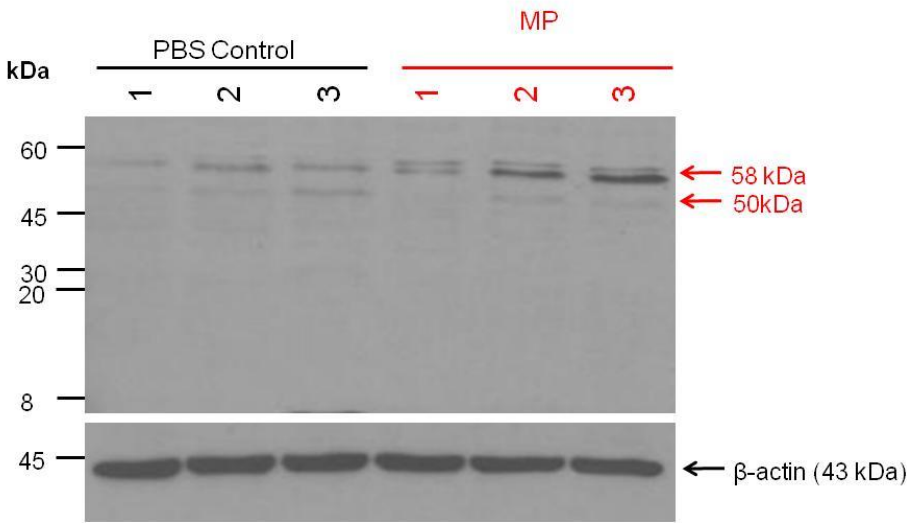

Figure 5.16: mRNA CXCL12 increases in MP liver but is not detected at the protein level. **A)** Representative qRT-PCR for the expression of CXCL12 variants in PBS control and Mp treated rat liver tissue. Total RNA was isolated using Trizol, as per manufacturer's instructions from whole mouse liver tissue. PCR controls were carried out in the absence of template RNA. Data are the mean and SD of mRNA CXCL12 variants for each treatment group and were tested for statistical significance using the Student's unpaired t-test. ** Represent significant between BDL and sham control ($p<0.001$). $n \geq 3$ for all groups. **B)** Representative Western blot for the expression of CXCL12. Whole liver tissue was homogenised followed by sonication and prepared for protein analysis by Western blot. 20µg of protein was loaded per lane and β-actin was used as a loading control. $n \geq 3$ for all groups.

5.3: Chapter Discussion

The results in this chapter demonstrated that liver injury was successfully achieved in all of the three different models of fibrosis induced by; CCl_4, BDL and MP treatment. The immunohistochemistry results also showed that CXCL12 was expressed by the biliary epithelial cells in each of the models and cells with morphology similar to myofibroblasts in the 12 wk CCl_4 fibrotic liver tissue were also observed. This is consistent with previous studies that have shown that both of these specific liver cell types express this chemokine (Terada, Yamamoto et al. 2003, Hong, Tuyama et al. 2009). However, in these studies it was difficult to confirm that the myofibroblasts expressed CXCL12 because as revealed by the immunofluorescence staining, biliary epithelial cells were also positive for α-SMA. Therefore, this would warrant further investigation by using additional markers of myofibroblasts for example, desmin.

Quantification of CXCL12 staining demonstrated increased expression in the CCl_4, MP and BDL models compared to the controls and furthermore, levels were greatest in the BDL model. This was not surprising since biliary epithelial cells are the main cellular source of CXCL12 and in this model a significant increase of CK-19 positive cells was observed. In the CCl_4 model, ICAM-1, IL-1 and CXCL9 were all up-regulated in the fibrotic liver tissue compared to the untreated tissue and these results are supported by previous studies. For example, in one study elevated levels of CXCL9 were observed in patients with hepatic fibrosis (Zeremski, Dimova et al. 2009). In another study, in comparison to healthy control, patients with liver disease displayed elevated serum levels of IL-1 compared to controls (Negash, Ramos et al. 2013). Furthermore, the expression of ICAM-1 has been shown to be increased in chronic liver tissues (Xu, Li et al. 2005). It was surprising that CXCL12 was not detected by the array assay; however, this may have been due to the expression levels being too low in this particular sample or it is possible that the chemokine may have been degraded during sample preparation.

Upon examination of the mRNA expression levels of CXCL12, the studies showed that variants were up regulated in each of the models with the exception of CXCL12-γ which was not detected in the mouse liver tissue (CCl_4 model). However, this supports the previous PCR data in Chapter 4 which showed that this variant was only expressed in the murine lungs and brain. Examination of protein CXCL12 expression by Western blotting showed that it was only detected in the BDL model (one sham control and one BDL rat liver) and bands were very faint. Nonetheless, as seen in the previous chapter, bands of greater molecular weights were observed in all three models. This may be a non-specific band i.e. the antibody may be reacting with another protein, alternatively, CXCL12 may be post translationally modified as discussed in the previous chapter.

Overall, the results demonstrated that mRNA expression of CXCL12 is increased in a centrilobular and two different periportal models of liver fibrosis. Thus, in the context of melanoma, it would be interesting to study metastasis in these three different models.

Chapter 6: Results 4

Modelling melanoma to the normal and damaged liver *in vivo*.

6.1: Introduction and Aims

Metastasis is the main cause of mortality for patients with cancer and the liver is a common site to which tumour cells metastasise. However, clinical studies have shown that for some cancers, metastasis rarely occurs to the cirrhotic liver (Uetsuji, Yamamura et al. 1992, Vanbockrijck and Kloppel 1992, Seymour and Charnley 1999, Gervaz, Pak-art et al. 2003, Pereira-Lima, Lichtenfels et al. 2003). For example, a study of 250 patients by Uetsuji et al revealed that hepatic metastasis of colorectal cancer was prevalent in patients with non-cirrhotic livers (20%) but was not evident in patients with cirrhosis (Uetsuji, Yamamura et al. 1992). Autopsy studies have also shown that colorectal cancer metastasis to the cirrhotic liver is rare (Seymour and Charnley 1999). The reasons for this are not yet fully understood, however, it has been postulated that venovenous shunting an event in cirrhosis, may prevent cells from entering the liver (Seymour and Charnley 1999). In addition, since alterations to the architecture of cirrhotic sinusoids are observed (Seymour and Charnley 1999), it has been suggested that liver injury may create an unfavourable site for cancer cells to both metastasise and reside in (Seymour and Charnley 1999). It has been suggested that the differences observed in experimental studies to clinical autopsy studies may be due to the difficulty of collecting controlled clinical groups (Qi, Qiu et al. 2004). For instance, patients with cirrhosis may have shorter life expectancies and therefore do not live long enough to develop metastasis (Qi, Qiu et al. 2004).

On the contrary, in the context of melanoma metastasis, an experimental study showed a greater incidence of tumours in animals with cirrhotic livers compared to control animals (Qi, Qiu et al. 2004). The authors suggested that as a consequence of changes in architecture and adhesion molecule expression expression in the cirrhotic livers, a greater number of tumour cells arrest in the terminal portal vein (TPV) (Qi, Qiu et al. 2004). However, whether or not cancer metastasizes more frequently to the fibrotic liver or to the liver exhibiting lower levels of damage is yet to be determined. To this end, in humans, it remains unclear as to whether the injured liver promotes or serves as a protective mechanism against melanoma metastasis. However, since chronic injury in the liver leads to an increase in pro-inflammatory cells (Wallace, Burt et al. 2008) releasing factors such as CXCL12, it is possible that liver injury may actually promote metastasis of CXCR4 positive melanoma cells.

An established model for studying melanoma is the C57BL/6-derived B16 mouse model for human melanoma (Overwijk and Restifo 2001). In this model, subcutaneous injection (s.c) and intravaneous injection (i.v) of B16 cells forms skin and lung tumours respectively (Overwijk and Restifo 2001). For example, in a study by Lee et al, CXCR4-luc-B16 cells were injected i.v into C57BL/6-derived mice and pulmonary metastasis was observed (Lee, Kakinuma et al. 2006). Additionally, xenograft mouse models for studying skin cancer have already been performed successfully utilising nude mice (Hill, Martin et al. 2009, Horie, Tsuchihara et al. 2010). In a study by Hill et al, fenretinide and bortezomib were tested for their ability to reduce tumour volume in a nude mouse model (Hill, Martin et al. 2009). Prior to the injection of these agents, three human melanoma cell lines (A375, CHL-1 and Wm2664) were inoculated into the right flank of nude mice and skin tumours were established (125mm^3 volume). The results demonstrated that clinically achievable concentrations of fenretinide and bortezomib markedly reduced tumour growth.

Therefore, the aims of this chapter were to perform *in vivo* pilot studies to examine whether melanoma cells (murine and human) metastasise to the normal and/or damaged liver and to any other organ based upon these existing models. A further aim of this chapter was to generate a hepatic stellate specific CXCL12 knockout mouse model because as yet, attempts to knock down this gene *in vivo* have been unsuccessful. If this was achieved, melanoma cells would be injected into both experimental (KO) and control (WT) groups to determine if CXCL12 secreted by myofibroblasts has an effect on melanoma growth and/or metastasis.

6.2: Results

6.2.1: Modelling human melanoma metastasis to the normal and damaged liver.

Initial attempts were made to establish a human model of melanoma metastasis. A summary of the experimental study is illustrated in Figure 6.1A (a detailed description is given in section 2.1.4). A375 human melanoma cells transfected with a fluorescent red protein (A375^{red}) (Figure 6.1B) were injected intravenously (i.v) into nude mice with either normal or damaged livers induced by intraperitoneal injection (i.p) of paracetamol. Control animals received PBS alone. Tumours were not observed by IVIS imaging and therefore H and E staining was performed on sections of all of the animal organs. The results showed that tumours were not observed in the brain, heart, lungs, kidney, spleen, pancreas or skin as shown by the representative images from an animal in each group in Figure 6.1C.

A

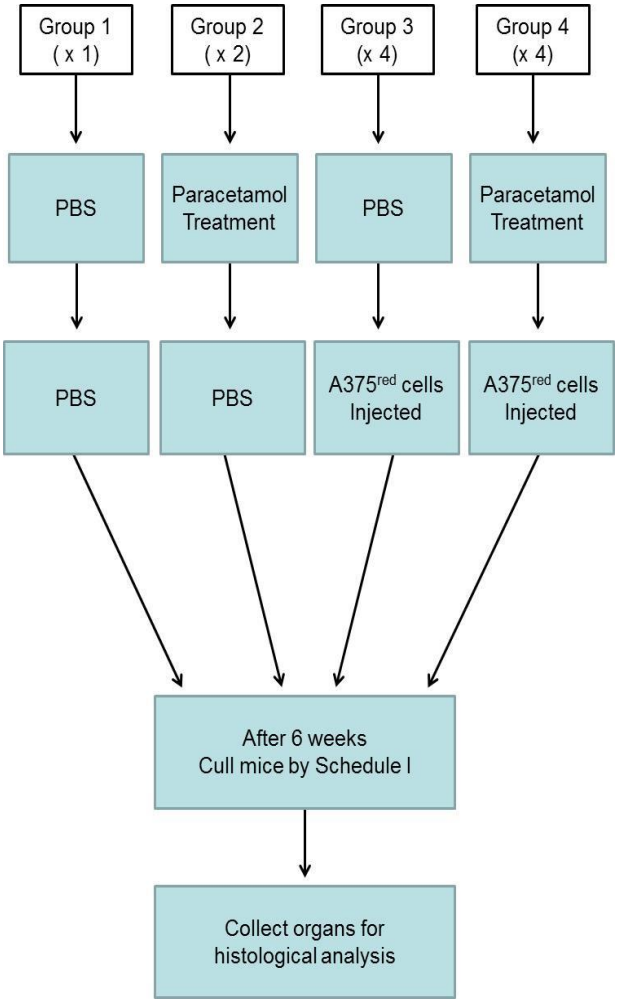

B

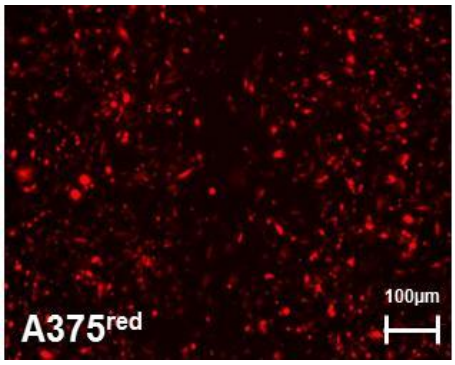

C

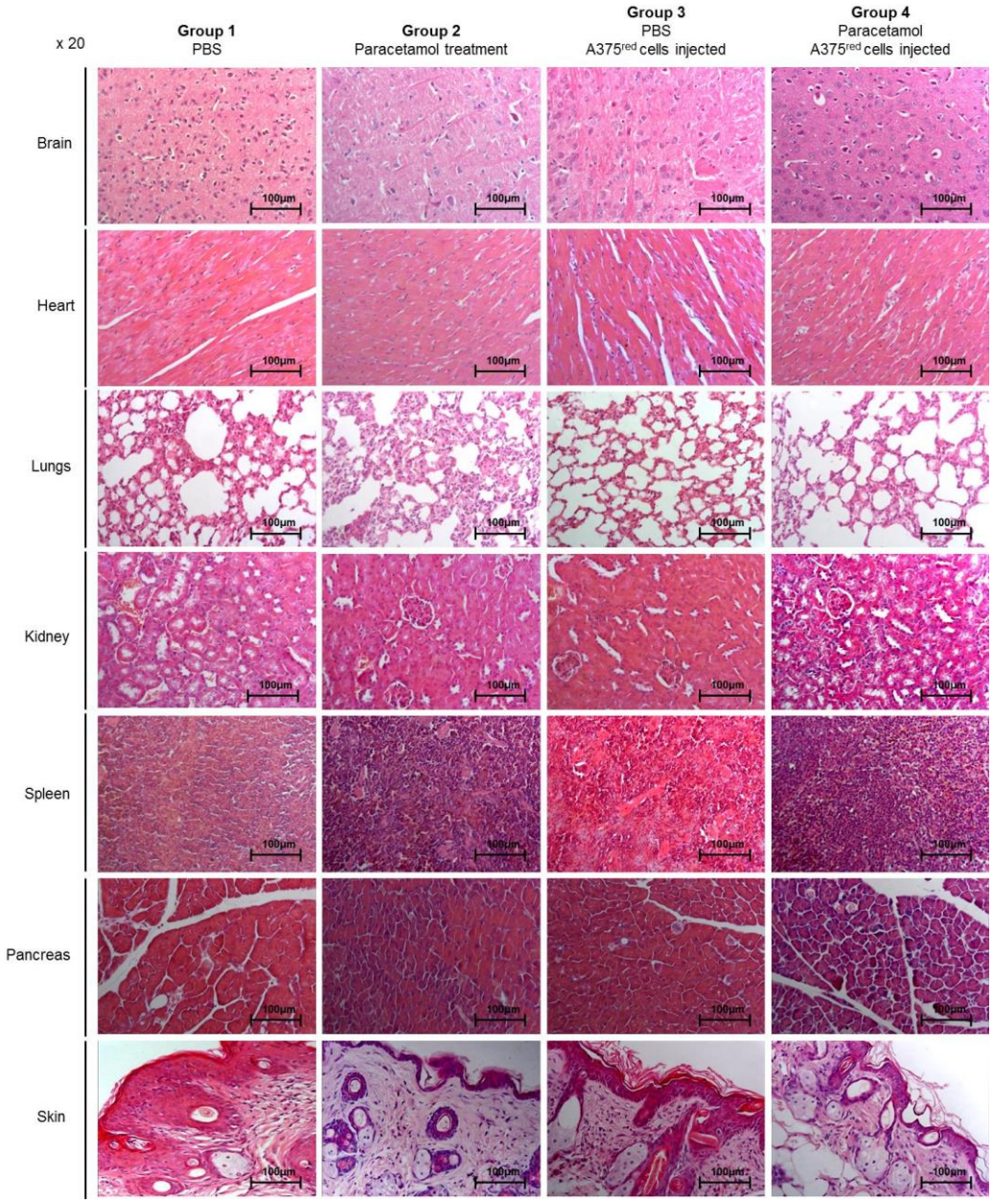

Figure 6.1: A375^{red} cells do not engraft in the organs of female nude mice.
A) Experimental plan for modelling human melanoma in nude mice. **B)** Representative image of A375 cells transfected with a red fluorescent protein (DS red). Images were taken by

fluorescence microscopy at x 10 magnification. Scale bar =100µM. **C)** Nude mice were culled and organs were harvested and fixed for 24 hours in 10% formalin made up in 1 x PBS. Samples were then processed, embedded in paraffin and sectioned (5µm) and haematoxylin and eosin (H and E) staining was performed. Tumours were not observed in the brain, heart, lungs, kidney, spleen, pancreas or skin. Images were acquired at x 20 magnification. Scale bars = 100µm.

The H and E staining results from the liver sections showed that in the majority of animals, tumour cells did not engraft in this organ (Figure 6.2A). Cells resembling the A375^{red} cells were observed (Figure 6.2B) in one animal from Group 3, indicating that the cells had metastasized to the liver in this mouse alone.

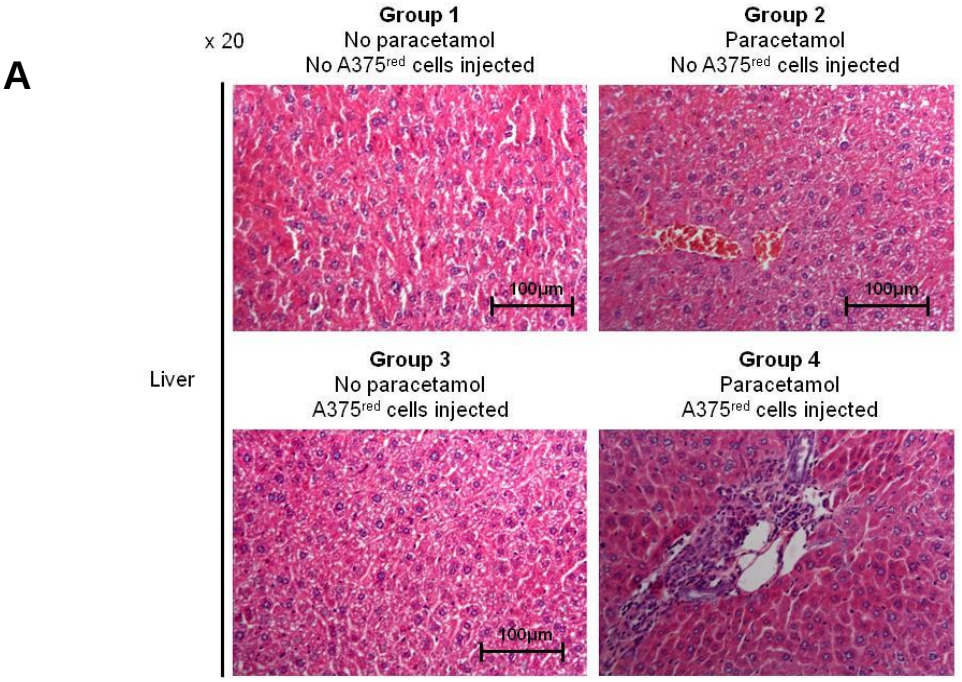

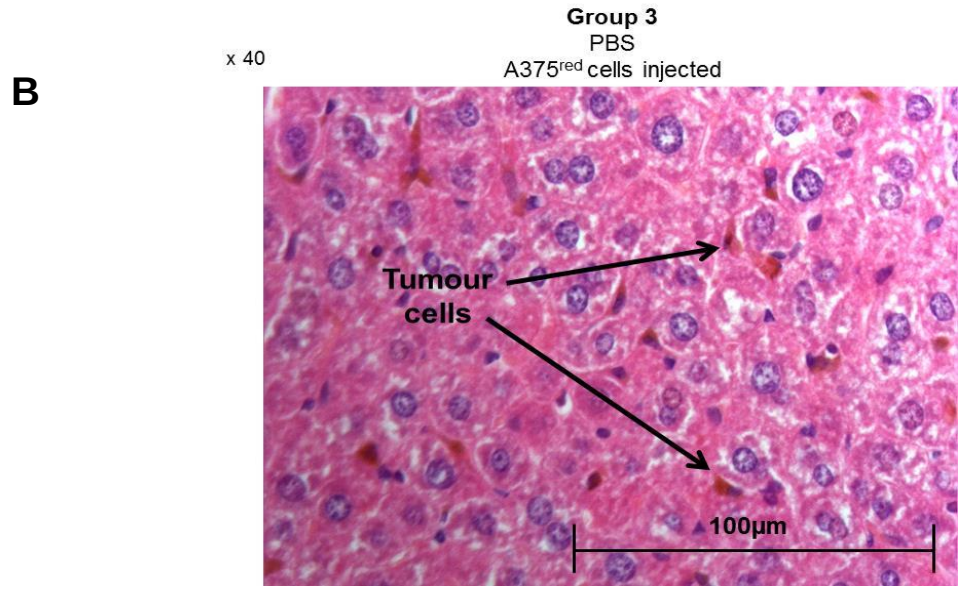

Figure 6.2: A375^{red} cells engrafted into one normal liver of a nude mouse.
Nude mice were culled and organs were harvested and fixed for 24 hours in 10% formalin made up in 1 x PBS. Samples were then processed, embedded in paraffin and sectioned (5µm) and haematoxylin and eosin (H and E) staining was performed. **A)** Tumours were not observed in the majority of the livers. **B)** Tumour cells resembling the A375^{red} cells were observed in one nude mouse. Images were acquired at x 20 or x 40 magnification. Scale bars = 100µm.

6.2.2: B16 as a mouse model for human melanoma to the normal and fibrotic liver.

To determine which organs in the female C57BL/6 mice the B16-F10 cell line engraft in, cells were injected either subcutaneously (s.c) or intravenously (i.v). A summary of the study carried out is illustrated in Figure 6.3 (further details are given in section 2.1.5). To reduce animal numbers, Group 1 organs were used from archived tissue from a previous study.

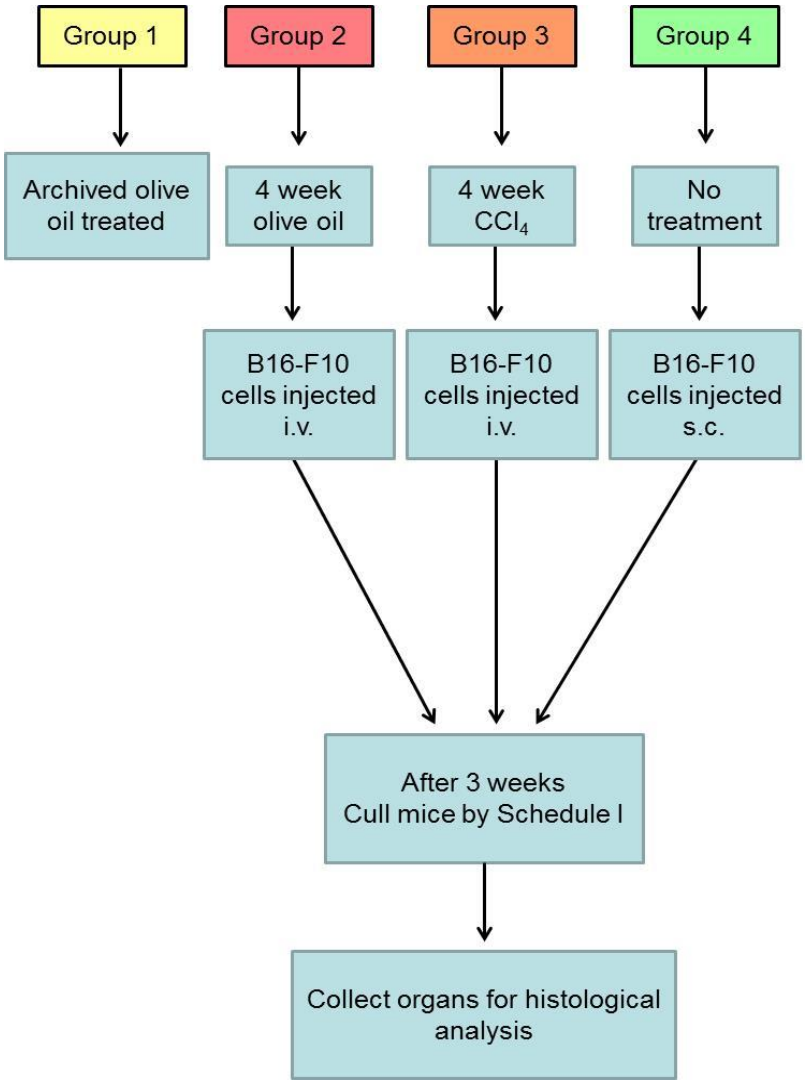

Figure 6.3: Experimental plan for the B16 as a mouse model of melanoma to the normal and fibrotic liver.

To confirm that CCl_4 had induced fibrosis in the animals in Group 3, the formalin fixed paraffin embedded liver sections were stained with H and E and sirius red. As illustrated by the bridging effect in Figure 6.4A (denoted by the arrows) fibrosis was established in all three mice and was most prominent in M7. Furthermore, collagen levels were significantly increased compared to untreated animals and levels were greatest in M7 (Figure 6.4B and C).

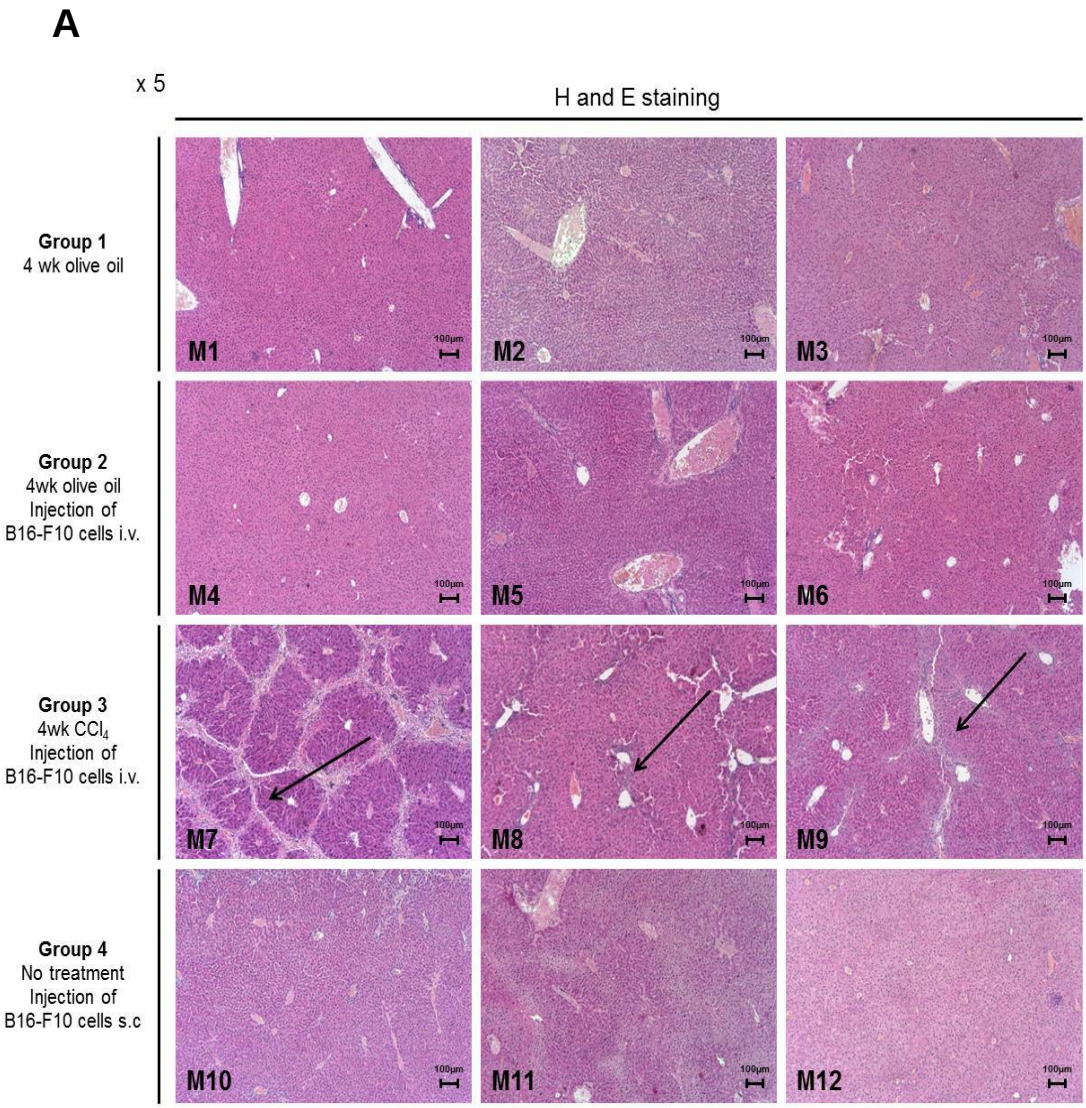

B

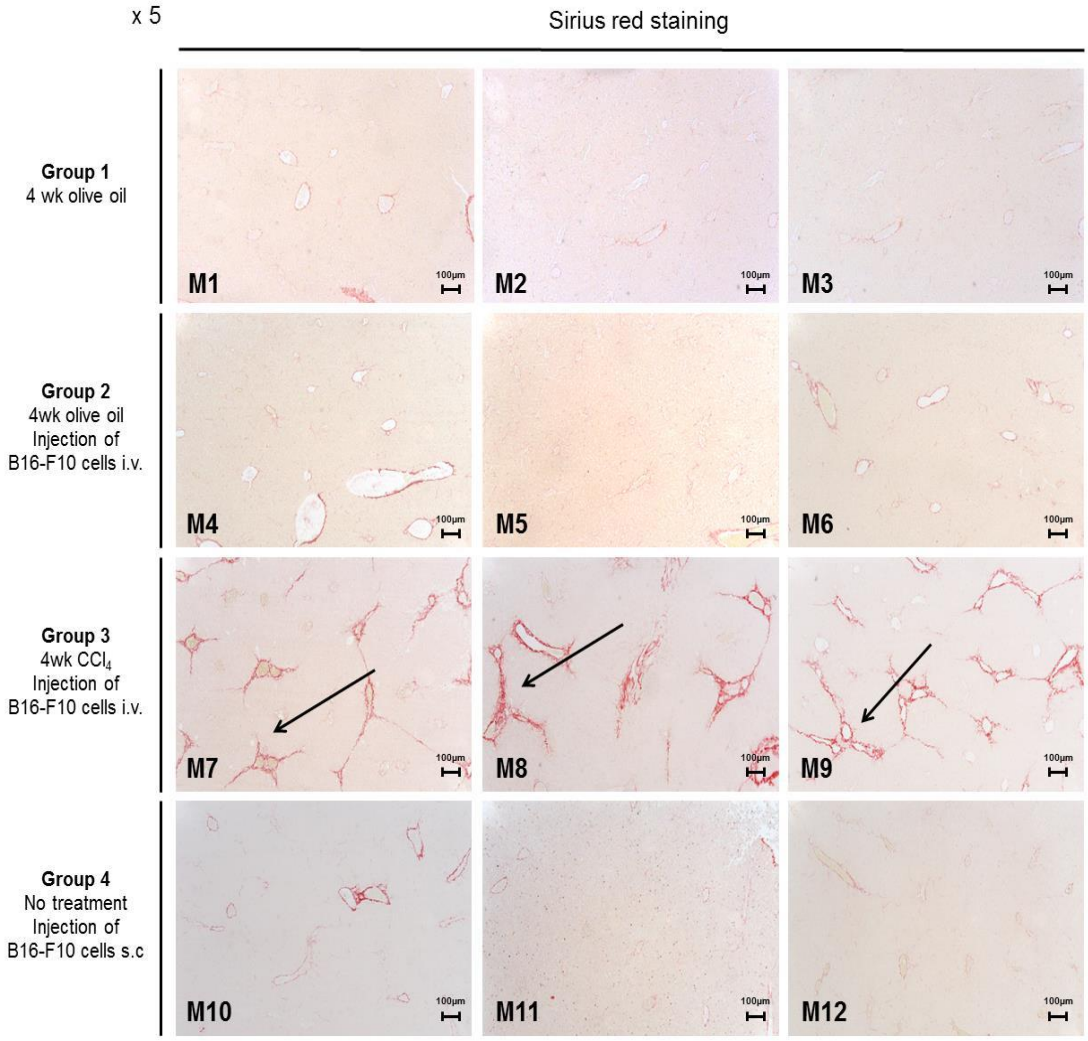

C

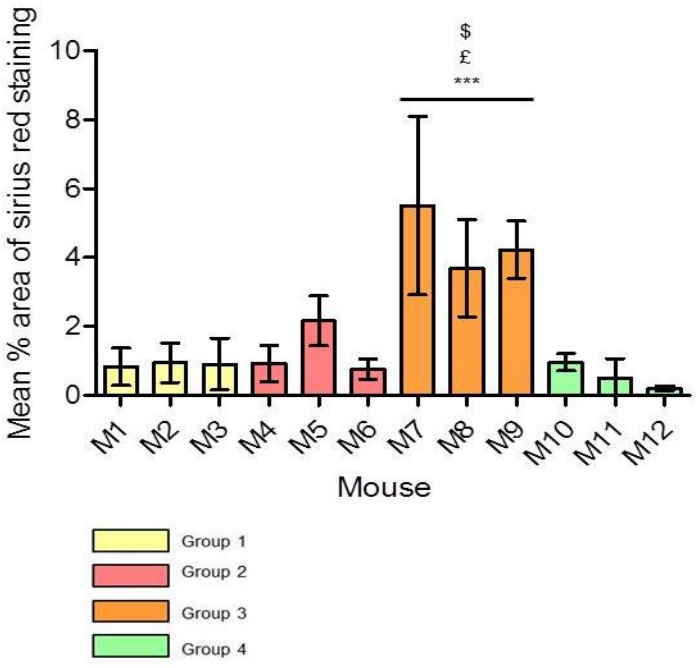

Figure 6.4: Assessment of fibrosis in the B16-F10 liver tissue.

C57BL/6 mice from the B16-F10 study were culled and livers were harvested and fixed for 24 hours in 10% formalin made up in 1 x PBS. Samples were then processed, embedded in paraffin and sectioned (5µm). Sections were then de-waxed, stained and mounted. **A)** Haematoxylin and Eosin (H and E) staining showing fibrosis in the Group 3 mice as denoted by the arrows **B)** Sirius red staining showing increased levels of collagen in the Group 3 mice as denoted by the arrows. Images were acquired at x 5 magnification. Scale bars = 100µm. **C)** For quantification of sirius red staining, pictures were taken in 10 random fields of view at x 10 magnification. Bars are the mean +SD. Statistical analyses were compared by one way ANOVA with Bonferroni's post hoc correction. *** indicates a significant difference compared to Group 1 mice, £ indicates a significant difference compared to the Group 2 mice and $ indicates a significant difference compared to the Group 4 mice (all $p<0.0001$).

To further confirm that CCl_4 treatment had resulted in fibrosis in the Group 3 mice, α-SMA immunofluorescence (Figure 6.5A) and immunohistochemistry (Figure 6.5B and C) staining was performed on the liver sections. As shown by the representative images (one animal from each group) the immunofluorescence staining revealed fibrotic bands in the animals treated with CCl_4 (Figure 6.5A). Additionally, the immunohistochemistry results demonstrated that the percentage of α-SMA positively stained cells was significantly greater in the animals treated with CCl_4 compared to the untreated animals (Figure 6.5B and C).

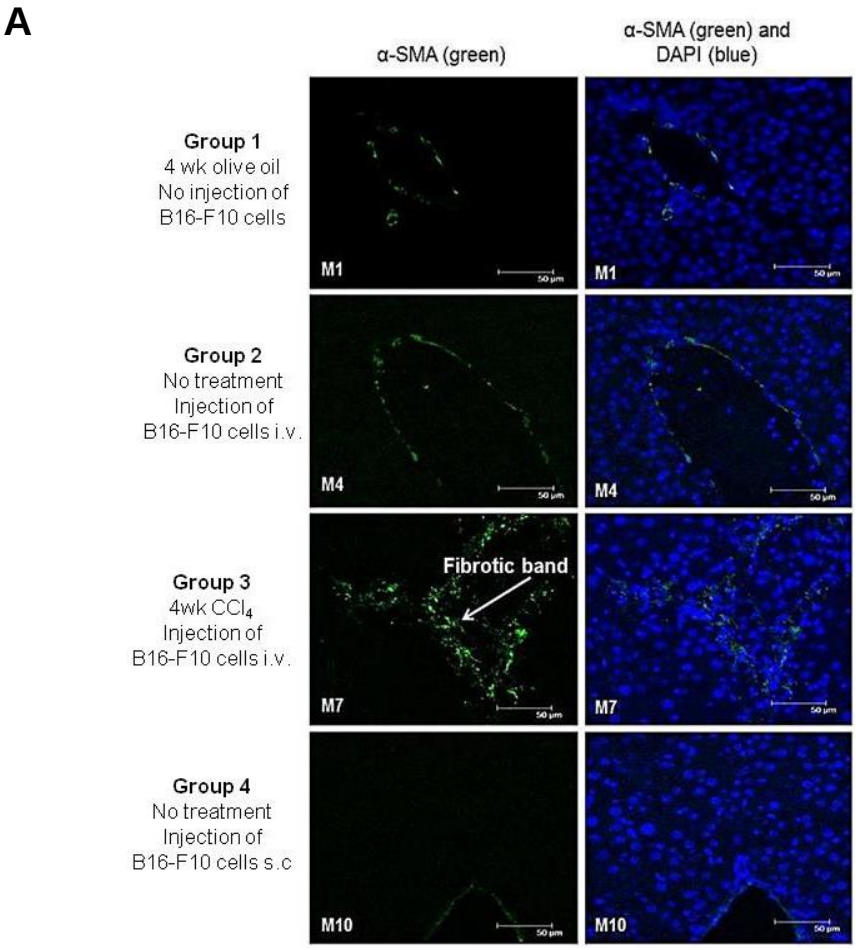

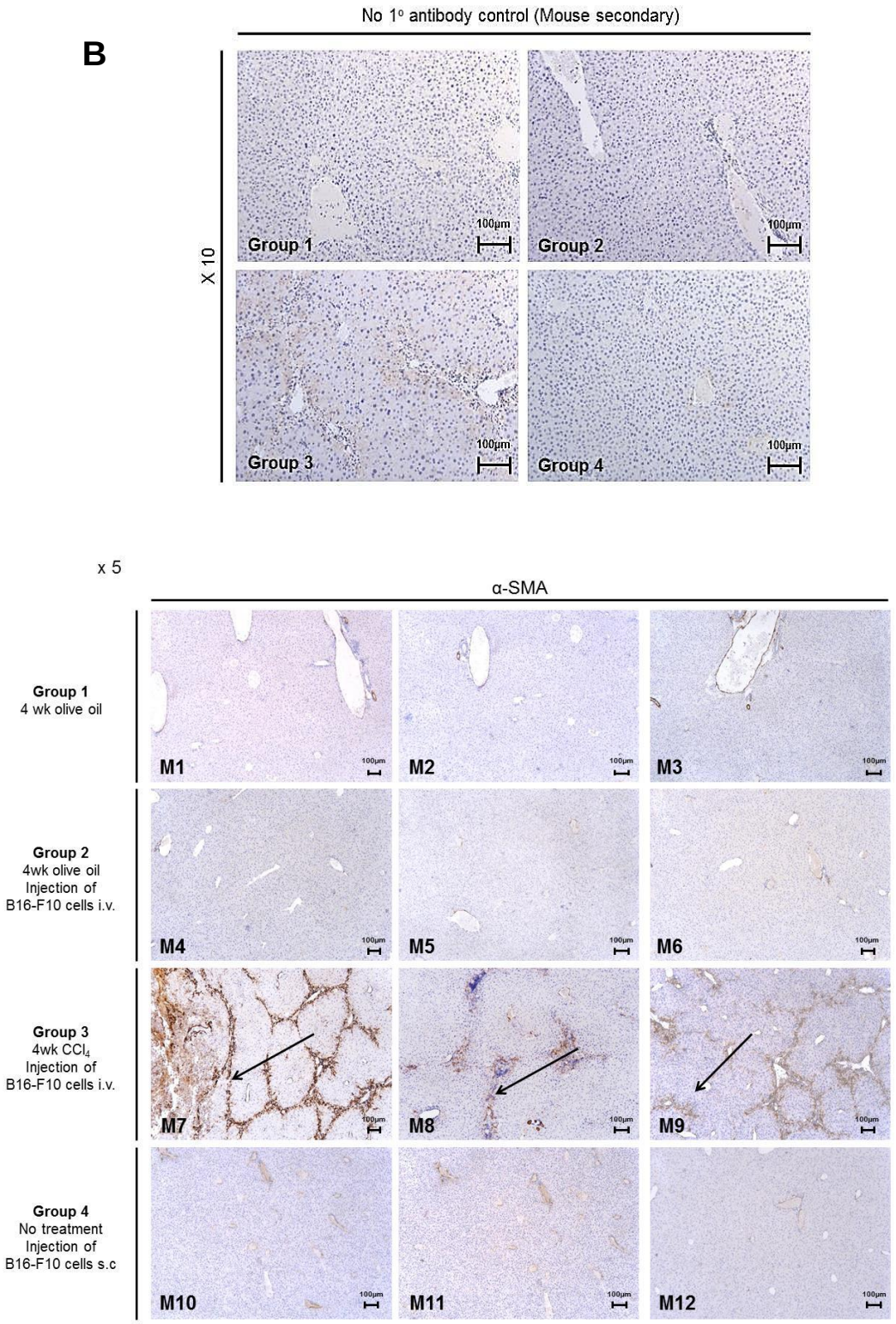
B
No 1° antibody control (Mouse secondary)
X 10
Group 1
Group 2
Group 3
Group 4
100µm
x 5
α-SMA
Group 1
4 wk olive oil
Group 2
4wk olive oil
Injection of
B16-F10 cells i.v.
Group 3
4wk CCl4
Injection of
B16-F10 cells i.v.
Group 4
No treatment
Injection of
B16-F10 cells s.c
M1
M2
M3
M4
M5
M6
M7
M8
M9
M10
M11
M12

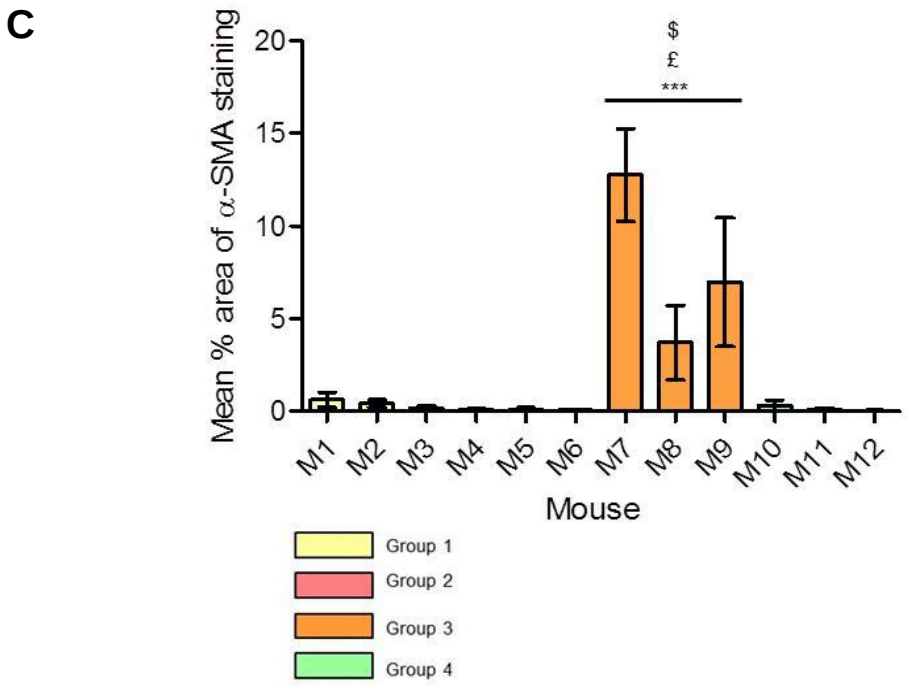

Figure 6.5: α-SMA staining in the B16-F10 liver tissue.
C57BL/6 mice from the B16-F10 study were culled and livers were harvested and fixed for 24 hours in 10% formalin made up in 1 x PBS. Samples were then processed, embedded in paraffin and sectioned (5µm) and de-waxed and immunochemically stained **A)** The expression α-SMA (green) was determined by confocal microscopy and background levels were set against the no primary control. DAPI was used to stain the nuclei. Representative images were acquired at x 40 magnification **B)** Sections were stained α-SMA. No primary antibody controls were included and were stained with the secondary anti-mouse IgG antibody alone. As indicated by the arrows positive staining was observed around the periportal regions. Representative images were acquired at x 5 magnification. Staining is typical of three separate experiments. Scale bars = 100µm. **C)** For quantification of α-SMA staining, pictures were taken in 10 random fields of view at x 10 magnification. Bars are the mean +SD. Statistical analyses were compared by one way ANOVA with Bonferroni's post hoc correction. *** indicates a significant difference compared to Group 1 mice, £ indicates a significant difference compared to the Group 2 mice and $ indicates a significant difference compared to the Group 4 mice (all $p<0.0001$).

B16-F10 tumour cells were identified macroscopically and microscopically (H and E staining) as black nodules, in the lungs (M4, M6, M7, M9 and M11) (Figure 6.6A and B), spleen (M7 and M11) (Figure 6.6A and C) and by s.c. injection in the pancreas (M11) (Figure 6.6A and D). A closer view of these tumour cells can be seen in Figure 6.6E. A summary of these results are given in Table 6.1.

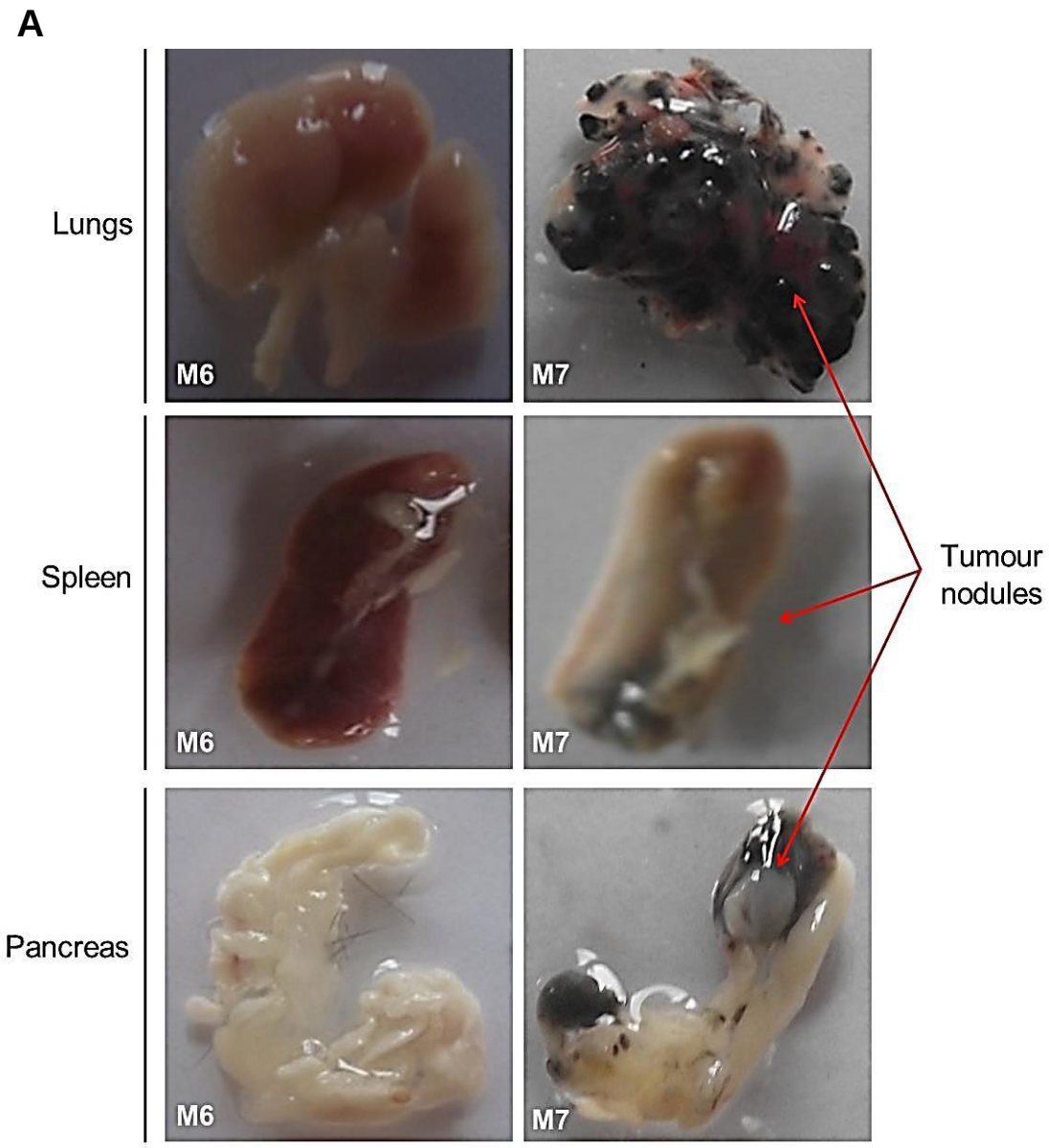
A
Lungs
Spleen
Pancreas
M6
M7
M6
M7
M6
M7
Tumour nodules

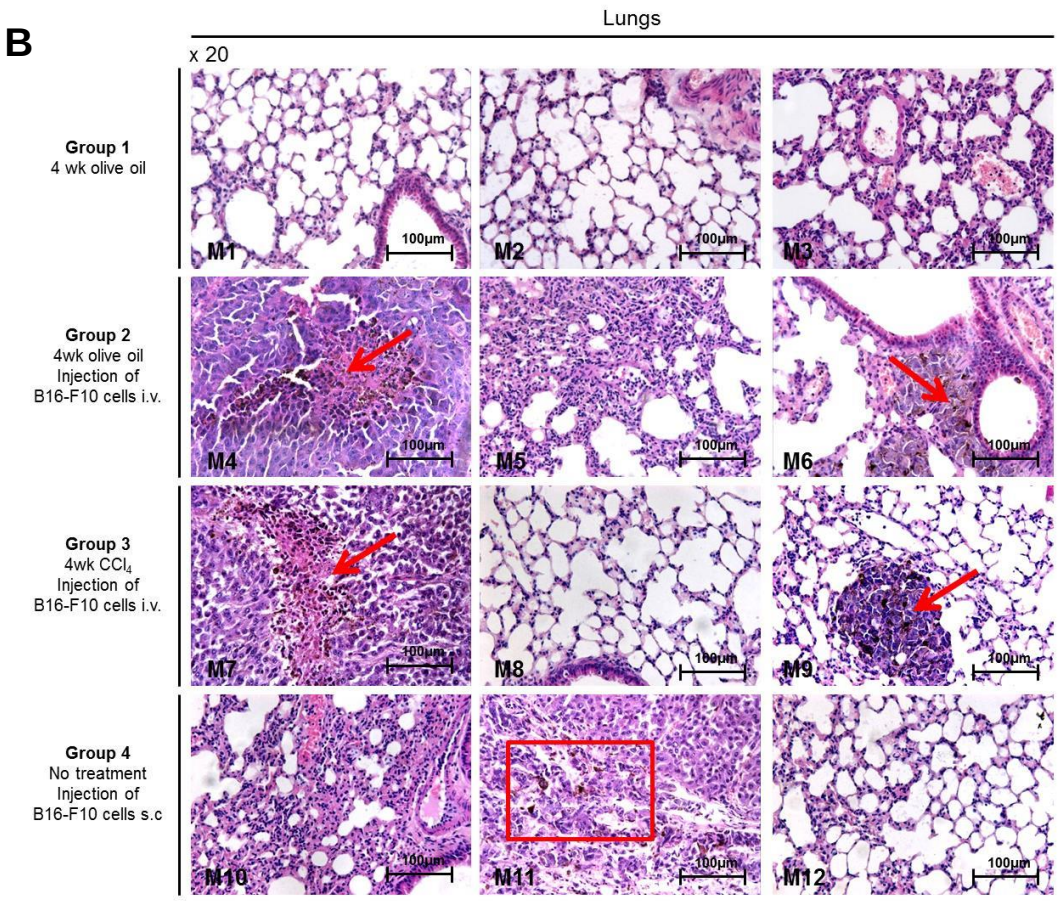
B
Lungs
x 20
Group 1
4 wk olive oil
Group 2
4wk olive oil
Injection of
B16-F10 cells i.v.
Group 3
4wk CCl4
Injection of
B16-F10 cells i.v.
Group 4
No treatment
Injection of
B16-F10 cells s.c
M1
M2
M3
M4
M5
M6
M7
M8
M9
M10
M11
M12
100µm

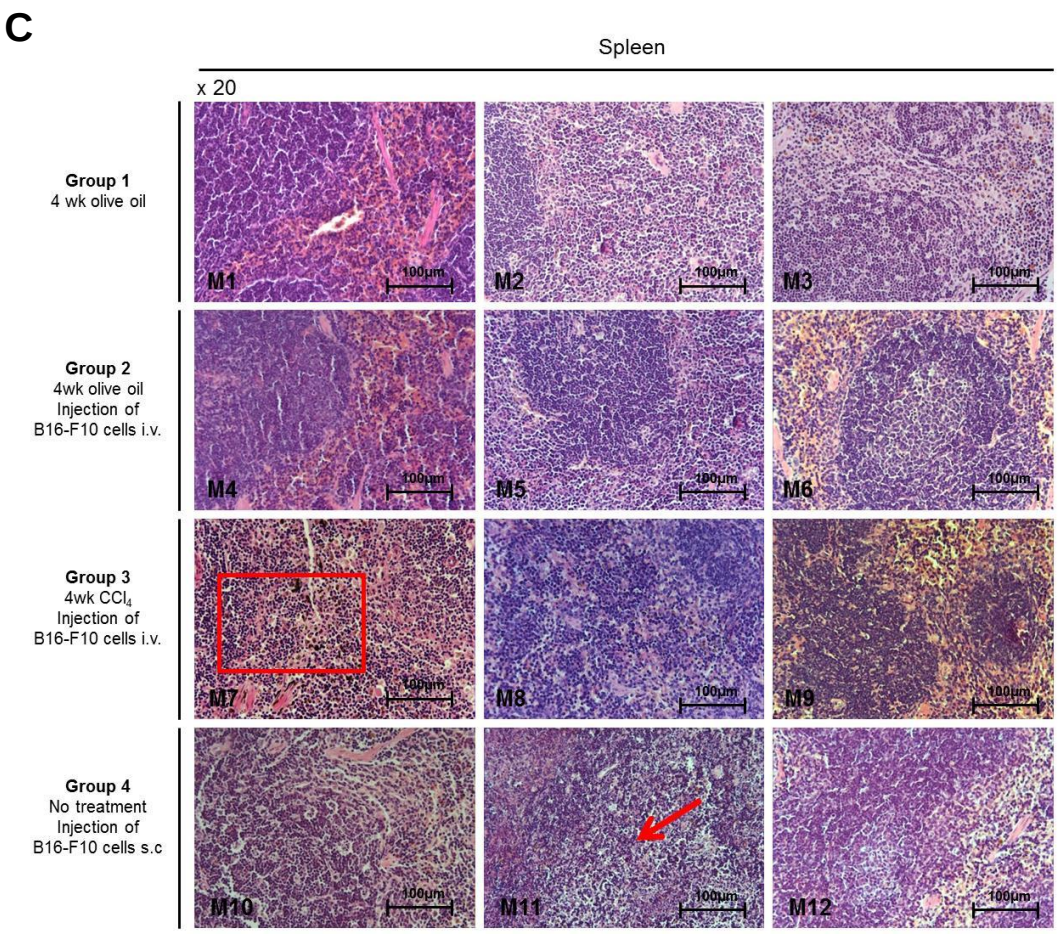
C
Spleen
x 20
Group 1
4 wk olive oil
Group 2
4wk olive oil
Injection of
B16-F10 cells i.v.
Group 3
4wk CCl4
Injection of
B16-F10 cells i.v.
Group 4
No treatment
Injection of
B16-F10 cells s.c
M1
M2
M3
M4
M5
M6
M7
M8
M9
M10
M11
M12
100µm

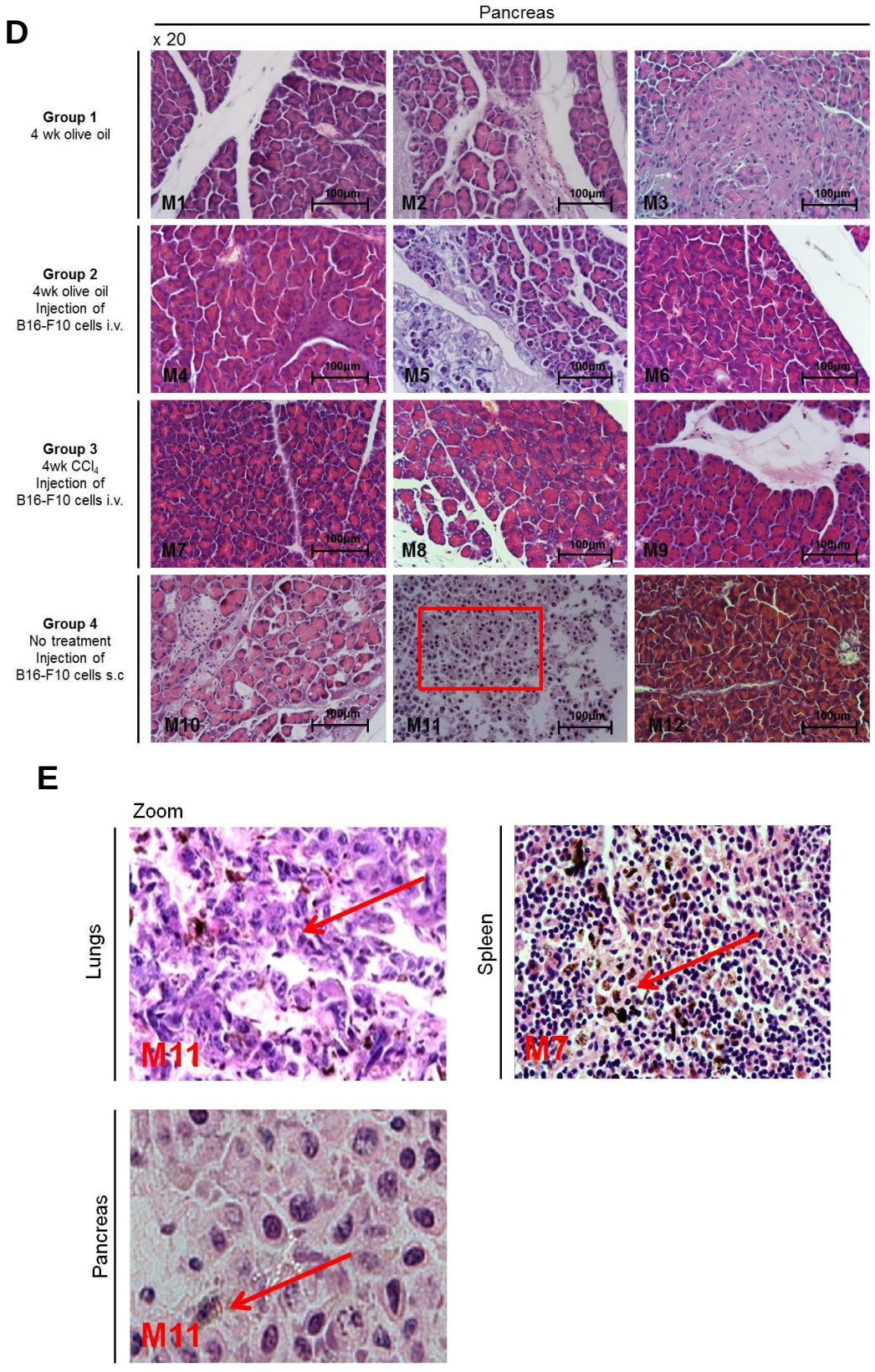

Figure 6.6: Tumour cells observed in the lungs, spleen and pancreas in the B16 mouse model.

A) Gross appearance of tumour nodules in the lungs, spleen and pancreas. Images were taken 21 days after injection. C57BL/6 mice from the B16-F10 study were culled and the organs were harvested and fixed for 24 hours in 10% formalin made up in 1 x PBS. Samples were then processed, embedded in paraffin and sectioned (5µm). Sections were then de-waxed, stained and mounted and haematoxylin and eosin (H and E) staining was performed. Tumours were

observed in the **B)** lungs of M4, M6, M7, M9 and M11 **C)** spleens of M7 and M11 and **D)** Pancreas in M11. Images were acquired at x 20 magnification. Scale bars = 100µm. **E)** Zoomed in images of the lungs, spleen and pancreas showing the black tumour cells observed.

Tumours were also observed in one normal (M11) and one fibrotic (M7) liver (Figure 6.7A and B) and these are clearly shown in Figure 6.7C. Tumour nodules were evident throughout the normal liver tissue and two large tumour nodules were observed in the fibrotic liver (Figure 6.7A).

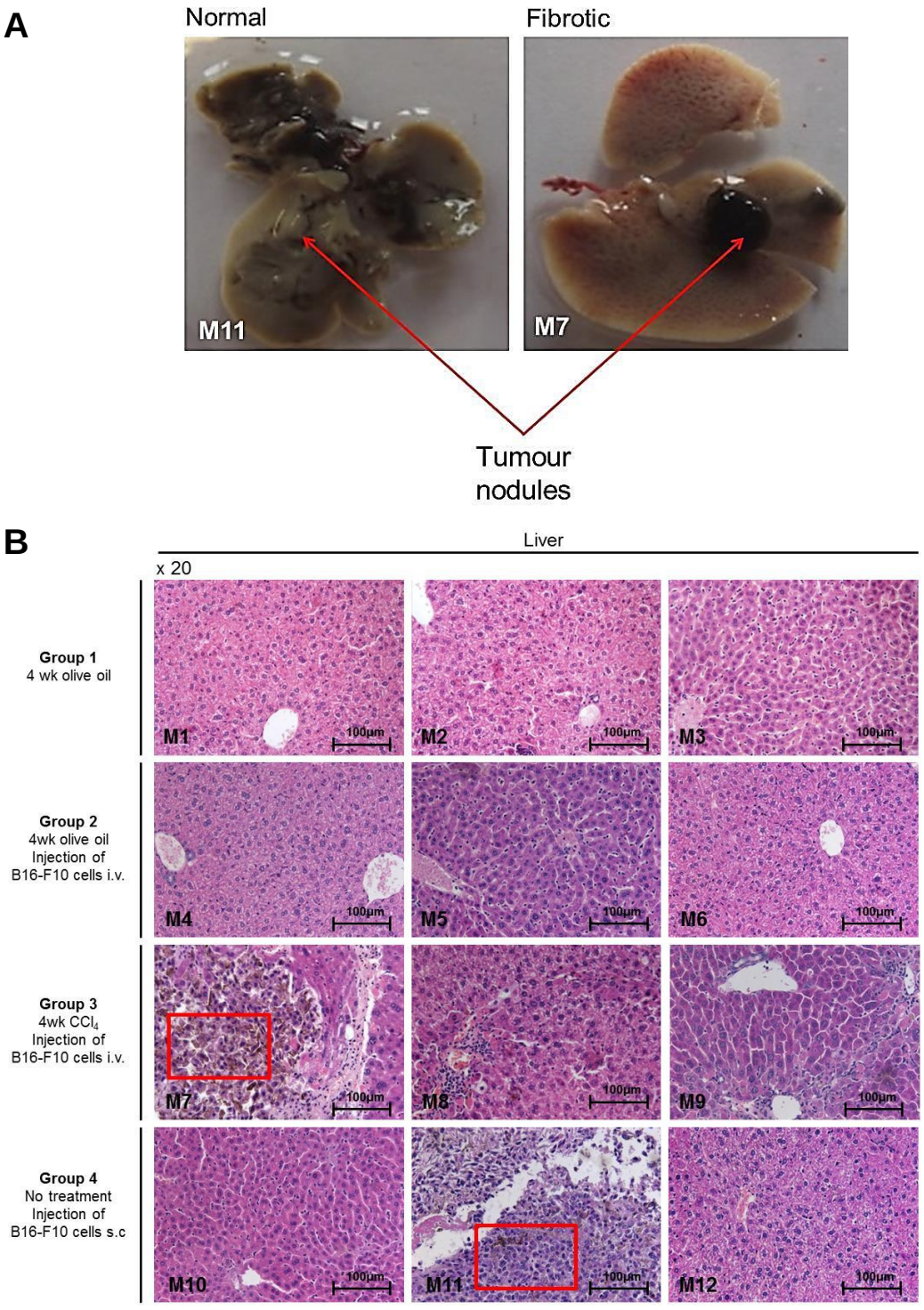

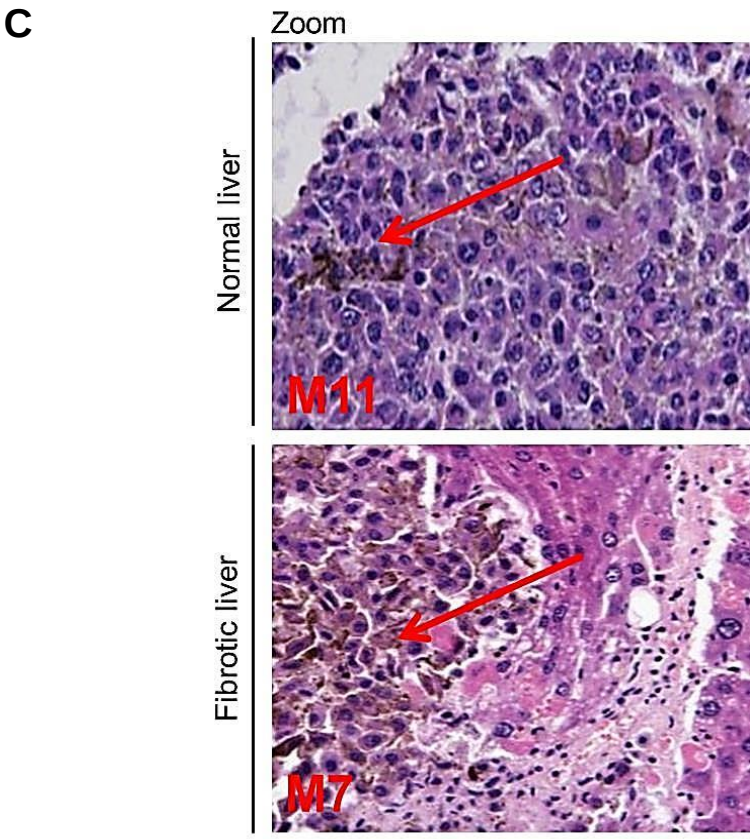

Figure 6.7: Tumour cells observed in the normal and fibrotic liver in the B16 mouse model.
A) Photographs showing tumours observed in the normal (M11) and fibrotic (M7) liver. **B)** The organs were harvested and fixed for 24 hours in 10% formalin made up in 1 x PBS. Samples were then processed, embedded in paraffin and sectioned (5µm). Sections were then de-waxed, stained and mounted and Haematoxylin and Eosin (H and E) staining was performed. H and E images were acquired at x 20 magnification. Scale bars = 100µm. **C)** Zoomed in images of the normal and fibrotic liver showing the black tumour cells observed. Staining is typical of three separate experiments.

Animals in Group 4 were injected with B16-F10 cells s.c. and as mentioned previously, this route of injection should initiate skin tumours, however, results showed that tumour cells were only observed in the skin of one animal (M10) (Figure 6.8A and B).

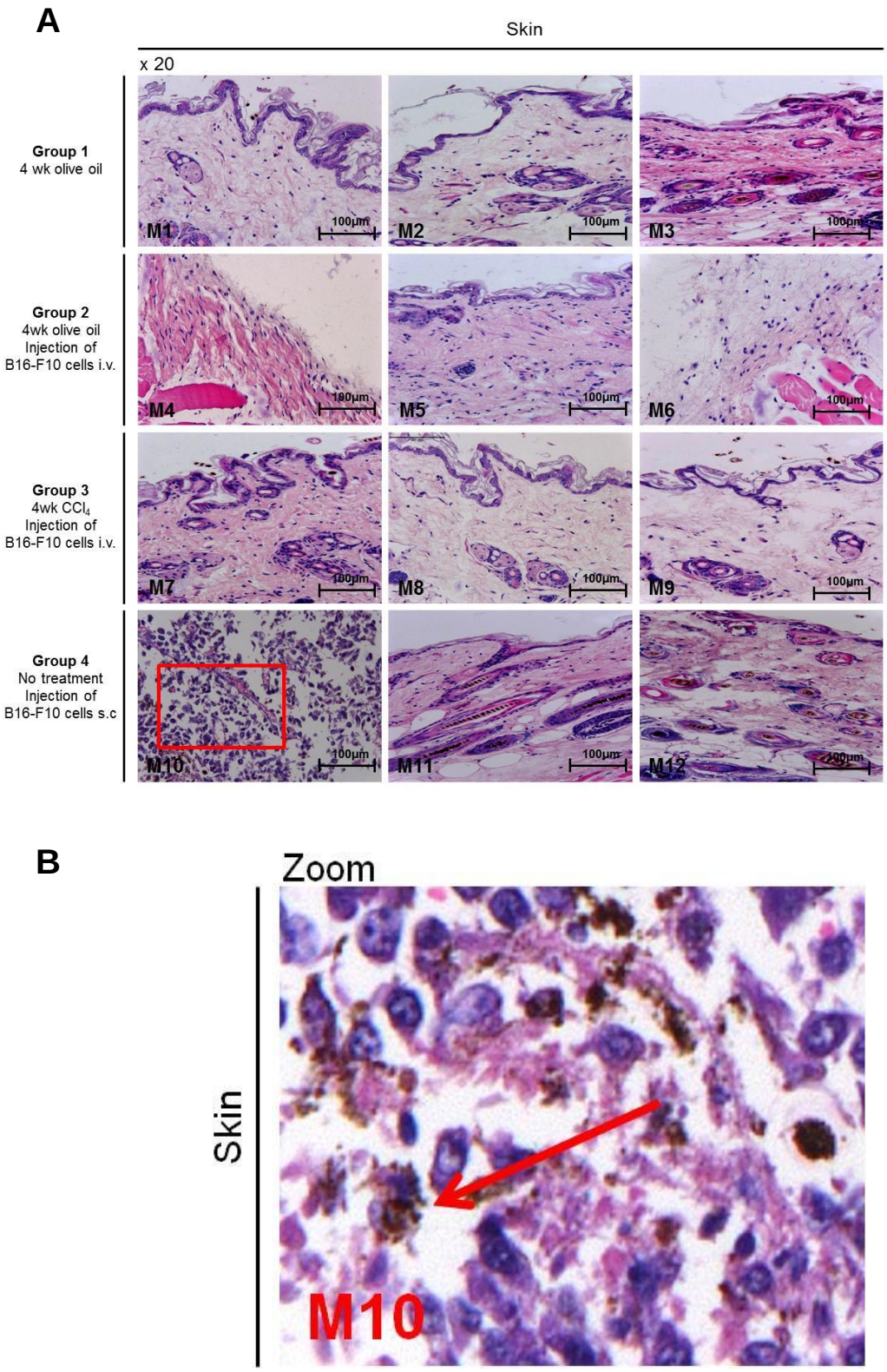

Figure 6.8: Tumours engrafted into the skin of one mouse in the B16-F10 model.
C57BL/6 mice from the B16-F10 study were culled and the skin was harvested and fixed for 24 hours in 10% formalin made up in 1 x PBS. Samples were then processed, embedded in paraffin and sectioned (5µm). Sections were then de-waxed, stained, mounted and stained with Haematoxylin and Eosin (H and E), Tumours were not observed in the skin.

In the brain, heart and kidney results demonstrated that tumours in these organs were not present in any of the animals (Figure 6.9 A-C)

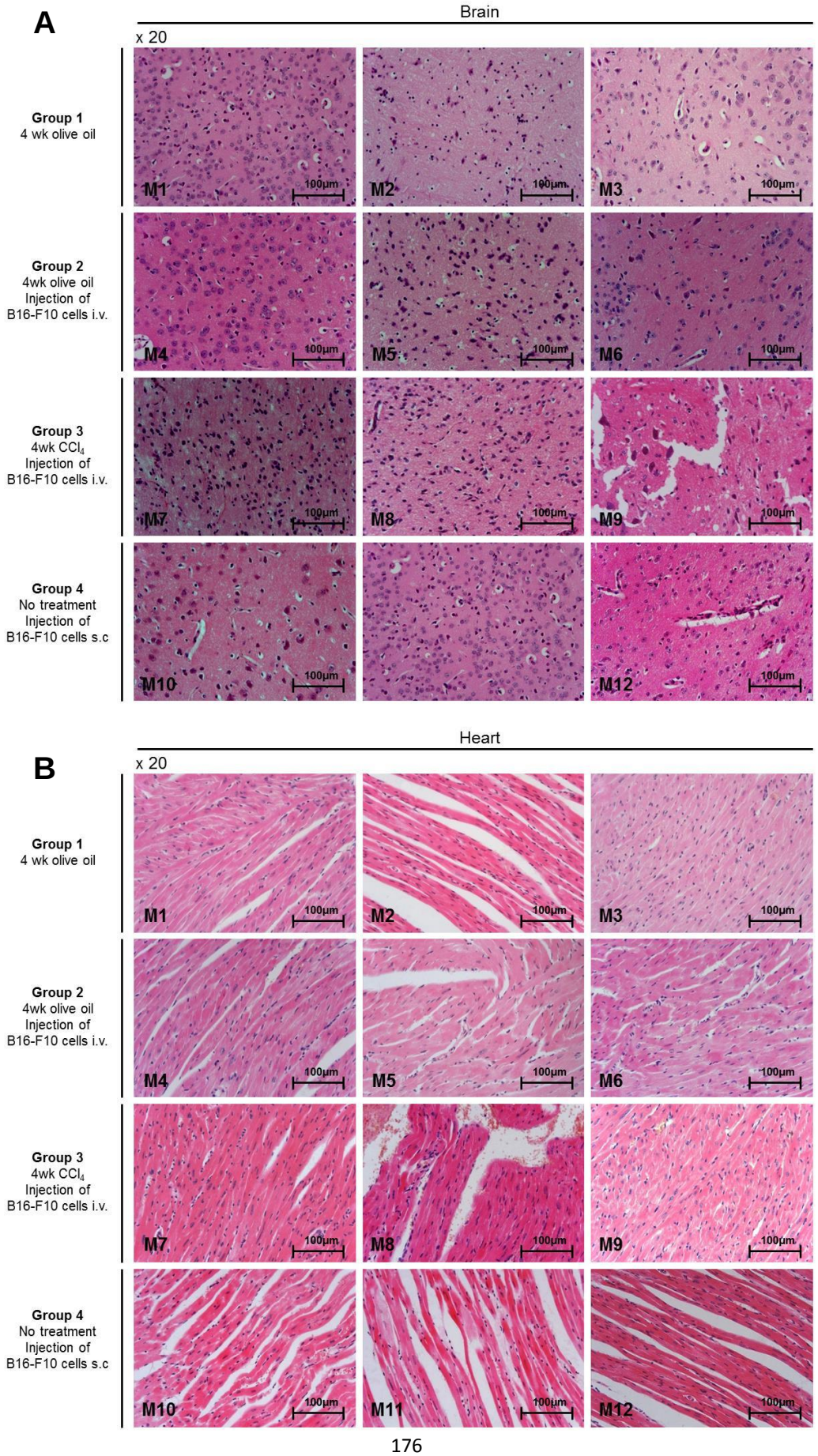

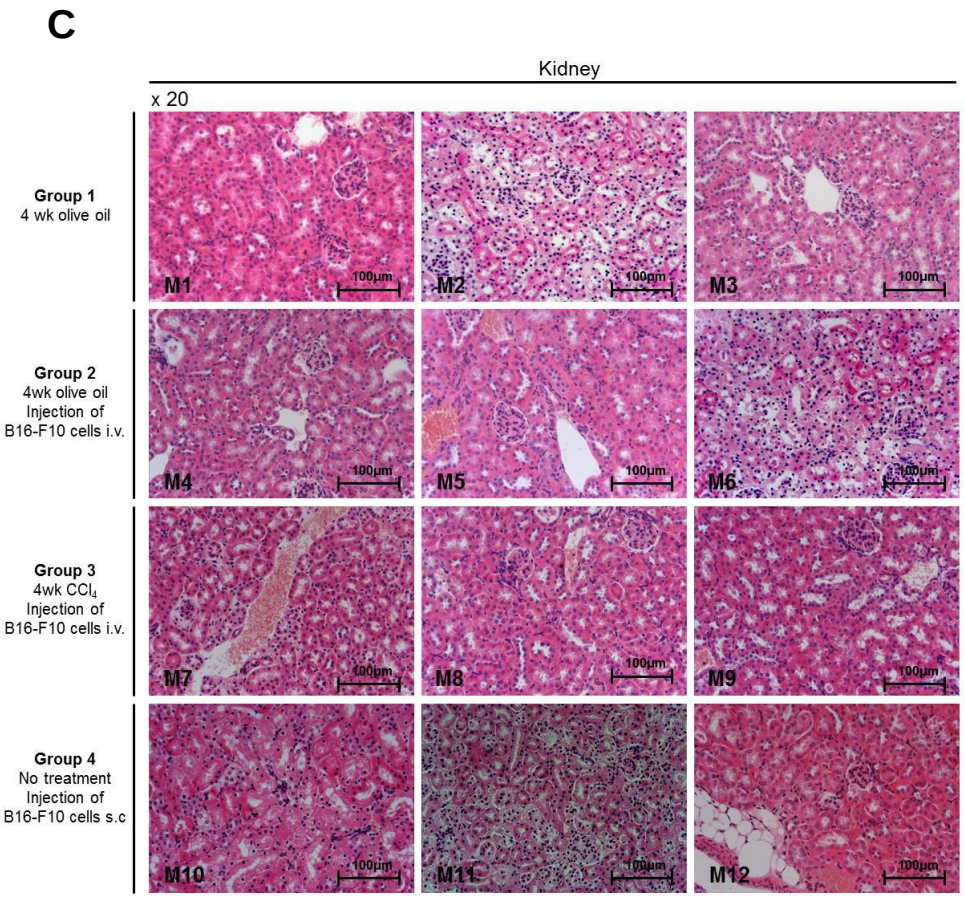

Figure 6.9: Tumours do not engraft in the brain, heart or kidney the normal and fibrotic liver of the B16-F10 mice.
C57BL/6 mice from the B16-F10 study were culled and the organs were harvested and fixed for 24 hours in 10% formalin made up in 1 x PBS. Samples were then processed, embedded in paraffin and sectioned (5µm). Sections were then de-waxed, stained and mounted. Haematoxylin and Eosin (H and E) staining of the A) Brain, B) Heart and C) Kidney. Tumours were not observed in these organs

A summary of the results of the tumours observed in each of the animals is given in Table 6.1.

	Mouse	Brain	Heart	Lungs	Liver	Kidney	Spleen	Pancreas	Skin
Group 1	1	–	–	–	–	–	–	–	–
4wk olive oil	2	–	–	–	–	–	–	–	–
	3	–	–	–	–	–	–	–	–
Group 2	4	–	–	Yes	–	–	–	–	–
4wk olive oil	5	–	–	–	–	–	–	–	–
Injection of B16-F10 cells i.v	6	–	–	Yes	–	–	–	–	–
Group 3	7	–	–	Yes	Yes	–	Yes	–	–
4wk CCl_4	8	–	–	–	–	–	–	–	–
Injection of B16-F10 cells i.v	9	–	–	Yes	–	–	–	–	–
Group 4	10	–	–	–	–	–	–	–	Yes
No treatment	11	–	–	Yes	Yes	–	Yes	Yes	–
Injection of B16-F10 cells s.c	12	–	–	–	–	–	–	–	–

Table 6.1: Summary of the tumours observed in the B16-F10 mouse model for melanoma.

Serial sections of the liver from an animal (M7) in Group 3 treated with CCl_4 and injected with B16-F10 cells were stained with H and E, α-SMA and vimentin. As shown in Figure 6.10 a band of myofibroblasts surrounding the tumour cell was observed.

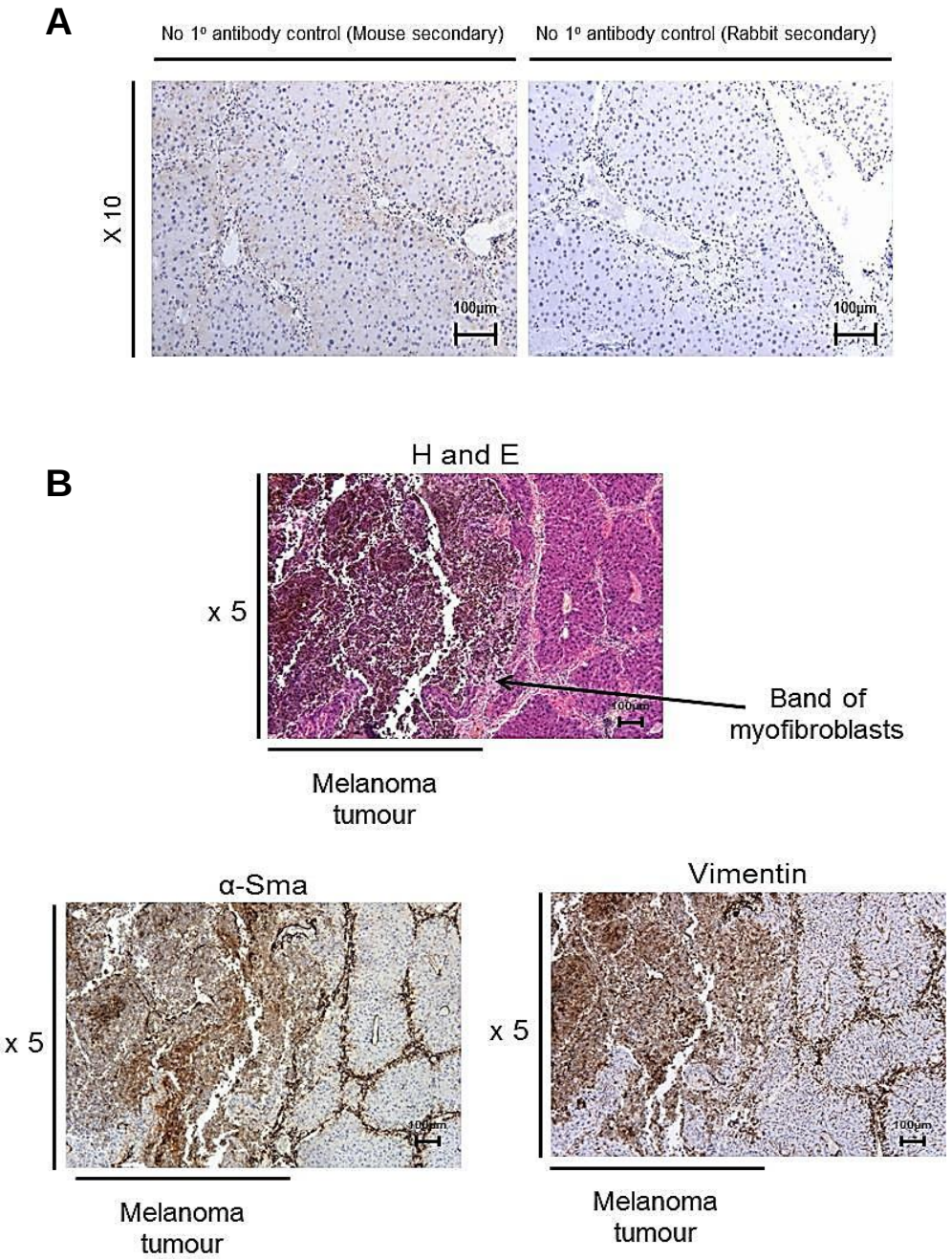

Figure 6.10: Myofibroblasts surrounding the B16-F10 melanoma tumour.
C57BL/6 mice from the B16-F10 study were culled and livers were harvested and fixed for 24 hours in 10% formalin made up in 1 x PBS. Samples were then processed, embedded in paraffin and sectioned (5µm) and de-waxed and stained **A)** No primary antibody controls were included and were stained with the secondary anti-mouse IgG antibody alone. **B)** Sections were stained with H and E or antibodies to either α-SMA or Vimentin as previously outlined in section 2.10. Specific dilutions are given in Table 2.4. As indicated by the arrow a band of myofibroblasts was observed surrounding the melanoma tumour cells. Representative images were acquired at x 5 magnification. Scale bars = 100µm.

Since B16-F10 cells express CXCL12 (section 3.2.1), to determine if this protein could be detected in the samples injected with these cells Western blotting was performed and the house-keeping protein ß-actin was used as a loading control. The results demonstrated that CXCL12 was not observed, however, as shown previously in mouse liver tissue (section 3.2.1) a band of greater intensity was observed in all of the samples (M1-M12) at ~62 kDa (Figure 6.11).

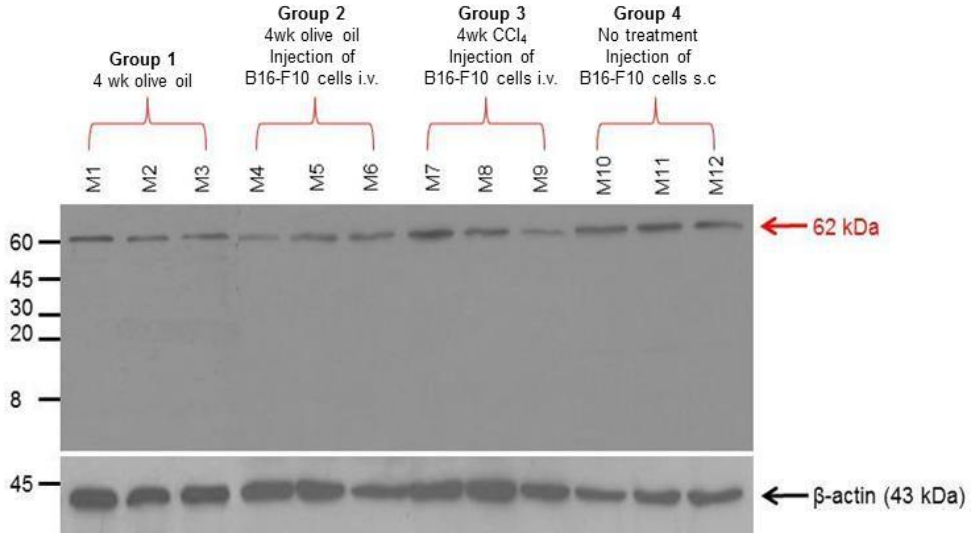

Figure 6.11: CXCL12 expression is not observed in the mice from the B16-F10 melanoma model.
Representative Western blot for the expression of CXCL12 in the livers of the B16-F10 melanoma model mice. Whole liver tissue was homogenised followed by sonication and prepared for protein analysis by Western blot. 20µg of protein was loaded per lane and β-actin was used as a loading control. M = Mouse liver.

6.2.3: Development of a hepatic stellate specific CXCL12 knockout mouse model.

A conditional knockout mouse using the Cre-loxP system (as described in section 2.1.3) in which CXCL12 is knocked out specifically in stellate cells (Gift from Professor Nagasawa, Kyoto University, Japan) was examined. All the mice used were cre+/- and flox+/+ and the crosses were female cre+/+, flox+/+ with males cre -/-,flox+/+. In order to separate the wild-type (WT) from the knockout (KO) mice genotyping was performed (Figure 6.12A) and the results demonstrated that cre was present in KO mice.

Conditioned media (both serum free and 10% FCS) was collected at 24, 48 and 72 hours from the stellate cells isolated from both the WT and the KO mice and an ELISA was performed. However, the results showed that secretion levels of CXCL12 were comparable between both groups in both serum free and 10% FCS media conditions (Figure 6.12B). Therefore the stellate cell isolation was repeated and RNA was extracted and qRT-PCR was performed immediately (without culturing the cells) however, there was no significant difference of CXCL12 expression between the WT and KO mice (Figure 6.12C). The isolation was repeated by Schwabe's group at Columbia University by using cell markers of stellate cells to obtain a purer population of cells, however similar results were observed (data not shown). Thus, unfortunately the results demonstrated that the CXCL12 gene was still functioning in the stellate cells.

A

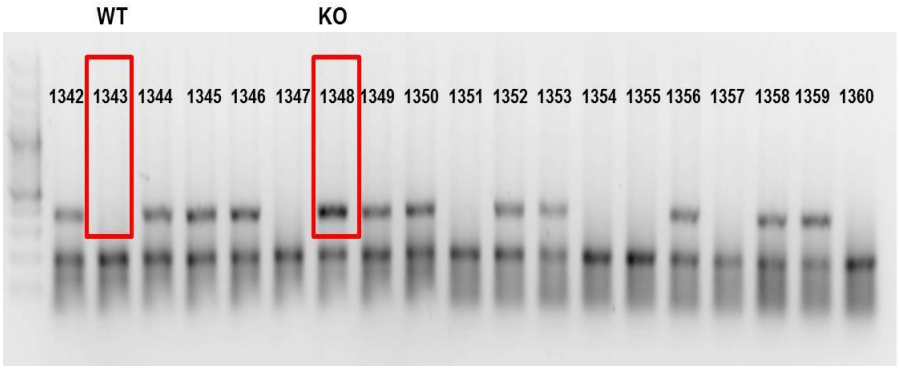

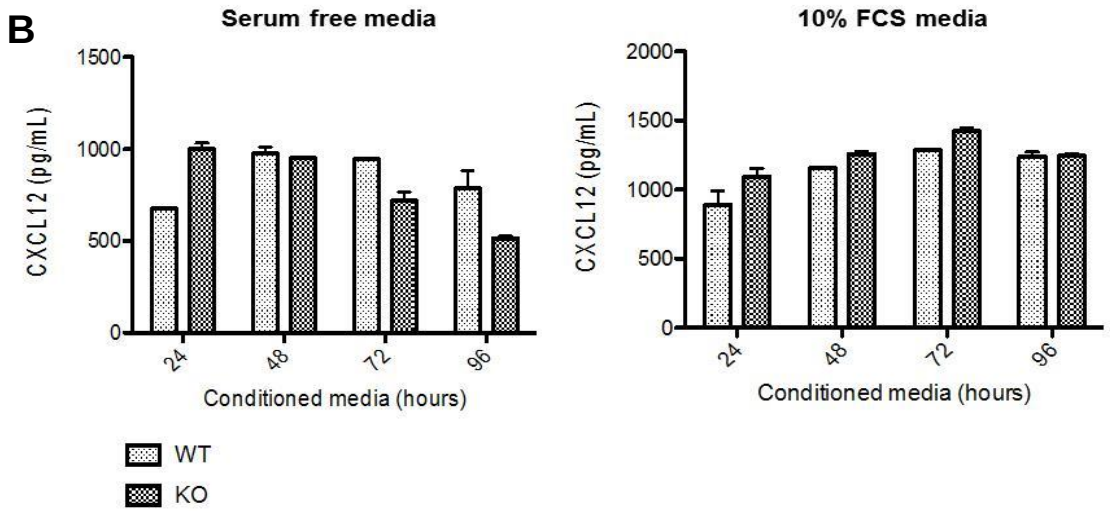

C

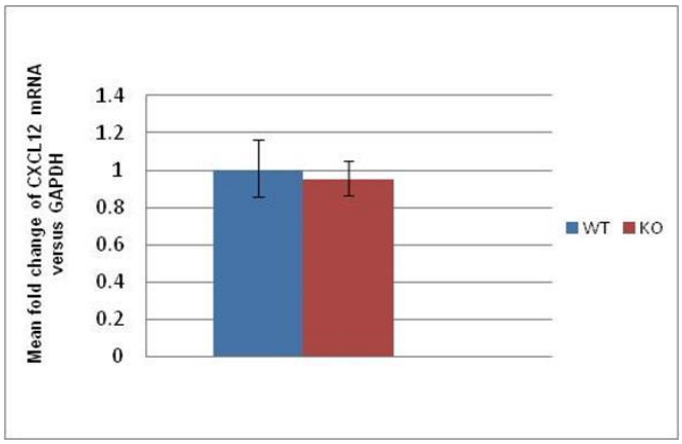

Figure 6.12: Development of a CXCL12 hepatic stellate cell knockout model.
A) Genotyping was performed on DNA isolated from the CXCL12 mice. PCR analysis was carried out for the presence of the transgene. Primer sequences and PCR conditions are detailed in table 2.7.1. PCR products were electrophoresed on a 2% agarose gel with ethidium bromide. **B)** ELISA was performed on conditioned media collected from both WT and KO stellate cells at 24, 48, and 72 hours but no significant differences between the two groups was observed. Bars are the mean +SD. **C)** qRT-PCR analysis for the expression of CXCl12-α was performed on the stellate cells isolated from both WT and KO mice, however no changes were seen in CXCL12 mRNA expression between the two groups. Bars are the mean +/-SD.

6.3: Chapter Discussion

The results from this study demonstrated that in the human model of melanoma metastasis, A375^{red} cells were only observed in the liver of one animal and not in any other organ. However, these data were based on the examination of liver sections since DSred was not visualised under the IVIS. Hence, these results may not give an accurate number of the animals that formed tumours since the whole organ was not examined and therefore another fluorescent protein would need to be used for example, a green fluorescent protein (GFP). However, another reason as to the low incidence of animals receiving tumours could be due to the genetic background of the mice. Thus, severe combined immunodeficiency (SCID) mice could be used as they are both T and B cell deficient and therefore should not reject the melanoma cells.

In the B16-F10 model of melanoma, compared to any other organ the incidence of tumours was highest in the lungs and this supports previous studies which have used this model (Overwijk and Restifo 2001, D'Alterio, Barbieri et al. 2012). The reason for pulmonary metastasis is because the lung vascular bed is the first microvasculature that the tumor cells pass through, hence, it is more difficult for the cells to pass on to other organs. In the s.c injected mice, skin tumours were only observed in one animal. The reason for not observing tumours in the other two animals is likely to be due to the injection technique. A ‘bleb’ under the skin may not have been achieved and it has been reported that this can result in delayed tumour growth or no growth at all (Overwijk and Restifo 2001). On examining the livers, tumours were observed in one normal and one fibrotic liver. Additionally, in the fibrotic liver a band of myofibroblasts was observed surrounding the tumour nodules which suggests that these cells may secrete a factor that attracts the tumour cells. Since the B16-F10 cells express CXCR4 and the myofibroblasts secrete CXCL12 this could be one possible mechanism, however this would need to be investigated much further.

As mentioned previously, many clinical studies have shown that hepatic metastasis is less common in cirrhotic livers compared to non-cirrhotic livers (Uetsuji, Yamamura et al. 1992, Vanbockrijck and Kloppel 1992, Seymour and Charnley 1999, Gervaz, Pak-art et al. 2003, Pereira-Lima, Lichtenfels et al. 2003),

however, in melanoma, studies have shown the opposite (Qi, Qiu et al. 2004). Although the B16 study in this present chapter was too small to determine if fibrosis increases melanoma metastasis to the liver, it does support this previous study showing that the tumour cells metastasize to the fibrotic liver (Qi, Qiu et al. 2004). A much larger study would need to be performed and in addition to determine if myofibroblasts promote melanoma migration, it would be interesting to deplete these cells. One method of doing this would be to use the C1-3 antibody developed previously by our group (Douglass, Wallace et al. 2008).

C1-3 is a human monoclonal antibody fragment which targets the extracellular domain of synaptophysin present on myofibroblasts (Elrick, Leel et al. 2005). Previous results have demonstrated that in culture, FITC (fluorescein isothiocyanate) conjugated C1-3 scAb interacts with human myofibroblasts but does affect hepatocytes (Elrick, Leel et al. 2005). In addition, when toxin tributyl tin is conjugated to C1-3, myofibroblasts are killed indicating that C1-3 is sequestered intracellularly. In a later study published by our group, it was shown that targeting gliotoxin to myofibroblasts with C1-3 reduced fibrosis *in vivo* in contrast to free gliotoxin alone (Douglass, Wallace et al. 2008). Furthermore, the C1-3 conjugated to gliotoxin did not affect the number of monocytes or macrophages and also it did not cross the blood brain barrier (Douglass, Wallace et al. 2008). As C1-3 specifically depletes myofibroblasts another application for this antibody would be the reduction of CXCL12 levels in the liver. Therefore, it would be interesting to inject the melanoma cells into this model and also other models of fibrosis to determine the specific cells that are involved in promoting migration in *in vivo*. Additionally, as well as injecting i.v. intrasplenic injections should be performed as this has been shown to induce metastasis in other cancers effectively (Vidal-Vanaclocha, Alonso-Varona et al. 1990).

Finally, the results here demonstrate the difficulty of generating a specific CXCL12 knock out model and this would need to be repeated using another promoter. If this were to be successful, injection of melanoma cells into this model would help to elucidate the specific role of the CXCR4-CXCL12 chemokine axis in melanoma metastasis to the liver.

7.0 Final Discussion and Future Prospects

7.0 Final Discussion and Future prospects

Malignant melanoma represents an increasing world health problem and over the past 30 years incidence rates in the UK have quadrupled (Cancer Research UK). Although early stage disease is treatable through surgical excision alone, once metastasis occurs prognosis for these patients remains extremely poor and therefore novel treatment strategies are urgently needed.

Recently, the importance of the CXCR4-CXCL12 chemokine axis in melanoma progression has been reported. Indeed, it has been found that CXCR4 is over expressed in melanoma cells and its sole ligand CXCL12 has been found to be highly expressed in organs which are prone to metastasis such as the lungs, brain and liver (Zlotnik, Yoshie et al. 2006). Furthermore, studies have shown that by inhibiting this axis melanoma metastasis is reduced to organs such as the lungs (D'Alterio, Barbieri et al. 2012). Based on these observations this has led to the hypothesis that the CXCR4-CXCL12 chemokine axis plays an important role in directing the migration of a wide range of tumour cells expressing CXCR4 to organs that express high levels of CXCL12. Hence, this chemokine axis may represent a promising novel treatment approach for preventing melanoma metastasis.

However, the specific liver cell types involved in the migration of melanoma have not been determined and studies focusing on metastasis to the fibrotic and/or damaged liver are somewhat limited. Furthermore, there have been a number of challenges in the development of chemokine inhibitors and as yet in the context of melanoma there has been little success. Therefore the main aims of this thesis were to confirm the expression of CXCR4 and CXCL12 in melanoma cells and various liver cell types in *in vitro* and in *in vivo*. Then to examine the migration of melanoma cells towards conditioned media collected from specific liver cells and also to test the ability of the novel CXCR4 inhibitor AMD11070 to inhibit migration. Additionally, to determine the levels of CXCL12 expression in different chronic liver injury models and finally to examine whether melanoma cells migrate towards both the normal and damaged/fibrotic liver.

Supporting previous data, the studies carried out confirmed that melanoma cells express both CXCR4 and CXCL12 and furthermore that myofibroblasts and biliary epithelial cells express these proteins both *in vitro* and *in v*ivo (Terada, Yamamoto et al. 2003, Scala, Ottaiano et al. 2005, Hong 2009). The secretion levels of CXCL12 by myofibroblasts compared to the biliary epithelial cells (both human and mouse) were greater, however, this may have been due to differences in cell number. Nonetheless, the main aim was to determine if the protein was secreted or not rather than quantifying the exact amount. However, in light of this data it would be interesting to specifically knockdown the expression of CXCL12 in the biliary epithelial cells in an *in vivo* setting in order to determine if melanoma metastasis was inhibited.

Inconsistent with a previous study which showed that CXCL12 and CXCR4 at the protein level is expressed (Hong 2009), on examination in these studies, bands of higher molecular weights for both proteins were observed. As discussed previously, the antibodies used may be detecting non-specific proteins; alternatively, the proteins may be post-translationally modified. Based on these findings, additional studies to confirm this are warranted, for example, performing mass spectrometry.

Migration assays demonstrated that murine melanoma cells migrated towards conditioned media collected from both biliary epithelial cells and myofibroblasts *in vitro*. However, as inhibitors were not used in these studies it was not possible to determine if it was CXCL12 or another factor/s that promoted the migration. Thus, additional studies would need to be performed by adding inhibitors and also by screening the media, for example, performing a cytokine array. However, in the migration assays using human melanoma cells it was demonstrated that the CXCR4-CXCL12 axis was involved in the migration of the cells and furthermore AMD11070 inhibited this (O'Boyle, Swidenbank et al. 2013). Interestingly, melanoma cell migration was increased by the over expression of BRAF (O'Boyle, Swidenbank et al. 2013) but importantly the ability of AMD11070 to inhibit migration was not affected by this. This has important implications as it would mean that it could be used in patients with both WT BRAF and also those harbouring the BRAF mutation.

Additionally, recent studies have shown that up regulation of the VEGF receptor is observed in a range of tumours expressing CXCR4 (Franco, Botti et al. 2010) and therefore it may also be of benefit to combine VEGF inhibitors which are currently being developed with AMD11070 to determine if efficacy is improved. Furthermore, since CXCR4 has found to be over expressed in a wide range of cancers including colorectal, prostate and ovarian this compound may also have benefits in a wide range of cancer settings. However, in order to develop the use of this inhibitor, translational studies would need to be performed to determine its effectiveness of inhibition *in vivo* and to evaluate any detrimental side effects.

In accordance with previous studies, showing that damage to the liver increases chemokine production (Hong 2009), mRNA CXCL12 expression levels in chronic liver injury models increased. In order to study melanoma metastasis to the liver it will be important to perform these studies in liver models of both centrilobular and periportal damage. Since liver fibrosis aetiology and pathology can vary considerably amongst patients (Wallace, Burt et al. 2008). Hence, the injection of melanoma cells into various models of fibrosis with differing levels of damage would shed light on whether the damaged liver promotes migration of melanoma or serves as a protective mechanism. Furthermore, it would be interesting to examine other chemokines and cytokines that are up-regulated in these models of liver injury.

In the *in vivo* studies, the results showed that human melanoma cells migrated to the liver in the nude mouse, however, this study would need to be repeated in SCID mice in order to increase the incidence numbers. In the B16 model of melanoma, murine melanoma cells migrated to both the normal and fibrotic liver. However, future larger animal studies and knockout animals with statistical analyses would be essential in establishing which cells *in vivo* are responsible for the migration of the melanoma cells.

Overall this study reinforces the importance of the chemokine axis in the role of melanoma metastasis to the liver more specifically the effect of myofibroblasts and biliary epithelial cells. Moreover, the AMD11070 data points towards the current approach of developing personalised therapies for specific groups of patients to improve clinical outcome for melanoma patients. However,

antagonizing CXCR4 alone may not be as effective *in vivo* due to the involvement of other chemokine axes in melanoma (Payne and Cornelius 2002). For example, in uveal melanoma, both CXCR4 and CCR7 showed to promote the migration of uveal melanoma cells towards the liver (Li, Alizadeh et al. 2008). In a recent study, it was shown that although CXCR7 did not directly promote the migration of melanoma cells it did regulate trans-endothelial migration of cancer cells (Zabel, Lewen et al. 2011). In comparison to melanocytes, melanoma cells have shown to express increased levels of CCR7 and CCR10 mRNA (Muller, Homey et al. 2001). In another study, the CCR9-CCL25 chemokine axis has been shown to be involved in the migration of melanoma cells to the small intestine (Amersi, Terando et al. 2008). The CCL27-CCR10 chemokine axis was shown to be associated with the metastasis of melanoma (Monteagudo, Ramos et al. 2012).

Thus, inhibiting CXCR4 alone may not be effective due to other chemokine expression. One of the reasons for this is that a single molecule usually does not result in complete inhibition due to chemokine redundancy in the system (Schall and Proudfoot 2011). Indeed, it has been reported that for successful inhibition at least 90% of the receptor needs to be blocked, however, many inhibitors fail to achieve this (Schall and Proudfoot 2011). Additionally, due to the importance of chemokine axes in other physiological processes, many inhibitors have shown unfavourable side effects. For example, studies carried out by the Bansal laboratory have demonstrated that AMD3100 induces liver fibrosis (Saiman 2012). It has also been argued that the reason as to why inhibitors have not been successful is also a result of inappropriate target selection and ineffective dosing(Schall and Proudfoot 2011). Furthermore, it has been suggested that since malignant cells have the ability to evolve and survive in many types of niches inhibition may promote the outgrowth of malignant cells that secrete a different array of chemokines (Balkwill 2012). Hence, targeting chemokine receptors may just simply re-direct the cancer cells to other locations in the body (Balkwill 2012). Thus, a greater insight into the chemokine system should lead to an increased understanding of melanoma and other cancers and therefore new treatment approaches.

8.0 References

Adjei, A. A., R. B. Cohen, W. Franklin, C. Morris, D. Wilson, J. R. Molina, L. J. Hanson, L. Gore, L. Chow, S. Leong, L. Maloney, G. Gordon, H. Simmons, A. Marlow, K. Litwiler, S. Brown, G. Poch, K. Kane, J. Haney and S. G. Eckhardt (2008). "Phase I pharmacokinetic and pharmacodynamic study of the oral, small-molecule mitogen-activated protein kinase kinase 1/2 inhibitor AZD6244 (ARRY-142886) in patients with advanced cancers." J Clin Oncol **26**(13): 2139-2146.

Affo, S. and R. Bataller (2011). "RANTES antagonism: a promising approach to treat chronic liver diseases." J Hepatol **55**(4): 936-938.

Ajuebor, M. N., J. A. Carey and M. G. Swain (2006). "CCR5 in T cell-mediated liver diseases: what's going on?" J Immunol **177**(4): 2039-2045.

Ajuebor, M. N., Q. Chen, R. M. Strieter, P. A. Adegboyega and T. Y. Aw (2010). "V(alpha)14iNKT cells promote liver pathology during adenovirus infection by inducing CCL5 production: implications for gene therapy." J Virol **84**(17): 8520-8529.

Ajuebor, M. N., C. M. Hogaboam, T. Le, A. E. Proudfoot and M. G. Swain (2004). "CCL3/MIP-1alpha is pro-inflammatory in murine T cell-mediated hepatitis by recruiting CCR1-expressing CD4(+) T cells to the liver." Eur J Immunol **34**(10): 2907-2918.

Ajuebor, M. N., C. M. Hogaboam, T. Le and M. G. Swain (2003). "C-C chemokine ligand 2/monocyte chemoattractant protein-1 directly inhibits NKT cell IL-4 production and is hepatoprotective in T cell-mediated hepatitis in the mouse." J Immunol **170**(10): 5252-5259.

Ajuebor, M. N., Z. Wondimu, C. M. Hogaboam, T. Le, A. E. Proudfoot and M. G. Swain (2007). "CCR5 deficiency drives enhanced natural killer cell trafficking to and activation within the liver in murine T cell-mediated hepatitis." Am J Pathol **170**(6): 1975-1988.

Ali, S. and G. Lazennec (2007). "Chemokines: novel targets for breast cancer metastasis." Cancer Metastasis Rev **26**(3-4): 401-420.

Amaravadi, R. K., L. M. Schuchter, D. F. McDermott, A. Kramer, L. Giles, K. Gramlich, M. Carberry, A. B. Troxel, R. Letrero, K. L. Nathanson, M. B. Atkins, P. J. O'Dwyer and K. T. Flaherty (2009). "Phase II Trial of Temozolomide and Sorafenib in Advanced Melanoma Patients with or without Brain Metastases." Clin Cancer Res **15**(24): 7711-7718.

Amersi, F. F., A. M. Terando, Y. Goto, R. A. Scolyer, J. F. Thompson, A. N. Tran, M. B. Faries, D. L. Morton and D. S. Hoon (2008). "Activation of CCR9/CCL25 in cutaneous melanoma mediates preferential metastasis to the small intestine." Clin Cancer Res **14**(3): 638-645.

Anthony, P. P., K. G. Ishak, N. C. Nayak, H. E. Poulsen, P. J. Scheuer and L. H. Sobin (1977). "The morphology of cirrhosis: definition, nomenclature, and classification." Bull World Health Organ **55**(4): 521-540.

Aoyama, T., S. Inokuchi, D. A. Brenner and E. Seki (2010). "CX3CL1-CX3CR1 interaction prevents carbon tetrachloride-induced liver inflammation and fibrosis in mice." Hepatology **52**(4): 1390-1400.

Apolinario, A., P. L. Majano, E. Alvarez-Perez, A. Saez, C. Lozano, J. Vargas and C. Garcia-Monzon (2002). "Increased expression of T cell chemokines and their receptors in chronic hepatitis C: relationship with the histological activity of liver disease." Am J Gastroenterol **97**(11): 2861-2870.

Apte, M. V., P. S. Haber, T. L. Applegate, I. D. Norton, G. W. McCaughan, M. A. Korsten, R. C. Pirola and J. S. Wilson (1998). "Periacinar stellate shaped cells in rat pancreas: identification, isolation, and culture." Gut **43**(1): 128-133.

Atallah, E. and L. Flaherty (2005). "Treatment of metastatic malignant melanoma." Curr Treat Options Oncol **6**(3): 185-193.

Bacon, K., M. Baggiolini, H. Broxmeyer, R. Horuk, I. Lindley, A. Mantovani, K. Maysushima, P. Murphy, H. Nomiyama, J. Oppenheim, A. Rot, T. Schall, M. Tsang, R. Thorpe, J. Van Damme, M. Wadhwa, O. Yoshie, A. Zlotnik, K. Zoon and I. W. S. o. C. Nomenclature (2002). "Chemokine/chemokine receptor nomenclature." J Interferon Cytokine Res **22**(10): 1067-1068.

Baggiolini, M., B. Dewald and B. Moser (1997). "Human chemokines: an update." Annu Rev Immunol **15**: 675-705.

Balabanian, K., B. Lagane, S. Infantino, K. Y. Chow, J. Harriague, B. Moepps, F. Arenzana-Seisdedos, M. Thelen and F. Bachelerie (2005). "The chemokine SDF-1/CXCL12 binds to and signals through the orphan receptor RDC1 in T lymphocytes." J Biol Chem **280**(42): 35760-35766.

Balch, C. M., J. E. Gershenwald, S. J. Soong, J. F. Thompson, M. B. Atkins, D. R. Byrd, A. C. Buzaid, A. J. Cochran, D. G. Coit, S. Ding, A. M. Eggermont, K. T. Flaherty, P. A. Gimotty, J. M. Kirkwood, K. M. McMasters, M. C. Mihm, Jr., D. L. Morton, M. I. Ross, A. J. Sober and V. K. Sondak (2009). "Final version of 2009 AJCC melanoma staging and classification." J Clin Oncol **27**(36): 6199-6206.

Balkwill, F. (2004). "Cancer and the chemokine network." Nat Rev Cancer **4**(7): 540-550.

Balkwill, F. R. (2012). "The chemokine system and cancer." J Pathol **226**(2): 148-157.

Ballardini, G., Groff, P, Badiali de Giorgi, L. et al. (1988). "Desmin and actin in the identification of Ito cells and in monitoring their evolution to myofibroblasts in experimental liver fibrosis." Cell Pathol Incl Mol PAthol **56**: 45-49.

Banerji, U., D. R. Camidge, H. M. Verheul, R. Agarwal, D. Sarker, S. B. Kaye, I. M. Desar, J. N. Timmer-Bonte, S. G. Eckhardt, K. D. Lewis, K. H. Brown, M. V. Cantarini, C. Morris, S. M. George, P. D. Smith and C. M. van Herpen (2010). "The first-in-human study of the hydrogen sulfate (Hyd-sulfate) capsule of the MEK1/2 inhibitor AZD6244 (ARRY-142886): a phase I open-label multicenter trial in patients with advanced cancer." Clin Cancer Res **16**(5): 1613-1623.

Barbero, S., R. Bonavia, A. Bajetto, C. Porcile, P. Pirani, J. L. Ravetti, G. L. Zona, R. Spaziante, T. Florio and G. Schettini (2003). "Stromal cell-derived factor 1alpha stimulates human glioblastoma cell growth through the activation of both extracellular signal-regulated kinases 1/2 and Akt." Cancer Res **63**(8): 1969-1974.

Barra, R. and J. C. Hall (1977). "Liver regeneration in normal and alloxan-induced diabetic rats." J Exp Zool **201**(1): 93-99.

Bartolome, R. A., S. Ferreiro, M. E. Miquilena-Colina, L. Martinez-Prats, M. L. Soto-Montenegro, D. Garcia-Bernal, J. J. Vaquero, R. Agami, R. Delgado, M. Desco, P. Sanchez-Mateos and J. Teixido (2009). "The chemokine receptor CXCR4 and the metalloproteinase MT1-MMP are mutually required during melanoma metastasis to lungs." Am J Pathol **174**(2): 602-612.

Bataller, R., Brenner, D.A. (2001). "Hepatic stellare cells as a target for the treatment of liver fibrosis." Semin Liver Dis **21**: 437-451.

Bataller, R., Schwabe, R, F., Choi, Y,H et al. (2003). "NADPH oxidase signal transduces angiotensin II in hepatic stellate cells and is critical in hepatic fibrosis." J. Clin. Invest. **112**: 1383-1394.

Belperio, J. A., M. P. Keane, D. A. Arenberg, C. L. Addison, J. E. Ehlert, M. D. Burdick and R. M. Strieter (2000). "CXC chemokines in angiogenesis." J Leukoc Biol **68**(1): 1-8.

Bieche, I., C. Chavey, C. Andrieu, M. Busson, S. Vacher, L. Le Corre, J. M. Guinebretiere, S. Burlinchon, R. Lidereau and G. Lazennec (2007). "CXC chemokines located in the 4q21 region are up-regulated in breast cancer." Endocr Relat Cancer **14**(4): 1039-1052.

Boissy, R. E. (2003). "Melanosome transfer to and translocation in the keratinocyte." Exp Dermatol **12 Suppl 2**: 5-12.

Bollag, G., P. Hirth, J. Tsai, J. Zhang, P. N. Ibrahim, H. Cho, W. Spevak, C. Zhang, Y. Zhang, G. Habets, E. A. Burton, B. Wong, G. Tsang, B. L. West, B. Powell, R. Shellooe, A. Marimuthu, H. Nguyen, K. Y. Zhang, D. R. Artis, J. Schlessinger, F. Su, B. Higgins, R. Iyer, K. D'Andrea, A. Koehler, M. Stumm, P. S. Lin, R. J. Lee, J. Grippo, I. Puzanov, K. B. Kim, A. Ribas, G. A. McArthur, J. A. Sosman, P. B. Chapman, K. T. Flaherty, X. Xu, K. L. Nathanson and K. Nolop (2010). "Clinical efficacy of a RAF inhibitor needs broad target blockade in BRAF-mutant melanoma." Nature **467**(7315): 596-599.

Breslow, A. (1970). "Thickness, cross-sectional areas and depth of invasion in the prognosis of cutaneous melanoma." Ann Surg **172**(5): 902-908.

Broelsch, C. E., J. C. Emond, P. F. Whitington, J. R. Thistlethwaite, A. L. Baker and J. L. Lichtor (1990). "Application of reduced-size liver transplants as split grafts, auxiliary orthotopic grafts, and living related segmental transplants." Ann Surg **212**(3): 368-375; discussion 375-367.

Burger, M., A. Glodek, T. Hartmann, A. Schmitt-Graff, L. E. Silberstein, N. Fujii, T. J. Kipps and J. A. Burger (2003). "Functional expression of CXCR4 (CD184) on small-cell lung cancer cells mediates migration, integrin activation, and adhesion to stromal cells." Oncogene **22**(50): 8093-8101.

Burns, J. M., B. C. Summers, Y. Wang, A. Melikian, R. Berahovich, Z. Miao, M. E. Penfold, M. J. Sunshine, D. R. Littman, C. J. Kuo, K. Wei, B. E. McMaster, K. Wright, M. C. Howard and T. J. Schall (2006). "A novel chemokine receptor for SDF-1 and I-TAC involved in cell survival, cell adhesion, and tumor development." J Exp Med **203**(9): 2201-2213.

Burr, A. W., M. R. Carpenter, J. E. Hines, W. J. Gullick and A. D. Burt (1993). "Intrahepatic distribution of transforming growth factor-alpha (TGF alpha) during liver regeneration following carbon tetrachloride-induced necrosis." J Pathol **170**(1): 95-100.

Burt, A., D., Robertson, J,H., Hair, J. et al. (1986). "Desmin-containing stellate cells in rat liver; distribution in normal animals and response to experimental acute liver injury " J Path **150**: 29-35.

Caruz, A., M. Samsom, J. M. Alonso, J. Alcami, F. Baleux, J. L. Virelizier, M. Parmentier and F. Arenzana-Seisdedos (1998). "Genomic organization and promoter characterization of human CXCR4 gene." FEBS Lett **426**(2): 271-278.

Casini, A., Ceni, E., Salzano, R. et al. "Neutrophil-derived superoxide anion induces lipid peroxidation and stimulates collagen synthesis in human hepatic stellate cells: role of nitric oxide" Hepatology **25**: 361-367.

Cassiman, D., Van Pelt, J., De Vos, R.et al. (1999). "Synaptophysin: a novel marker for human and rat hepatic stellate cells." Am J Pathol **155**: 1831-1839.

Chambers, A. F., A. C. Groom and I. C. MacDonald (2002). "Dissemination and growth of cancer cells in metastatic sites." Nat Rev Cancer **2**(8): 563-572.

Chapman, P. B., A. Hauschild, C. Robert, J. B. Haanen, P. Ascierto, J. Larkin, R. Dummer, C. Garbe, A. Testori, M. Maio, D. Hogg, P. Lorigan, C. Lebbe, T. Jouary, D. Schadendorf, A. Ribas, S. J. O'Day, J. A. Sosman, J. M. Kirkwood, A. M. Eggermont, B. Dreno, K. Nolop, J. Li, B. Nelson, J. Hou, R. J. Lee, K. T. Flaherty, G. A. McArthur and B.-S. Group (2011). "Improved survival with vemurafenib in melanoma with BRAF V600E mutation." N Engl J Med **364**(26): 2507-2516.

Chatzipantelis, P., A. C. Lazaris, G. Kafiri, K. Papadimitriou, T. G. Papathomas, A. Nonni and E. S. Patsouris (2006). "Cytokeratin-7, cytokeratin-19, and c-Kit: Immunoreaction during the evolution stages of primary biliary cirrhosis." Hepatol Res **36**(3): 182-187.

Chavey, C., F. Bibeau, S. Gourgou-Bourgade, S. Burlinchon, F. Boissiere, D. Laune, S. Roques and G. Lazennec (2007). "Oestrogen receptor negative breast cancers exhibit high cytokine content." Breast Cancer Res **9**(1): R15.

Chen, B., C. Tardell, B. Higgins, K. Packman, J. F. Boylan and H. Niu (2012). "BRAFV600E negatively regulates the AKT pathway in melanoma cell lines." PLoS One **7**(8): e42598.

Chiloeches, A. and R. Marais (2006). "Is BRAF the Achilles' Heel of thyroid cancer?" Clin Cancer Res **12**(6): 1661-1664.

Chu, C. Y., Y. S. Sheen, S. T. Cha, Y. F. Hu, C. T. Tan, H. C. Chiu, C. C. Chang, M. W. Chen, M. L. Kuo and S. H. Jee (2013). "Induction of chemokine receptor CXCR4 expression by transforming growth factor-beta1 in human basal cell carcinoma cells." J Dermatol Sci.

Costin, G. E. and V. J. Hearing (2007). "Human skin pigmentation: melanocytes modulate skin color in response to stress." FASEB J **21**(4): 976-994.

Coulomb-L'Hermin, A., A. Amara, C. Schiff, I. Durand-Gasselin, A. Foussat, T. Delaunay, G. Chaouat, F. Capron, N. Ledee, P. Galanaud, F. Arenzana-Seisdedos and D. Emilie (1999). "Stromal cell-derived factor 1 (SDF-1) and antenatal human B cell lymphopoiesis: expression of SDF-1 by mesothelial cells and biliary ductal plate epithelial cells." Proc Natl Acad Sci U S A **96**(15): 8585-8590.

D'Alterio, C., A. Barbieri, L. Portella, G. Palma, M. Polimeno, A. Riccio, C. Ierano, R. Franco, G. Scognamiglio, J. Bryce, A. Luciano, D. Rea, C. Arra and S. Scala (2012). "Inhibition of stromal CXCR4 impairs development of lung metastases." Cancer Immunol Immunother **61**(10): 1713-1720.

Davies, H., G. R. Bignell, C. Cox, P. Stephens, S. Edkins, S. Clegg, J. Teague, H. Woffendin, M. J. Garnett, W. Bottomley, N. Davis, E. Dicks, R. Ewing, Y. Floyd, K. Gray, S. Hall, R. Hawes, J. Hughes, V. Kosmidou, A. Menzies, C. Mould, A. Parker, C. Stevens, S. Watt, S. Hooper, R. Wilson, H. Jayatilake, B. A. Gusterson, C. Cooper, J. Shipley, D. Hargrave, K. Pritchard-Jones, N. Maitland, G. Chenevix-Trench, G. J. Riggins, D. D. Bigner, G. Palmieri, A. Cossu, A. Flanagan, A. Nicholson, J. W. Ho, S. Y. Leung, S. T. Yuen, B. L. Weber, H. F. Seigler, T. L. Darrow, H. Paterson, R. Marais, C. J. Marshall, R. Wooster, M. R. Stratton and P. A. Futreal (2002). "Mutations of the BRAF gene in human cancer." Nature **417**(6892): 949-954.

Davis, D. A., K. E. Singer, M. De La Luz Sierra, M. Narazaki, F. Yang, H. M. Fales, R. Yarchoan and G. Tosato (2005). "Identification of carboxypeptidase N as an enzyme responsible for C-terminal cleavage of stromal cell-derived factor-1alpha in the circulation." Blood **105**(12): 4561-4568.

De Fabo, E. C., F. P. Noonan, T. Fears and G. Merlino (2004). "Ultraviolet B but not ultraviolet A radiation initiates melanoma." Cancer Res **64**(18): 6372-6376.

De Falco, V., V. Guarino, E. Avilla, M. D. Castellone, P. Salerno, G. Salvatore, P. Faviana, F. Basolo, M. Santoro and R. M. Melillo (2007). "Biological role and potential therapeutic targeting of the chemokine receptor CXCR4 in undifferentiated thyroid cancer." Cancer Res **67**(24): 11821-11829.

Di Cesare, S., J. C. Marshall, B. F. Fernandes, P. Logan, E. Antecka, V. B. Filho and M. N. Burnier, Jr. (2007). "In vitro characterization and inhibition of the CXCR4/CXCL12 chemokine axis in human uveal melanoma cell lines." Cancer Cell Int **7**: 17.

Doitsidou, M., M. Reichman-Fried, J. Stebler, M. Koprunner, J. Dorries, D. Meyer, C. V. Esguerra, T. Leung and E. Raz (2002). "Guidance of primordial germ cell migration by the chemokine SDF-1." Cell **111**(5): 647-659.

Douglass, A., K. Wallace, R. Parr, J. Park, E. Durward, I. Broadbent, C. Barelle, A. J. Porter and M. C. Wright (2008). "Antibody-targeted myofibroblast apoptosis reduces fibrosis during sustained liver injury." J Hepatol **49**(1): 88-98.

Douglass, A., Wallace, K., Parr, R. et al. (2008). "Antibody-targeted myofibroblast apoptosis reduces fibrosis during sustained liver injury." Hepatology **49**: 88-98.

Eisen, T., T. Ahmad, K. T. Flaherty, M. Gore, S. Kaye, R. Marais, I. Gibbens, S. Hackett, M. James, L. M. Schuchter, K. L. Nathanson, C. Xia, R. Simantov, B. Schwartz, M. Poulin-Costello, P. J. O'Dwyer and M. J. Ratain (2006). "Sorafenib in advanced melanoma: a Phase II randomised discontinuation trial analysis." Br J Cancer **95**(5): 581-586.

Elrick, L. J., V. Leel, M. G. Blaylock, L. Duncan, M. R. Drever, G. Strachan, K. A. Charlton, M. Koruth, A. J. Porter and M. C. Wright (2005). "Generation of a monoclonal human single chain antibody fragment to hepatic stellate cells--a potential mechanism for targeting liver anti-fibrotic therapeutics." J Hepatol **42**(6): 888-896.

Ewing, J. (1928). Neoplastic diseases : a treatise on tumors. [S.l.], W. B. Saunders.

Falchook, G. S., G. V. Long, R. Kurzrock, K. B. Kim, T. H. Arkenau, M. P. Brown, O. Hamid, J. R. Infante, M. Millward, A. C. Pavlick, S. J. O'Day, S. C. Blackman, C. M. Curtis, P. Lebowitz, B. Ma, D. Ouellet and R. F. Kefford (2012). "Dabrafenib in patients with melanoma, untreated brain metastases, and other solid tumours: a phase 1 dose-escalation trial." Lancet **379**(9829): 1893-1901.

Feng, Y., C. C. Broder, P. E. Kennedy and E. A. Berger (1996). "HIV-1 entry cofactor: functional cDNA cloning of a seven-transmembrane, G protein-coupled receptor." Science **272**(5263): 872-877.

Fisher, R. and J. Larkin (2012). "Vemurafenib: a new treatment for BRAF-V600 mutated advanced melanoma." Cancer Manag Res **4**: 243-252.

Flaherty, K. T., I. Puzanov, K. B. Kim, A. Ribas, G. A. McArthur, J. A. Sosman, P. J. O'Dwyer, R. J. Lee, J. F. Grippo, K. Nolop and P. B. Chapman (2010). "Inhibition of mutated, activated BRAF in metastatic melanoma." N Engl J Med **363**(9): 809-819.

Flomenberg, N., R. L. Comenzo, K. Badel and G. Calandra (2010). "Plerixafor (Mozobil) alone to mobilize hematopoietic stem cells from multiple myeloma

patients for autologous transplantation." Biol Blood Marrow Transplant **16**(5): 695-700.

Fogh, J. and B. C. Giovanella (1978). The Nude mouse in experimental and clinical research. New York, Academic Press.

Folkman, J. (2002). "Role of angiogenesis in tumor growth and metastasis." Semin Oncol **29**(6 Suppl 16): 15-18.

Folkman, J., K. Watson, D. Ingber and D. Hanahan (1989). "Induction of angiogenesis during the transition from hyperplasia to neoplasia." Nature **339**(6219): 58-61.

Franco, R., G. Botti, M. Mascolo, G. Loquercio, G. Liguori, G. Ilardi, S. Losito, A. La Mura, R. Calemma, C. Ierano, J. Bryce, C. D'Alterio and S. Scala (2010). ""CXCR4-CXCL12 and VEGF correlate to uveal melanoma progression"." Front Biosci (Elite Ed) **2**: 13-21.

Frederick, M. J. and G. L. Clayman (2001). "Chemokines in cancer." Expert Rev Mol Med **3**(19): 1-18.

Fricker, S. P., V. Anastassov, J. Cox, M. C. Darkes, O. Grujic, S. R. Idzan, J. Labrecque, G. Lau, R. M. Mosi, K. L. Nelson, L. Qin, Z. Santucci and R. S. Wong (2006). "Characterization of the molecular pharmacology of AMD3100: a specific antagonist of the G-protein coupled chemokine receptor, CXCR4." Biochem Pharmacol **72**(5): 588-596.

Friedman, B. H., J. H. Wolf, L. Wang, M. E. Putt, A. Shaked, J. D. Christie, W. W. Hancock and K. M. Olthoff (2012). "Serum cytokine profiles associated with early allograft dysfunction in patients undergoing liver transplantation." Liver Transpl **18**(2): 166-176.

Friedman, S. (2000). "Molecular regulation of hepatic fibrosis, an integrated cellular response to tissue injury." J Biol Chem(275): 2247-2250.

Furutani, Y., H. Nomura, M. Notake, Y. Oyamada, T. Fukui, M. Yamada, C. G. Larsen, J. J. Oppenheim and K. Matsushima (1989). "Cloning and sequencing of the cDNA for human monocyte chemotactic and activating factor (MCAF)." Biochem Biophys Res Commun **159**(1): 249-255.

Gale, L. M. and S. R. McColl (1999). "Chemokines: extracellular messengers for all occasions?" Bioessays **21**(1): 17-28.

Galun, E. and S. Rose-John (2013). "The regenerative activity of interleukin-6." Methods Mol Biol **982**: 59-77.

Gao, Z., X. Wang, K. Wu, Y. Zhao and G. Hu (2010). "Pancreatic stellate cells increase the invasion of human pancreatic cancer cells through the stromal cell-derived factor-1/CXCR4 axis." Pancreatology **10**(2-3): 186-193.

Gerard, C. and B. J. Rollins (2001). "Chemokines and disease." Nat Immunol **2**(2): 108-115.

Gervaz, P., R. Pak-art, S. Nivatvongs, B. G. Wolff, D. Larson and S. Ringel (2003). "Colorectal adenocarcinoma in cirrhotic patients." J Am Coll Surg **196**(6): 874-879.

Goddard, S., A. Williams, C. Morland, S. Qin, R. Gladue, S. G. Hubscher and D. H. Adams (2001). "Differential expression of chemokines and chemokine receptors shapes the inflammatory response in rejecting human liver transplants." Transplantation **72**(12): 1957-1967.

Grisham, J. W. (1994). "Migration of hepatocytes along hepatic plates and stem cell-fed hepatocyte lineages." Am J Pathol **144**(5): 849-854.

Halaban, R., W. Zhang, A. Bacchiocchi, E. Cheng, F. Parisi, S. Ariyan, M. Krauthammer, J. P. McCusker, Y. Kluger and M. Sznol (2010). "PLX4032, a selective BRAF(V600E) kinase inhibitor, activates the ERK pathway and enhances cell migration and proliferation of BRAF melanoma cells." Pigment Cell Melanoma Res **23**(2): 190-200.

Hatzivassiliou, G., K. Song, I. Yen, B. J. Brandhuber, D. J. Anderson, R. Alvarado, M. J. Ludlam, D. Stokoe, S. L. Gloor, G. Vigers, T. Morales, I. Aliagas, B. Liu, S. Sideris, K. P. Hoeflich, B. S. Jaiswal, S. Seshagiri, H. Koeppen, M. Belvin, L. S. Friedman and S. Malek (2010). "RAF inhibitors prime wild-type RAF to activate the MAPK pathway and enhance growth." Nature **464**(7287): 431-435.

Hauschild, A., S. S. Agarwala, U. Trefzer, D. Hogg, C. Robert, P. Hersey, A. Eggermont, S. Grabbe, R. Gonzalez, J. Gille, C. Peschel, D. Schadendorf, C. Garbe, S. O'Day, A. Daud, J. M. White, C. Xia, K. Patel, J. M. Kirkwood and U. Keilholz (2009). "Results of a phase III, randomized, placebo-controlled study of sorafenib in combination with carboplatin and paclitaxel as second-line treatment in patients with unresectable stage III or stage IV melanoma." J Clin Oncol **27**(17): 2823-2830.

Hill, D. S., S. Martin, J. L. Armstrong, R. Flockhart, J. J. Tonison, D. G. Simpson, M. A. Birch-Machin, C. P. Redfern and P. E. Lovat (2009). "Combining the endoplasmic reticulum stress-inducing agents bortezomib and fenretinide as a novel therapeutic strategy for metastatic melanoma." Clin Cancer Res **15**(4): 1192-1198.

Hokeness, K. L., E. S. Deweerd, M. W. Munks, C. A. Lewis, R. P. Gladue and T. P. Salazar-Mather (2007). "CXCR3-dependent recruitment of antigen-specific T lymphocytes to the liver during murine cytomegalovirus infection." J Virol **81**(3): 1241-1250.

Hong, F., A. Tuyama, T. F. Lee, J. Loke, R. Agarwal, X. Cheng, A. Garg, M. I. Fiel, M. Schwartz, J. Walewski, A. Branch, A. D. Schecter and M. B. Bansal (2009). "Hepatic stellate cells express functional CXCR4: role in stromal cell-derived factor-1alpha-mediated stellate cell activation." Hepatology **49**(6): 2055-2067.

Horie, K., M. Tsuchihara and T. Nakatsura (2010). "Silencing of secreted protein acidic and rich in cysteine inhibits the growth of human melanoma cells with G arrest induction." Cancer Sci **101**(4): 913-919.

Hsia, C. C., C. A. Axiotis, A. M. Di Bisceglie and E. Tabor (1992). "Transforming growth factor-alpha in human hepatocellular carcinoma and coexpression with hepatitis B surface antigen in adjacent liver." Cancer **70**(5): 1049-1056.

Ilmakunnas, M., K. Hockerstedt, H. Makisalo, S. Siitonen, H. Repo and E. J. Pesonen (2010). "Hepatic IL-8 release during graft procurement is associated with impaired graft function after human liver transplantation." Clin Transplant **24**(1): 29-35.

James, L. P., H. C. Farrar, T. L. Darville, J. E. Sullivan, T. G. Givens, G. L. Kearns, G. S. Wasserman, P. M. Simpson and J. A. Hinson (2001). "Elevation of serum interleukin 8 levels in acetaminophen overdose in children and adolescents." Clin Pharmacol Ther **70**(3): 280-286.

Janowski, M. (2009). "Functional diversity of SDF-1 splicing variants." Cell Adh Migr **3**(3): 243-249.

Jiang, Y., L. A. Tabak, A. J. Valente and D. T. Graves (1991). "Initial characterization of the carbohydrate structure of MCP-1." Biochem Biophys Res Commun **178**(3): 1400-1404.

Jo, S. Y., P. I. Wang, J. E. Nor, E. L. Bellile, Z. Zhang, F. P. Worden, A. Srinivasan and S. K. Mukherji (2013). "CT Perfusion Can Predict Overexpression of CXCL8 (Interleukin-8) in Head and Neck Squamous Cell Carcinoma." AJNR Am J Neuroradiol.

Johnston, D. G., G. A. Johnson, K. G. Alberti, G. H. Millward-Sadler, J. Mitchell and R. Wright (1986). "Hepatic regeneration and metabolism after partial hepatectomy in diabetic rats: effects of insulin therapy." Eur J Clin Invest **16**(5): 384-390.

Joseph, E. W., C. A. Pratilas, P. I. Poulikakos, M. Tadi, W. Wang, B. S. Taylor, E. Halilovic, Y. Persaud, F. Xing, A. Viale, J. Tsai, P. B. Chapman, G. Bollag, D. B. Solit and N. Rosen (2010). "The RAF inhibitor PLX4032 inhibits ERK signaling and tumor cell proliferation in a V600E BRAF-selective manner." Proc Natl Acad Sci U S A **107**(33): 14903-14908.

Kam, I., S. Lynch, G. Svanas, S. Todo, L. Polimeno, A. Francavilla, R. J. Penkrot, S. Takaya, B. G. Ericzon, T. E. Starzl and et al. (1987). "Evidence that host size determines liver size: studies in dogs receiving orthotopic liver transplants." Hepatology **7**(2): 362-366.

Kim, J., T. Mori, S. L. Chen, F. F. Amersi, S. R. Martinez, C. Kuo, R. R. Turner, X. Ye, A. J. Bilchik, D. L. Morton and D. S. Hoon (2006). "Chemokine receptor CXCR4 expression in patients with melanoma and colorectal cancer liver metastases and the association with disease outcome." Ann Surg **244**(1): 113-120.

Kim, M., Y. J. Koh, K. E. Kim, B. I. Koh, D. H. Nam, K. Alitalo, I. Kim and G. Y. Koh (2010). "CXCR4 signaling regulates metastasis of chemoresistant melanoma cells by a lymphatic metastatic niche." Cancer Res **70**(24): 10411-10421.

Knittel, T., Kobold, D., Saile, B et al. (1999). "Rat liver myofibroblasts and hepatic stellate cells: different cell populations of the fibroblast lineage with fibrogenic potential." Gastroenterology **117**: 1205-1221.

Knowles, M. A. and P. Selby (2005). Introduction to the cellular and molecular biology of cancer. Oxford, Oxford University Press.

Kocabayoglu, P. and S. L. Friedman (2013). "Cellular basis of hepatic fibrosis and its role in inflammation and cancer." Front Biosci (Schol Ed) **5**: 217-230.

Kryczek, I., S. Wei, E. Keller, R. Liu and W. Zou (2007). "Stroma-derived factor (SDF-1/CXCL12) and human tumor pathogenesis." Am J Physiol Cell Physiol **292**(3): C987-995.

Kuhnelt-Leddihn, L., H. Muller, K. Eisendle, B. Zelger and G. Weinlich (2012). "Overexpression of the chemokine receptors CXCR4, CCR7, CCR9, and CCR10 in human primary cutaneous melanoma: a potential prognostic value for CCR7 and CCR10?" Arch Dermatol Res **304**(3): 185-193.

Land, E. J. and P. A. Riley (2000). "Spontaneous redox reactions of dopaquinone and the balance between the eumelanic and phaeomelanic pathways." Pigment Cell Res **13**(4): 273-277.

Lee, C. H., T. Kakinuma, J. Wang, H. Zhang, D. C. Palmer, N. P. Restifo and S. T. Hwang (2006). "Sensitization of B16 tumor cells with a CXCR4 antagonist increases the efficacy of immunotherapy for established lung metastases." Mol Cancer Ther **5**(10): 2592-2599.

Leiter, U., F. Meier, B. Schittek and C. Garbe (2004). "The natural course of cutaneous melanoma." J Surg Oncol **86**(4): 172-178.

Lev, D. C., A. Onn, V. O. Melinkova, C. Miller, V. Stone, M. Ruiz, E. C. McGary, H. N. Ananthaswamy, J. E. Price and M. Bar-Eli (2004). "Exposure of melanoma cells to dacarbazine results in enhanced tumor growth and metastasis in vivo." J Clin Oncol **22**(11): 2092-2100.

Levoye, A., K. Balabanian, F. Baleux, F. Bachelerie and B. Lagane (2009). "CXCR7 heterodimerizes with CXCR4 and regulates CXCL12-mediated G protein signaling." Blood **113**(24): 6085-6093.

Li, H., H. Alizadeh and J. Y. Niederkorn (2008). "Differential expression of chemokine receptors on uveal melanoma cells and their metastases." Invest Ophthalmol Vis Sci **49**(2): 636-643.

Li, H., W. Yang, P. W. Chen, H. Alizadeh and J. Y. Niederkorn (2009). "Inhibition of chemokine receptor expression on uveal melanomas by CXCR4 siRNA and its

effect on uveal melanoma liver metastases." Invest Ophthalmol Vis Sci **50**(12): 5522-5528.

Liang, Z., Y. Yoon, J. Votaw, M. M. Goodman, L. Williams and H. Shim (2005). "Silencing of CXCR4 blocks breast cancer metastasis." Cancer Res **65**(3): 967-971.

Lin, J. Y. and D. E. Fisher (2007). "Melanocyte biology and skin pigmentation." Nature **445**(7130): 843-850.

Livak, K. J. and T. D. Schmittgen (2001). "Analysis of relative gene expression data using real-time quantitative PCR and the 2(-Delta Delta C(T)) Method." Methods **25**(4): 402-408.

Loos, T., A. Mortier, M. Gouwy, I. Ronsse, W. Put, J. P. Lenaerts, J. Van Damme and P. Proost (2008). "Citrullination of CXCL10 and CXCL11 by peptidylarginine deiminase: a naturally occurring posttranslational modification of chemokines and new dimension of immunoregulation." Blood **112**(7): 2648-2656.

LoRusso, P. M., S. S. Krishnamurthi, J. J. Rinehart, L. M. Nabell, L. Malburg, P. B. Chapman, S. E. DePrimo, S. Bentivegna, K. D. Wilner, W. Tan and A. D. Ricart (2010). "Phase I pharmacokinetic and pharmacodynamic study of the oral MAPK/ERK kinase inhibitor PD-0325901 in patients with advanced cancers." Clin Cancer Res **16**(6): 1924-1937.

Luster, A. D. (1998). "Chemokines--chemotactic cytokines that mediate inflammation." N Engl J Med **338**(7): 436-445.

MacSween, R., N,M., Burt, A, D., Portmann, B,C. (2002). Pathology of the Liver. London, Churchill Livingstone

MacSween, R. N. M. P. o. t. l., A. D. Burt, B. Portmann and L. D. Ferrell (2007). MacSween's pathology of the liver. [London], Elsevier Churchill Livingstone.

Margolin, K. A., J. Moon, L. E. Flaherty, C. D. Lao, W. L. Akerley, 3rd, M. Othus, J. A. Sosman, J. M. Kirkwood and V. K. Sondak (2012). "Randomized phase II trial of sorafenib with temsirolimus or tipifarnib in untreated metastatic melanoma (S0438)." Clin Cancer Res **18**(4): 1129-1137.

Marshall, H. (2010). The use of a recombinant single chainantibody in the investigation of liver fibrosis. PhD Newcastle University.

Matsumoto, T. and M. Kawakami (1982). "The unit-concept of hepatic parenchyma--a re-examination based on angioarchitectural studies." Acta Pathol Jpn **32 Suppl 2**: 285-314.

Matsusue, R., Kubo, H., Hisamori, S. et al. (2009). "Hepatic stellate cells promote liver metastasis of colon cancer cells by the action of SDF-1/CXCR4 axis." Ann Surg Oncol **16**: 2645-2653.

McQuibban, G. A., J. H. Gong, E. M. Tam, C. A. McCulloch, I. Clark-Lewis and C. M. Overall (2000). "Inflammation dampened by gelatinase A cleavage of monocyte chemoattractant protein-3." Science **289**(5482): 1202-1206.

Mendt, M. and J. E. Cardier (2012). "Stromal-derived factor-1 and its receptor, CXCR4, are constitutively expressed by mouse liver sinusoidal endothelial cells: implications for the regulation of hematopoietic cell migration to the liver during extramedullary hematopoiesis." Stem Cells Dev **21**(12): 2142-2151.

Michalopoulos, G. K. (1990). "Liver regeneration: molecular mechanisms of growth control." FASEB J **4**(2): 176-187.

Moelants, E. A., A. Mortier, J. Van Damme and P. Proost (2013). "In vivo regulation of chemokine activity by post-translational modification." Immunol Cell Biol **91**(6): 402-407.

Monteagudo, C., D. Ramos, A. Pellin-Carcelen, R. Gil, R. C. Callaghan, J. M. Martin, V. Alonso, A. Murgui, L. Navarro, S. Calabuig, J. A. Lopez-Guerrero, E. Jorda and A. Pellin (2012). "CCL27-CCR10 and CXCL12-CXCR4 chemokine ligand-receptor mRNA expression ratio: new predictive factors of tumor progression in cutaneous malignant melanoma." Clin Exp Metastasis **29**(6): 625-637.

Mosi, R. M., V. Anastassova, J. Cox, M. C. Darkes, S. R. Idzan, J. Labrecque, G. Lau, K. L. Nelson, K. Patel, Z. Santucci, R. S. Wong, R. T. Skerlj, G. J. Bridger, D. Huskens, D. Schols and S. P. Fricker (2012). "The molecular pharmacology of AMD11070: an orally bioavailable CXCR4 HIV entry inhibitor." Biochem Pharmacol **83**(4): 472-479.

Moyle, G., E. DeJesus, M. Boffito, R. S. Wong, C. Gibney, K. Badel, R. MacFarland, G. Calandra, G. Bridger and S. Becker (2009). "Proof of activity with AMD11070, an orally bioavailable inhibitor of CXCR4-tropic HIV type 1." Clin Infect Dis **48**(6): 798-805.

Muller, A., B. Homey, H. Soto, N. Ge, D. Catron, M. E. Buchanan, T. McClanahan, E. Murphy, W. Yuan, S. N. Wagner, J. L. Barrera, A. Mohar, E. Verastegui and A. Zlotnik (2001). "Involvement of chemokine receptors in breast cancer metastasis." Nature **410**(6824): 50-56.

Murphy, J. W., Y. Cho, A. Sachpatzidis, C. Fan, M. E. Hodsdon and E. Lolis (2007). "Structural and functional basis of CXCL12 (stromal cell-derived factor-1 alpha) binding to heparin." J Biol Chem **282**(13): 10018-10027.

Murphy, P. M., M. Baggiolini, I. F. Charo, C. A. Hebert, R. Horuk, K. Matsushima, L. H. Miller, J. J. Oppenheim and C. A. Power (2000). "International union of pharmacology. XXII. Nomenclature for chemokine receptors." Pharmacol Rev **52**(1): 145-176.

Nagasawa, T., S. Hirota, K. Tachibana, N. Takakura, S. Nishikawa, Y. Kitamura, N. Yoshida, H. Kikutani and T. Kishimoto (1996). "Defects of B-cell lymphopoiesis and bone-marrow myelopoiesis in mice lacking the CXC chemokine PBSF/SDF-1." Nature **382**(6592): 635-638.

Naumann, U., E. Cameroni, M. Pruenster, H. Mahabaleshwar, E. Raz, H. G. Zerwes, A. Rot and M. Thelen (2010). "CXCR7 functions as a scavenger for CXCL12 and CXCL11." PLoS One **5**(2): e9175.

Negash, A. A., H. J. Ramos, N. Crochet, D. T. Lau, B. Doehle, N. Papic, D. A. Delker, J. Jo, A. Bertoletti, C. H. Hagedorn and M. Gale, Jr. (2013). "IL-1beta production through the NLRP3 inflammasome by hepatic macrophages links hepatitis C virus infection with liver inflammation and disease." PLoS Pathog **9**(4): e1003330.

Neubauer, K., Knittel, T., Aursch, S., et al. (1996). "Glial fibrillary acidic protein-a cell type specific marker for Ito cells in vivo and in vitro." Hepatology **24**: 719-730.

Newton, P., G. O'Boyle, Y. Jenkins, S. Ali and J. A. Kirby (2009). "T cell extravasation: demonstration of synergy between activation of CXCR3 and the T cell receptor." Mol Immunol **47**(2-3): 485-492.

Niesner, B. and N. Maheshri (2013). "Using the Cre-lox System to Randomize Target Gene Expression States and Generate Diverse Phenotypes." Biotechnol Bioeng.

O'Boyle, G., I. Swidenbank, H. Marshall, C. E. Barker, J. Armstrong, S. A. White, S. P. Fricker, R. Plummer, M. Wright and P. E. Lovat (2013). "Inhibition of CXCR4-CXCL12 chemotaxis in melanoma by AMD11070." Br J Cancer **108**(8): 1634-1640.

Onai, N., Y. Zhang, H. Yoneyama, T. Kitamura, S. Ishikawa and K. Matsushima (2000). "Impairment of lymphopoiesis and myelopoiesis in mice reconstituted with bone marrow-hematopoietic progenitor cells expressing SDF-1-intrakine." Blood **96**(6): 2074-2080.

Otsuka, S. and G. Bebb (2008). "The CXCR4/SDF-1 chemokine receptor axis: a new target therapeutic for non-small cell lung cancer." J Thorac Oncol **3**(12): 1379-1383.

Overwijk, W. W. and N. P. Restifo (2001). "B16 as a mouse model for human melanoma." Curr Protoc Immunol **Chapter 20**: Unit 20 21.

Paget, S. (1989). "The distribution of secondary growths in cancer of the breast. 1889." Cancer Metastasis Rev **8**(2): 98-101.

Payne, A. S. and L. A. Cornelius (2002). "The role of chemokines in melanoma tumor growth and metastasis." J Invest Dermatol **118**(6): 915-922.

Pease, J. E. and R. Horuk (2009). "Chemokine receptor antagonists: part 2." Expert Opin Ther Pat **19**(2): 199-221.

Pereira-Lima, J. E., E. Lichtenfels, F. S. Barbosa, C. G. Zettler and J. M. Kulczynski (2003). "Prevalence study of metastases in cirrhotic livers." Hepatogastroenterology **50**(53): 1490-1495.

Possamai, L. A., C. G. Antoniades, Q. M. Anstee, A. Quaglia, D. Vergani, M. Thursz and J. Wendon (2010). "Role of monocytes and macrophages in experimental and human acute liver failure." World J Gastroenterol **16**(15): 1811-1819.

Probert, P. M. E., M. R. Ebrahimkhani, F. Oakley, J. Mann, A. D. Burt, D. A. Mann and M. C. Wright (In press). "A reversible model for periportal fibrosis and refined alternative to bile duct ligation " Journal of Toxicology 1-10.

Proost, P., T. Loos, A. Mortier, E. Schutyser, M. Gouwy, S. Noppen, C. Dillen, I. Ronsse, R. Conings, S. Struyf, G. Opdenakker, P. C. Maudgal and J. Van Damme (2008). "Citrullination of CXCL8 by peptidylarginine deiminase alters receptor usage, prevents proteolysis, and dampens tissue inflammation." J Exp Med **205**(9): 2085-2097.

Qi, K., H. Qiu, D. Sun, G. Y. Minuk, M. Lizardo, J. Rutherford and F. W. Orr (2004). "Impact of cirrhosis on the development of experimental hepatic metastases by B16F1 melanoma cells in C57BL/6 mice." Hepatology **40**(5): 1144-1150.

Rajpar, S. and J. Marsden (2008). ABC of skin cancer. Malden, Mass. ; Oxford, Blackwell Pub.

Ratajczak, M. Z., E. Zuba-Surma, M. Kucia, R. Reca, W. Wojakowski and J. Ratajczak (2006). "The pleiotropic effects of the SDF-1-CXCR4 axis in organogenesis, regeneration and tumorigenesis." Leukemia **20**(11): 1915-1924.

Raz, E. and H. Mahabaleshwar (2009). "Chemokine signaling in embryonic cell migration: a fisheye view." Development **136**(8): 1223-1229.

Robinson, E. A., T. Yoshimura, E. J. Leonard, S. Tanaka, P. R. Griffin, J. Shabanowitz, D. F. Hunt and E. Appella (1989). "Complete amino acid sequence of a human monocyte chemoattractant, a putative mediator of cellular immune reactions." Proc Natl Acad Sci U S A **86**(6): 1850-1854.

Rossi, D. and A. Zlotnik (2000). "The biology of chemokines and their receptors." Annu Rev Immunol **18**: 217-242.

Saiman, Y. (2012). The Role of Stellate Cell-derived CXCL12 in Liver Injury, PhD, Mount Sinai School of Medicine 1-125.

Saiman, Y. and S. L. Friedman (2012). "The role of chemokines in acute liver injury." Front Physiol **3**: 213.

Sakai, N., H. Yoshidome, T. Shida, F. Kimura, H. Shimizu, M. Ohtsuka, D. Takeuchi, M. Sakakibara and M. Miyazaki (2012). "CXCR4/CXCL12 expression profile is associated with tumor microenvironment and clinical outcome of liver metastases of colorectal cancer." Clin Exp Metastasis **29**(2): 101-110.

Scala, S., P. Giuliano, P. A. Ascierto, C. Ierano, R. Franco, M. Napolitano, A. Ottaiano, M. L. Lombardi, M. Luongo, E. Simeone, D. Castiglia, F. Mauro, I. De Michele, R. Calemma, G. Botti, C. Caraco, G. Nicoletti, R. A. Satriano and G.

Castello (2006). "Human melanoma metastases express functional CXCR4." Clin Cancer Res **12**(8): 2427-2433.

Scala, S., A. Ottaiano, P. A. Ascierto, M. Cavalli, E. Simeone, P. Giuliano, M. Napolitano, R. Franco, G. Botti and G. Castello (2005). "Expression of CXCR4 predicts poor prognosis in patients with malignant melanoma." Clin Cancer Res **11**(5): 1835-1841.

Schall, T. J. and A. E. Proudfoot (2011). "Overcoming hurdles in developing successful drugs targeting chemokine receptors." Nat Rev Immunol **11**(5): 355-363.

Schioppa, T., B. Uranchimeg, A. Saccani, S. K. Biswas, A. Doni, A. Rapisarda, S. Bernasconi, S. Saccani, M. Nebuloni, L. Vago, A. Mantovani, G. Melillo and A. Sica (2003). "Regulation of the chemokine receptor CXCR4 by hypoxia." J Exp Med **198**(9): 1391-1402.

Schroder, J. M., M. Sticherling, H. H. Henneicke, W. C. Preissner and E. Christophers (1990). "IL-1 alpha or tumor necrosis factor-alpha stimulate release of three NAP-1/IL-8-related neutrophil chemotactic proteins in human dermal fibroblasts." J Immunol **144**(6): 2223-2232.

Schutyser, E., Y. Su, Y. Yu, M. Gouwy, S. Zaja-Milatovic, J. Van Damme and A. Richmond (2007). "Hypoxia enhances CXCR4 expression in human microvascular endothelial cells and human melanoma cells." Eur Cytokine Netw **18**(2): 59-70.

Scotton, C. J., J. L. Wilson, K. Scott, G. Stamp, G. D. Wilbanks, S. Fricker, G. Bridger and F. R. Balkwill (2002). "Multiple actions of the chemokine CXCL12 on epithelial tumor cells in human ovarian cancer." Cancer Res **62**(20): 5930-5938.

Sell, S. (2001). "Heterogeneity and plasticity of hepatocyte lineage cells." Hepatology **33**(3): 738-750.

Sell, S. (2003). "The hepatocyte: heterogeneity and plasticity of liver cells." Int J Biochem Cell Biol **35**(3): 267-271.

Seymour, K. and R. M. Charnley (1999). "Evidence that metastasis is less common in cirrhotic than normal liver: a systematic review of post-mortem case-control studies." Br J Surg **86**(10): 1237-1242.

Sgroi, A., C. Gonelle-Gispert, P. Morel, R. M. Baertschiger, N. Niclauss, G. Mentha, P. Majno, V. Serre-Beinier and L. Buhler (2011). "Interleukin-1 receptor antagonist modulates the early phase of liver regeneration after partial hepatectomy in mice." PLoS One **6**(9): e25442.

Shirozu, M., T. Nakano, J. Inazawa, K. Tashiro, H. Tada, T. Shinohara and T. Honjo (1995). "Structure and chromosomal localization of the human stromal cell-derived factor 1 (SDF1) gene." Genomics **28**(3): 495-500.

Simeonova, P. P., Gallucci, R.M., Hulderman, T. et al. (2001). "The role of tumour necrosis factor-alpha in liver toxicity, inflammation and fibrosis induced by carbon tetrachloride." Toxicol. Appl. Pharmacol **177**: 112-120.

Singh, S., A. P. Singh, B. Sharma, L. B. Owen and R. K. Singh (2010). "CXCL8 and its cognate receptors in melanoma progression and metastasis." Future Oncol **6**(1): 111-116.

Smith, M. C., K. E. Luker, J. R. Garbow, J. L. Prior, E. Jackson, D. Piwnica-Worms and G. D. Luker (2004). "CXCR4 regulates growth of both primary and metastatic breast cancer." Cancer Res **64**(23): 8604-8612.

Steinberg, M. and M. Silva (2010). "Plerixafor: A chemokine receptor-4 antagonist for mobilization of hematopoietic stem cells for transplantation after high-dose chemotherapy for non-Hodgkin's lymphoma or multiple myeloma." Clin Ther **32**(5): 821-843.

Stone, N. D., S. B. Dunaway, C. Flexner, C. Tierney, G. B. Calandra, S. Becker, Y. J. Cao, I. P. Wiggins, J. Conley, R. T. MacFarland, J. G. Park, C. Lalama, S. Snyder, B. Kallungal, K. L. Klingman and C. W. Hendrix (2007). "Multiple-dose escalation study of the safety, pharmacokinetics, and biologic activity of oral AMD070, a selective CXCR4 receptor inhibitor, in human subjects." Antimicrob Agents Chemother **51**(7): 2351-2358.

Strain, A. J. (1992). "Transforming growth factor-beta: the elusive hepatic chalone?" Hepatology **16**(1): 269-270.

Strong, R. W. (2006). "Living-donor liver transplantation: an overview." J Hepatobiliary Pancreat Surg **13**(5): 370-377.

Su, L. P., J. P. Zhang, H. B. Xu, J. Chen, Y. Wang and S. D. Xiong (2005). "[The role of CXCR4 in lung cancer metastasis and its possible mechanism]." Zhonghua Yi Xue Za Zhi **85**(17): 1190-1194.

Sullivan, R. J. and K. Flaherty (2013). "MAP kinase signaling and inhibition in melanoma." Oncogene **32**(19): 2373-2379.

Sun, Y. X., J. Wang, C. E. Shelburne, D. E. Lopatin, A. M. Chinnaiyan, M. A. Rubin, K. J. Pienta and R. S. Taichman (2003). "Expression of CXCR4 and CXCL12 (SDF-1) in human prostate cancers (PCa) in vivo." J Cell Biochem **89**(3): 462-473.

Syed Khaja, A. S., N. Dizeyi, P. K. Kopparapu, L. Anagnostaki, P. Harkonen and J. L. Persson (2013). "Cyclin A1 modulates the expression of vascular endothelial growth factor and promotes hormone-dependent growth and angiogenesis of breast cancer." PLoS One **8**(8): e72210.

Takekoshi, T., J. J. Ziarek, B. F. Volkman and S. T. Hwang (2012). "A locked, dimeric CXCL12 variant effectively inhibits pulmonary metastasis of CXCR4-expressing melanoma cells due to enhanced serum stability." Mol Cancer Ther **11**(11): 2516-2525.

Tashiro, K., H. Tada, R. Heilker, M. Shirozu, T. Nakano and T. Honjo (1993). "Signal sequence trap: a cloning strategy for secreted proteins and type I membrane proteins." Science **261**(5121): 600-603.

Teicher, B. A. and S. P. Fricker (2010). "CXCL12 (SDF-1)/CXCR4 pathway in cancer." Clin Cancer Res **16**(11): 2927-2931.

Terada, R., K. Yamamoto, T. Hakoda, N. Shimada, N. Okano, N. Baba, Y. Ninomiya, M. E. Gershwin and Y. Shiratori (2003). "Stromal cell-derived factor-1 from biliary epithelial cells recruits CXCR4-positive cells: implications for inflammatory liver diseases." Lab Invest **83**(5): 665-672.

Thompson, J. F., R. A. Scolyer and R. F. Kefford (2005). "Cutaneous melanoma." Lancet **365**(9460): 687-701.

Todorovic, M., Z. Radisavljevic, B. Balint, B. Andjelic, V. Todorovic, M. P. Jovanovic and B. Mihaljevic (2012). "Increased angiogenesis-associated poor outcome in acute lymphoblastic leukemia: a single center study." Appl Immunohistochem Mol Morphol **20**(5): 488-493.

Uetsuji, S., M. Yamamura, K. Yamamichi, Y. Okuda, H. Takada and K. Hioki (1992). "Absence of colorectal cancer metastasis to the cirrhotic liver." Am J Surg **164**(2): 176-177.

Ugurel, S. and D. Schadendorf (2003). "Systemic treatment in advanced melanoma: innovative perspectives." Onkologie **26**(3): 234-238.

Van Coillie, E., P. Proost, I. Van Aelst, S. Struyf, M. Polfliet, I. De Meester, D. J. Harvey, J. Van Damme and G. Opdenakker (1998). "Functional comparison of two human monocyte chemotactic protein-2 isoforms, role of the amino-terminal pyroglutamic acid and processing by CD26/dipeptidyl peptidase IV." Biochemistry **37**(36): 12672-12680.

Van Coillie, E., J. Van Damme and G. Opdenakker (1999). "The MCP/eotaxin subfamily of CC chemokines." Cytokine Growth Factor Rev **10**(1): 61-86.

Van Damme, J., J. Van Beeumen, R. Conings, B. Decock and A. Billiau (1989). "Purification of granulocyte chemotactic peptide/interleukin-8 reveals N-terminal sequence heterogeneity similar to that of beta-thromboglobulin." Eur J Biochem **181**(2): 337-344.

Van den Steen, P. E., P. Proost, A. Wuyts, J. Van Damme and G. Opdenakker (2000). "Neutrophil gelatinase B potentiates interleukin-8 tenfold by aminoterminal processing, whereas it degrades CTAP-III, PF-4, and GRO-alpha and leaves RANTES and MCP-2 intact." Blood **96**(8): 2673-2681.

Vanbockrijck, M. and G. Kloppel (1992). "Incidence and morphology of liver metastasis from extrahepatic malignancies to cirrhotic livers." Zentralbl Pathol **138**(2): 91-96.

Verbeke, H., G. De Hertogh, S. Li, J. Vandercappellen, S. Noppen, E. Schutyser, A. A. El-Asrar, G. Opdenakker, J. Van Damme, K. Geboes and S. Struyf (2010).

"Expression of angiostatic platelet factor-4var/CXCL4L1 counterbalances angiogenic impulses of vascular endothelial growth factor, interleukin-8/CXCL8, and stromal cell-derived factor 1/CXCL12 in esophageal and colorectal cancer." Hum Pathol **41**(7): 990-1001.

Vidal-Vanaclocha, F., A. Alonso-Varona, R. Ayala and E. Barbera-Guillem (1990). "Functional variations in liver tissue during the implantation process of metastatic tumour cells." Virchows Arch A Pathol Anat Histopathol **416**(3): 189-195.

Vlahakis, S. R., A. Villasis-Keever, T. S. Gomez, G. D. Bren and C. V. Paya (2003). "Human immunodeficiency virus-induced apoptosis of human hepatocytes via CXCR4." J Infect Dis **188**(10): 1455-1460.

Wald, O., O. Pappo, R. Safadi, M. Dagan-Berger, K. Beider, H. Wald, S. Franitza, I. Weiss, S. Avniel, P. Boaz, J. Hanna, G. Zamir, A. Eid, O. Mandelboim, U. Spengler, E. Galun and A. Peled (2004). "Involvement of the CXCL12/CXCR4 pathway in the advanced liver disease that is associated with hepatitis C virus or hepatitis B virus." Eur J Immunol **34**(4): 1164-1174.

Wallace, K., A. D. Burt and M. C. Wright (2008). "Liver fibrosis." Biochem J **411**(1): 1-18.

Xu, X., Y. M. Li, H. Ji, C. Z. Hou, Y. B. Cheng and F. P. Ma (2005). "Changes of ECM and CAM gene expression profile in the cirrhotic liver after HCV infection: analysis by cDNA expression array." World J Gastroenterol **11**(14): 2184-2187.

Yokoi, Y., Namihisa, T., Kuroda, H et al. (1984). "Immunocytochemical detection of desmin in fat-storing (Ito cells)." Hepatology **4**: 709-714.

Yoshimura, T., E. A. Robinson, E. Appella, K. Matsushima, S. D. Showalter, A. Skeel and E. J. Leonard (1989). "Three forms of monocyte-derived neutrophil chemotactic factor (MDNCF) distinguished by different lengths of the amino-terminal sequence." Mol Immunol **26**(1): 87-93.

Yu, L., J. Cecil, S. B. Peng, J. Schrementi, S. Kovacevic, D. Paul, E. W. Su and J. Wang (2006). "Identification and expression of novel isoforms of human stromal cell-derived factor 1." Gene **374**: 174-179.

Zabel, B. A., S. Lewen, R. D. Berahovich, J. C. Jaen and T. J. Schall (2011). "The novel chemokine receptor CXCR7 regulates trans-endothelial migration of cancer cells." Mol Cancer **10**: 73.

Zepper, M. (2008). "CreLoxP experiment." 2012.

Zeremski, M., R. Dimova, Q. Brown, I. M. Jacobson, M. Markatou and A. H. Talal (2009). "Peripheral CXCR3-associated chemokines as biomarkers of fibrosis in chronic hepatitis C virus infection." J Infect Dis **200**(11): 1774-1780.

Zhang, T., R. Somasundaram, K. Berencsi, L. Caputo, P. Rani, D. Guerry, E. Furth, B. J. Rollins, M. Putt, P. Gimotty, R. Swoboda, M. Herlyn and D. Herlyn (2005). "CXC chemokine ligand 12 (stromal cell-derived factor 1 alpha) and

CXCR4-dependent migration of CTLs toward melanoma cells in organotypic culture." J Immunol **174**(9): 5856-5863.

Zhu, Y., R. Zhou, H. Yang, J. Tan, X. Zhang and Q. Liu (2012). "[Effect of ulinastatin pretreatment on liver regeneration and TNF-alpha/IL-6/STAT-3 signal pathway in rats with major hepatectomy and ischemia-reperfusion injury]." Nan Fang Yi Ke Da Xue Xue Bao **32**(9): 1301-1306.

Zlotnik, A., A. M. Burkhardt and B. Homey (2011). "Homeostatic chemokine receptors and organ-specific metastasis." Nat Rev Immunol **11**(9): 597-606.

Zlotnik, A. and O. Yoshie (2000). "Chemokines: a new classification system and their role in immunity." Immunity **12**(2): 121-127.

Zlotnik, A., O. Yoshie and H. Nomiyama (2006). "The chemokine and chemokine receptor superfamilies and their molecular evolution." Genome Biol **7**(12): 243.

9.0 Abstracts and publications

Abstracts:

The Inhibition of chemokine signalling in metastatic melanoma to the liver.

Isabella Swidenbank[1], Professor Matthew Wright[1], Dr Graeme O'Boyle[1], Dr Penny Lovat[1].
[1]*Institute of Cellular Medicine, Newcastle University, Newcastle upon Tyne, UK*

Malignant melanoma represents the most aggressive skin cancer. Although early stage disease is treatable through surgical excision, late stage tumours frequently metastasise to the liver, at which point treatment options are limited. Recently, migration of melanoma towards metastatic sites has been shown to be associated with the chemokine CXCR4-CXCL12 receptor-ligand complex. In this context, novel receptor antagonists may offer therapeutic potential. The aim of the present study was therefore to test the hypothesis that inhibition of the CXCR4-CXCL12 receptor-ligand complex may provide a novel strategy for the prevention of melanoma metastasis.

Results demonstrated increased expression of CXCR4 in human metastatic melanoma cell lines, as demonstrated by both Western blotting and immunohistochemistry. Conversely, CXCL12 was expressed in human fibrotic liver cells but absent in hepatocytes and both metastatic melanoma cell lines. Dose response studies to test the potential of novel CXCR4 receptor antagonists to inhibit melanoma cell viability using a commercially available assay demonstrated that one inhibitor significantly reduced viability of both melanoma cell lines at clinically achievable concentrations. Live cell-imaging analysis of melanoma cell migration and chemotaxis assays also demonstrated that AMD11070 inhibited melanoma cell migration and chemotaxis towards recombinant CXCL12. Collectively, these data support the hypothesis that inhibition of the CXCR4-CXCL12 chemokine axis may represent a novel strategy through which to inhibit melanoma cell metastasis to the liver.

North East Post Graduate Conference (NEPG)
Newcastle University

The investigation of the role of liver damage/myofibroblasts on tumour metastasis to the liver.

Isabella Swidenbank[1], Dr Penny Lovat[1], Dr Graeme O'Boyle[1], Dr Keith Charlton[1], Dr Helen Reeves[2], Dr Steve White[3], Professor Matthew Wright[1]

[1]Institute of Cellular Medicine, Newcastle University, Newcastle upon Tyne, UK
[2]Northern Institute for Cancer Research, Newcastle University, Newcastle upon Tyne, UK
[3] Freeman Hospital, Newcastle upon Tyne, UK

Liver fibrosis is characterised by the accumulation of extracellular matrix proteins (ECM) caused by a range of toxins including xenobiotics and alcohol. Hepatic stellate cells (HSC) are pivotal in liver fibrosis. In the normal liver, HSCs exist in a quiescent state to store Vitamin A. Upon liver injury HSCs become 'activated' producing ECM and also pro-inflammatory proteins such as chemokines. The C1-3 antibody developed by our laboratory specifically targets HSCs and has already shown to be successful in liver fibrosis models. Another role for C1-3 may be in preventing cancer metastasis to the liver as chemokines are known to be involved in tumour progression. Many cancer cells over express the chemokine receptor CXCR4 and therefore, this current study was carried out to see if HSCs express SDF alpha. Western blot and PCR analysis was carried out in human liver tissue to determine SDF-alpha expression. Immunofluorescence was performed on human liver tissue sections and immunocytochemistry on HSCs for SDF-alpha localization. Sirius red staining on human liver sections was quantified to study fibrosis levels. Western Blot and PCR analysis demonstrated that SDF-alpha is expressed by the liver. Immunofluroescence showed co-staining of SDF-alpha with a marker of HSCs and Immunocytochemistry revealed the cytoplasmic expression of SDF-alpha in HSCs. Finally, sirius red staining showed varying levels of fibrosis and western blot results confirmed a correlation between increased levels of fibrosis with increased SDF-alpha expression. Thus, C1-3 may not only have important benefits for liver fibrosis but also for preventing cancer metastasis to the liver.

BTS Annual meeting 2012
Warwick University

Hepatic Stellate Cell-derived CXCL12 promotes T cell adhesion to Sinusoidal Endothelial Cells

[1]Dr Yedidya Saiman, [2]Isabella Swidenbank, [1]Professor Meena Bansal

[1]Mount Sinai School of Medicine, Division of Liver Diseases, New York, USA.
[2]Institute of Cellular Medicine, Newcastle University, Newcastle upon Tyne, UK

Lymphocyte migration into the liver is an important component of both chronic and acute liver injury and involves both binding to endothelial surfaces and transmigration into the hepatic parenchyma. During injury, endothelial cells undergo a process of activation by which they can up regulate their cell surface expression of chemokines to be presented to inflammatory cells. CXCL12, a chemokine increased in patients with liver disease, can be transcytosed and presented on endothelial cell surface. This transcytosed CXLC12 is more potent at promoting T cell chemotaxis than free CXCL12. Since stellate cells are considered liver specific tissue pericytes which are adjacent to endothelial cells and express high levels of CXCL12, we ***hypothesized*** that hepatic stellate cell-derived CXCL12 is transcytosed by sinusoidal endothelial cells and presented on their cell surface promoting lymphocyte adhesion. **Methods:** Monolayers of endothelial cells were cultured on the apical side of 3μm transwell inserts with or without stellate cells on the basal side. After 48 hours of co-culture, freshly isolated splenic T cells were added to the endothelial cell monolayer, incubated 1 hour, and the number of adhering T cells quantified. Adhesion assays were repeated with murine fibroblasts and with addition of a CXCL12 neutralizing antibody or monensin, a transcytosis inhibitor. **Results:** T cell adhesion to endothelial cell monolayers is enhanced by the presence of hepatic stellate cells and 3T3 murine fibroblasts (~2-fold increase) and did not require direct cell-cell contact. Pre-incubation of endothelial cell monolayers with a CXCL12 neutralizing antibody abolished the stellate cell dependent increase in T cells adhesion. Finally, addition of monensin, a transcytosis inhibitor, to the monolayers decreased the number of adhering T cells. **Conclusions:** Stellate cell-derived CXCL12 is transcytosed by endothelial cells thereby promoting T cell adhesion. These studies present a new paradigm for the role of stellate cells in inflammatory cell migration into the liver. Studies are currently underway to determine the role of stellate cell-derived CXCL12 in rodent models of liver injury. The availability of small molecule inhibitors of the CXCL12/CXCR4 axis makes it an attractive therapeutic target.

ASSLD Meeting 2012
Boston, USA

Publication:

Inhibition of CXCR4–CXCL12 chemotaxis in melanoma by AMD11070

G O'Boyle[1], I Swidenbank[1,5], H Marshall[1], C E Barker[1], J Armstrong[2], S A White[1], S P Fricker[3], R Plummer[4,6], M Wright[1,6] and P E Lovat[1,6]

[1]Institute of Cellular Medicine, Newcastle University, Newcastle upon Tyne NE2 4HH, UK
[2]University of Sunderland, Sunderland, UK
[3]Genzyme Corporation, Framingham, MA 01701, USA
[4]Northern Institute for Cancer Research, Newcastle University, Newcastle upon Tyne NE2 4HH, UK

Br J Cancer. 2013 Apr 30;108(8):1634-40. doi: 10.1038/bjc.2013.124. Epub 2013 Mar 2